

**STRAIN RATE EFFECTS ON TENSILE FRACTURE
AND DAMAGE TOLERANCE
OF COMPOSITE LAMINATES**

by

Yew-Poh Mak

B.S. Aerospace Engineering, The University of Michigan (1990)

**Submitted to the Department of Aeronautics and Astronautics in
Partial Fulfillment of the Requirements for the Degree of**

MASTER OF SCIENCE

at the

MASSACHUSETTS INSTITUTE OF TECHNOLOGY

June 1992

Copyright © Massachusetts Institute of Technology, 1992. All rights reserved.

Signature of Author _____
Department of Aeronautics and Astronautics
May 15, 1992

Certified by _____
Professor Hugh L. McManus
Thesis Supervisor

Accepted by _____
Professor Harold Y. Wachman
Chairman, Department Graduate Committee

Aero
MASSACHUSETTS INSTITUTE
OF TECHNOLOGY

JUN 05 1992

Strain Rate Effects on Tensile Failure and Damage Tolerance of Composite Laminates

by

Yew-Poh Mak

Submitted to the Department of Aeronautics and Astronautics on May 15,
1992, in partial fulfillment of the requirements for the Degree of
Master of Science.

ABSTRACT

An experimental study was carried out to investigate the behavior of graphite/epoxy laminates under uniaxial tensile loading at strain rates ranging from 0.0042 ϵ /min to 2 ϵ /min. The specimens were manufactured using two methods: automated tow placement and manual tape layup. The two material systems used were IM7/977-2 and AS4/938. The failure strengths, failure modes and laminate properties of both unnotched and notched specimens were measured. IM7/977-2 tape layup specimens were insensitive to strain rates between 0.005 ϵ /min and 0.5 ϵ /min, except for observed differences in the failure modes of the notched specimens. Although the undamaged response of the AS4/938 specimens was not dependent on manufacturing technique or strain rate, their damage tolerance was dependent on both factors. Notched tow placed specimens were stronger than notched tape layup specimens at all strain rates. The failure strengths of the notched tape layup specimens were significantly strain rate dependent, decreasing by about 20% at 2 ϵ /min; the notched tow placed specimens showed little strain rate sensitivity. The failure modes of the notched tow placed and notched tape layup specimens differed, but were independent of strain rates. The notched tow placed specimens exhibited a progressive failure, surviving to loads well beyond the load at which damage initiated at the notch tip. Conversely, the notched tape layup specimens at high strain rates exhibited a brittle failure; they failed soon after damage initiation.

Thesis Supervisor: Hugh L. McManus

Title: Boeing Assistant Professor, Department of
Aeronautics and Astronautics, Massachusetts
Institute of Technology

ACKNOWLEDGMENTS

The completion of this thesis is by no means an individual effort. Professor Hugh McManus has provided immeasurable guidance and patience throughout the conduct of this research. He is always available and approachable for all the questions and doubts I have, or just to talk about anything other than work. My gratitude also goes to Professor Paul Lagace, for giving me the opportunity to work at TELAC, and Professors John Dugundji and Michael Graves, for their concern and advise for my work. Professor Anthony Waas deserves special mention for generating my interest in composites.

Albert Supple taught me how to do things the way they are done in the 'real' world. Thanks Al, for all your help and concern. My team of UROPs deserves all the credit for expediting the experimental work and helping to prepare this document. Thank you, Kimberly Kohlhepp, Amy Gardner and Attila Lengyel, for all your help. Matt Beaumont programmed and debugged the data acquisition program and Narendra Bhat answered all my little and big questions. Thank you! My colleagues at TELAC have made going to work a little less boring. Thanks to all and especially: Mary, Laura, Peter, Wilson, Ed and Hiroto.

Life at MIT would have been a painful experience if not for the dudes, Jose (Pep) Ferrer, Mark (Camster) Campbell, and the rest of the gang: Charrissa, Kathy, Dave, Norm, Eric (Strang'O), Len, Pete, and John. Also, my two incredibly hilarious best friends, Scott (the armchair rocket-scientist) Heifetz and Nitin (the rational romantic) Subhedar, have provided tremendous encouragement all this while. Your long distance calls have kept me in touch with sanity.

DEDICATION

This document is dedicated to my parents and family, whose love and concern through all these years of separation, is very much appreciated. You have provided me with the strength and purpose to move ahead, especially in the worst of times.

To the Powerful and the Wise:

*Graduate School - it's a test of ultimate will
a heartbreak climb uphill
We're lost in a world of our own -
a world under anaesthetic -
subdivided and synthetic
Time becomes a spiral and space a curve
and though we might get dizzy
we try not to lose our nerve.*

*At the same time we're looking into
the eye of the storm
we try to maintain an air of joie de vivre
to improvise and orchestrate
illusions of careless flight
through our graduate school years
We hope our wild kinetic dreams
will transport our desires
and drive us when we're down.*

*Every day we're standing in a wind tunnel
racing towards the future
We often wonder whether we're
in a groove and on a roll
or in a rut and on a slide
But we keep heading down those tracks
driven on without a moment to spend
on anything but our work.*

*Throughout our graduate school years
we physically punish our bodies
while our spirits fly on dangerous missions
and our imaginations are on fire
We're focused high on soaring ambitions
consumed in a single desire
In the grip of a nameless possession
we are slaves to a driving obsession.*

*And finally it comes - graduation
As we examine our scars of pleasure
and scars of pain
We realize that good work
is the key to good fortune
And then we receive our degree -
one moment's high and glory rolls on by
like a streak of lightning
that flashes and fades in the summer sky
The moment may be brief
but it can be so bright.*

We're only immortal for a limited time...

*RUSH, a compilation
N.S., 1992*

FOREWORD

This investigation was conducted in the Technology Laboratory for Advanced Composites (TELAC) of the Department of Aeronautics and Astronautics at the Massachusetts Institute of Technology. This work was sponsored by Boeing Commercial Airplane under Purchase Order Number FZ-282568-0755N.

TABLE OF CONTENTS

<u>Chapter</u>		<u>Page</u>
1	INTRODUCTION	17
2	BACKGROUND.....	22
	2.1 Fracture of Composite Laminates	22
	2.1.1 Unnotched Specimens.....	22
	2.1.2 Notched Specimens.....	24
	2.2 Strain Rate Effects on Composite Laminates.....	27
	2.2.1 Strain Rate Effects on Composite Properties.....	28
	2.2.2 Strain Rate Effects on Composite Failure.....	31
	2.3 Tape Layup and Tow Placement Manufacturing Techniques.....	33
3	EXPERIMENTAL PROCEDURE.....	37
	3.1 Experimental Approach.....	37
	3.2 Material Specification and Fabrication	39
	3.3 Preparation of Specimens for Testing.....	46
	3.3.1 Measurement of Coupons.....	46
	3.3.2 Measurement of Panels.....	47
	3.3.3 Attachment of Fiberglass End Tabs	50
	3.3.4 Machining of Slits	51
	3.3.5 Attachment of Mounting Jigs for Panels	53

<u>Chapter</u>	<u>Page</u>
3.4 Instrumentation.....	57
3.4.1 Unnotched and Notched Coupons.....	57
3.4.2 Notched Panels	58
3.5 Testing Procedures.....	61
3.6 Data Collection.....	62
3.7 Data Reduction	66
4 RESULTS.....	68
4.1 Expected Strain Rate versus Measured Strain Rate	68
4.2 IM7/977-2 Test Results	69
4.2.1 Unnotched Coupon Results.....	69
4.2.2 Notched Panel Results	72
4.3 AS4/938 Tests Results	83
4.3.1 Unnotched Coupon Results.....	83
4.3.2 Notched Specimen Results.....	93
4.3.3 Strain Distribution of Notched Panels	101
4.3.4 Mar-Lin Correlation of Notched Specimens	107
5 DISCUSSION	113
5.1 Strain Rate Effects on IM7/977-2 Specimens.....	113
5.1.1 Unnotched Coupons.....	113
5.1.2 Notched Panels	114
5.2 Strain Rate Effects on AS4/938 Specimens	119
5.2.1 Unnotched Coupons.....	119
5.2.2 Notched Specimens.....	122

<u>Chapter</u>	<u>Page</u>
6	CONCLUSIONS AND RECOMMENDATIONS.....131
	6.1 Conclusions.....131
	6.2 Recommendations.....132
	REFERENCES.....133
	APPENDIX A.....139
	APPENDIX B143
	APPENDIX C153
	APPENDIX D165
	APPENDIX E185

LIST OF FIGURES

Figure		Page
Figure 2.1	Loading Regimes at Different Strain Rates.....	29
Figure 2.2	Schematic of the Tow Placement Process.....	35
Figure 3.1	Tensile Coupon Configuration.....	44
Figure 3.2	Tensile Panel Configuration.....	45
Figure 3.3	Schematic of Coupon Measurement Locations.....	48
Figure 3.4	Schematic of Panel Measurement Locations.	49
Figure 3.5	Schematic Representation of a Slit.	52
Figure 3.6	Jig Plate Dimensions and Bolt Tightening Sequence.	55
Figure 3.7	Side View of Panel Secured in Mounting Jig.	56
Figure 3.8	Strain Gage Placement for Unnotched and Notched Coupons.....	59
Figure 3.9	Strain Gage Placement for Notched Panels.....	60
Figure 3.10	Photograph of tensile coupon in hydraulic grips prior to testing.	64
Figure 3.11	Photograph of tensile panel in hydraulic grips prior to testing.	65
Figure 4.1	Average Failure Stress vs. Strain Rate for IM7/977-2 Specimens.....	71
Figure 4.2	Sketches of Different Failure Modes.	73
Figure 4.3	Failure Modes of IM7/977-2 Unnotched Coupon and AS4/938 Unnotched Coupon.....	74
Figure 4.4	Photograph of Failed IM7/977-2 Unnotched Coupon at Different Strain Rates.....	75
Figure 4.5	Stress-Strain Curves of IM7/977-2 Unnotched Coupons at Different Strain Rates.	76
Figure 4.6	Failure Modes of IM7/977-2 Notched Panels at Different Strain Rates.....	79

Figure	Page
Figure 4.7 Distribution of Failure Modes for IM7/977-2 Notched Panels.	80
Figure 4.8 Photographs of Failed IM7/977-2 Notched Panel at (a) 0.005 e/min and (b) 0.025 e/min.	81
Figure 4.9 Photographs of Failed IM7/977-2 Notched Panel at (c) 0.1 e/min and (d) 0.5 e/min.	82
Figure 4.10 Average Failure Stress vs. Strain Rate for AS4/938 Tape Layup Specimens.	85
Figure 4.11 Average Failure Stress vs. Strain Rate for AS4/938 Tow Placed Specimens.	86
Figure 4.12 Photograph of Failed AS4/938 Tape Layup Unnotched Coupon at Different Strain Rates.	88
Figure 4.13 Photograph of Failed AS4/938 Tow Placed Unnotched Coupon at Different Strain Rates.	89
Figure 4.14 Stress-Strain Curves of AS4/938 Tape Layup Unnotched Coupons at Different Strain Rates.	90
Figure 4.15 Stress-Strain Curves of AS4/938 Tow Placed Unnotched Coupons at Different Strain Rates.	91
Figure 4.16 Failure Modes of AS4/938 Tape Layup and Tow Placed Notched Specimens.	95
Figure 4.17 Photograph of Typical Failed AS4/938 Tape Layup and Tow Placed Notched Specimens.	96
Figure 4.18 Photograph of Failed AS4/938 Tape Layup Notched Coupon at Different Strain Rates.	97
Figure 4.19 Photograph of Failed AS4/938 Tape Layup Notched Panel at Different Strain Rates.	98
Figure 4.20 Photograph of Failed AS4/938 Tow Placed Notched Coupon at Different Strain Rates.	99
Figure 4.21 Photograph of Failed AS4/938 Tow Placed Notched Panel at Different Strain Rates.	100
Figure 4.22 Average Strain Distribution of AS4/938 notched panel at 0.0042 strain/min.	103

<u>Figure</u>	<u>Page</u>
Figure 4.23 Average Strain Distribution of AS4/938 notched panel at 0.1 strain/min.....	104
Figure 4.24 Average Strain Distribution of AS4/938 notched panel at 2 strain/min.....	105
Figure 4.25 AS4/938 Notched Failure Stresses and Fracture Prediction Curve at 0.0042 e/min.....	110
Figure 4.26 Notched AS4/938 Specimens Failure Stresses and Fracture Prediction Curve at 0.1 e/min.....	111
Figure 4.27 AS4/938 Notched Failure Stresses and Fracture Prediction Curve at 2 e/min.....	112
Figure 5.1 Experimental and Predicted Stress-Strain Curves of IM7/977-2 Unnotched Coupons.	115
Figure 5.2 Strain Readings Collected of Typical IM7/977-2 Notched Panel.	116
Figure 5.3 Plot of Notch Tip Strain versus Normalized Time of Representative IM7/977-2 Notched Specimens at Different Strain Rates.....	117
Figure 5.4 Experimental and Predicted Stress-Strain Curves of AS4/938 Unnotched Coupons.....	121
Figure 5.5 Strain Readings Collected of Typical IM7/977-2 Notched Panel.	124
Figure 5.6 Failure Initiation Stress and Final Failure Stress of AS4/938 Notched Specimens, 19 mm Slit.....	125
Figure 5.7 Failure Initiation Stress and Final Failure Stress of AS4/938 Notched Specimens, 19 mm Slit.....	126
Figure C.1-Figure C.12 Strain Distribution of AS4/938 Notched Panels at Different Strain Rates.....	153-164
Figure D.1-Figure D.20 Collected Data of Tensile Tests conducted on IM7/977-2 Specimens.....	165-184
Figure E.1-Figure E.90 Collected Data of Tensile Tests conducted on AS4/938 Specimens	185-274

LIST OF TABLES

Table	Page
Table 3.1	Material and Calculated Laminate Properties.....40
Table 3.2	Test Matrix for Tensile IM7/977-2 Specimens41
Table 3.3	Material and Calculated Laminate Properties.....42
Table 3.4	Test Matrix for Tensile AS4/938 Specimens43
Table 3.5	Stroke Rate Settings and Data Collection Frequencies Used in Tensile Tests.....63
Table 4.1	Average Failure Stress of IM7/977-2 Specimens at Different Strain Rates.....70
Table 4.2	IM7/977-2 Unnotched Coupon Stiffness Data at Different Strain Rates.....77
Table 4.3	Average Failure Stress of AS4/938 Specimens at Different Strain Rates.....84
Table 4.4	AS4/938 Unnotched Coupon Stiffness Data at Different Strain Rates.....92
Table 4.5	Average Mar-Lin Fracture Parameter (Hc) for AS4/938 specimens at Different Strain Rates109
Table 5.1	Average Stress at Failure Initiation and Ratio of Initiation Stress to Failure Stress for the IM7/977-2, 51 mm Notched Specimens.....118
Table 5.2	Average Stress at Failure Initiation and Ratio of Initiation Stress to Failure Stress for the AS4/938, 19 mm Notched Specimens.....127
Table 5.3	Average Stress at Failure Initiation and Ratio of Initiation Stress to Failure Stress for the AS4/938, 51 mm Notched Specimens.....128
Table A.1	IM7/977-2 Unnotched Coupon Parameters139
Table A.2	IM7/977-2 Notched Panel Parameters.....140
Table A.3	IM7/977-2 Unnotched Coupon Failure and Stiffness Data141

<u>Table</u>	<u>Page</u>
Table A.4	IM7/977-2 Notched Panels Failure Data142
Table B.1	AS4/938 Tape Layup Unnotched Coupon Parameters143
Table B.2	AS4/938 Tow Placed Unnotched Coupon Parameters.....144
Table B.3	AS4/938 Tape Layup Notched Coupon Parameters145
Table B.4	AS4/938 Tow Placed Notched Coupon Parameters.....146
Table B.5	AS4/938 Tape Layup Notched Panel Parameters147
Table B.6	AS4/938 Tow Placed Notched Panel Parameters.....148
Table B.7	AS4/938 Tape Layup Unnotched Coupon Failure and Stiffness Data149
Table B.8	AS4/938 Tow Placed Unnotched Coupon Failure and Stiffness Data150
Table B.9	AS4/938 Tape Layup Notched Specimens Failure Data151
Table B.10	AS4/938 Tow Placed Notched Specimens Failure Data152

NOMENCLATURE

a	half length of slit
d_{bolt}	diameter of jig bolt
E	modulus of elasticity
G	shear modulus
H_C	laminate fracture parameter in Mar-Lin correlation
K_{IC}	fracture toughness
m	singularity from Mar-Lin correlation
M	torque applied to jig bolt
n_{bolt}	number of jig bolts
n_s	number of shear planes in jig
p	maximum load introduced through shear to each jig bolt
2r	size of discontinuity
W	width of specimen
Y₁	finite width correction factor
ε	strain
μ	coefficient of friction between jig plates and specimen
μ_{strain}	microstrain (=10⁻⁶ strain)
σ_f	failure stress
σ_y	stress in the transverse direction
σ_{y(far-field)}	far-field stress in the transverse direction
σ_y[∞]	transverse far-field stress with finite width corrections
v	Poisson's Ratio
AS4/938	graphite/epoxy prepreg used in the investigation
CLPT	Classical Laminated Plate Theory

GPa	Gigapascals (=10⁹ pascals)
Hz	Hertz
IM7/977-2	graphite/epoxy used in the investigation
in	inches
kN	Kilonewton (=10³ newtons)
LEFM	Linear Elastic Fracture Mechanics
min	minutes
m m	millimeters
MCLAM	computer code used for progressive failure analysis
MPa	Megapascals (=10⁶ pascals)
sec	seconds
TELAC	Technology Laboratory for Advanced Composites

Chapter 1

INTRODUCTION

Advanced composite materials consist of reinforcements, such as glass or graphite fibers, that are impregnated in a resin or binder. The usage of these materials in aerospace structures has increased significantly in the past decade. The main advantages of composite materials are their high strength-to-weight and stiffness-to-weight ratios. By using composite materials, weight savings of 5% to 30% can be realized over conventional metal structures. In commercial air transports, this advantage translates into lower fuel costs, greater operating range and higher payloads. Composite materials also have greater fatigue and corrosion resistance than metals, leading to a longer service life and lower maintenance costs.

Presently, composite materials are utilized in primary and secondary structures in aircraft. The Beechcraft Starship I, for example, has an all-composite airframe. Examples of military and commercial aircraft that utilize composites in secondary structures include the McDonnell Douglas F/A-18, Northrop F-117A, Airbus A320 and Boeing 767. Boeing may use composite materials in the fuselage of its next generation of wide body commercial aircraft.

The high level of confidence that is required for the use of composite materials in primary structures of civilian transport aircraft, equivalent to that established for conventional metals, has yet to be achieved. Composite materials have different elastic properties than metals and they fail by different mechanisms. Reliable analytical techniques have been developed

to predict the elastic behavior of composite materials. Failure behavior, on the other hand, is still not fully understood. Current state-of-the-art understanding of failure mechanisms can be used to bound failure loads and predict sensitivities to various design parameters such as layup. Testing is still required to prove that a structure is capable of withstanding design loads. There is substantial room for improvement in the understanding of composite failure mechanisms, and substantial pay-offs if this improvement simplifies the design and certification of composite structures.

The area of interest addressed by this investigation is the effect of strain rates on the fracture of composite laminates containing damage. Composite structures may be damaged in service, and subsequently may be subjected to a variety of loading conditions. Primary composite structures must be able to tolerate damage, i.e., they must be able to survive the destruction or degradation of a small region and continue to perform for a specified period of time. Severe damage propagation leading to an eventual catastrophic failure of the structure is unacceptable.

Damage to composite structures not only includes visible penetrations on the exterior but also less obvious damage beneath the surface. Visible damage can be caused by errant fan blades or bird strikes, while less obvious damage can be caused by a tool dropped during maintenance, or a stone kicked up from the runway during takeoff or landing. Also, realistic composite structures are designed with features such as free edges and cutouts. These features cause stress concentrations very similar to those caused by damage. Graphite/epoxy composites are brittle materials, and their tensile strengths can be severely degraded by damage and stress concentrations.

Composite structures in service are subjected to variable loading conditions. In addition to regular aerodynamic and cabin pressure loads, loading conditions also include gusts, sudden maneuvers, landing shocks, depressurizations and impacts. The strain rates invoked in these events vary drastically and these variations may affect the response of the structure. In the worst case, high strain rates may cause premature failure of the structure.

The effects of variable strain rates on composite structures are not well understood. Currently, most of the published strength data of various composite material systems is obtained experimentally at the 'static' rate, at approximately 0.005 ϵ /min. This strain rate is also assumed in the formulation of failure prediction methodologies for unflawed and flawed composites. However, it is not known if damage mechanisms observed at the 'static' rate are still applicable at higher strain rates. Therefore, there is a necessity to conduct an investigation to identify strain rate sensitivity, if any, on damaged composite structures.

The technique used to manufacture advanced composite materials may affect the quality of the structure and its ability to withstand damage. The traditional method of laying up composite materials is manual layup. In recent years, automated or semi-automated methods have been used to simplify various aspects of the manual layup operation. These include the use of machines to perform the laying, cutting and trimming of plies. An automated method of laying up composites, known as tow placement, is relatively new in the composite manufacturing industry. It involves using a machine that is programmed to process individual tows of fibers and position them precisely next to each other. This method is especially

efficient when laying up a contoured surface. However, little data on the performance of laminates manufactured using this technique is available.

In this investigation, the effects of strain rate on composite failure were studied experimentally. The material systems used were IM7/977-2 and AS4/938 graphite/epoxy. The former is a 'toughened' (i.e., high strain-to-failure) resin composite. It was used for preliminary tests in this investigation. The latter material was used in the bulk of this work. AS4/938 specimens manufactured by manual tape layup and automated tow placement were tested. Tensile tests were conducted on both unflawed and flawed specimens over strain rates ranging from 0.0042 ϵ /min to 2 ϵ /min. Load, stroke and strain data were collected from each test. Longitudinal and transverse strains were collected from the unflawed specimens; strains were collected from strategic points (e.g., far-field and near flaw) on the flawed specimens. The raw data was reduced to laminate elastic properties, failure loads, approximate damage initiation loads, strain distributions near flaws and Mar-Lin damage tolerance parameters.

It was found that the elastic properties and undamaged failure strengths are independent of both strain rate and manufacturing technique. In contrast, damage tolerance of these materials is significantly strain rate dependent. It is also strongly dependent on manufacturing technique. It appears that the mechanism by which damage progresses from the existing flaw to final failure of the specimen is sensitive to strain rate and manufacturing technique.

A literature review on the topic of composite fracture at different strain rates is presented in Chapter 2. This chapter contains a review of the failure prediction methodologies applicable to both unflawed and flawed composites, previous work done in the area of strain rate effects, and an

overview of the manual tape layup and automated tow placement manufacturing techniques. In Chapter 3, experimental procedures are presented. An account of the preparation of specimens, testing, data acquisition and reduction of data is given. Chapter 4 presents the results obtained in this experimental investigation. Further discussions and possible explanations of the findings are presented in Chapter 5. Chapter 6 presents conclusions and recommendations for subsequent investigations.

Chapter 2
BACKGROUND

This chapter presents reviews and discussions on three topics: the fracture of notched and unnotched composite laminates, strain rate effects on composite behavior, and an overview of manual tape layup and automated tow placement manufacturing techniques.

2.1 Fracture of Composite Laminates

The study of composite fracture has been aggressively pursued in the last twenty years. This section examines the theories and correlations used to predict failure of both unnotched and notched composite laminates.

2.1.1 Unnotched Specimens

In this section, existing theories on the failure of composite laminates are reviewed. Nahas [1] surveyed 30 failure criteria for composites and he classified them into 4 different categories: the limit criteria, the interaction criteria, the tensor polynomial criteria, and the direct laminate criteria. The first category involves failure theories, e.g., maximum stress and maximum strain [2], that stipulate failure when a stress or strain parameter reaches its limit. No interaction between stresses is accounted for but the failure mode is identified. Failure criteria in the second category, e.g., Hill [3], Hoffman [4], use a quadratic formula of stress. Failure occurs when this formula is satisfied. The onset but not the mode of failure is predicted. The third category of failure criteria, e.g., Tsai-Wu [5], Gol'denblat-Kopnov [6], is similar to the second, except that more general formulae are evaluated. Different tensile and compressive

strengths and all possible quadratic interaction terms are accounted for. Again, the onset and not the mode of failure is predicted. The last category, e.g., Puppo-Evensen [7] consists of failure criteria that can be directly applied to the entire laminate. Lamination theory or constitutive assumptions are not involved. This category of failure criteria requires experimental determination of laminate strength for every new design.

Laminate failure can be predicted by either the ply-by-ply approach or total laminate approach. The former treats the laminate as consisting of many bonded layers. These layers are treated as homogenous, orthotropic materials. Using Classical Laminated Plate Theory (CLPT) [8], the ply stresses and strains in each ply are obtained and any of the failure criteria in the first three categories described above applied to each ply. The failure envelopes are obtained for all plies and the innermost envelope is selected as the laminate failure envelope. The total laminate approach considers the entire laminate as a homogenous and anisotropic material. CLPT is not used and the failure criteria are applied directly to the laminate. This approach requires strength characterization of the entire laminate. The ply-by-ply approach requires only strength characterization of one ply.

The ply-by-ply approach predicts the first ply failure (FPF) load, i.e., when the first ply will fail. Often, the laminate as a whole will not fail at this load. Progressive failure of a laminate can be analyzed by removing or degrading the properties of a failed ply, recalculating the laminate properties, and again applying a failure criterion to the remaining plies. This procedure is repeated until all plies have failed. The maximum load reached is often referred to as the last ply failure (LPF) load. Specific procedures for this kind of analyses include the Hahn-Tsai method [9], the

Chou-Orringer-Rainey method [10] and the Petit-Waddoups method [11], just to name a few.

The results of progressive failure analyses are dependent on the choice of ply failure criteria and failed ply degradation method. The degradation modulus are often arbitrary, and the continued use of ply-by-ply failure criteria in a damaged laminate is problematic [12]. These methods are, however, useful for bounding the laminate failure strength and achieving insight into the laminate failure process.

2.1.2 Notched Specimens

Early researchers used Linear Elastic Fracture Mechanics (LEFM) to model the behavior of composites with notches [13]. In classical LEFM, the failure stress is predicted by the expression:

$$\sigma_f = K_{IC} (\pi r)^{-0.5} \quad (2.1)$$

where σ_f is the notched failure stress, K_{IC} is the fracture toughness and r is half of the crack length. This theory provides good correlation with experimental results of unidirectional laminates but not angle-ply laminates. According to an overview on notched composite laminate analyses and experimental work compiled by Awerbach and Madhukar [14], two major approaches were undertaken by researchers in this area. One of them is an extension of LEFM concepts while the other explicitly considers the stress distribution at the notch.

The Mar-Lin prediction is an extension of LEFM concepts that accounts for the inhomogeneity of composite materials. Lin and Mar [15] contended that for composites, the mathematical stress singularity at the

notch tip should not be set at 0.5. Their expression for predicting the fracture stress is:

$$\sigma_f = H_C (2r)^{-m} \quad (2.2)$$

where H_C is known as the laminate fracture parameter [16] and m is the stress singularity of the notch tip at the fiber/matrix interface. The variable, m , is governed by the shear moduli and Poisson's ratios of the fiber and matrix. In the Mar-Lin equation, it is the length and not the shape of the discontinuity that determines the failure stress. The laminate fracture parameter, H_C , is a function of the laminate and it is determined experimentally. Fenner found the value of m for graphite/epoxy to be 0.28 [17]. Correlation of experimental results with the Mar-Lin failure prediction using this m value was good in some cases [18, 19] and not so good in others [20]. The best fits of the Mar-Lin equation with experimental data did not correspond to an m value of 0.28. Lagace [20] attributed these variations to fracture resulting from interlaminar stresses, instead of in-plane stresses. Although H_C is laminate and stacking sequence dependent, it is not dependent on notch geometries. Hence, the laminate fracture parameter determined from a single notch geometry can be used to correlate results obtained from testing other kinds of notches within the same laminate type.

Whitney and Nuismer [21, 22] formulated the point stress and average stress criteria for predicting the failure stresses of composite laminates in the presence of holes and slits. These criteria represent the other approach where the concept of the damage zone, analogous to the plastic zone found in metals, is utilized. Explicit calculations of the

stresses at the notch tip show singularity or very high values at this location. Due to both local stress redistribution and the inhomogenous nature of composite materials, these concentrations do not necessarily result in failure. In both of their failure prediction methodologies, this aspect is accounted for by assuming a characteristic length ahead of the crack. When the stress within or at the characteristic length reaches the unnotched failure stress, failure occurs. In the point stress criterion, failure occurs when the normal stress at some fixed distance ahead of the notch equals to the unnotched tensile strength; in the average stress criterion, failure occurs when the averaged normal stress value over some fixed distance ahead of the notch reaches the untouched tensile strength. These failure criteria are notch geometry dependent; the unnotched failure strengths and the characteristic lengths of the laminate are determined experimentally. Theoretically, the characteristic lengths in both criteria are dependent only on the materials. However, experimental correlation using these criteria indicates that the characteristic lengths are dependent on layup as well [23, 24].

Another group of researchers used similar concepts of damage zones and characteristic crack lengths to formulate their failure criterion. Waddoups, Eisenmann and Kaminski (WEK) [25] treated the composite material as an ideal, brittle, Griffith solid, and postulated that the energy for crack extension is stored in a region ahead of the crack. This region has a characteristic length which is independent of hole size. So far, all the predictive models discussed are semi-empirical and they require a large amount of data for successful applications.

The initiation of damage at the tip of a notch does not necessarily fail the notched structure. This is analogous to the fact that the first ply failure

does not necessarily cause failure of an unnotched laminate. 'Progressive' failure of a notched laminate is very complex. Large in-plane stress gradients exist near the notch, and the strains also vary ply by ply through the thickness. Predicting a progressive failure involves applying a failure criterion to all plies at many in-plane locations, and each time a failure occurs, recalculating the stiffness and load distribution in the entire structure. Chang [26], for example, investigated progressive failure of notched composites. Considerations of progressive failure can help justify an approach such as Whitney-Nuismer's. If failure near the notch tip results in reduced stiffness, then the load will be transferred, and the stress concentrations at the notch tip will be reduced.

2.2 Strain Rate Effects on Composite Laminates

Research conducted in this area covers a wide range of strain rates. Different testing techniques and procedures are employed for tests at different strain rates. The lowest strain rate region is associated with creep where a constant load is applied and the strain variation with time recorded. The effective strain rates of such test are extremely small. The quasi-static region corresponds to strain rates up to 6 ϵ/min [27]. In this regime, it is assumed that no time dependent mechanisms act. Standard hydraulic machines are capable of testing specimens at a constant strain rate in this regime. The next strain rate region, referred to as intermediate strain rates (up to about 3,000 ϵ/min), are applied by means of fast-acting or pneumatic machines and/or falling weight apparatus. Inertia effects become important in this rate regime. Higher strain rates, primarily in compression, can be obtained by mechanical impact devices or explosively generated pulses. The Split Hopkinson bar is an example of this type of

impact devices that can invoke strain rates up to 60,000 ϵ /min in compression. Wave propagation effects are dominant in this strain rate regime and must be accounted for. Figure 2.1 shows the different strain rate regimes, and the loading methods and dynamic considerations associated with these regimes [28].

The strain rates used in this investigation are in the quasi-static range. Some of the reviews in this section present research that is performed at strain rates beyond this range. Two topics on strain rate effects on composite materials are discussed: strain rate effects on composite properties and strain rate effects composite failure.

2.2.1 Strain Rate Effects on Composite Properties

It is well known that the mechanical properties of metals vary with strain rates [29]. Research performed on composite materials indicates that these materials also have strain rate dependent properties.

Strain rate effects on the longitudinal properties of unidirectional laminates are influenced by the type of fibers present. Glass fibers are strain rate sensitive, while carbon fibers are not [30]. Daniel et al. [31] and Harding et al. [32] conducted tensile tests on unidirectional carbon reinforced epoxy and the results showed no strain rate sensitivity. On the other hand, tensile tests conducted on glass fiber reinforced epoxy showed strain rate sensitivity. Armenakas and Sciammarella [33] tested 0° unidirectional glass/epoxy specimens up to strain rates of 3000 ϵ /min using an explosively driven machine. They found that the modulus and tensile strength increased and the ultimate dynamic strain decreased with strain rate. These results are also confirmed in tests conducted by Harding and Welsh [32].

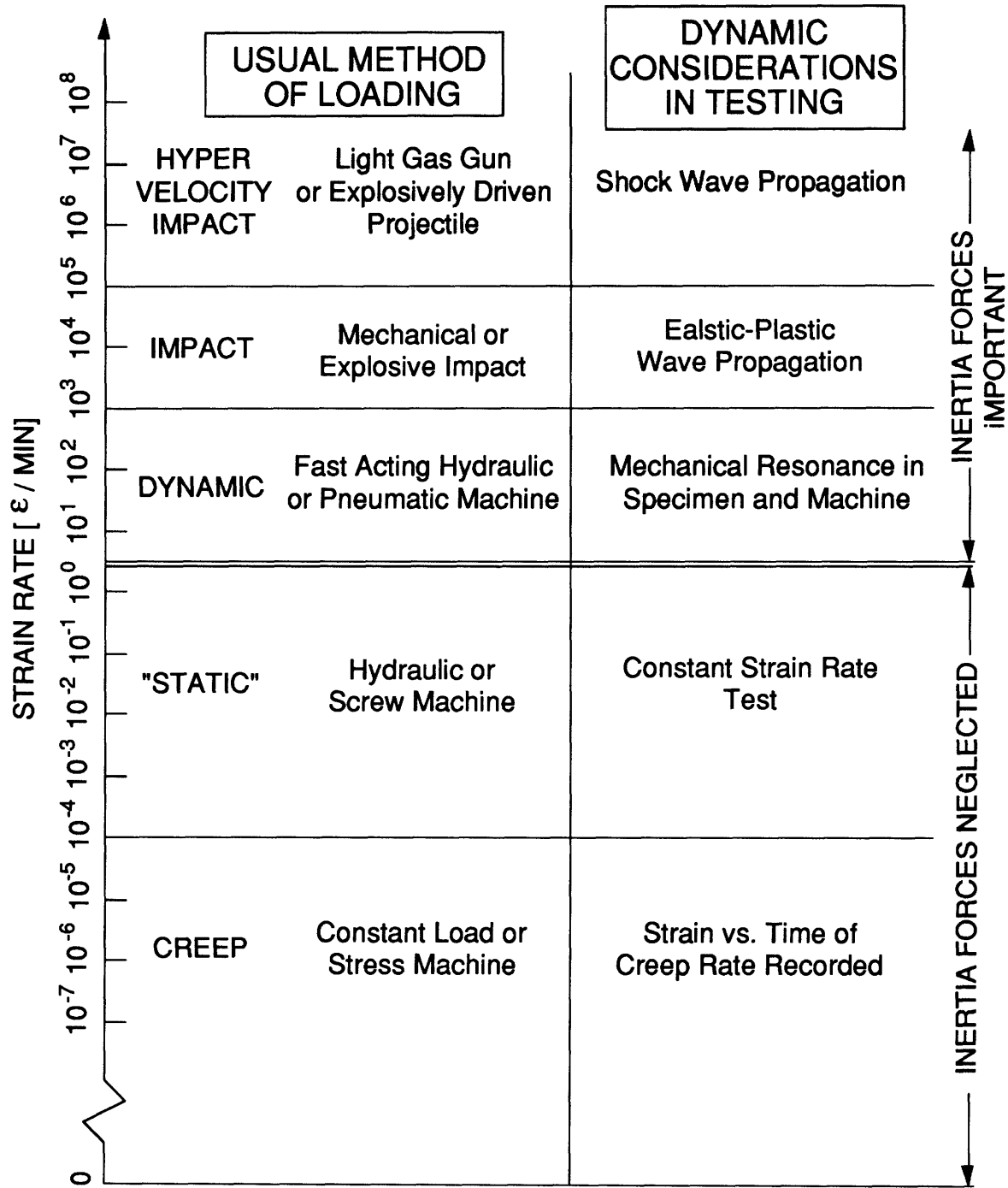


Figure 2.1 Loading Regimes at Different Strain Rates.

Most resin materials, such as epoxy, are sensitive to strain rates. Hence, the transverse properties of unidirectional laminates are also strain rate sensitive. Daniel [31] tested 90° unidirectional laminates and showed that the transverse modulus of carbon/epoxy unidirectional laminates doubled and the strength increased by almost 200% at strain rates of 9,000 ϵ /min. Daniel [34] also showed that at 300 ϵ /min, the transverse modulus and strength increased by about 15% and the failure strain decreased by about 10%.

Tests conducted on angle-ply laminates also showed strain rate sensitivity. Harding [32] tested angle-ply glass/epoxy laminates at strain rates up to 70,000 ϵ /min and found a large increase in strength, failure strain and modulus with strain rate. At 9,000 ϵ /min, Al-Salehi et al. [35] found that while the modulus remained constant, there was a slight increase in the failure stress and strain of the angle-ply laminates they tested. At 180 ϵ /min, Rotem and Lifshitz [36] found that the high strain rate strength of angle-ply laminates was about three times higher than the static value and the laminate modulus increased by about 50%. The ultimate strains remained unchanged in these tests. Daniel [34] also conducted similar tests at this rate and obtained identical results.

Strain rate effects on compressive properties of composites were studied by Sierakowski et al. [37] and Frey et al. [38] utilizing the Split Hopkinson Pressure Bar at strain rates up to 12,000 ϵ /min. They showed that increasing the strain rates resulted in an increase in compressive strength and different failure modes of the composite specimens.

Strain rate effects on interlaminar fracture toughness have also been studied. Mall et al. [39] and Smiley et al. [40] showed that the interlaminar fracture toughness of composite materials is loading rate sensitive. For

most 'toughened' resin composite materials, it decreased with increasing strain rate. For example, tests conducted on T300/F185 decreased by 20% over three decades of loading rates [41]. For the AS4/3501-6 graphite/epoxy material system, Mode I interlaminar fracture toughness remained constant up to about 0.01 ϵ /min and decreased by 70% with further increase in strain rate. However, Aliyu and Daniel [41] performed similar tests and found that Mode I interlaminar fracture toughness increased by 20% at the same strain rate instead.

2.2.2 Strain Rate Effects on Composite Failure

Published papers on the mechanisms of composite failure at low and high strain rates are rare. Mullin et al. [42] attempted to study the failure modes of specimens made of five boron filaments embedded in an epoxy matrix. They were tensile tested at 0.008 ϵ /min and 0.8 ϵ /min. Examination of the specimens tested at the slower strain rate showed more fiber breaks than those tested at the higher strain rate. Also, the specimens failed at higher stresses at the slower rate. The explanation given was that gradual redistribution of load was possible at the slower rate of loading. As a break in the fiber occurs, a slower strain rate allows stresses to be transferred, via the matrix, to other surrounding fibers. The fibers are hence able to fail according to their variations in strength. However, when a higher strain rate is used, rapid propagation of fracture through the matrix occurs, causing instantaneous loading of adjacent fibers. The failure stress at the higher strain rate decreases because it is not possible for load to be transferred gradually. Although tests conducted with these kinds of specimens are highly idealized compared to practical composites, the results are, nonetheless, interesting.

Suvorova [43] pointed out that changes in loading rates affect the final failure modes of composite structures. He conducted tensile tests at various strain rates and showed that as strain rate increased, strength increased in some regimes and decreased in others. He postulated that when damage accumulation is the cause of final failure of a specimen, the strength of the specimen increases with strain rate. At higher strain rates, the loading time decreases and hence there is less time for damage to accumulate. This results in stronger specimens. The failure surfaces of these specimens are rough and the fibers are pulled out of the matrix. On the other hand, he postulated that when the dominant failure mode of a specimen is due to the growth of macrocracks, the failure strength decreases with increasing strain rate. As with tests conducted by Mullin et al. on boron filaments, failure propagation is assumed to be faster at a higher loading rate, resulting in lower failure stresses. The failure surfaces of these specimens are smooth and clean. Adhesion strength between the fibers and the matrix also plays an important role in the transition from one mode of failure to another. Weak adhesion causes debonding of the material and divides the fibers from the resin, thus preventing the growth of the macrocrack. As a result, when propagation of macrocracks is the dominant failure mode, weak fiber/matrix adhesion delays failure propagation and results in an increase in the failure strength of the specimen.

In summary, the literature reviewed above showed that the mechanical properties of some of the materials present in composites, such as most resins and glass fibers, are strain rate sensitive while others, such as carbon fibers, are not. Also, some materials are strain rate sensitive only above a certain strain rate. Laminate parameters, such as

interlaminar fracture toughness, are also investigated and no conclusive results are obtained. Varying strain rates are also shown to affect the failure process and failure modes of unidirectional plies, angle ply laminates, and idealized specimens such as individual boron filaments embedded in epoxy matrices.

So far, not much information is available on the failure of multidirectional laminates under different strain rates. There is evidence that strengths and modes of failure are strain rate dependent. This dependence may vary with material, ply angle and other factors. In the first section of this chapter, it was shown that the presence of material discontinuities, such as holes or cracks, changes the behavior of composite structures. These discontinuities may also affect the already complex failure phenomenon of laminates at different strain rates.

2.3 Tape Layup and Tow Placement Manufacturing Techniques

An overview of the conventional manual tape layup [44] and automated tow placement methods [45] are presented below.

Hand layup using prepreg tape is a slow and labor intensive procedure. It is dependent on the skills of the individual doing the laminating. Prepreg is a material containing the fiber reinforcement that has been pre-impregnated with resin and then cured slightly to increase its viscosity. It comes in rolls of various widths, typically 12 inches to 24 inches, and in various forms, unidirectional tape or woven fabric. The prepreg is cut to the desired shape and manually laid up, layer by layer, to the desired thickness. The assembly requires vacuum bagging and curing at elevated temperatures in an autoclave. Laying up unidirectional tape on a contoured tool is difficult because the tape tends to follow a geodesic path.

However, because this method is manual, a skilled individual can adapt to variations in the tack and width of the prepreg. Unlike using automated techniques, the tolerance of the gaps and overlaps between each layer can be reduced and controlled by a skillful worker. Low tolerances in the gaps and overlaps help to provide a good resin distribution in the final manufactured part.

Automated tow placement, also known as automated fiber placement, involves positioning unidirectional prepreg tows precisely next to one another on a layup tool. The tows are typically 0.125 inches wide. The tow placement machine is programmed to follow a pre-defined geodesic path for all passes. Cutting and trimming are done automatically. A schematic of the fiber placement process is shown in Figure 2.2 [45]. Once the laying up is accomplished, the assembly is cured. As the tow placement machine does not have the versatility of a human being, the tows fed into the machine have to be of exact width. Otherwise, undesirable gaps and overlaps will occur. Also, the tack of the prepreg is important. An excessively tacky material will gum up the chutes of the machine and cause clogging. On the other hand, materials that are not tacky enough will not adhere properly and maintain their position. Producing prepreg tows with minimal width variations and the correct tack are challenges facing the prepreg manufacturers. Unless these obstacles are overcome, automated tow placement will be inefficient, with extensive delays and cost overruns caused by machine downtime.

Tow placed specimens have been tested to determine their properties relative to that of conventional manual tape layup. Walker et al. [46] conducted tensile tests on notched tape layup and tow placed laminates with the same volume of fiber and matrix constituents. They found that

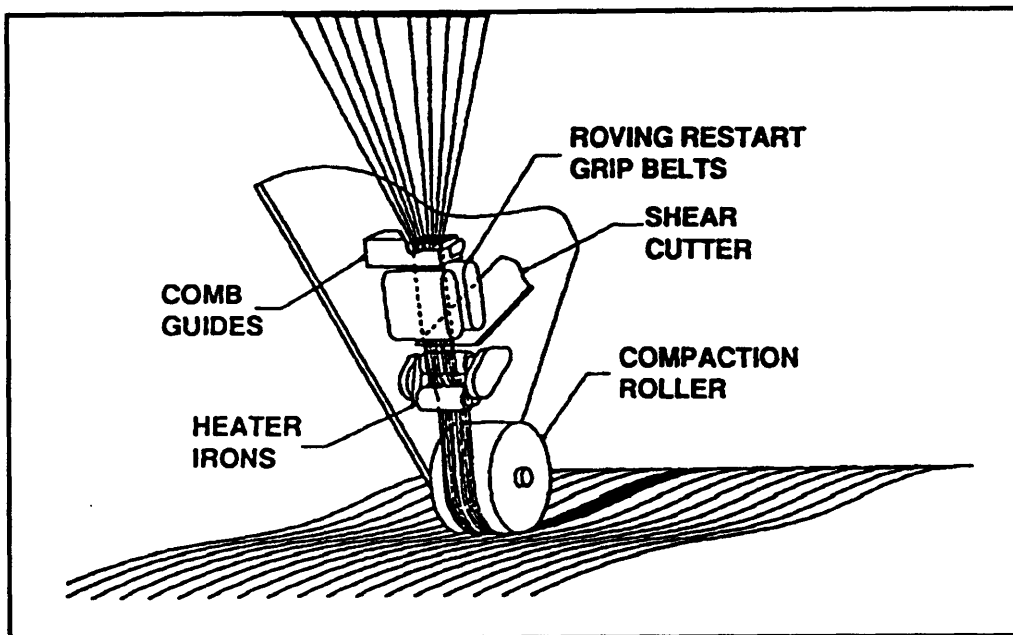


Figure 2.2 Schematic of the Tow Placement Process.

compared to the tape layup specimens, the tow-placed specimens had lower notch sensitivity.

A possible explanation for the lowered notch sensitivity was the presence of resin rich zones between the tows within each ply. These zones facilitate ply splitting, which may lead to a more easily damaged laminate. This process enhances redistribution of stresses around the notch tip, resulting in higher ultimate failure strengths in the tow placed notched specimens. There are also other material differences between the tow placed and tape layup laminates that can account for the higher failure strengths. These include fiber sizing, fiber bundle size, and resin impregnation method. So far, there has been no conclusive explanations for the higher fracture strength of notched tow placed laminates compared to notched tape layup laminates.

Chapter 3

EXPERIMENTAL PROCEDURE

The experimental investigation was carried out to determine the effects of different strain rates on tensile failure of composite laminates. Specimens were manufactured from two material systems, IM7/977-2 and AS4/938. They were manufactured and cut to size by Boeing. In this section, the test matrices used in the investigation are presented and the rationale for their design explained. Also, detailed specimen pre-test preparation, instrumentation, testing, data collection and reduction procedures are described.

3.1 Experimental Approach

Unnotched and notched composite laminates were tested at various strain rates and their laminate properties, failure mechanisms and modes of failure observed. IM7/977-2 and AS4/938 were the chosen material systems for this investigation. The AS4/938 specimens were manufactured by two different methods: manual tape layup and automated tow placement.

The IM7/977-2 specimens were 13 plies thick. The layup was $[\pm 45/90/0/\pm 60/90]_s$. The material properties and calculated laminate properties for this system are shown in Table 3.1. Tests were conducted on both unnotched and notched specimens. A total of 8 unnotched coupons and 12 notched panels were tested at 4 different strain rates. The unnotched coupons were 50 mm wide and their gage lengths were 200 mm. The notched panels were 203 mm wide with gage lengths of 406 mm. A

51 mm slit was machined at the center of the notched panel, perpendicular to the loading axis. This slit size was chosen to produce a width-of-specimen to slit length ratio ($W/2a$) of four. This ratio was experimentally found to produce good correlation with analytical predictions [46]. The configurations of the tensile test coupon and panel are shown in Figure 3.1 and Figure 3.2 respectively.

The lowest strain rate chosen for tests on the IM7/977-2 specimens was 0.005 ϵ/min , equivalent to the strain rate used for standard 'static' tests at the Technology Laboratory of Advanced Composites (TELAC). Higher strain rates were set at 0.025 ϵ/min , 0.1 ϵ/min and 0.5 ϵ/min . These strain rates covered three orders of magnitude and were evenly spaced when plotted on a logarithmic scale. The test matrix for the IM7/977-2 specimens is presented in Table 3.2.

The layup for the AS4/938 specimens was $[\bar{+}45/0/90/\bar{+}30/\bar{0}]_s$. Material properties and calculated laminate properties for this material system are shown in Table 3.3. Two types of AS4/938 specimens were tested: manual tape layup and automated tow-placement. For each specimen type, 15 unnotched coupons, 15 notched coupons with a 19 mm slit and 15 notched panels with a 51 mm slit were tested. The coupons were 76 mm wide with gage lengths of 178 mm and the panels were 203 mm wide with gage lengths of 406 mm. The slits were machined at the center of the specimen perpendicular to the loading axis. The specimen configurations are shown in Figure 3.1 and Figure 3.2. Notched coupons and panels had the same width-of-specimen to slit length ratio.

The three strain rates used to test the AS4/938 specimens were 0.0042 ϵ/min , 0.1 ϵ/min and 2 ϵ/min . The lowest strain rate corresponds to the 'static' rate used to conduct tensile tests at Boeing. Based on the results

of preliminary tests conducted on the IM7/977-2, 2 ϵ /min was chosen to be the highest rate used on the AS4/938 specimens. This was the maximum practical rate attainable using existing hardware at TELAC. The tensile test matrix for the AS4/938 material system is shown in Table 3.4.

3.2 Material Specification and Fabrication

The designations IM7/977-2 and AS4/938 represent graphite/epoxy material system. Fiber types IM7 and AS4 are graphite fibers produced by Hercules, Inc. Resin type 977-2, also produced by Hercules, is a representative 'toughened' resin. Type 938 is an untoughened resin produced by ICI/Fiberite.

All the specimens were manufactured and cut to the required dimensions at Boeing before they were shipped to TELAC. The following is a brief outline of the manufacturing process and sizing of specimens conducted at Boeing [46].

Panels were manufactured for each of the material types used in this investigation. The panels for all the IM7/977-2 and half of the AS4/938 specimens were fabricated using the standard hand layup techniques. The material for the tape layup process was furnished in 12 inch wide continuous unidirectional prepreg tape. The AS4/938 tow placed specimens were fabricated by means of the Hercules 6-axis fiber placement machine that places twelve tows simultaneously. The panels were autoclave cured according to the manufacturers' cure cycle. Upon completion of the curing process, the test coupons were cut to slightly oversized dimensions with a band saw, and subsequently sanded to the exact dimensions. A 125 surface finish was designated for all cut edges.

Table 3.1 Material and Calculated Laminate Properties

	E_L (GPa)	E_T (GPa)	ν_{LT}	G_{LT} (GPa)
Material				
IM7/977-2	152.1	8.5	0.35	4.2
Laminate				
$[\pm 45/90/0/\pm 60/90]_s$	39.5	68.5	0.28	22.9

Ply Thickness = 0.188 mm

Laminate Thickness = 2.44 mm

Table 3.2 Test Matrix for Tensile IM7/977-2 Specimens

Specimen Type	Strain Rate (ϵ/min)			
	0.005	0.025	0.1	0.5
Unnotched ^a	2 ^c	2	2	2
Notched ^b	3	3	3	3

^a Tensile coupon size of 350 mm by 50 mm

^b Tensile panel size of 610 mm by 203 mm with 51 mm slit

^c Indicates number of specimens tested

Table 3.3 Material and Calculated Laminate Properties

	E_L (GPa)	E_T (GPa)	ν_{LT}	G_{LT} (GPa)
Material				
AS4/938	135.4	9.37	0.32	4.96
Laminate				
[$\mp 45/0/90/\mp 30/\bar{0}$]s	62.7	37.0	0.46	21.1

Ply Thickness = 0.188 mm

Laminate Thickness = 2.44 mm

Table 3.4 Test Matrix for Tensile AS4/938 Specimens

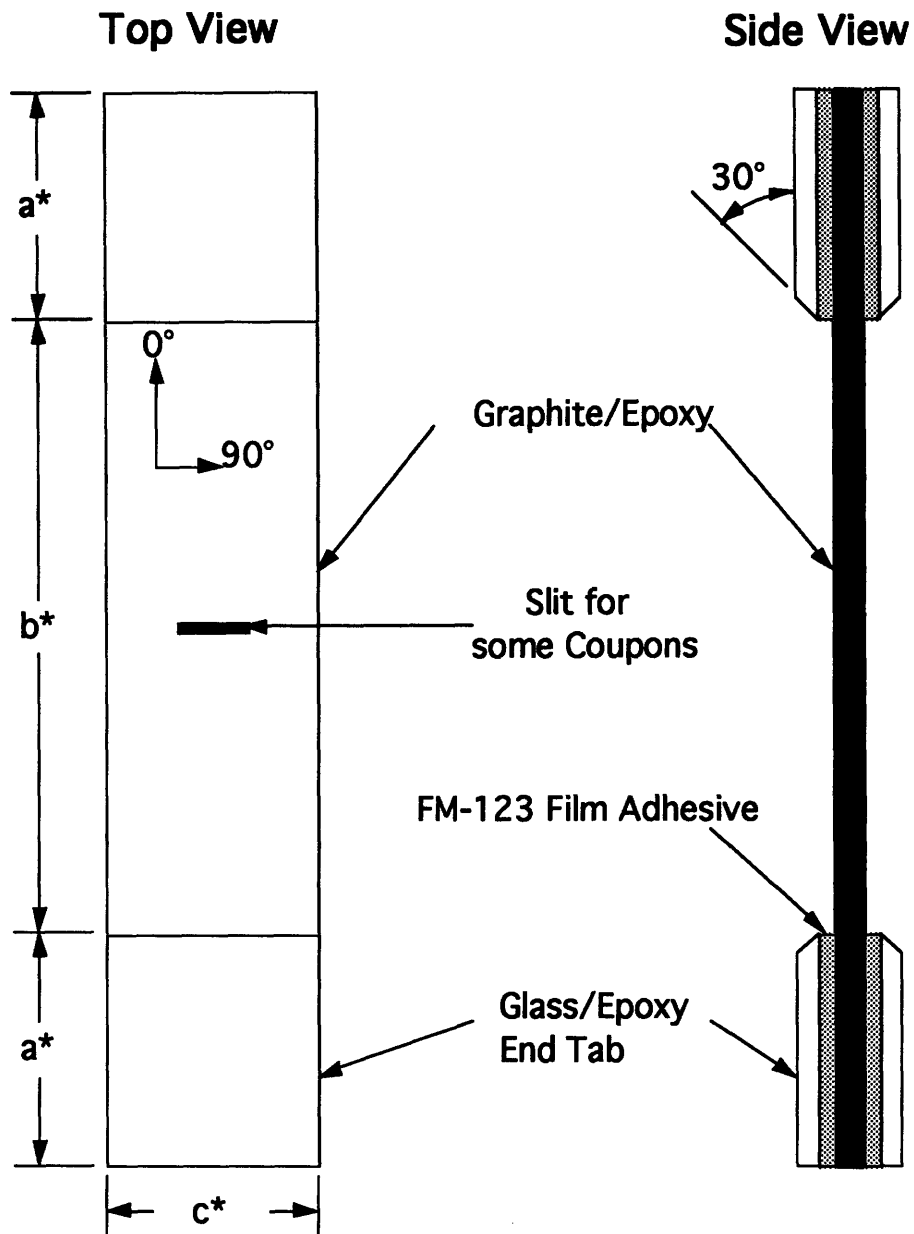
Specimen Type	Strain Rate (ϵ/min)		
	0.0042	0.1	2
Tape Layup:			
Unnotched Coupons ^a	5 ^d	5	5
Notched Coupons ^b	5	5	5
Notched Panels ^c	5	5	5
Tow Placement:			
Unnotched Coupons	5	5	5
Notched Coupons	5	5	5
Notched Panels	5	5	5

^a Tensile coupon size of 306 mm by 76 mm

^b Tensile coupon size of 306 mm by 76 mm with 19 mm slit

^c Tensile panel size of 610 mm by 203 mm with 51 mm slit

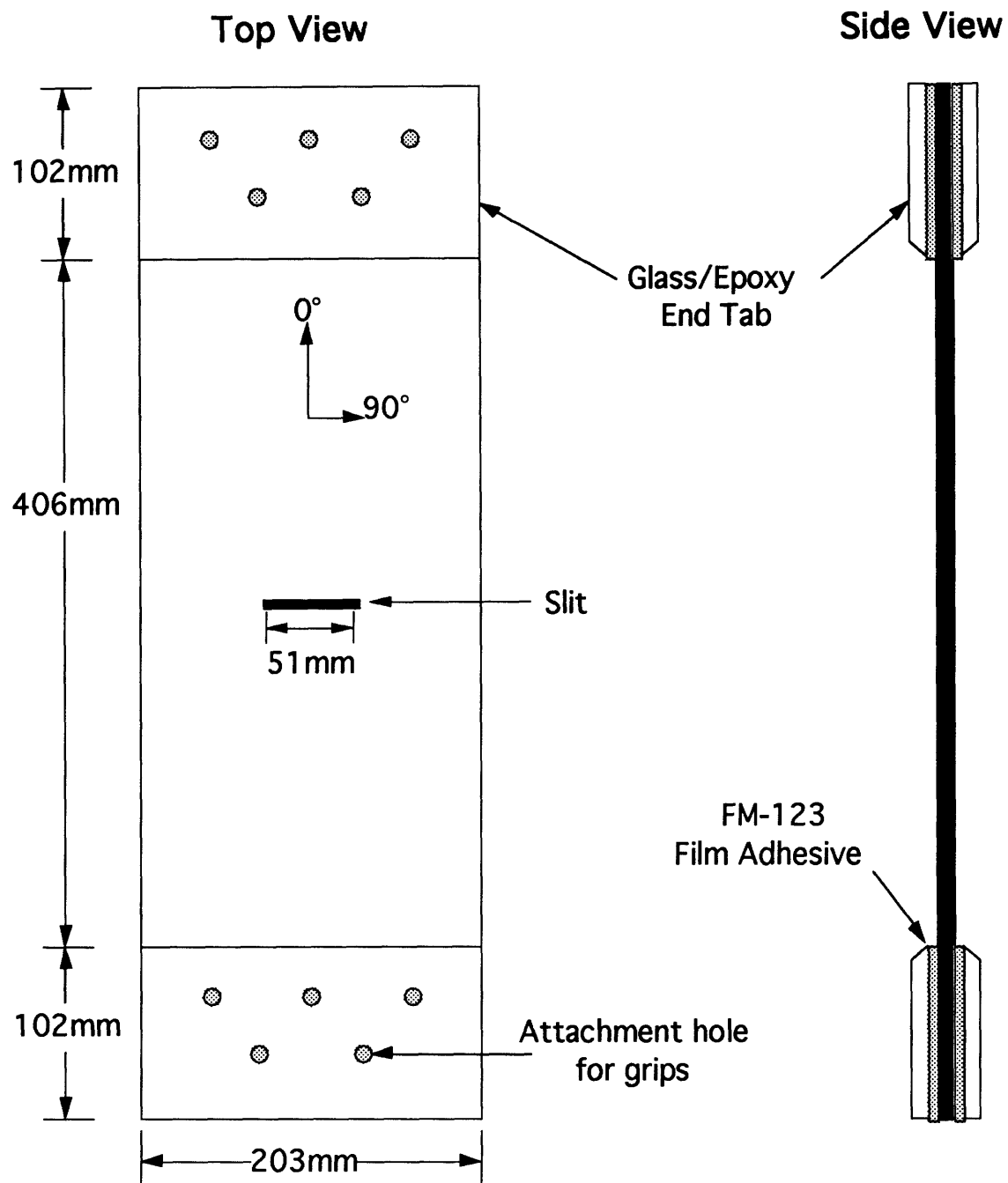
^d Indicates number of specimens tested



NOTE: Not to Scale

* for IM7/977-2 coupons, $a = 76$ mm, $b = 200$ mm, $c = 50$ mm
 for AS4/938 coupons, $a = 64$ mm, $b = 178$ mm, $c = 76$ mm

Figure 3.1 Tensile Coupon Configuration.



NOTE: Not to Scale

Figure 3.2 Tensile Panel Configuration.

Inspection of the specimens upon arrival at TELAC showed that the edges were damaged from cutting and sanding. The outer plies were split and delaminated. These splits extended for about 3 mm inwards from the panel edge. No attempts were made to correct these defects before the specimens were prepared for testing.

3.3 Preparation of Specimens for Testing

Pre-test preparation of the specimens was conducted at the Technology Laboratory of Advanced Composites (TELAC). This work was carried out in accordance to procedures developed at TELAC. In the course of the investigation, additional experimental methodology was developed as required. These procedures are outlined in this section, and further details can be found in the TELAC Manufacturing Class Notes [47].

3.3.1 Measurement of Coupons

A total of 3 width and 9 thickness measurements were taken from each coupon. This was done to assure specimen uniformity and to compare thickness of the specimens with nominal values supplied by the manufacturer. A template with the thickness and width positions was made, aligned to the center of the test section of each specimen, and the positions marked out for measurements. Figure 3.3 shows a schematic of a tensile coupon with the measurement points.

The measured average laminate thickness of the IM7/977-2 tensile coupons was 2.44 mm. This corresponded to an average ply thickness of 0.188 mm, equivalent to the reported nominal value. The average width of these coupons was 50.3 mm, compared to the nominal width of 50 mm.

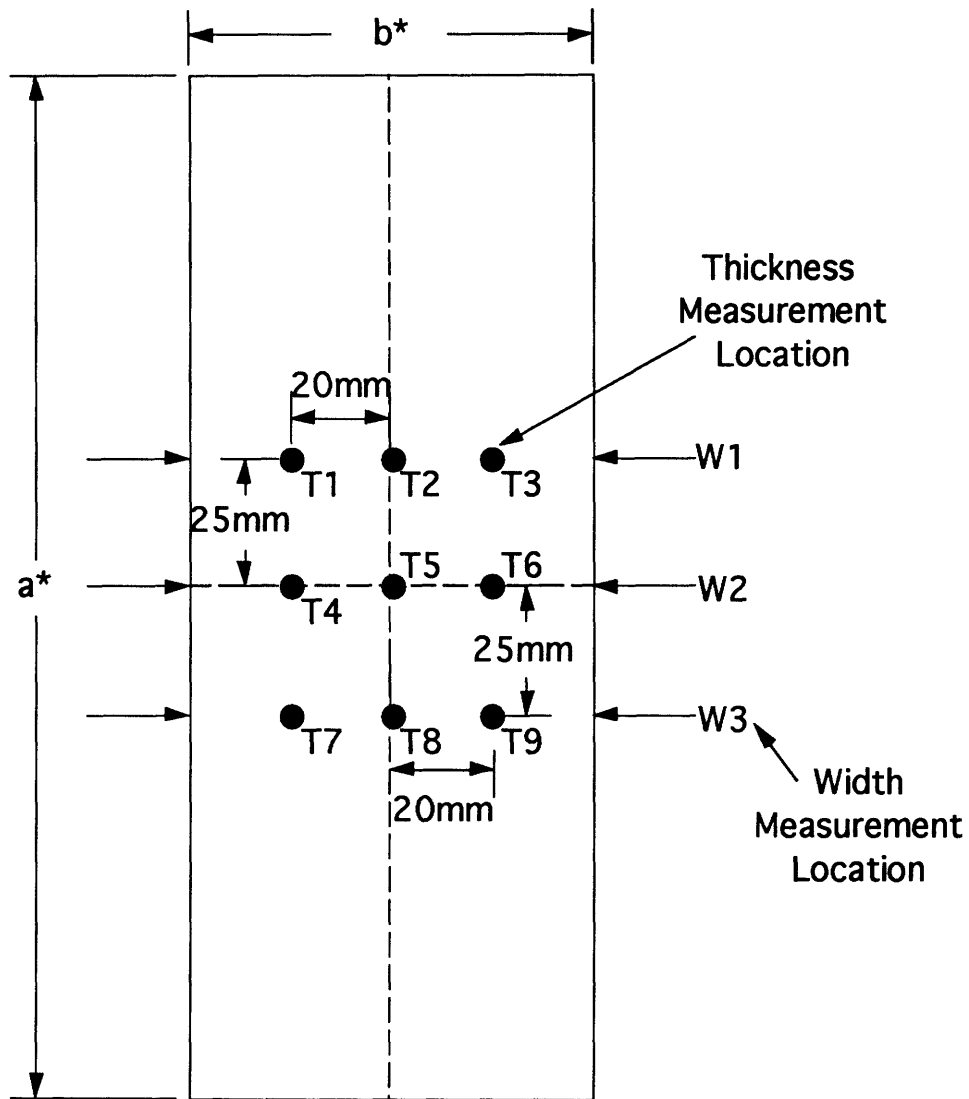
Measured average laminate thickness of the AS4/938 tape layup and tow placed coupons were 2.46 mm and 2.51 mm, corresponding to average

ply thicknesses of 0.189 mm and 0.193 mm respectively. Measured average widths of these specimens were 77.0 mm for the tape layup coupons and 76.3 mm for tow placed coupons. The nominal ply thickness and width of the AS4/938 specimens were 0.188 mm and 76 mm respectively. Individual measurements for the specimens used in this investigation are tabulated in Appendix A for the IM7/977-2 coupons and Appendix B for the AS4/938 coupons. For all subsequent calculations used in this investigation, nominal values for both thickness and width were used.

3.3.2 Measurement of Panels

Three width and five thickness measurements were taken from each tensile panel. The procedure was similar to that for the coupons and a schematic of the measurement locations is shown in Figure 3.4. The average laminate thickness of the IM7/977-2 panels was 2.46 mm, translating to an average ply thickness of 0.189 mm. The average width of these panels was 205.6 mm, compared to the nominal panel width of 203 mm.

For the AS4/938 tape layup panels, the average laminate thickness is 2.44 mm, corresponding to an average ply thickness of 0.188 mm. The average width for these panels was 204.6 mm. The average laminate thickness and width of the AS4/938 tow placed panels were 2.51 mm and 203.89 mm respectively. The resultant average ply thickness was 0.193 mm. Nominal width and ply thickness of these panels were 203 mm and 0.188 mm respectively. Again, individual measurements of the specimens are tabulated in Appendix A and Appendix B for the two respective material systems. Nominal values were used for all subsequent calculations.



* for IM7/977-2 coupons, $a = 200$ mm, $b = 50$ mm
 for AS4/938 coupons, $a = 178$ mm, $b = 76$ mm

Figure 3.3 Schematic of Coupon Measurement Locations.

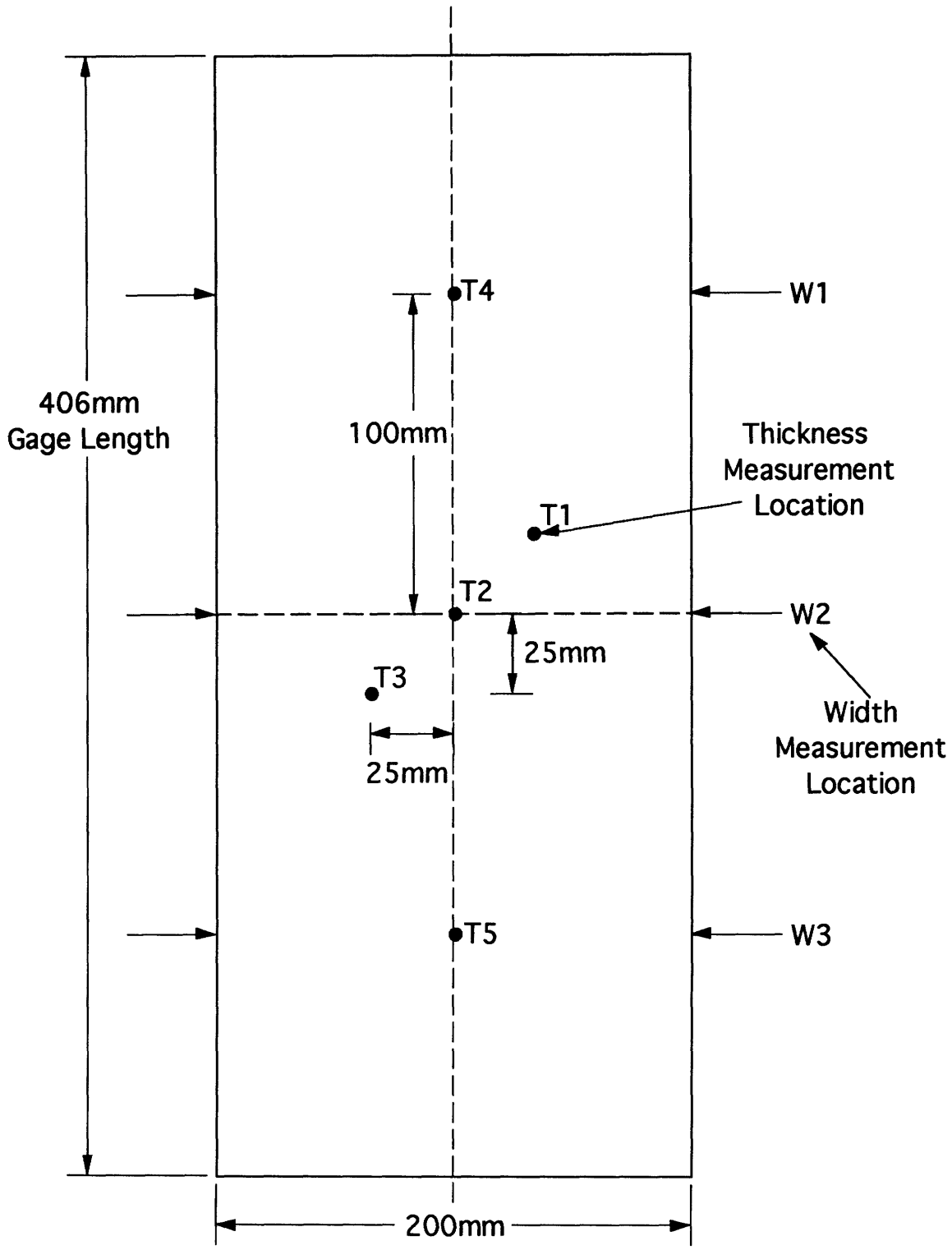


Figure 3.4 Schematic of Panel Measurement Locations.

3.3.3 Attachment of Fiberglass End Tabs

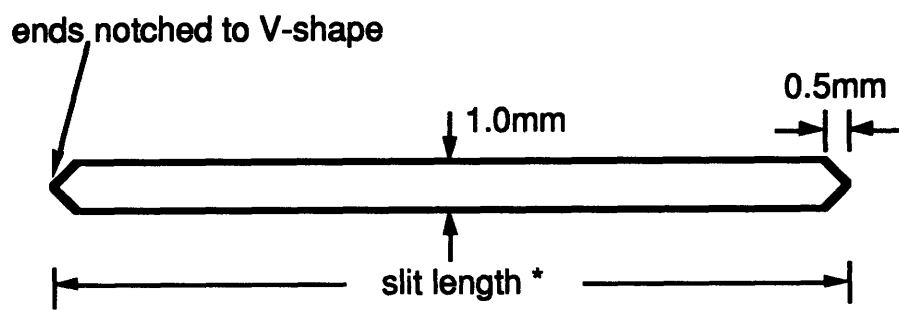
Fiberglass tabs were bonded to the ends of the test specimens to reinforce the gripping section where the tensile load was applied. The material for the end tabs was Scotchply Reinforced Plastic Type 1002, a non-woven crossply fiberglass reinforced epoxy resin material. The film adhesive used for bonding was American Cyanamid FM-123. The end tabs had a nominal thickness of 3.8 mm. In order to ensure smooth transfer of loads from the end tabs to the tensile coupons, the ends of the tabs nearest to the test section were beveled to an angle of 30°. For the IM7/977-2 tensile coupons, the tabs were 50 mm wide and 76 mm long, leaving a gage length of 200 mm. The end tabs used for the AS4/938 tensile coupons were 76 mm wide and 64 mm long. The resulting gage length was 178 mm. For the tensile panels of both material systems, the end tabs were 203 mm wide and 102 mm long, leaving a gage length of 406 mm.

The end tabs were cut from 380 mm by 600 mm sheets of pre-cured fiberglass with a bandsaw. A belt sander was used to sand the tabs to size and to bevel one of the edges. Before bonding, the bond faces of the tabs were roughened using 180-C Grit sandpaper and cleaned with cheesecloth and methanol to ensure good adhesion. Also, the ends of the specimens were cleaned thoroughly with cheesecloth and water. The tabs were placed on the film adhesive and a razor knife was used to cut the film adhesive around the edges. Using a heat gun to make the adhesive tacky, two tabs were placed onto the ends of one face of the specimen with the beveled edges facing inwards. A ruler was used to ensure that the required gage length was achieved. This procedure was repeated on the other face of the specimen, so that four end tabs were in place on each specimen.

The assembled specimens with the end tabs were placed on an aluminum caul plate to be cured in the autoclave. The caul plate was covered with a piece of Guaranteed Non-Porous Teflon (GNPT). A layer of GNPT was used to cover the specimens before steel top plates were placed on them. The steel plates were used to distribute an even loading during the cure. The entire assembly was covered with another layer of GNPT and four layers of fiberglass airbreather before being sealed with vacuum bagging and vacuum tape. In the autoclave, a vacuum was drawn on the vacuum bag and an external pressure of 0.07 MPa was applied. The temperature was raised at 3°C/minute to 107°C, and held for 2 hours. Cooling of the cure assembly was performed, at the same rate as the heating, until the autoclave temperature reached 66°C. The vacuum was vented and the autoclave was shut down.

3.3.4 Machining of Slits

Slits were manufactured at the center of some of the coupons and all the panels. They were oriented perpendicular to the loading direction. The slit size for the coupons was 19 mm while that for the panels was 51 mm. A scribe was used to mark out the required slit size on the specimen. A 'starter' slit, three quarters of the required slit length, was cut using a Dremel tool equipped with a 25 mm diameter rotary blade. The thickness of the blade was 0.6 mm. The speed used for machining the slits was 30,000 rpm. The blade was slowly lowered by hand onto the slit marking. Starting from the middle, a cut through the thickness of the panel was made and the blade was carefully moved along the rest of the marking. A jeweler's saw, with a nominal thickness of 0.5 mm, was used



* coupon slit length = 19mm
panel slit length = 51mm

Figure 3.5 Schematic Representation of a Slit.

to cut the slit to the required size. The ends of the slit were notched to a V-shape using a jeweler's saw blade with teeth filed to a point.

A schematic of a slit is shown in Figure 3.5. The nominal width of the slit was 1 mm and the nominal tip-to-tip slit length was 19 mm for the coupons and 51 mm for the panels. Each manufactured slit was examined under a microscope for quality and measured with a sliding caliper. The slit measurements for individual specimens are presented in Appendix A for the IM7/977-2 specimens and Appendix B for the AS4/938 specimens respectively.

The average slit length for the IM7/977-2 panels was 51.0 mm, equivalent to the nominal value. The average slit lengths of the AS4/938 tape layup coupons and panels were 18.5 mm and 50.6 mm respectively while that for the tow placed coupons and panels were 19.5 mm and 51.0 mm respectively. For all subsequent calculations, the nominal slit lengths of 19 mm for the coupons and 51 mm for the panels are used.

3.3.5 Attachment of Mounting Jigs for Panels

Mounting jigs were used to hold the panels onto the testing machine. The jigs consisted of four steel plates, two attached to each end of the panel. The jig plates were attached to the panel at each end by means of five bolts. They were tapered to fit into the grips of the testing machine. The thickness of each jig plate was 6.25 mm. A schematic of the jig plate is shown in Figure 3.6 [48].

Holes used for mounting the panels onto the jigs were drilled at the ends of the specimens after the end tabs were bonded. There were five attachment holes, 12.7 mm in diameter, on each end. The positions of the holes were determined by placing a set of jig plates on the specimen and

marking out the center of the hole by means of a template, transfer punch and hammer. Once the locations were marked, a 4.8 mm carbide tipped drill was used to make a 'starter' hole. The holes were drilled to size using another carbide tipped drill that was 12.7 mm in diameter.

A total of 10 bolts, 10 nuts, 40 washers and 2 spacers was required for mounting a panel onto the jig plates. The side view of one end of a panel clamped in the mounting jigs is shown in Figure 3.7. The bolts were Grade 8, 12.7 mm (0.5 inches) in diameter, 51 mm (2 inches) long with a 25.4 mm (1 inch) shoulder. Two spacers were required at each end of the panel. The thickness of each spacer was equivalent to that of the panel with bonded tabs. They were made by adhering two pieces of 19 ply fiberglass cut to fit into the spacing area. The adhesive used was Hysol 0151 epoxy patch. Mounting of the jigs was performed by first placing two jig plates on both sides of the panel, with the holes aligned. The spacer was then slipped between the plates and five bolts were placed through the attachment holes. The shoulder of each bolt was coated lightly with Bostik Never-Seez for lubrication. Washers were attached to the bolt on both sides of the jig plates to ensure proper tightening. The bolts and nuts were initially tightened by hand.

The required torque for each bolt was applied by means of a torque wrench. This was done in three stages, each stage with an increment of a third of the final required torque. The order of tightening the bolts is shown in Figure 3.6. As specified by Pemberton [49], the final torque was dependent on the maximum expected load. The equation used was:

$$M = \frac{d_{\text{bolt}} p}{5 (n_{\text{bolt}} \mu n_s)} \quad (3.1)$$

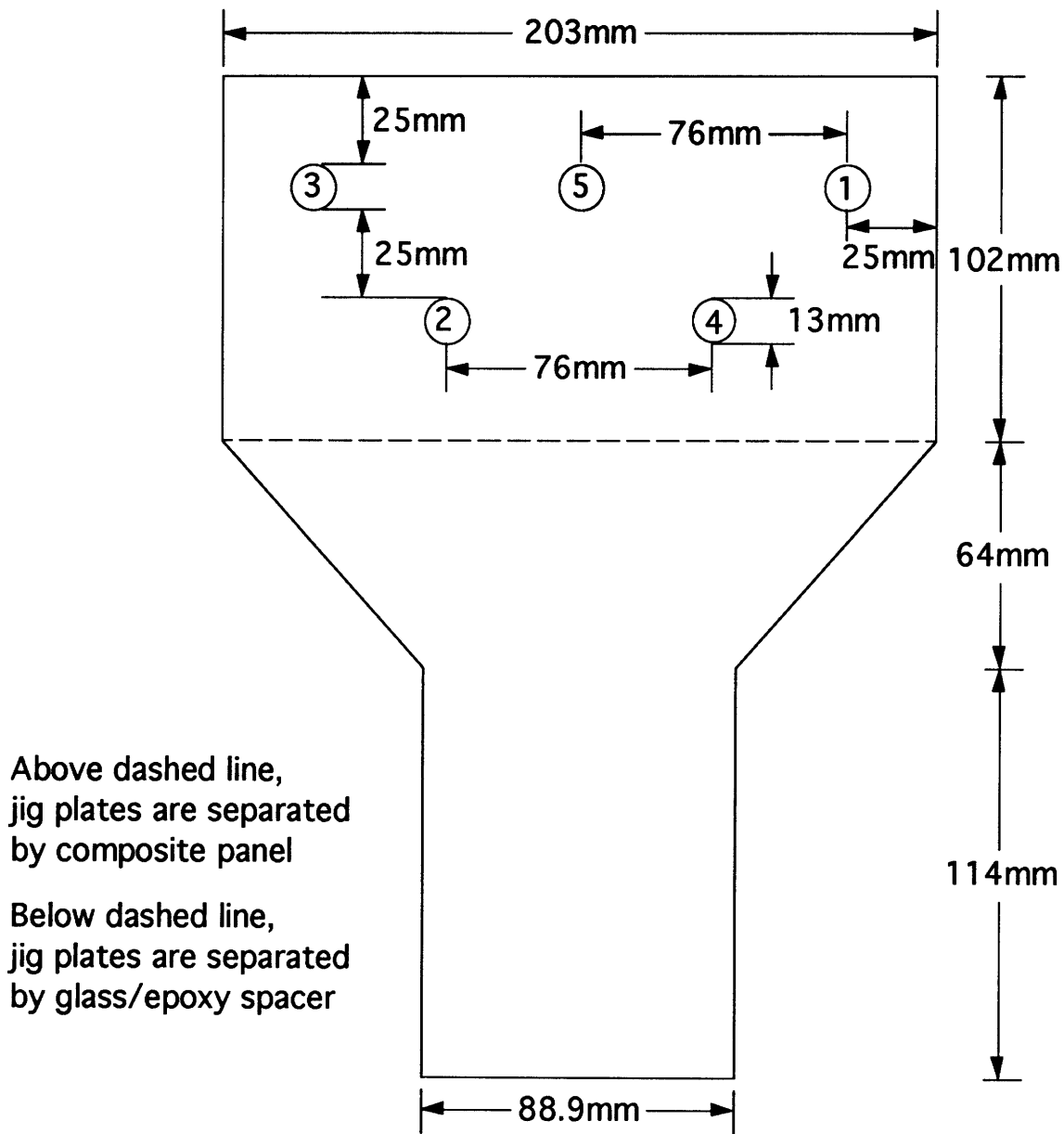


Figure 3.6 Jig Plate Dimensions and Bolt Tightening Sequence.

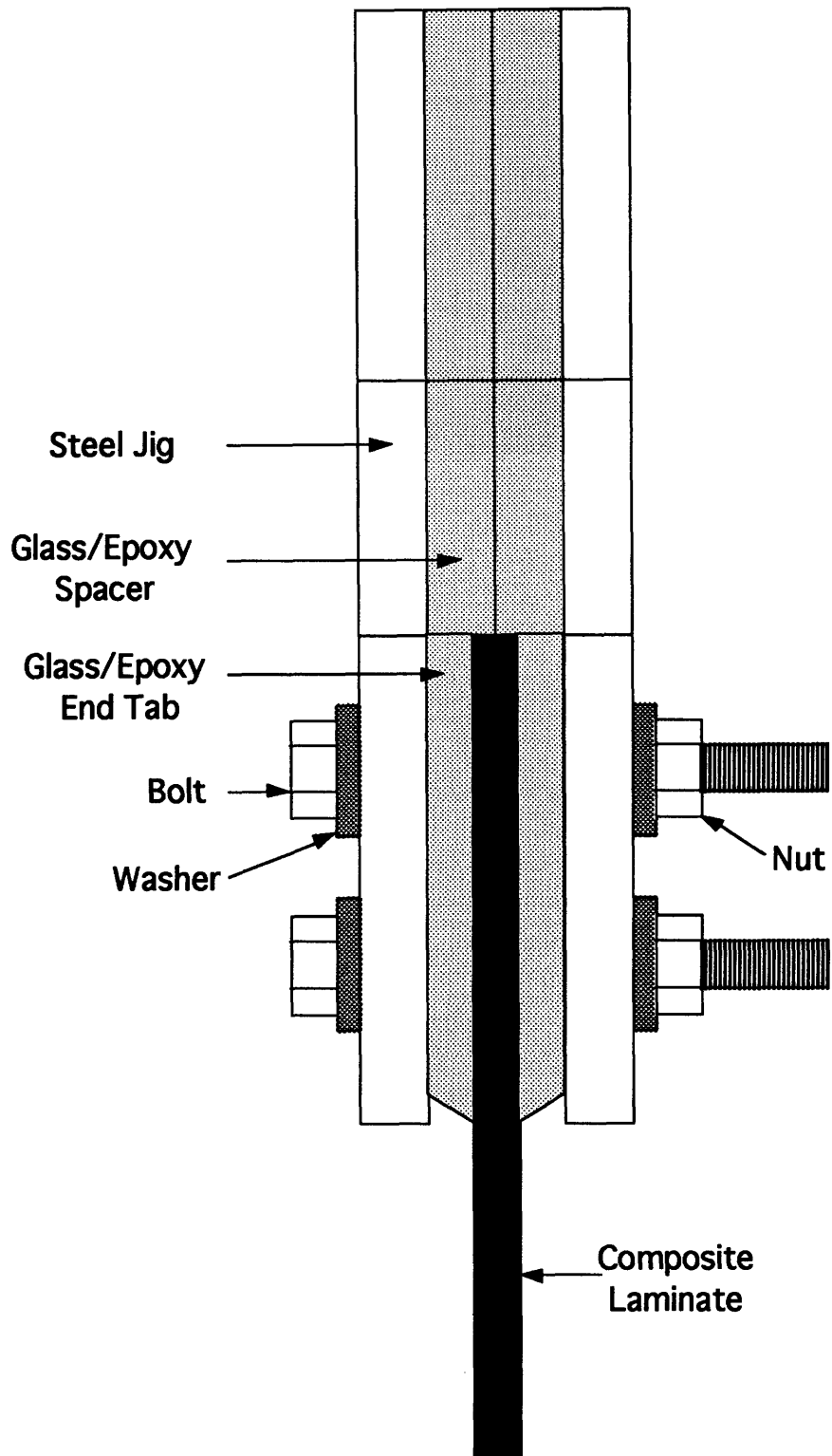


Figure 3.7 Side View of Panel Secured in Mounting Jig.

where M is the torque applied to each bolt, d_{bolt} is the diameter of the bolts, p is the maximum load to be transferred through the joints, n_{bolt} is the number of bolts used, μ is the coefficient of friction between the plates and specimen, and n_s is the number of shear planes.

The value for p was set as the maximum expected failure load of the panel. For both IM7/977-2 and AS4/938 panels, p was set as 150 kN. This value was obtained by assuming that the failure stress of the notched panel was approximately half that of the unnotched coupon. Five bolts were used and their diameters were 12.7 mm. There were two shear planes, one for each jig plate, and the coefficient of friction was set at 0.18. The resulting final torque used to tighten each bolt was 210 Nm.

3.4 Instrumentation

Both tensile coupons and panels were instrumented with strain gages manufactured by Micro Measurements Company. Two types of gages were used, EA-06-125-AD-120 and EA-06-031DE-120. The former gages were 5 mm by 10 mm, with a gage factor of 2.055 and accuracy of $\pm 0.5\%$. The latter were smaller gages, 3 mm by 6 mm, with a gage factor of 2.01 and accuracy of $\pm 1.0\%$. The area on the specimens where the gages were bonded was cleaned thoroughly with water and cheesecloth. The gages were bonded to the specimens using catalyst and adhesive (M-Bond 200) supplied by Micro Measurements. Electrical wire leads, 460 mm in length, were attached to the gages.

3.4.1 Unnotched and Notched Coupons

All unnotched coupons had one longitudinal and one transverse strain gage attached. The longitudinal gage was placed at the center of the test section while the transverse gage was placed on the centerline of the

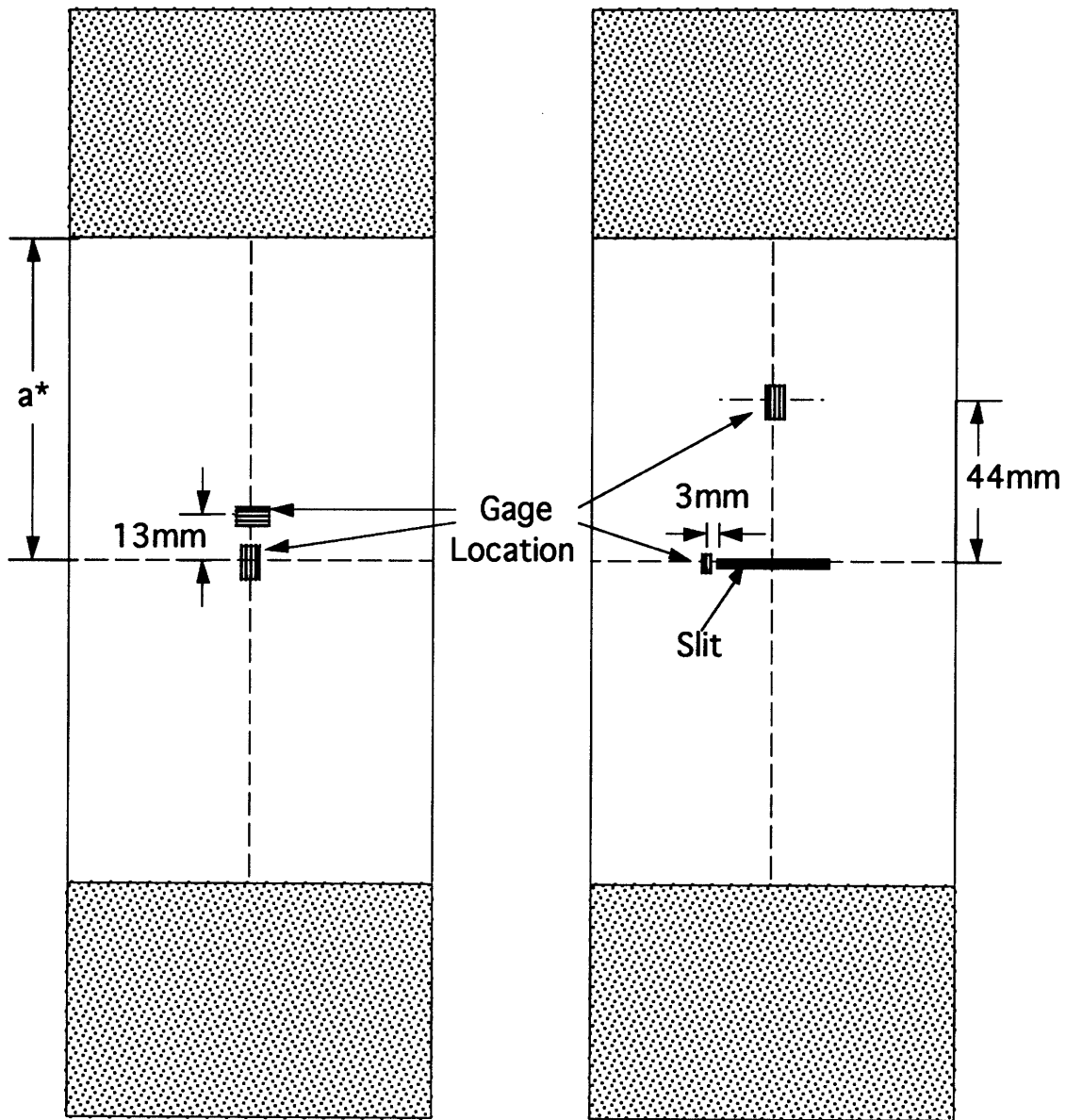
specimen, 13 mm above the longitudinal gage. Both gages were of type EA-06-125-AD-120. The strain gage arrangement for the unnotched coupons is shown in Figure 3.8.

The notched coupons had two longitudinal gages attached. This strain gage arrangement is also shown in Figure 3.8. The far-field strain gage was of type EA-06-125-AD-120. It was placed on the specimen's centerline, halfway between the slit and the end tab. The smaller gage, of type EA-06-031DE-120, was placed at one end of the notch, along the axis containing the notch. The distance from the notch tip to the middle axis of the strain gage was 3 mm.

3.4.2 Notched Panels

The strain gage arrangement for the IM7/977-2 notched panels was similar to that for the AS4/938 notched coupons. All the panels tested had a far-field longitudinal gage of type EA-06-125-AD-120 attached at the centerline of the specimen, 102 mm above the slit. The panels were also instrumented with the smaller strain gage (type EA-06-031DE-120) located at one end of the slit. The distance from the notch tip to the middle axis of the strain gage was 3 mm.

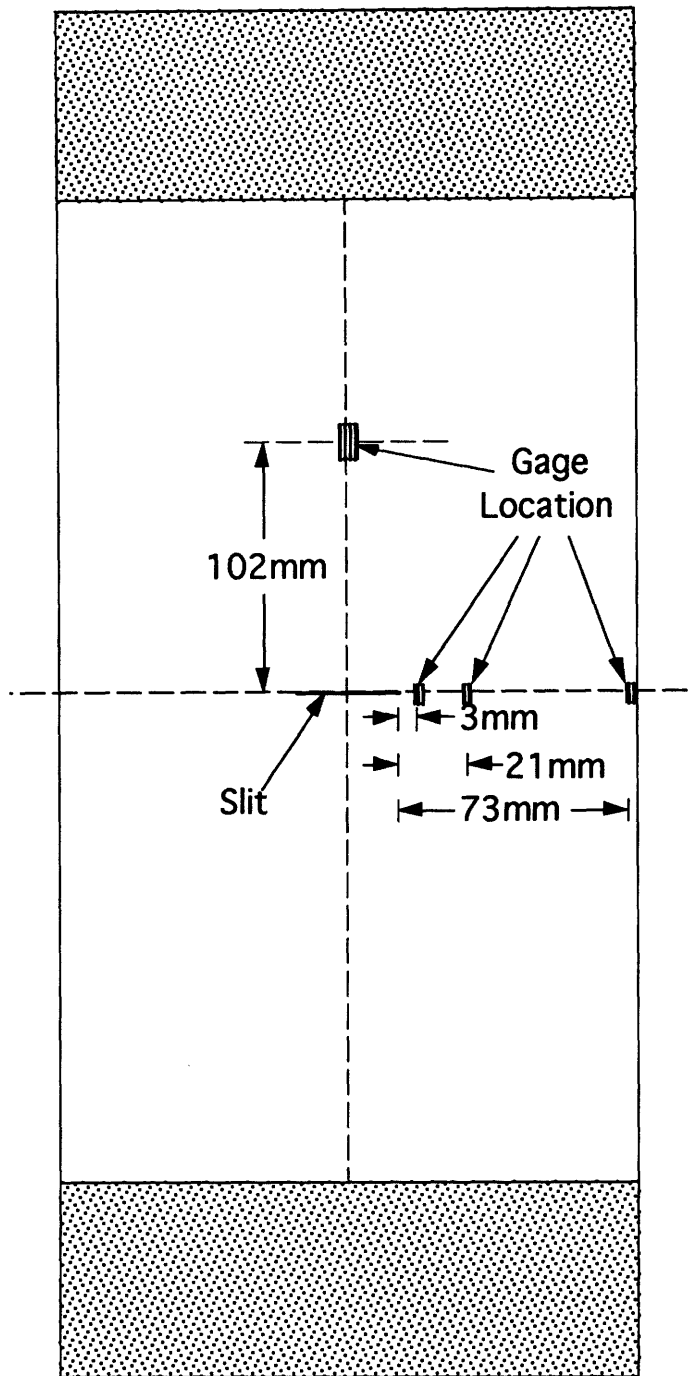
All thirty AS4/938 notched panels had a far-field longitudinal strain gage placed on the centerline of the panel, 102 mm above the slit. In addition, twelve AS4/938 panels had a strain gage arrangement designed to monitor the strain distribution during the tests. This strain gage arrangement is shown in Figure 3.9. Two tape layup panels and tow placed panels were tested at each strain rate with this strain gage arrangement. The arrangement consisted of three strain gages, type EA-06-031DE-120, aligned in a straight line along the axis containing the slit, from the notch



NOTE: Not to Scale

* for IM7/977-2 coupons, $a = 100$ mm
 for AS4/938 coupons, $a = 89$ mm

Figure 3.8 Strain Gage Placement for Unnotched and Notched Coupons.



NOTE: Not to Scale

Figure 3.9 Strain Gage Placement for Notched Panels.

tip to the edge of the panel. They were placed on either side of the slit. The distances from the notch tip to the middle axes of the strain gages were 3 mm, 21 mm and 73 mm.

3.5 Testing Procedures

All tensile tests were performed on the MTS 810 Material Test System equipped with hydraulic grips. The required strain rates for the tests were achieved by varying the stroke rate settings of the machine. Ideally, the strain rate is the ratio of the stroke rate setting to the specimen gage length. However, due to the existence of load train compliance, the measured strain rate, recorded by the far-field strain gage, was lower than this ideal strain rate. This discrepancy will be further discussed and accounted for in the next chapter. For all the tests conducted, the stroke rate setting was computed from multiplying the desired strain rate by the gage length of the specimen.

In this investigation, tensile tests were conducted at a total of 14 different stroke rates. They are presented in Table 3.5 for each test condition. The IM7/977-2 specimens were tested at 4 strain rates, resulting in 8 different stroke rates as the coupons and panels had different gage lengths. Similarly, the AS4/938 specimens required 6 different stroke rate settings to achieve the required 3 strain rates.

Mounting of the coupons or panels in the hydraulic grips was performed as followed: One end of the specimen was first placed between the jaws of the upper grips. For the coupon, this referred to one end of the specimen with the end tabs attached; for the panel assembled with the mounting jigs, this referred to one end of the jig plates. Alignment of the coupon was achieved by means of a machinist's square, while alignment of

the panel was done with a level. Special care was taken to make sure that the entire coupon end tab or jig plate gripping section was inside the grips before applying grip pressure. The upper crosshead, with the specimen attached, was slowly lowered into the jaws of the lower grips. At this 'zero condition', before gripping the lower jaws, the strain gages were balanced and calibrated. The load and stroke readings were also set to zero. Again, special care was taken to ensure that entire grip section of the specimen was gripped. The gripping pressure for the coupons was 7 GPa and that for the panels was 17 GPa. Pictures of a coupon and panel prior to the application of load are shown in Figure 3.10 and Figure 3.11 respectively.

Before starting the test machine, the data acquisition program was activated. All tests were conducted in stroke control and ran monotonically to fracture. At the lower rates of loading, splitting and cracking sounds were heard during the tests and they were recorded by noting down the load readings displayed on the testing machine. This information was incorporated into the recorded test data. At the end of each test, a photograph was taken of the failed specimen to record the failure modes.

3.6 Data Collection

Data for the tests was taken with an Apple Macintosh IIX computer running the LabVIEW2 data acquisition software developed by National Instruments. The hardware interface consisted of a MacADIOS breakout box and analog/digital converter card supplied by GW Instruments. Load and stroke readings from the testing machine were fed into a MacADIOS breakout box, through the analog/digital converter card and recorded by the LabVIEW2 data acquisition program. Similarly, the output from the strain gages was fed through the Vishay Instruments Strain Gage

Table 3.5 Stroke Rate Settings and Data Collection Frequencies Used in Tensile Tests

Specimen Type	Strain Rate (ϵ/min)			
	0.005	0.025	0.1	0.5
IM7/977-2:				
Unnotched Coupons	0.04 ^a [2] ^b	0.2 [10]	0.8 [50]	4 [150]
Notched Panels	0.08 [5]	0.4 [10]	1.6 [100]	8 [200]
	0.0042	0.1	2	
AS4/938:				
Unnotched Coupons	0.03 [2]	0.7 [50]	14.4 [750]	
Notched Coupons	0.03 [2]	0.7 [100]	14.4 [750]	
Notched Panels	0.07 [5]	1.7 [100]	33 [750]	

^a Stroke rate setting (inches/min)

^b Data collection frequency (Hz)

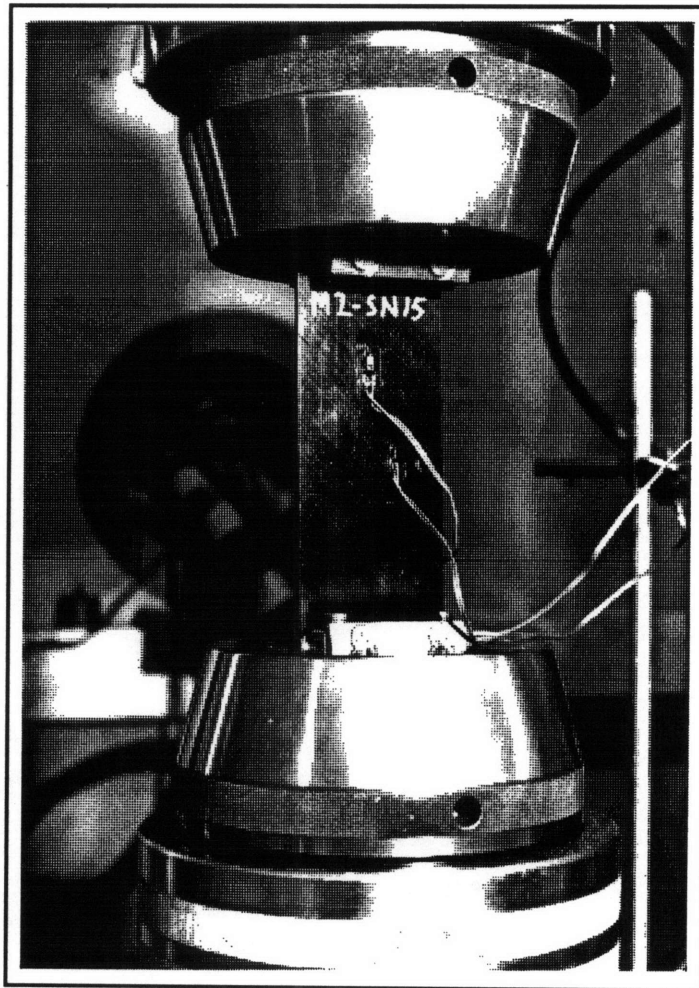


Figure 3.10 Photograph of tensile coupon in hydraulic grips prior to testing.

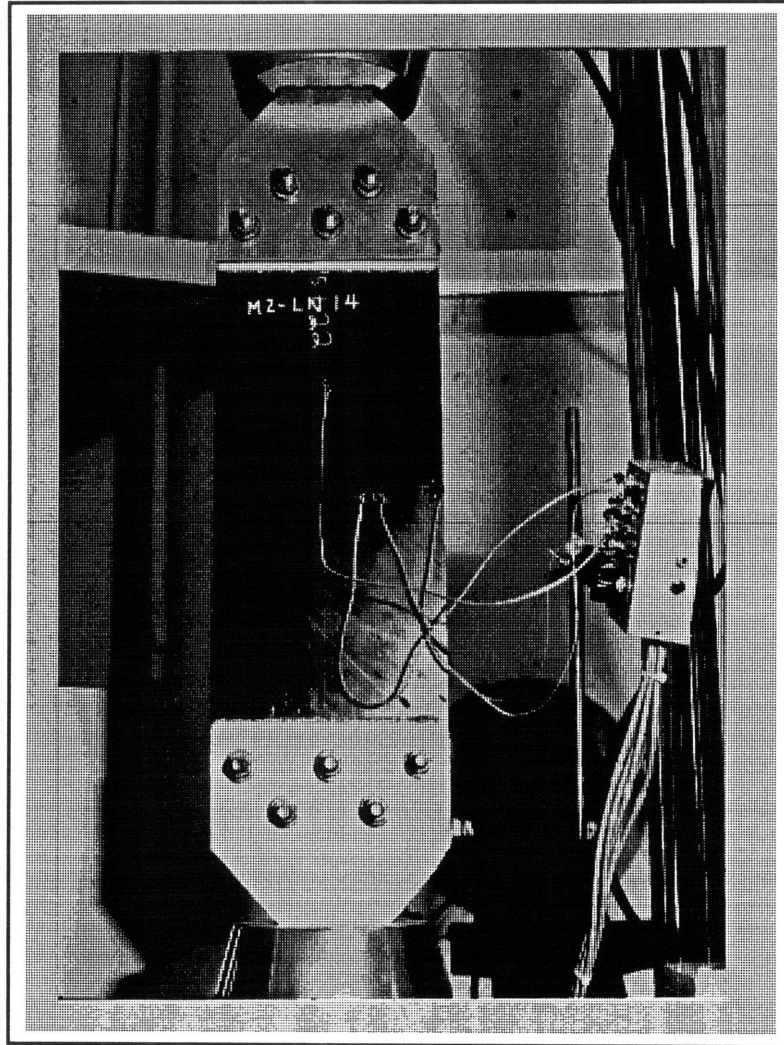


Figure 3.11 Photograph of tensile panel in hydraulic grips prior to testing.

Amplifiers/Balances, the MacADIOS breakout box and the analog/digital converter card, and recorded by the same program.

Different data collection frequencies were used at different strain rates to ensure that sufficient data was collected to record the tests. A total of eight different frequencies were used in the tests. They are tabulated in Table 3.5 with the corresponding stroke rate settings. For each test, an average of about 200 data points were collected. The data collection frequencies were determined by estimating the time required to fail each specimen configuration at each strain rate. A custom LabVIEW2 program, written by member of the laboratory for high frequency data acquisition, was used. This program utilizes the 'Digitize' data acquisition module [50] and is named 'TELAC 8 Channel Fast Acquisition'.

3.7 Data Reduction

All data reduction and analysis procedures were performed using Apple Macintosh computers. The data files created by the LabVIEW2 data acquisition software contained columns of data points corresponding to the data acquisition channels used during the tests. The first three channels were used to record the load, longitudinal or far-field strain, and stroke respectively. Additional channels were used to record readings from other strain gages. As the data files contained extra data points collected before and after the tests, they were 'trimmed' to a manageable size. This procedure was performed in the Microsoft Excel spreadsheet program, where the initial rows of data points before any noticeable increase in recorded stroke readings were deleted. Similarly, rows of data collected after attaining the maximum load (i.e., the failure of the specimen), were removed from the data file. A time column was added into the data file as

the time taken for the tests was not measured. It was determined from the data collection frequency used and 'zero' time was set at the instant where the stroke reading started to increase. From each 'trimmed' data file, pertinent parameters like maximum load and the corresponding strains were noted.

LIN6 [51] was used to compute the laminate moduli, major Poisson's ratios, stroke rates and strain rates for all the tests. LIN6 is an algorithm that selects linear regions of a curve, and performs linear regressions to compute the slopes of these regions. The laminate moduli was obtained from the slope of the stress versus longitudinal strain curve. Stress was computed from the ratio of the recorded load to nominal cross sectional area of each specimen configuration. The laminate major Poisson's ratio was obtained from the slope of the transverse strain versus longitudinal strain curve. Stroke and strain rates were obtained from the slopes of the stroke and longitudinal/far-field strain versus time curves respectively.

The outputs for the stroke rates were linear for all the tests conducted. However, the output for the laminate moduli, major Poisson's ratios and strain rates showed regions of non-linearity. The first substantial linear region in the trimmed output, consisting of at least ten data points, was used to calculate these properties.

Chapter 4

RESULTS

In this chapter, experimental results of strain rate effects on tensile failure of IM7/977-2 and AS4/938 laminates are presented. These include the failure stresses, failure modes, laminate longitudinal moduli and major Poisson's ratio at all the strain rates tested. The strain distributions of the AS4/938 panels are examined at varying strain rates. Also, the notched failure strengths of the AS4/938 specimens are correlated with the Mar-Lin theory.

All individual specimen measurements and laminate properties recorded in this investigation are tabulated in Appendix A for the IM7/977-2 specimens and Appendix B for the AS4/938 specimens. The load, stroke and strain gage readings collected for all the tests are shown, plotted against time, in Appendix D and Appendix E for the IM7/977-2 and AS4/938 specimens respectively.

4.1 Expected Strain Rate versus Measured Strain Rate

The stroke rate used to conduct each test was determined by multiplying the desired strain rate by the specimen gage length. Ideally, this stroke rate would invoke the required strain rate in the specimen. However, due to compliance in the load train, the actual strain rates measured by strain gages mounted on the specimen were lower than the ideal values. The variations between the measured strain rates and the ideal strain rates were dependent on the specimen configurations. Generally, the difference was about 20% for the coupons and 30% to 40% for

the panels. The measured strain rates were consistent within each set of test configuration.

Measured strain rates for individual specimens are shown in Appendix A and Appendix B for the IM7/977-2 and AS4/938 specimens respectively. The 'expected' or ideal strain rate will be used to label and categorize the various properties recorded when presenting the results. When applicable, failure properties will be plotted using the measured strain rates.

4.2 IM7/977-2 Test Results

The results of tensile tests conducted on unnotched and notched IM7/977-2 laminates at four strain rates are presented below.

4.2.1 Unnotched Coupon Results

The average failure stresses of the unnotched specimens, and their coefficients of variation, are shown in Table 4.1. At the lowest strain rate of 0.005 ϵ /min, the average failure stress was 544 MPa. At 0.025 ϵ /min, it was 560 MPa; at 0.1 ϵ /min, it was 510 MPa; and at 0.5 ϵ /min, it was 565 MPa. The average failure stresses are plotted against the measured strain rate in Figure 4.1. The differences between the average failure stress recorded at the 'static' rate of 0.005 ϵ /min and those recorded at higher strain rates were between 3% and 6%.

The failure modes of the unnotched IM7/977-2 coupons at different strain rates were similar when inspected. The fracture paths of all the failed coupons were relatively straight, extending across the specimen at an approximate angle of 30° to the loading axis. The failure surface showed a combination of failure modes that included fiber breakage at the non-90° plies and matrix cracking at the 90° plies. The outer 45° plies at the

Table 4.1 Average Failure Stress of IM7/977-2 Specimens at Different Strain Rates

Strain Rate (ϵ/min)	Average Failure Stress (MPa)	
	Unnotched Coupons ^a	Notched Panel ^b (51 mm Slit)
0.005	544 (9.2%) ^b	259 (2.7%)
0.025	560 (6.6%)	260 (0.2%)
0.1	510 (2.3%)	262 (2.1%)
0.5	565 (1.8%)	258 (4.5%)

a 2 specimens tested in each case

b 3 specimens tested in each case

c numbers in parentheses are coefficients of variation

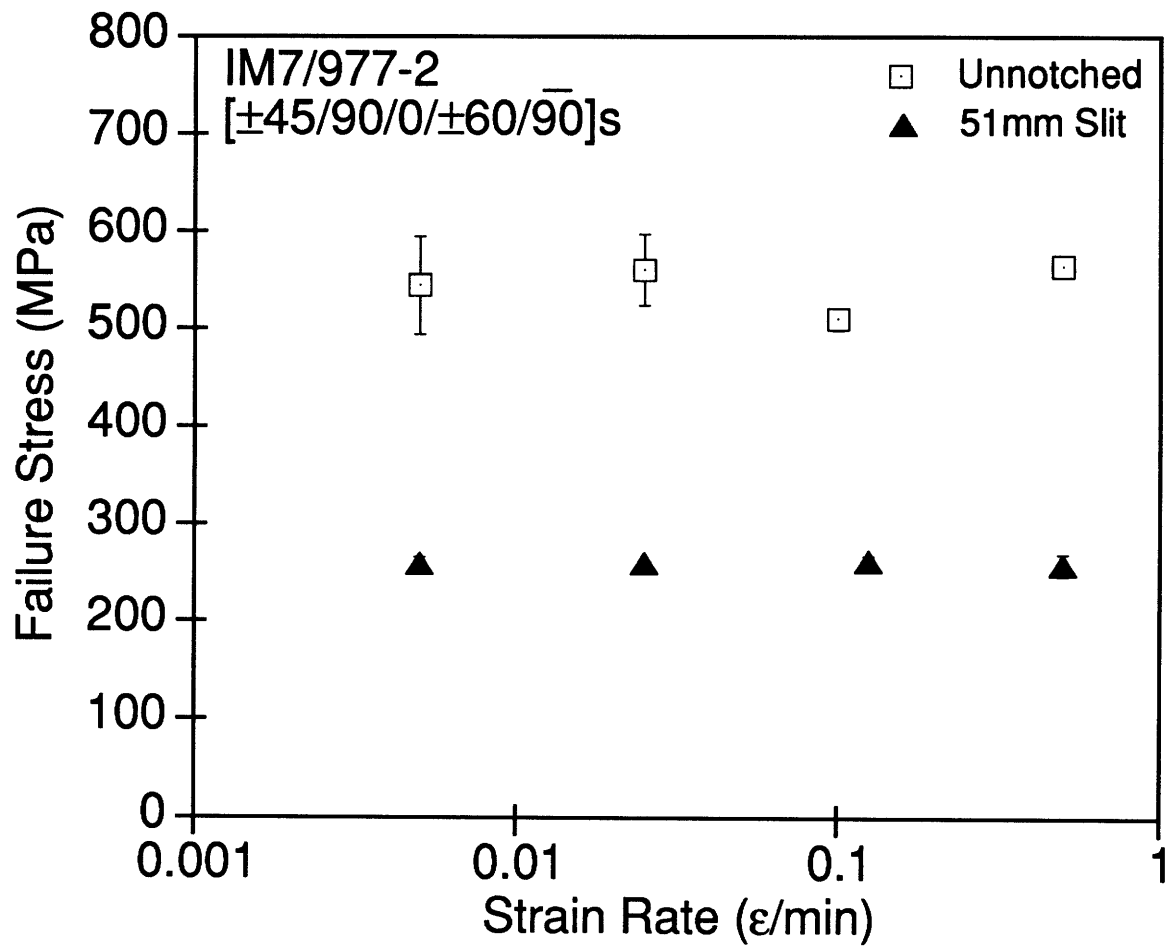


Figure 4.1 Average Failure Stress vs. Strain Rate for IM7/977-2 Specimens.

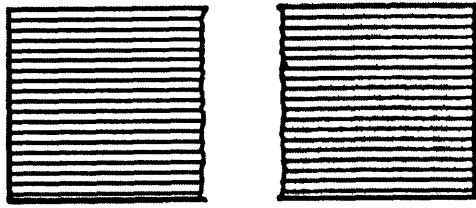
surfaces of the specimen were delaminated from the adjacent plies. The delaminations extended for about 50 mm from the failure surface. Sketches of the different failure modes described are shown in Figure 4.2. For some of the IM7/977-2 coupons, failure also occurred near the end of the specimens. These failures were perpendicular to the loading direction. A sketch of the failure modes of the unnotched coupons described above is shown in Figure 4.3, and a post test photograph of representative unnotched coupons tested at the various strain rates is shown in Figure 4.4.

The stress strain curves of representative IM7/977-2 unnotched coupons at the various strain rates tested are shown in Figure 4.5. The stress-strain behaviors were generally linear for at least one-third of the initial loading. After that, the curves showed load drops at about 350 MPa and 500 MPa. The locations where the drop in load occurs corresponded to audible 'clicks' heard and recorded during testing.

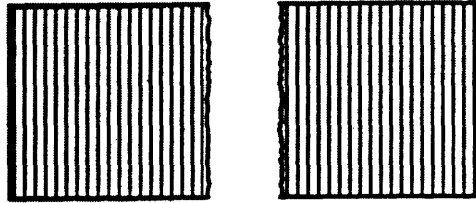
The average laminate longitudinal modulus was 35.2 GPa at 0.005 ϵ /min, 39.7 GPa at 0.025 ϵ /min, 37.8 GPa at 0.1 ϵ /min and 39.1 GPa at 0.5 ϵ /min. The laminate longitudinal modulus calculated for this layup using Classical Laminated Plate Theory (CLPT), shown in Table 3.1, was 39.5 GPa. The Poisson's ratio obtained experimentally was 0.26 at 0.005 ϵ /min and 0.27 at the rest of the strain rates tested. This was consistent with the CLPT computed value of 0.27. The average laminate moduli and Poisson's Ratios at different strain rates, with their coefficients of variation, are shown in Table 4.2.

4.2.2 Notched Panel Results

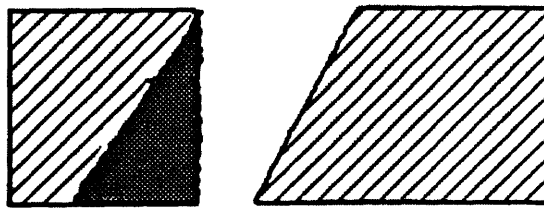
The average failure stress for the notched panels at the 'static' rate of 0.005 ϵ /min was 259 MPa. At 0.025 ϵ /min, the average failure stress was



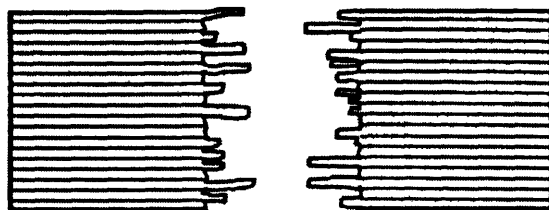
Fiber Breakage



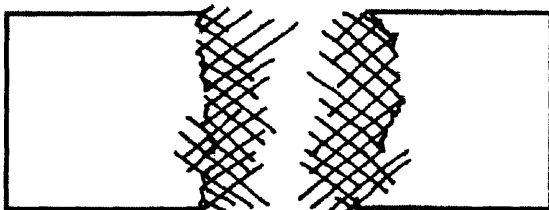
Matrix Cracking



Delamination

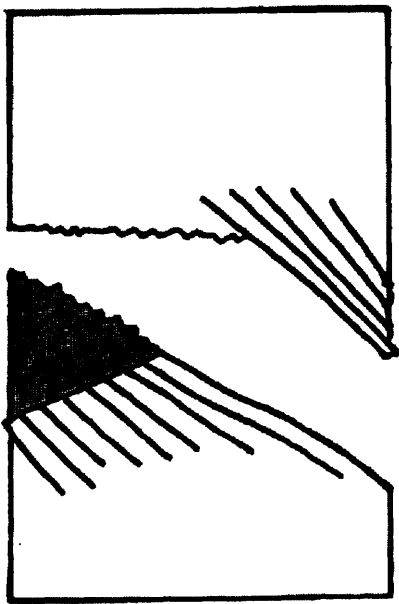


Bundle Pullout

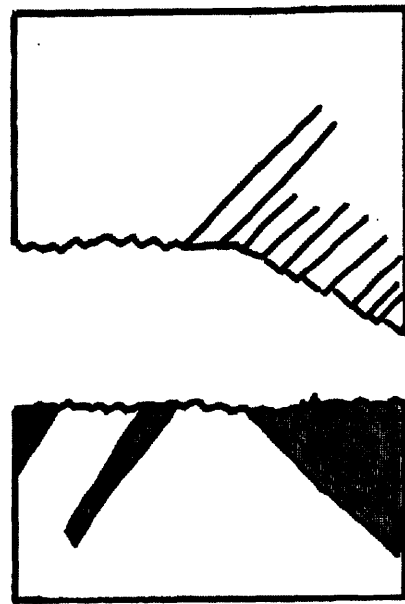


Splitting

Figure 4.2 Sketches of Different Failure Modes.



(a) IM7/977-2 Unnotched Coupon



(b) AS4/938 Unnotched Coupon

Key:

 Delaminated Area

 Matrix Splitting

Figure 4.3 Failure Modes of IM7/977-2 Unnotched Coupon and AS4/938 Unnotched Coupon.

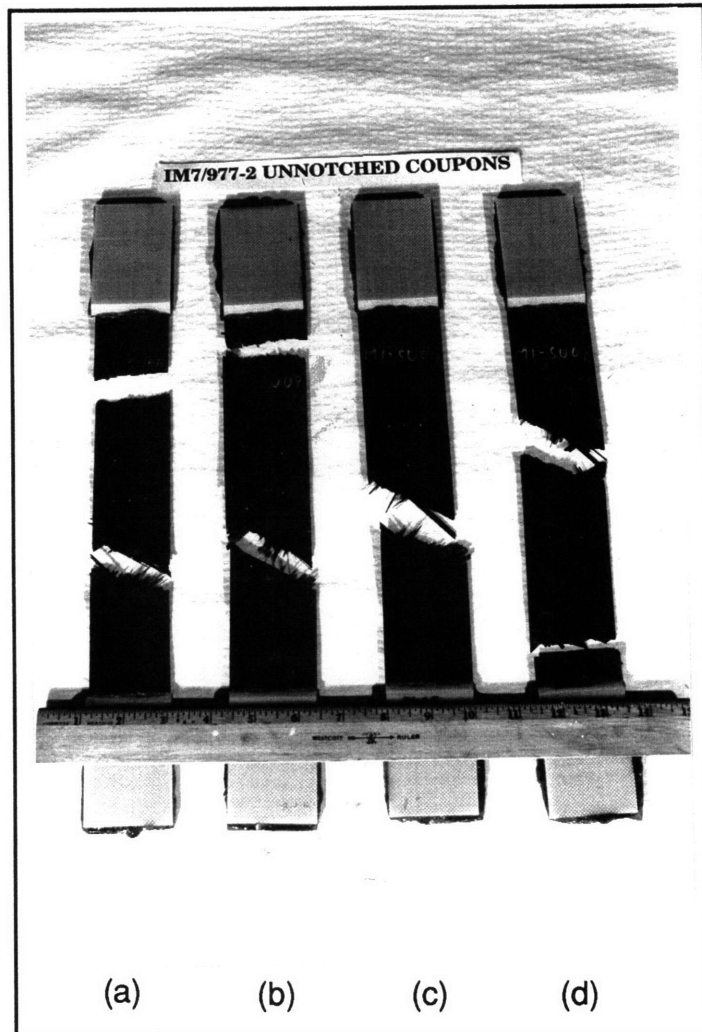


Figure 4.4 Photographs of Failed IM7/977-2 Unnotched Coupons at Different Strain Rates.

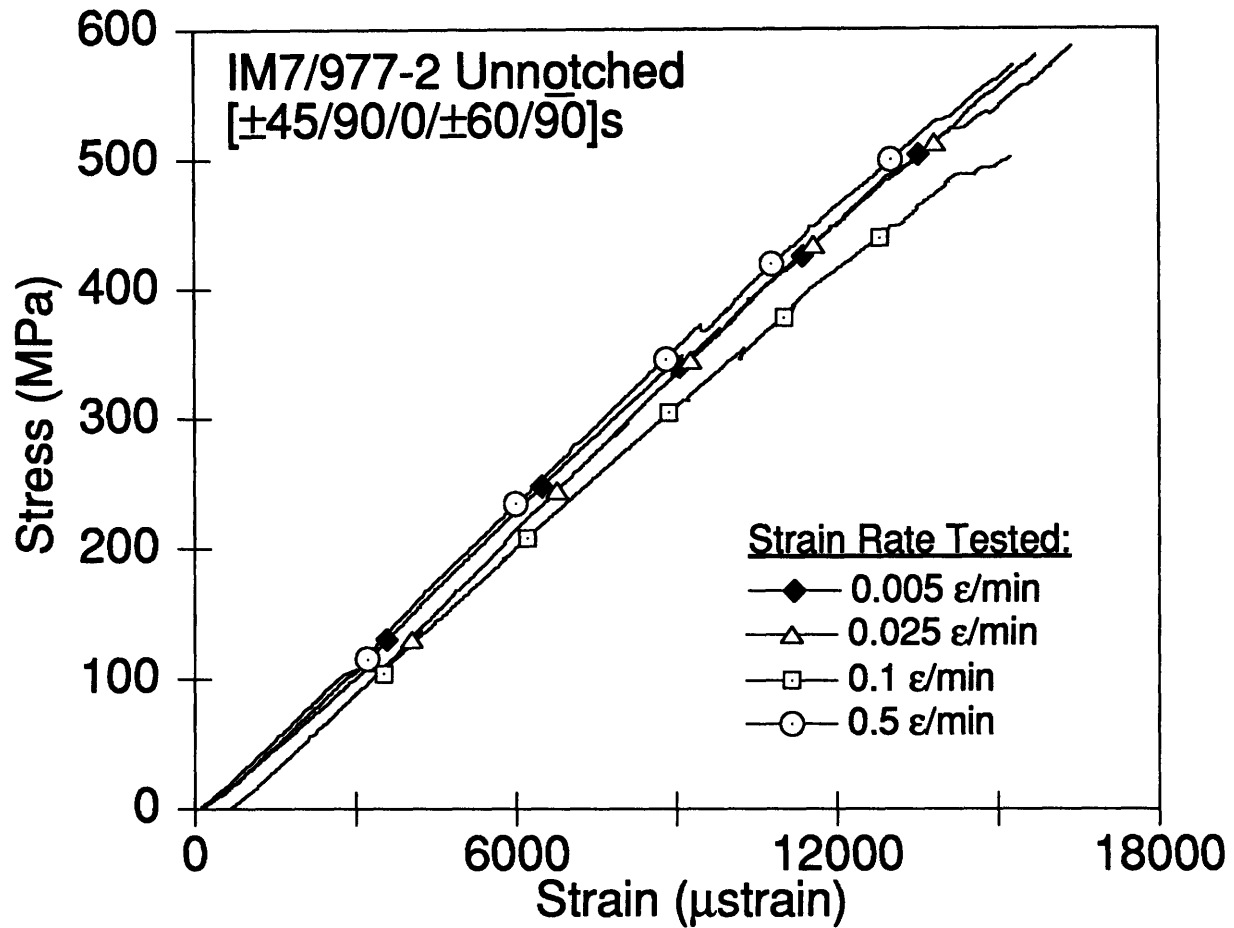


Figure 4.5 Stress-Strain Curves of IM7/977-2 Unnotched Coupons at Different Strain Rates.

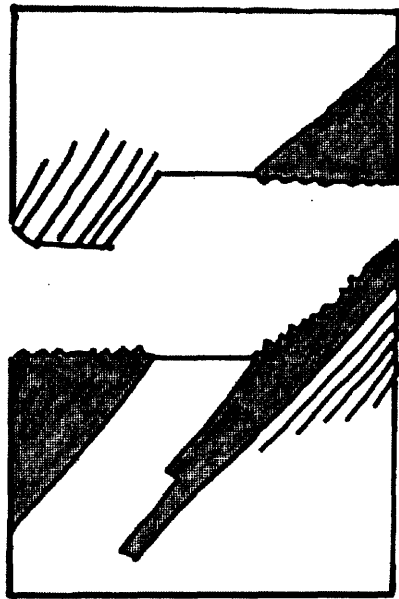
Table 4.2 IM7/977-2 Unnotched Coupon Stiffness Data at Different Strain Rates

Strain Rate (ϵ /min)	Average Laminate Longitudinal Modulus (GPa)	Average Laminate Poisson's Ratio
0.005	35.2 (13.4%) ^a	0.26 (0%)
0.025	39.7 (2.3%)	0.27 (2.7%)
0.1	37.8 (1.3%)	0.27 (0%)
0.5	39.1 (0.4%)	0.27 (2.7%)

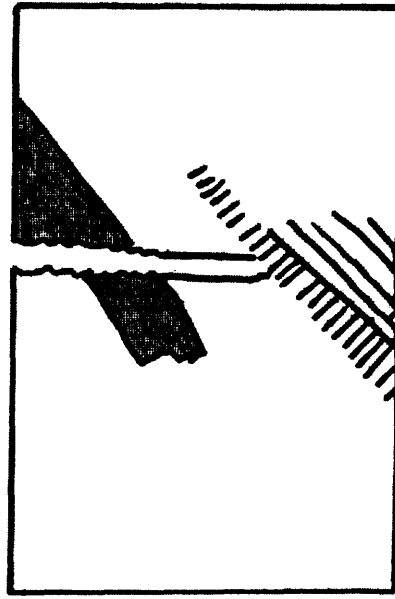
^a numbers in parentheses are coefficients of variation

260 MPa; it was 262 MPa at 0.1 ϵ /min and 258 MPa at 0.5 ϵ /min. These values and their coefficients of variation are shown in Table 4.1. The average failure stresses of the IM7/977-2 notched panels plotted against measured strain rates are shown in Figure 4.1.

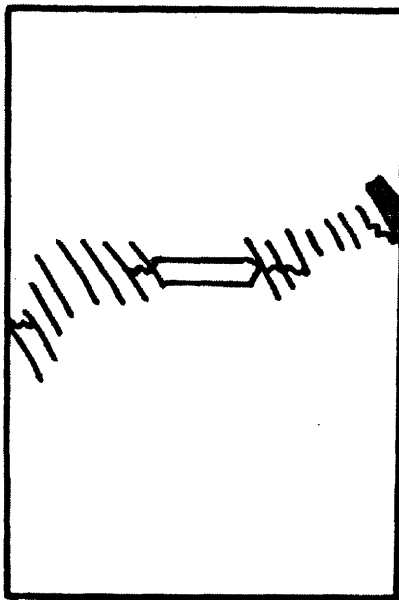
The appearance of the failed IM7/977-2 notched panels differed at the different strain rates tested. Failure of the notched panels started at the ends of the slits and propagated outwards to the edges of the panels. At 0.005 ϵ /min, fracture paths generally traveled at 60° or 90° to the loading direction. Along the failure surface, the 0° plies failed from fiber breakage and the 90° plies failed from matrix cracking. The other plies also failed from fiber breakage. Minor delamination was present at the outer 45° plies near the failure surface. At 0.025 ϵ /min, the fracture phenomenon was similar to that at 0.005 ϵ /min. However, some specimens tested at this strain rate did not break cleanly due to splitting in the matrix of the 45° and 60° plies. This resulted in the plies separating to strands about 5 mm long, along the fiber direction. At 0.1 ϵ /min and 0.5 ϵ /min, none of the specimens tested broke into separate pieces. Examination of the fracture path showed that it was jagged and not well defined. The severity of splitting of the outer 45° plies increased with strain rates. At 0.5 ϵ /min, the $\pm 45^\circ$ plies broke into very long and thin strands, about 100 mm long. Twisting of these strands from the delaminated 45° plies occurred as the panels were extended further apart. Examination of the internal 0° and 90° plies in these panels showed no splitting. These plies broke by fiber breakage and matrix cracking respectively. Sketches of the different failure modes described above are shown in Figure 4.2. Also, sketches of the IM7/977-2 notched panels at different strain rates are shown in Figure 4.6. A bar-chart summarizing the different modes of failure observed in the notched panels



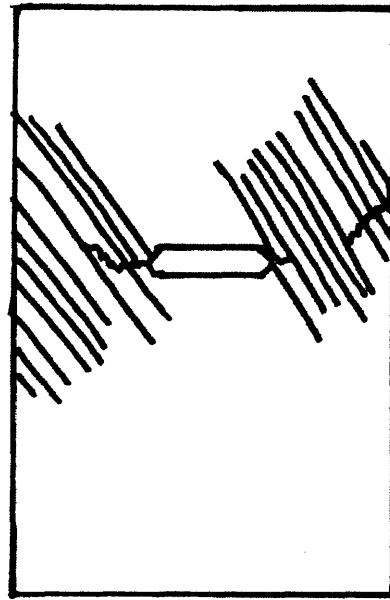
(a) 0.005 ϵ /min



(b) 0.025 ϵ /min




(b) 0.1 ϵ /min



(d) 0.5 ϵ /min

Key:

 Delaminated Area


 Matrix Splitting

Figure 4.6 Failure Modes of IM7/977-2 Notched Panels at Different Strain Rates.

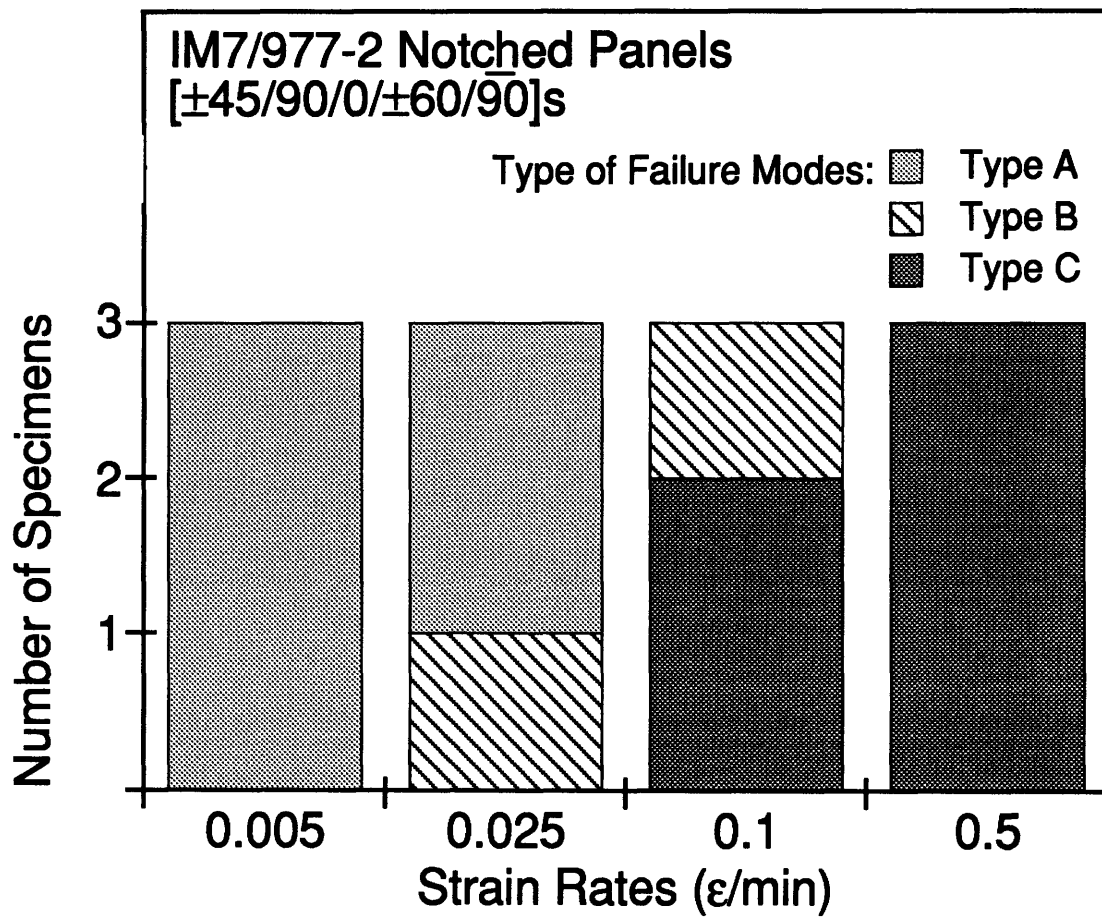


Figure 4.7 Distribution of Failure Modes for IM7/977-2 Notched Panels.

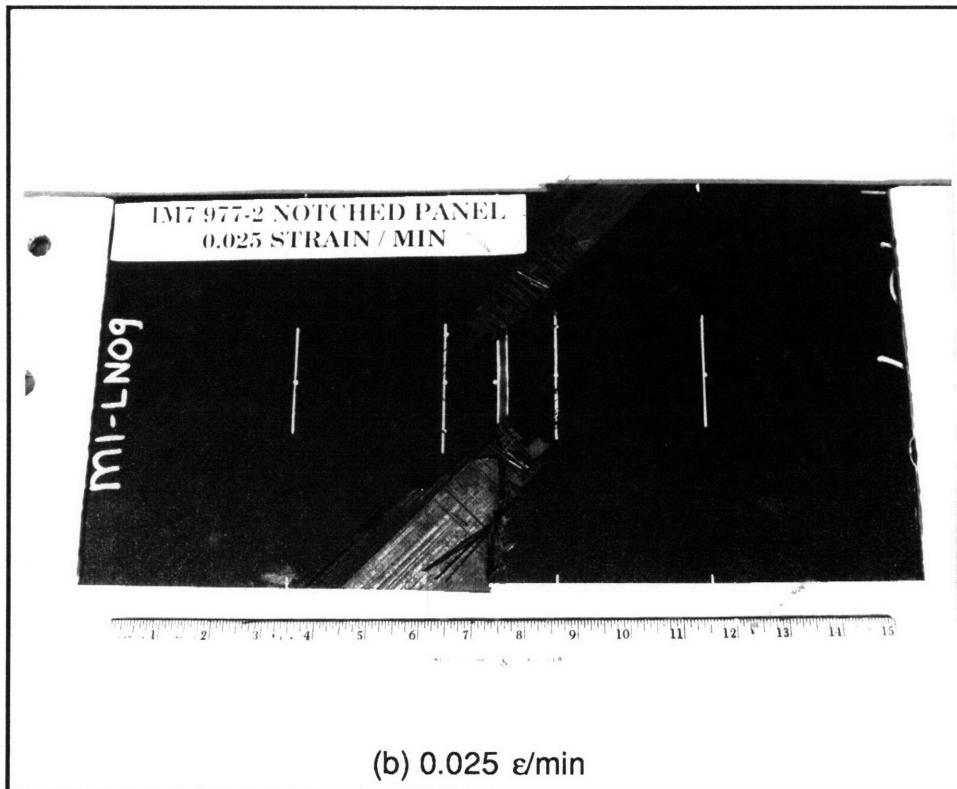
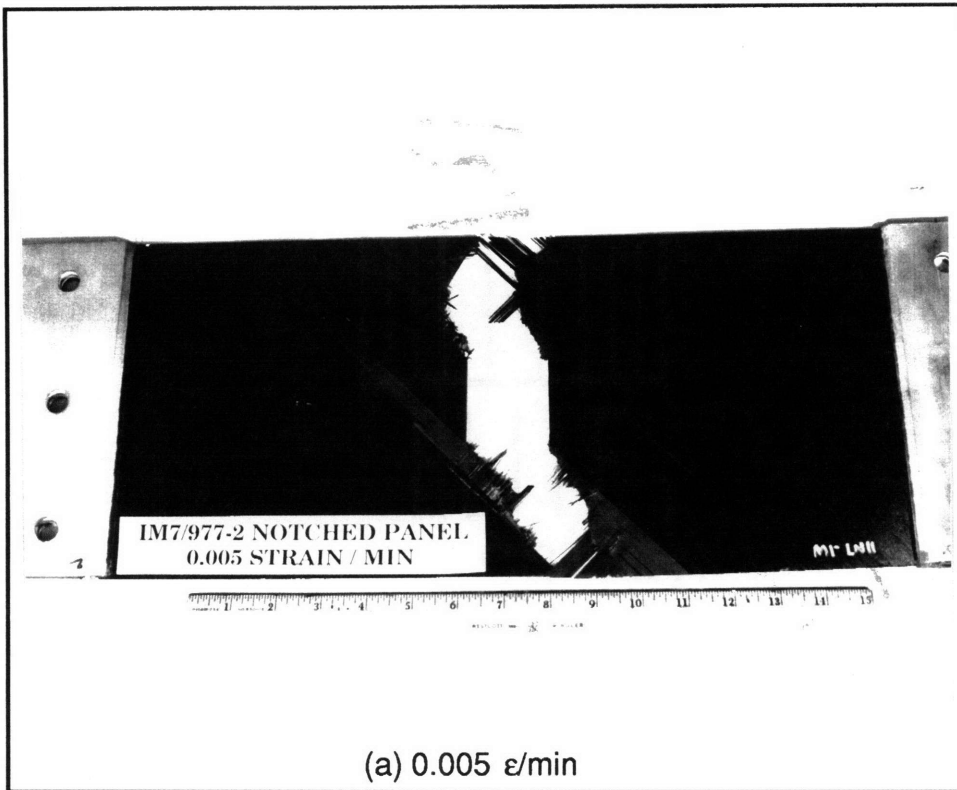


Figure 4.8 Photographs of Failed IM7/977-2 Notched Panels at (a) 0.005 ϵ /min and (b) 0.025 ϵ /min.

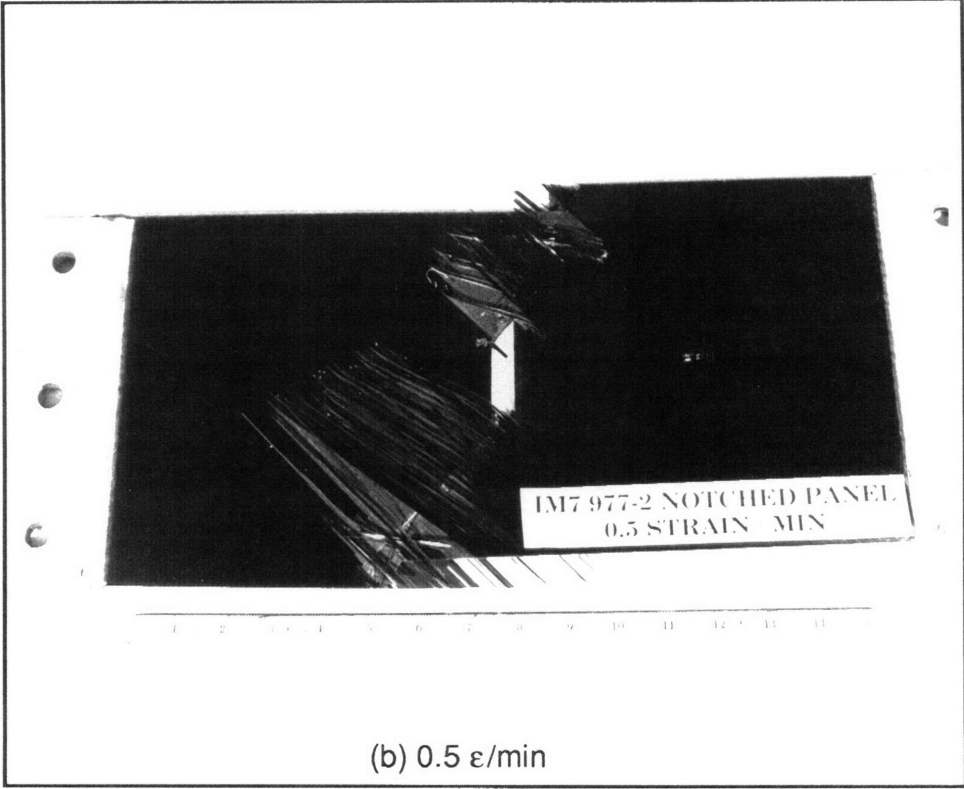
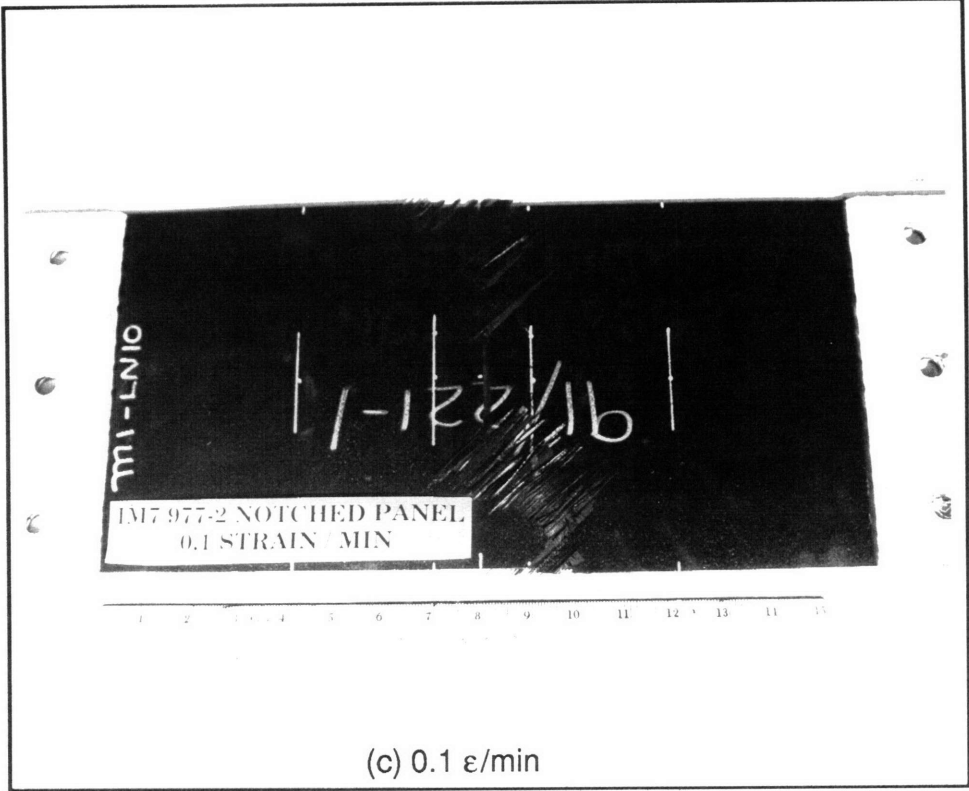


Figure 4.9 Photographs of Failed IM7/977-2 Notched Panels at (c) 0.1 ϵ /min and (d) 0.5 ϵ /min.

is shown in Figure 4.7. Failure due mainly to fiber breakage and matrix cracking, with the specimen breaking into two parts, is represented as Type A damage. Type C failure is typified by severe outer ply splitting and a jagged fracture path, with the specimen remaining intact and held together by the split plies. Type B damage is combination of both Type A and Type C damages. It represents a failure mode with less severe splitting on the plies and a more defined fracture path. Photographs of representative panel failure tested at the four strain rates are shown in Figure 4.8 and Figure 4.9.

4.3 AS4/938 Tests Results

The results of testing AS4/938 unnotched and notched specimens at three strain rates are presented below.

4.3.1 Unnotched Coupon Results

The average failure stress of the AS4/938 tape layup unnotched coupon was 608 MPa and 598 MPa at strain rates of 0.0042 ϵ /min and 0.1 ϵ /min respectively. When the loading rate was increased to 2 ϵ /min, the average failure stress decreased to 565 MPa. The difference in average failure stress between the slowest and fastest rate was 7%. The tow placed unnotched specimens failed at about the same values as the tape specimens. At 0.0042 ϵ /min, the average failure stress was 589 MPa and at 0.1 ϵ /min, it was 605 MPa. At the highest loading rate of 2 ϵ /min, the average failure stress was 582 MPa. The strength results are tabulated in Table 4.3. Failure stresses for tape layup and tow placed unnotched coupons are plotted against measured strain rate in Figures 4.10 and 4.11.

The failure modes of the unnotched AS4/938 tape layup and tow placed coupons were similar. Also, there were no significant changes in

Table 4.3 Average Failure Stress of AS4/938 Specimens at Different Strain Rates

Average Failure Stress ^a (MPa)			
Strain Rate (ϵ /min)	Unnotched Coupons	Notched Coupon (19 mm Slit)	Notched Panel (51 mm Slit)
Tape Layup:			
0.0042	608 (4.4%)	279 (7.8%)	197 (8.0%)
0.1	598 (2.8%)	288 (12.2%)	189 (8.6%)
2	565 (4.4%)	227 (7.8%)	168 (16.5%)
Tow Placement:			
0.0042	589 (2.6%)	351 (3.1%)	290 (3.3%)
0.1	605 (1.9%)	370 (8.7%)	293 (3.9%)
2	582 (0.8%)	339 (7.1%)	263 (8.8%)

a 5 specimens tested in each case

b numbers in parentheses are coefficients of variation

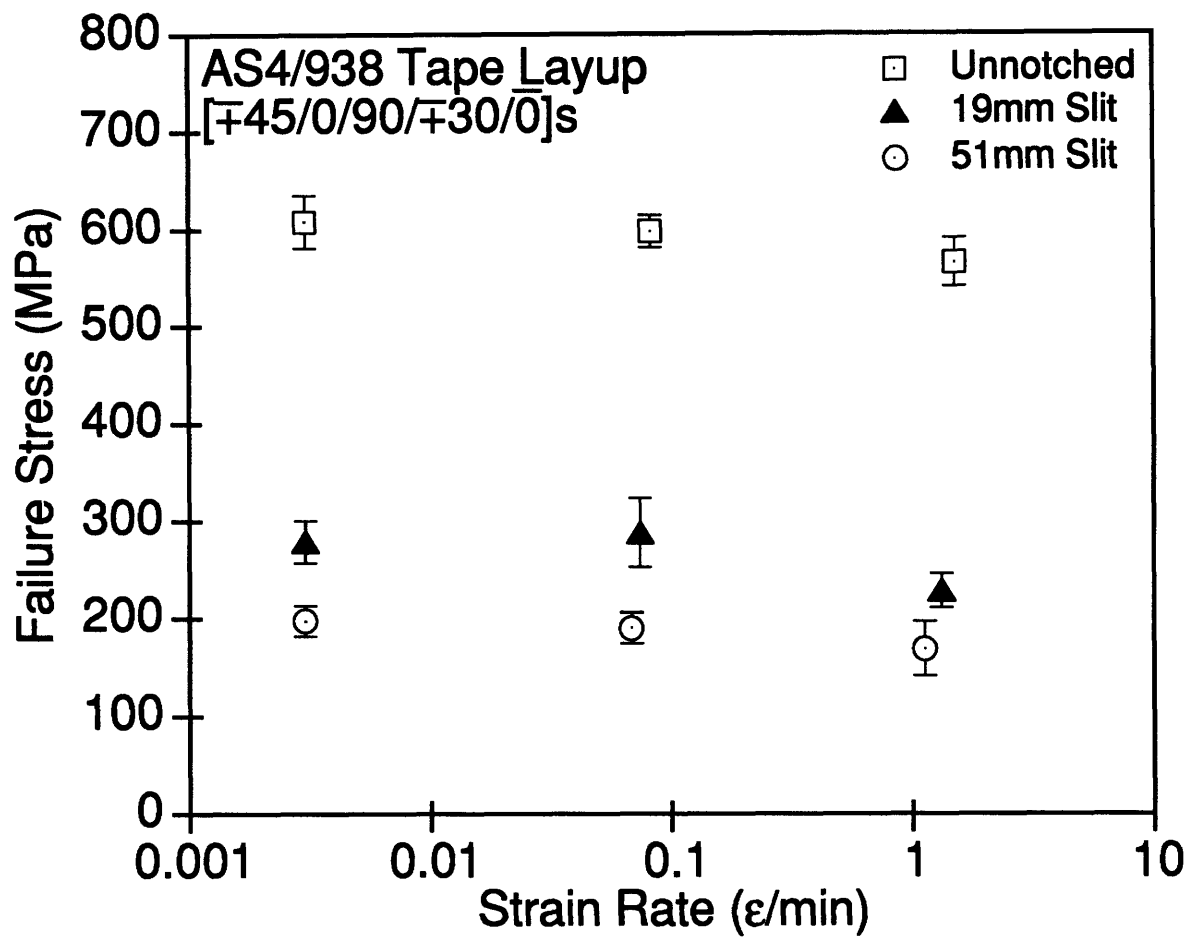


Figure 4.10 Average Failure Stress vs. Strain Rate for AS4/938 Tape Layup Specimens.

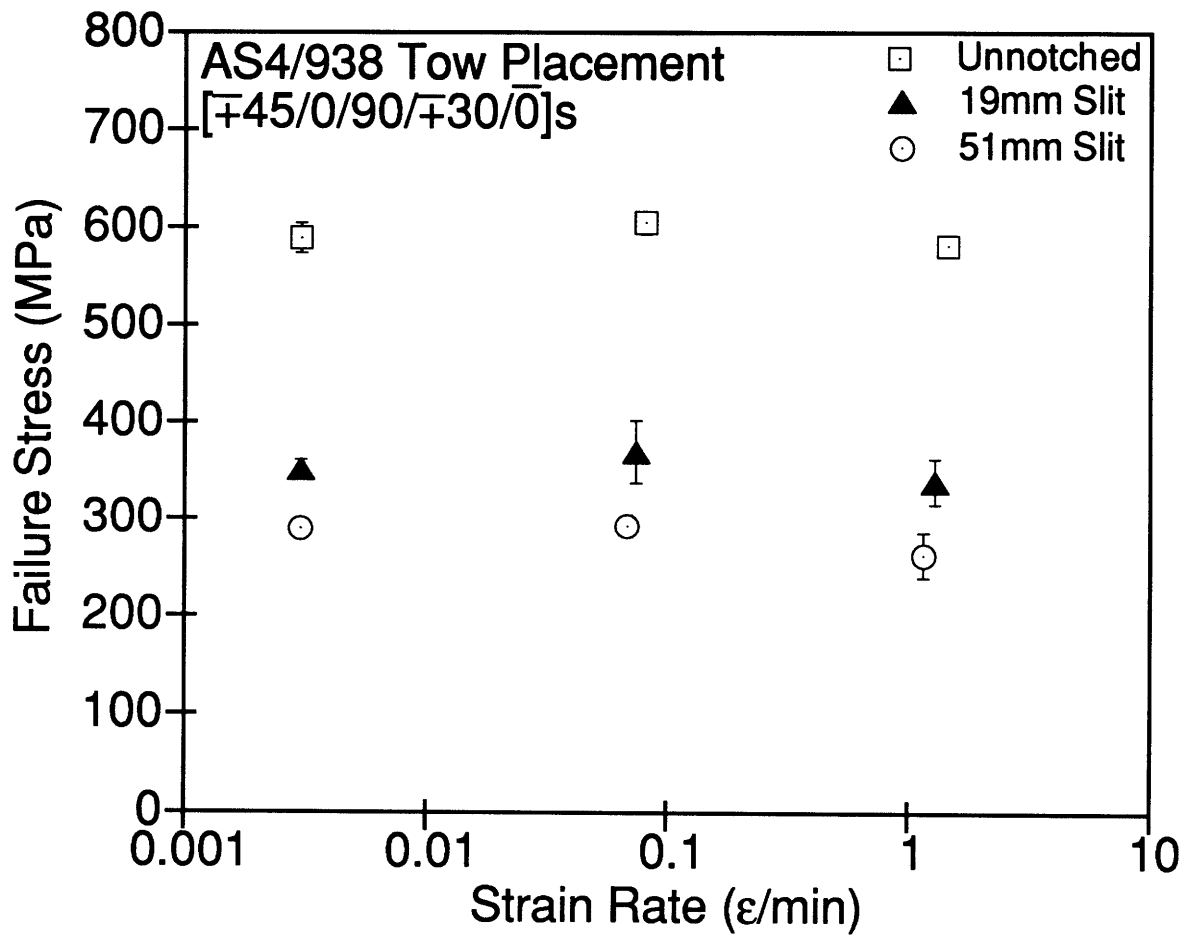
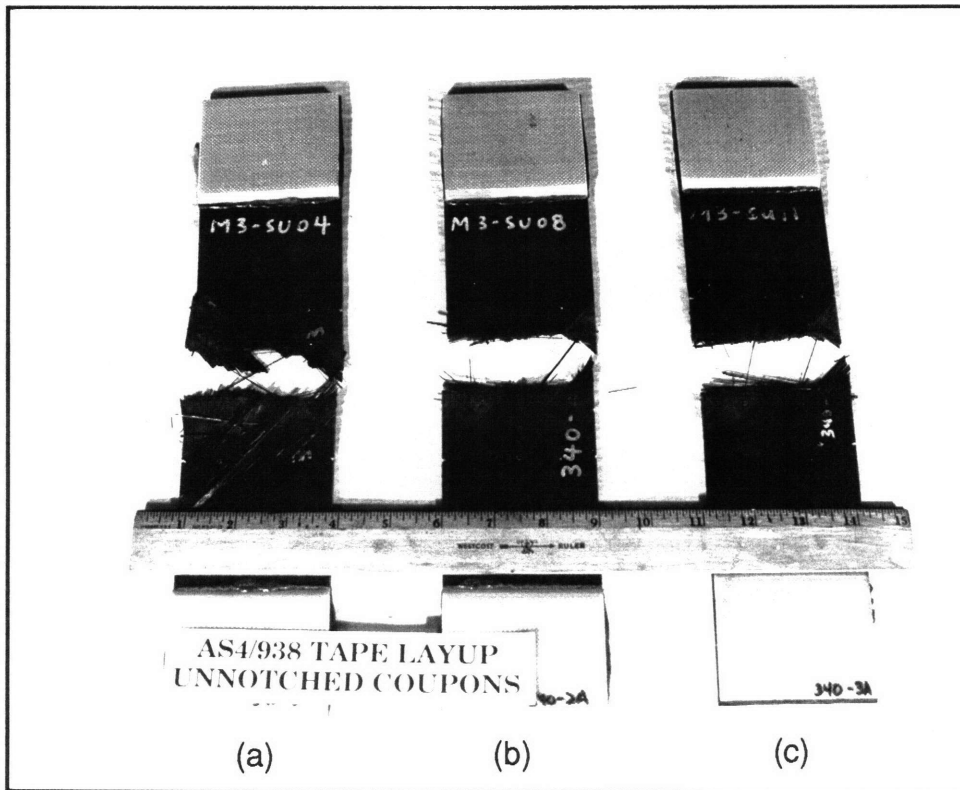


Figure 4.11 Average Failure Stress vs. Strain Rate for AS4/938 Tow Placed Specimens.

the failure modes for either type of specimen when the strain rates were varied. Sketches of the different failure modes described below are shown in Figure 4.2. All the specimens broke cleanly in the middle of the gage length. The fracture path was relatively straight and perpendicular to the loading axis. On the failure surface, bundle pullout was observed on the $\pm 45^\circ$ and $\pm 30^\circ$ plies. Fiber breakage was observed in the internal 0° plies and matrix cracking in the 90° plies. On the outer surfaces of the specimens, the $\pm 45^\circ$ plies delaminated. The delamination extended inwards from the failure surface and the delaminated surface broke after about 10 mm to 30 mm. A sketch of the failure modes of the AS4/938 unnotched coupon is shown in Figure 4.3. Representative photographs of the unnotched tape layup and tow placed coupons failed at different strain rates are shown in Figure 4.12 and Figure 4.13 respectively.

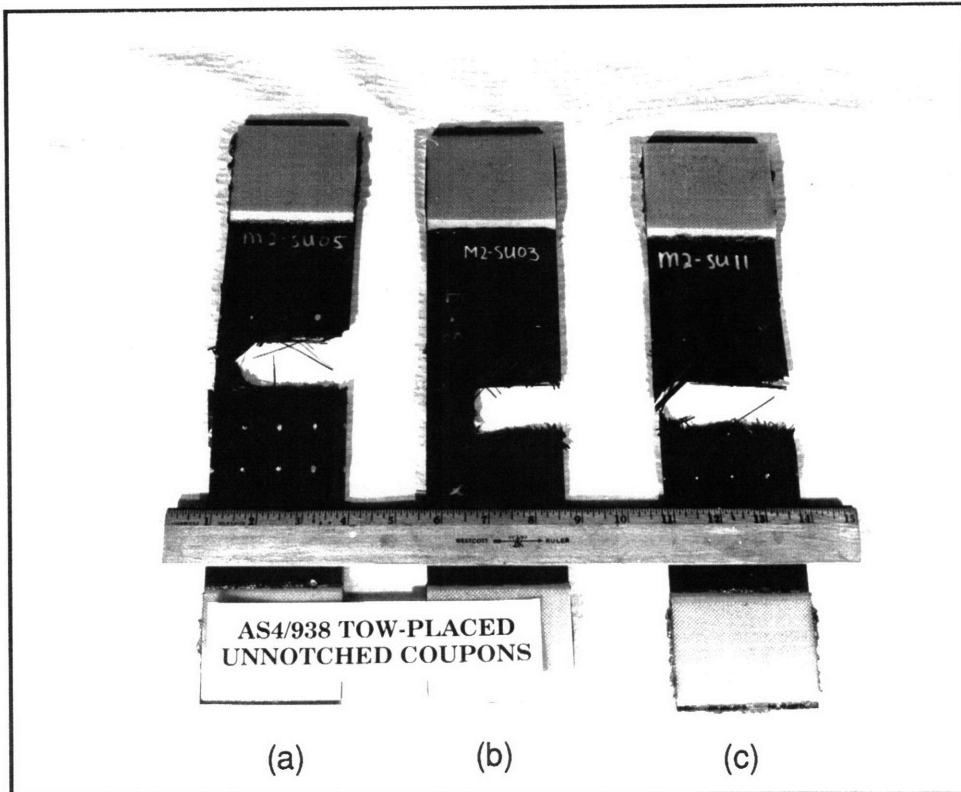
The stress-strain curves of the AS4/938 tape layup and tow placed unnotched coupons were similar. These curves at different strain rates are shown in Figure 4.14 and Figure 4.15 respectively. These specimens behaved linearly and the behavior was consistent at different strain rates. There were no visible load drops on the curves. However, 'clicks' were heard when testing the specimens at the slower strain rates.

For the tape layup specimens, the average longitudinal moduli were 60.7 GPa, 59.6 GPa and 61.7 GPa at increasing strain rates of 0.0042 ϵ /min, 0.1 ϵ /min and 2 ϵ /min respectively. Average laminate moduli for the tow placed coupons were 60.6 GPa, 62.2 GPa and 61.9 GPa at the equivalent strain rates. The laminate longitudinal modulus computed for this layup from CLPT was 62.7 GPa as shown in Table 3.3. The average laminate moduli obtained experimentally were within 3% of the value computed using CLPT.



Strain Rates: (a) 0.0042 ϵ /min
(b) 0.1 ϵ /min
(c) 2 ϵ /min

Figure 4.12 Photographs of Failed AS4/938 Tape Layup Unnotched Coupons at Different Strain Rates.



Strain Rates: (a) 0.0042 ϵ /min
(b) 0.1 ϵ /min
(c) 2 ϵ /min

Figure 4.13 Photographs of Failed AS4/938 Tow Placed Unnotched Coupons at Different Strain Rates.

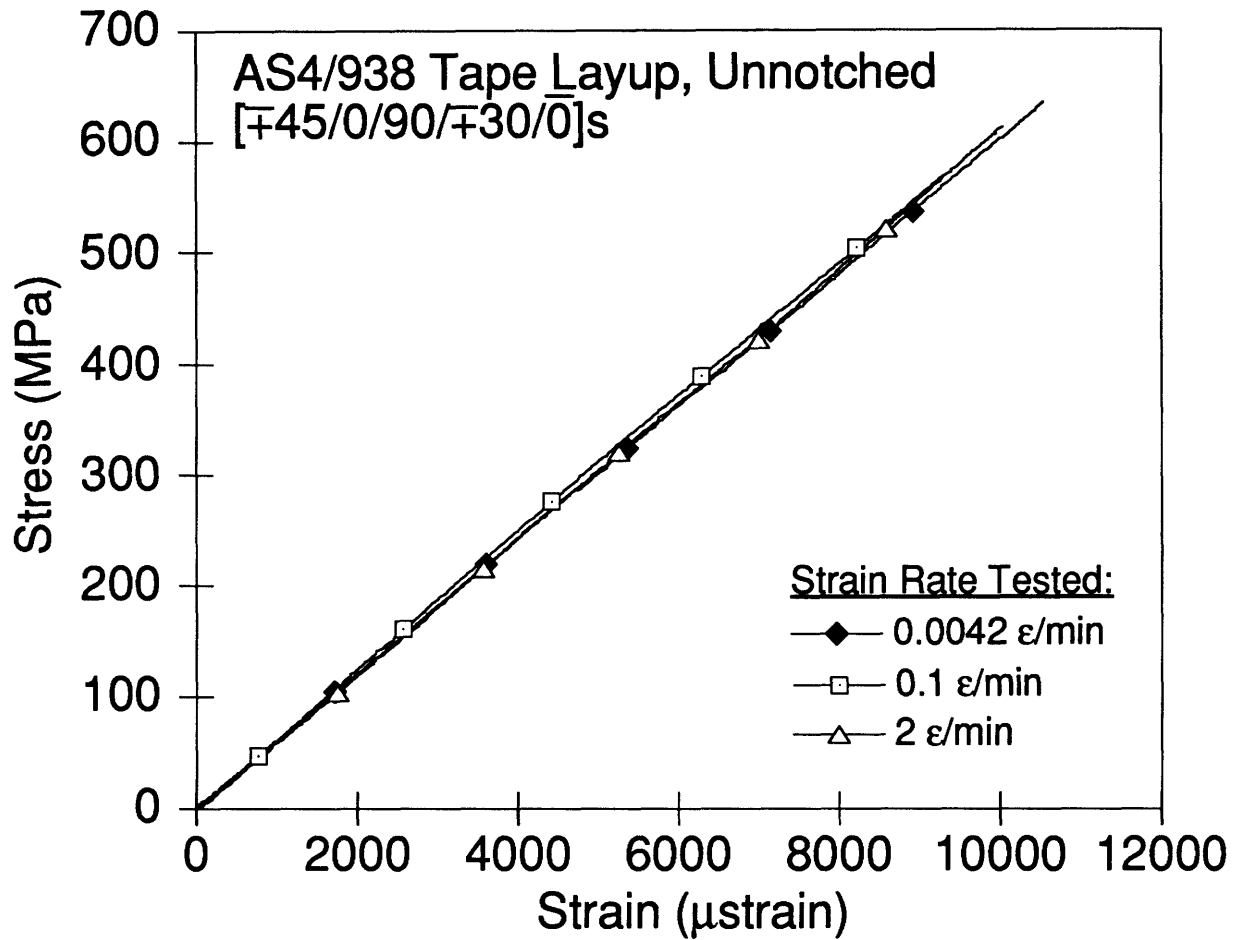


Figure 4.14 Stress-Strain Curves of AS4/938 Tape Layup Unnotched Coupons at Different Strain Rates.

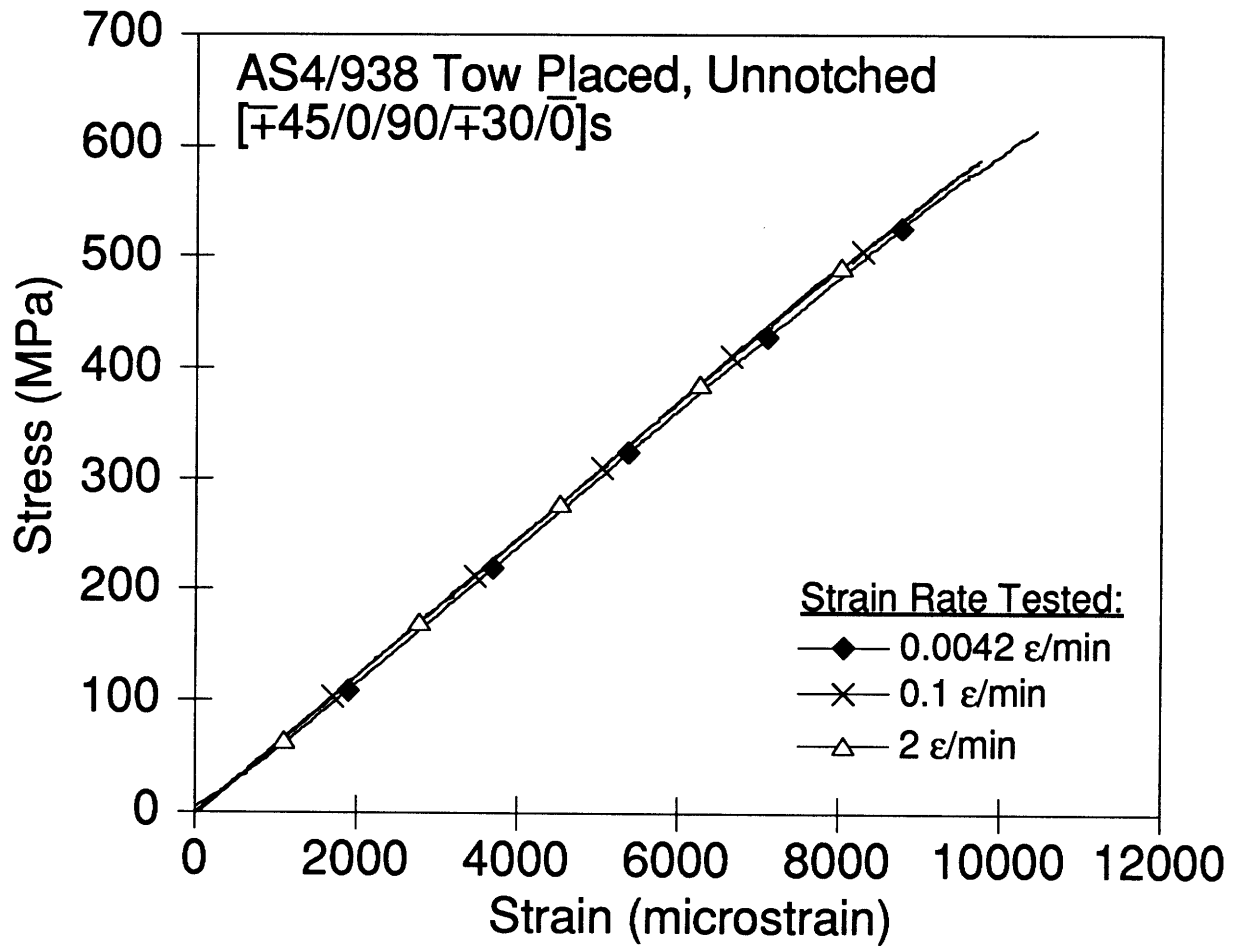


Figure 4.15 Stress-Strain Curves of AS4/938 Tow Placed Unnotched Coupons at Different Strain Rates.

Table 4.4 AS4/938 Unnotched Coupon Stiffness Data at Different Strain Rates

Strain Rate (ϵ/min)	Average Laminate Longitudinal Modulus (GPa)	Average Laminate Poisson's Ratio
Tape Layup:		
0.0042	60.7 (3.2%)	0.48 (2.4%)
0.1	59.6 (3.0%)	0.47 (3.0%)
2	61.7 (3.8%)	0.50 (3.2%)
Tow Placement:		
0.0042	60.6 (1.8%)	0.48 (6.2%)
0.1	62.2 (2.1%)	0.51 (5.3%)
2	61.9 (3.8%)	0.48 (4.6%)

^a numbers in parentheses are coefficients of variation

The laminate major Poisson's ratios for the tape layup and tow placed specimens were also insensitive to the strain rates tested. The Poisson's ratio calculated from CLPT was 0.46. The average experimental value obtained for the tape layup coupons at 0.0042 ϵ /min was 0.48. It was 0.47 at 0.1 ϵ /min and 0.50 at 2 ϵ /min. The average Poisson's ratios for the tow placement coupons were 0.48, 0.51 and 0.48 at 0.0042 ϵ /min, 0.1 ϵ /min and 2 ϵ /min respectively. Average laminate moduli and Poisson's ratios for the AS4/938 specimens, and their coefficients of variation, are shown in Table 4.4.

4.3.2 Notched Specimen Results

The average failure stress for tape layup notched coupons was 279 MPa at the strain rate of 0.0042 ϵ /min. At 0.1 ϵ /min, the average failure stress was 288 MPa and at 2 ϵ /min, the average failure stress decreased to 227 MPa. The difference in strength values between the slowest and fastest rates was 19%. Results obtained from the tape layup notched panels showed the same trend. At the 'static' rate of 0.0042 ϵ /min, the average failure stress was 197 MPa and at 0.1 ϵ /min, it was 189 MPa. When the loading rate was increased to 2 ϵ /min, the average failure stress was 168 MPa, a decrease of 15% from the 'static' rate.

Average failure stress results for the tow placed specimens showed less sensitivity to strain rates. Tow placed notched coupons failed, on the average, at 351 MPa, 370 MPa and 339 MPa at strain rates of 0.0042 ϵ /min, 0.1 ϵ /min and 2 ϵ /min respectively. From the 'static' strain rate of 0.0042 ϵ /min, the average failure stress increased by 5% at 0.1 ϵ /min and decreased by 3% at 2 ϵ /min. The average failure stresses for the tow placed panels were 290 MPa, 293 MPa and 263 MPa from the slowest to the highest

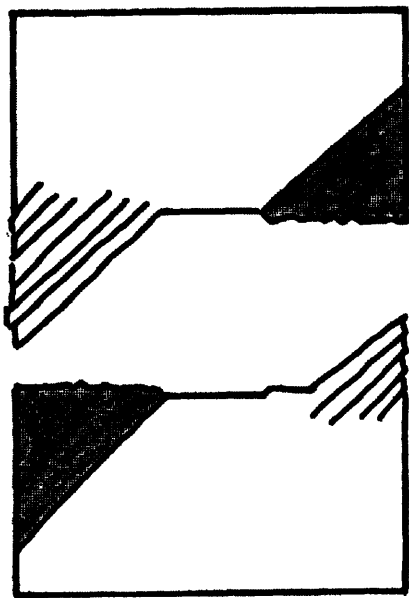
rate. The difference between the average failure stress of the panels at the slowest and fastest rate was 9%.

Notched specimens manufactured using automated tow placement exhibited higher failure strengths than those manufactured using manual tape layup. At 0.0042 ϵ /min, average failure stress differences between the tape layup and tow placed specimens were 26% for the coupons and 47% for the panels. At 0.1 ϵ /min, the differences were 28% for the coupons and 55% for the panels; and at 2 ϵ /min, the differences were 49% for the coupons and 56% for the panels. The average failure stresses and coefficients of variation for all notched specimens are summarized in Table 4.3. Failure stresses of the tape layup and tow placed specimens are plotted against measured strain rates in Figure 4.10 and Figure 4.11 respectively.

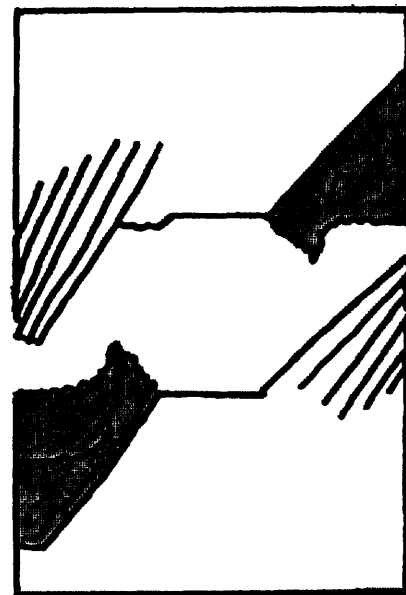
The tape layup and tow placed notched specimens had different failure modes. A sketch illustrating the differences in the failure modes of the notched tape layup and tow placed specimens is shown in Figure 4.16. Photographs taken of typical failed specimens of each type are shown in Figure 4.17. The failure modes were very consistent within each specimen type. They were not sensitive to strain rate.

The fracture path of the tape layup specimen was straight and perpendicular to the loading axis. The outer 45° plies on the top and bottom surfaces delaminated and split into strands about 30 mm long, which remained attached to the plies. Underneath, the rest of the laminate failed mainly due to fiber breakage and matrix cracking. The failure surface was smooth and straight.

The failure modes of the AS4/938 tow placed notched specimens were different. Failure initiated at the notch tip and the failure path was jagged and rough. The failure path did not cut through all the plies at the same



(a) AS4/938 Tape Layup, Notched



(b) AS4/938 Tow Placement, Notched

Key:

 Delaminated Area

 Matrix Splitting

Figure 4.16 Failure Modes of AS4/938 Tape Layup and Tow Placed Notched Specimens.

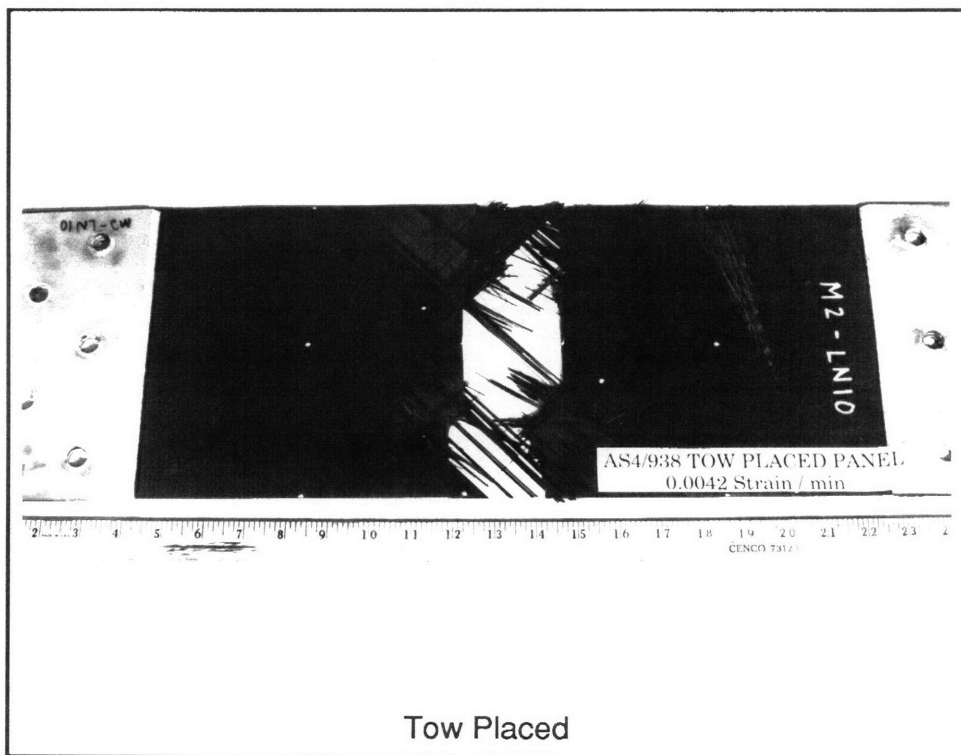
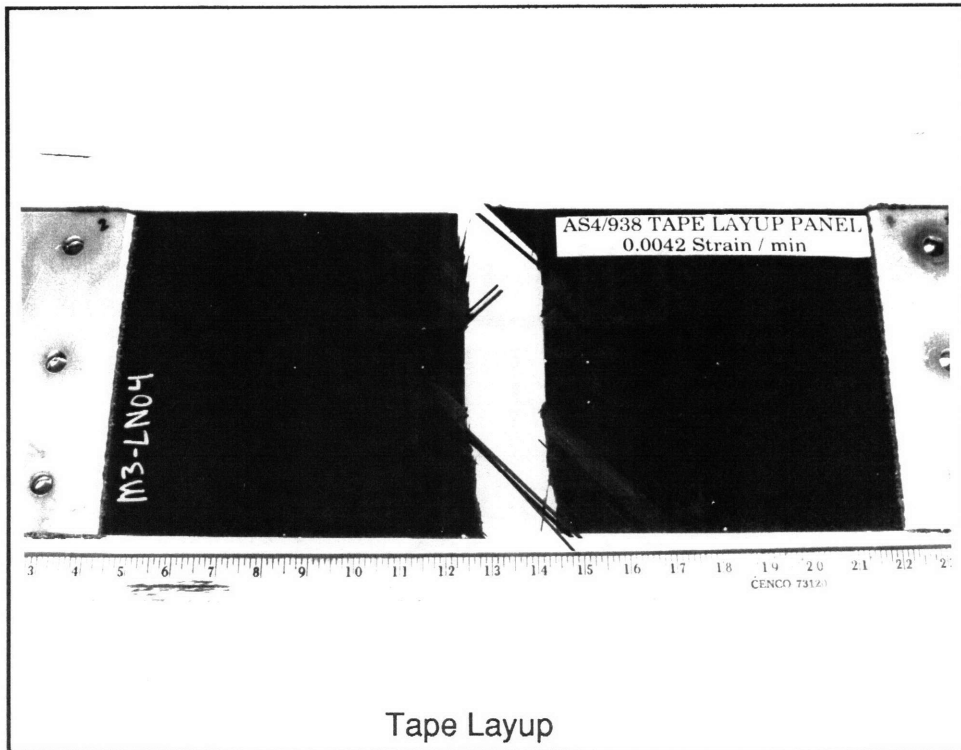
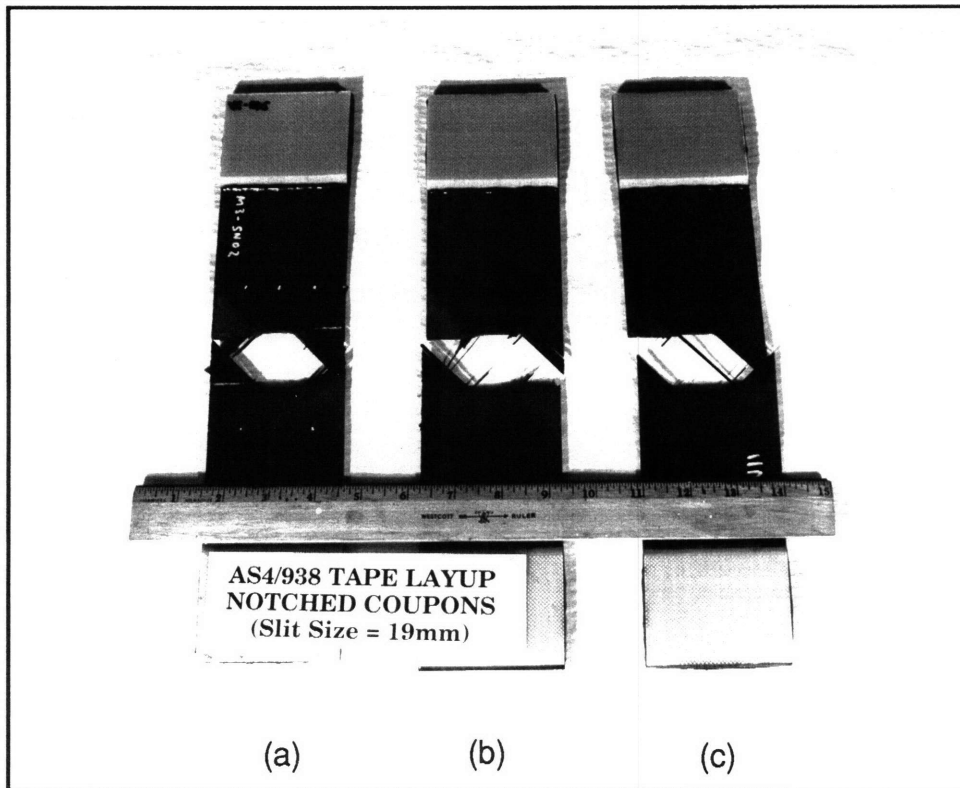
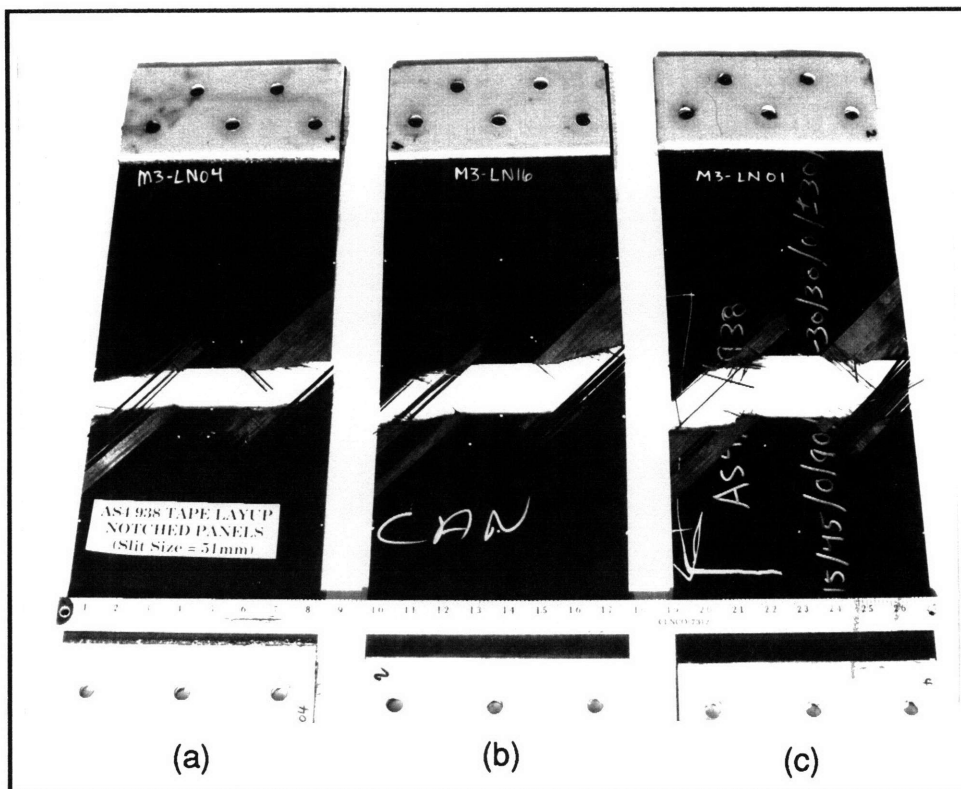


Figure 4.17 Photographs of Typical Failed AS4/938 Tape Layup and Tow Placed Notched Specimens.



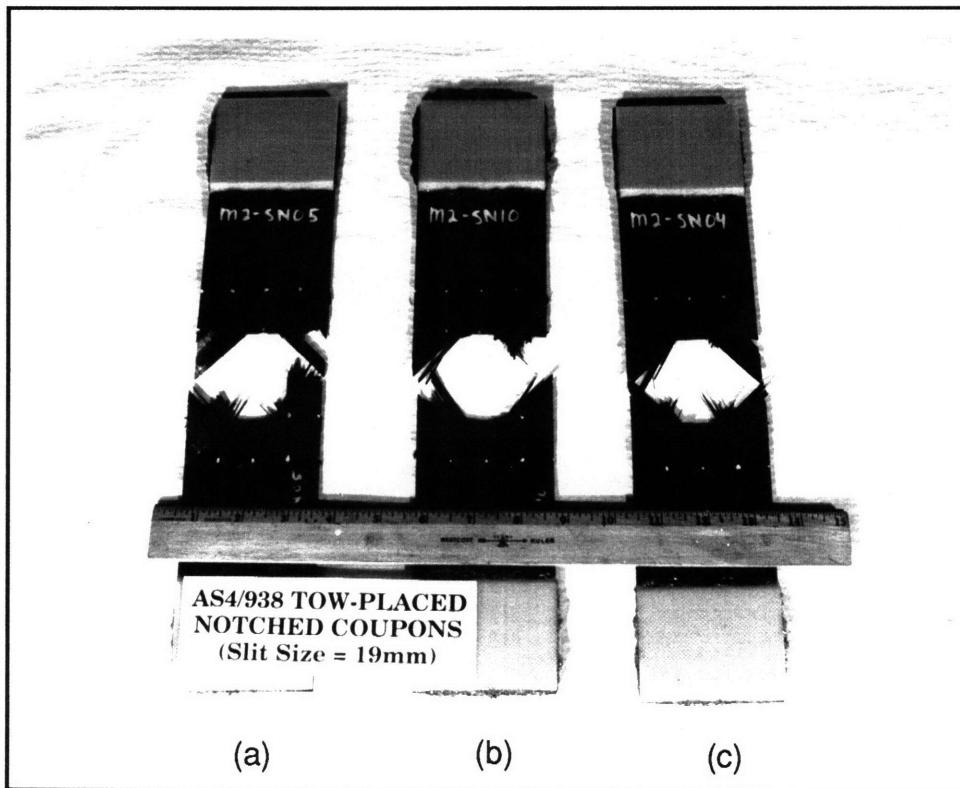
Strain Rates: (a) 0.0042 ϵ /min
(b) 0.1 ϵ /min
(c) 2 ϵ /min

Figure 4.18 Photographs of Failed AS4/938 Tape Layup Notched Coupons at Different Strain Rates.



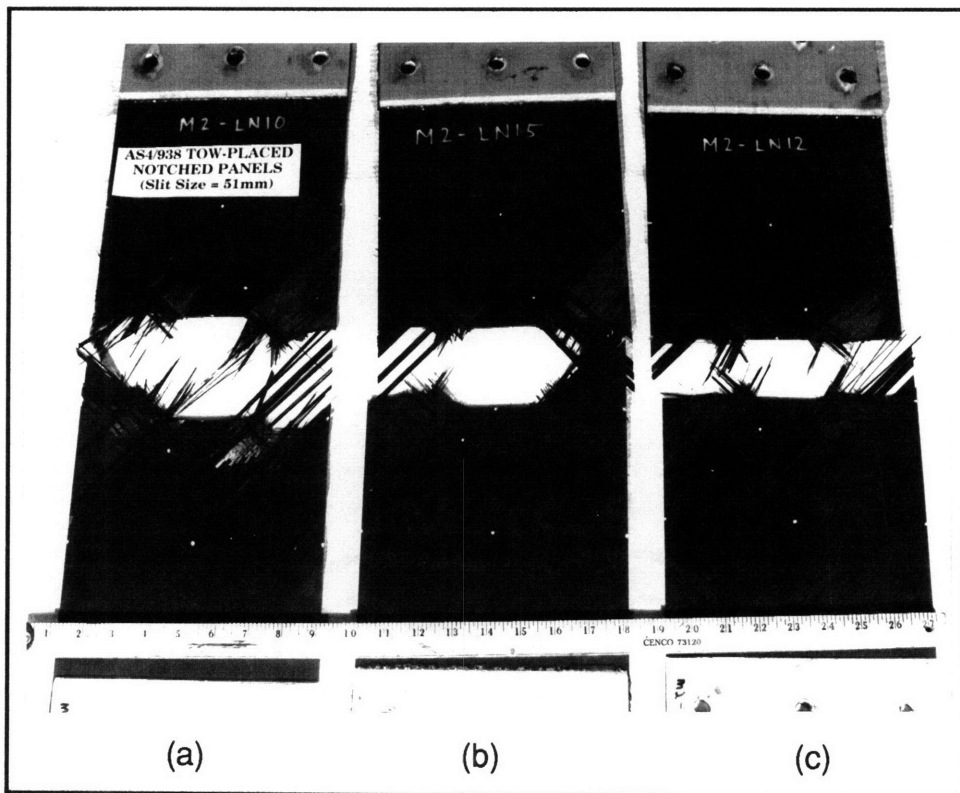
Strain Rates: (a) 0.0042 ϵ /min
 (b) 0.1 ϵ /min
 (c) 2 ϵ /min

Figure 4.19 Photographs of Failed AS4/938 Tape Layup Notched Panels at Different Strain Rates.



Strain Rates: (a) 0.0042 ϵ /min
(b) 0.1 ϵ /min
(c) 2 ϵ /min

Figure 4.20 Photographs of Failed AS4/938 Tow Placed Notched Coupons at Different Strain Rates.



Strain Rates: (a) 0.0042 ϵ /min
(b) 0.1 ϵ /min
(c) 2 ϵ /min

Figure 4.21 Photographs of Failed AS4/938 Tow Placed Notched Panels at Different Strain Rates.

location as different sets of plies were observed to have their own distinct failure surfaces. The 0° and 90° plies failed perpendicular to the loading axis due to fiber breakage and matrix cracking respectively; the other plies failed at an angle to the loading axis, notably, the 45° plies, which failed by matrix splitting. Delamination was present through the thickness of the specimens and it was especially severe at the outer 45° plies. Sketches of the failure modes described above are shown in Figure 4.2. Representative photographs taken of the AS4/938 tape layup specimens are shown in Figure 4.18 and Figure 4.19; representative photographs of the tow placed specimens are shown in Figure 4.20 and Figure 4.21.

4.3.3 Strain Distribution of Notched Panels

Twelve AS4/938 notched panels were instrumented with strain gages to monitor the strain distribution from the notch tip to the edge of the panels. Three strain gages were used. They were aligned along the axis of the slit. The distances from the notch tip to the centerline of the gages were 3 mm, 21 mm and 73 mm. Six tape layup and six tow placed panels had this strain gage arrangement. The panels were tested at the three strain rates, two at each rate.

Tape layup and tow placed panels showed identical strain distribution behaviors. They are averaged together and shown in Figure 4.22, Figure 4.23 and Figure 4.24 for panels tested at the three strain rates. Strain distribution plots for the individual panels tested are presented in Appendix C. Recorded strains at each gage location were normalized by the recorded far-field strains to produce the strain concentration factor. They were plotted against the distance from the notch tip to the specimen free edge.

The strain distributions were also compared to Lekhnitskii's analytical expression used for computing normal stresses ahead of a crack in a notched orthotropic laminate under uniaxial loading [52]. The expression used was:

$$\sigma_y(x,0) = \frac{\sigma_y^\infty x}{\sqrt{x^2 - a^2}} \quad (4.1)$$

The origins of the coordinates, x and y , are at the center of the crack with the x -axis in line with the crack and the y -axis on the centerline of the specimen. σ_y is the normal stress at the mid-plane ($y=0$) and the x coordinate ranges from a slight distance from the crack tip to the edge of the laminate. σ_y^∞ is the far-field stress corrected for finite width effects and the slit length is $2a$. This expression is independent of material properties and can be used for either isotropic or orthotropic laminates.

The finite width correction factor (Y_1) for isotropic materials was used in the computations. It was approximated by the expression [53]:

$$Y_1\left(\frac{2a}{W}\right) = 1 + 0.128\left(\frac{2a}{W}\right) - 0.288\left(\frac{2a}{W}\right)^2 + 1.52\left(\frac{2a}{W}\right)^3 \quad (4.2)$$

where $2a$ is the slit length and W is the width of the specimen. For the AS4/938 panels, the slit length to width of specimen ratio is 4, resulting in a finite width correction factor of 1.04.

In the plots, the normal stress corrected for finite width effects was normalized by the far-field stress. The resulting expression was used for plotting the prediction curves:

$$\frac{\sigma_y}{\sigma_{y(\text{far-field})}}(x,0) = \frac{1.04 x}{\sqrt{x^2 - a^2}} \quad (4.3)$$

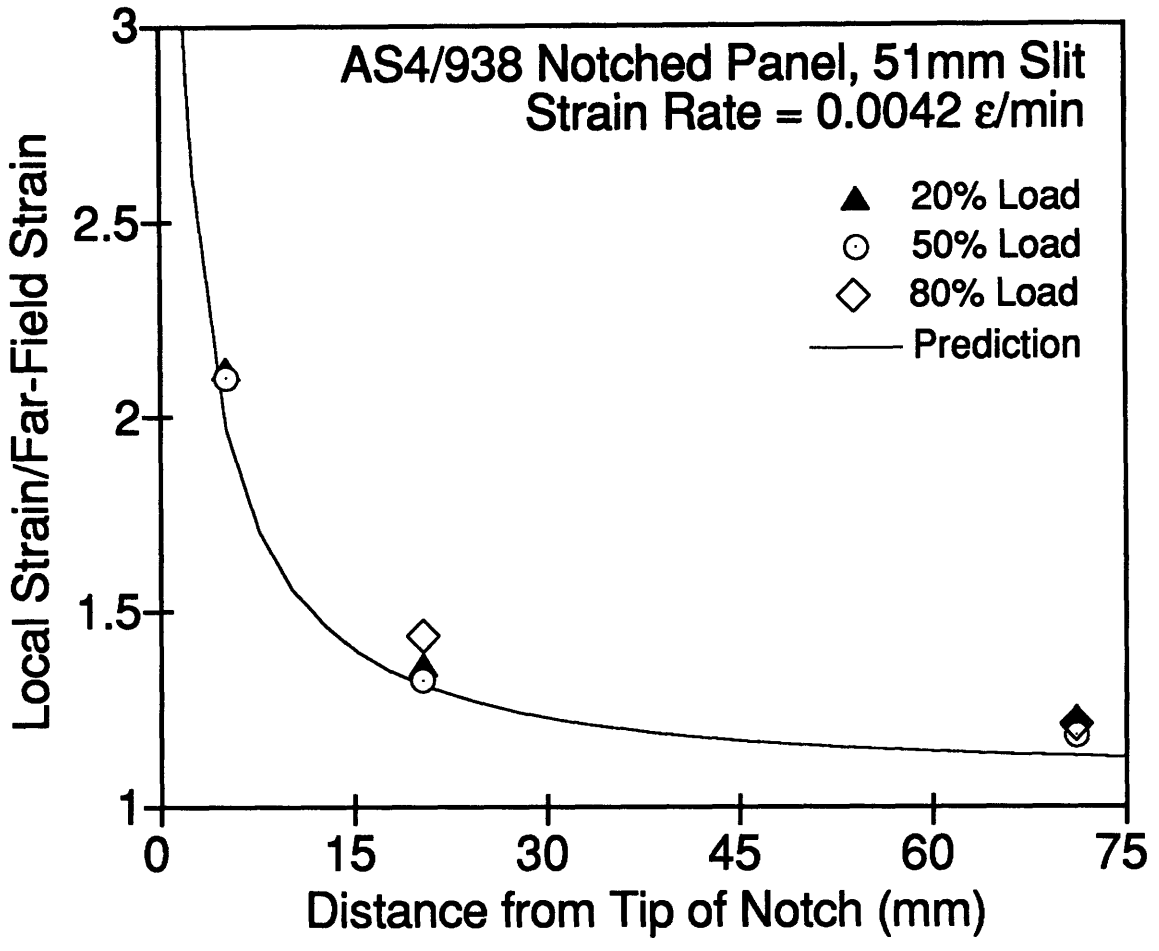


Figure 4.22 Average Strain Distribution of AS4/938 notched panel at 0.0042 strain/min.

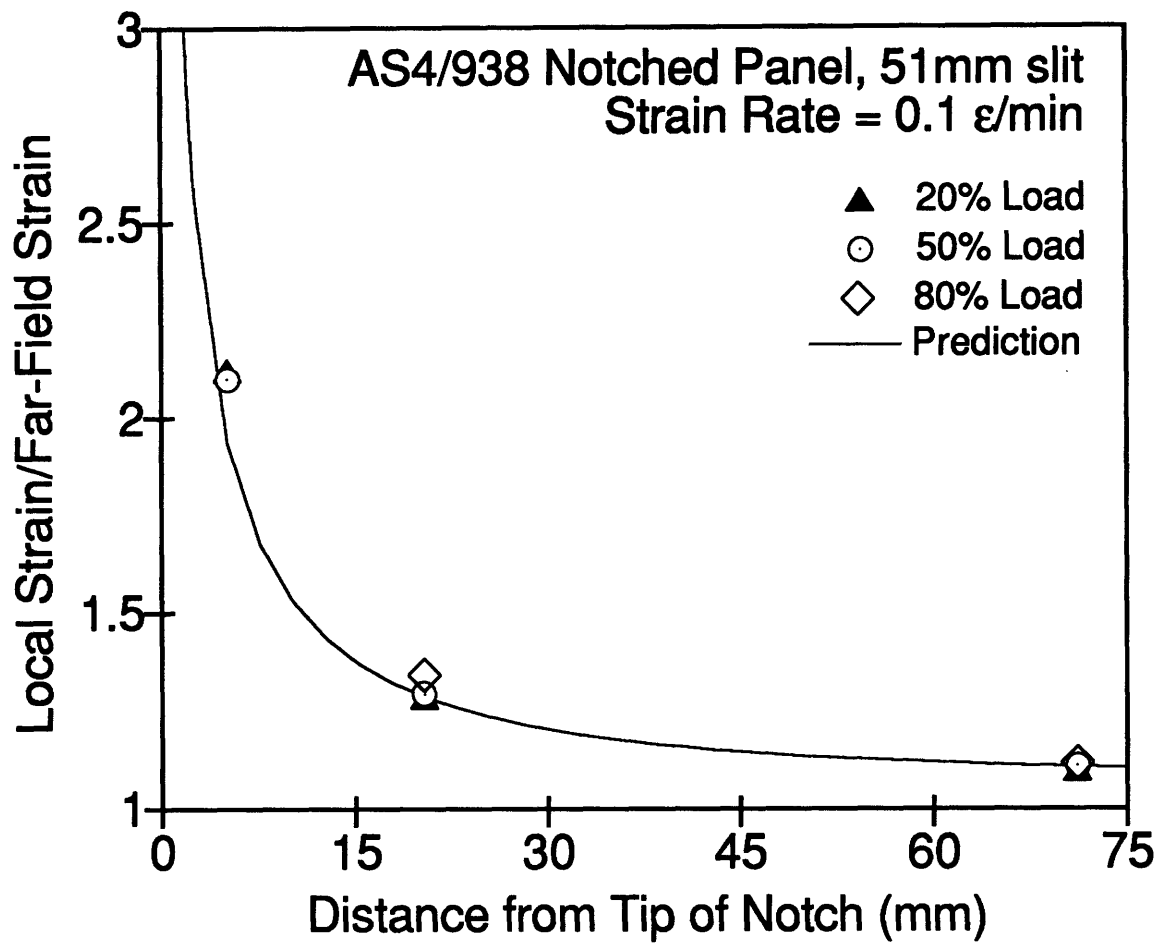


Figure 4.23 Average Strain Distribution of AS4/938 notched panel at 0.1 strain/min.

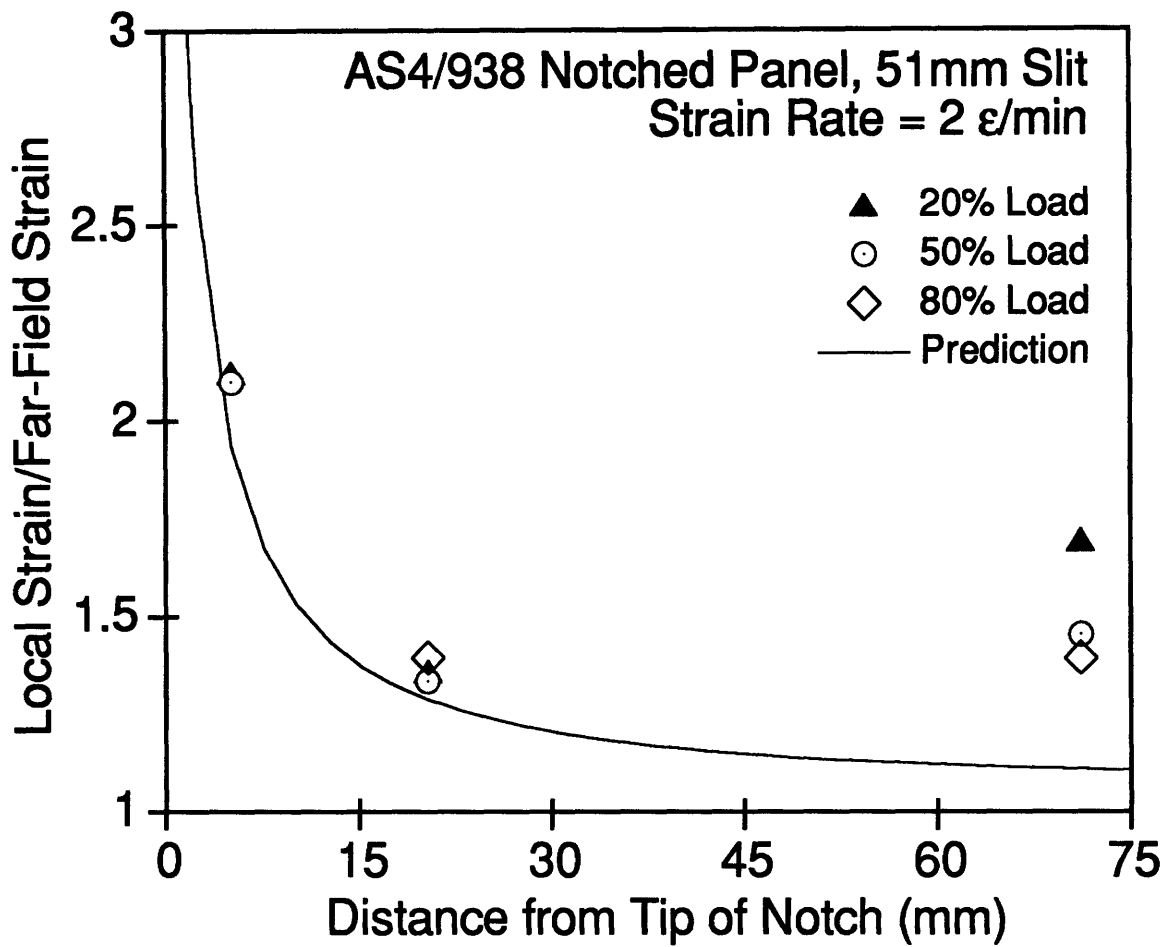


Figure 4.24 Average Strain Distribution of AS4/938 notched panel at 2 strain/min.

Also, the x-axis in the plots was shifted so that the origin was at the notch tip instead of the center of the slit. The above stress concentration was assumed to be the same as the strain concentration at low loads. This will be true as long as the laminate modulus remains constant.

At $0.0042 \text{ } \epsilon/\text{min}$, as shown in Figure 4.22, the average strain concentration recorded at 20% of the maximum stress agreed with the analytical prediction at all the three locations on the panel. When the stress level was increased to 50%, the average strain concentration recorded at the gage nearest to the notch tip increased. The strain concentrations at the other two locations remained the same. At 80% of the maximum stress level, the gage at the notch tip produced erratic readings. The middle gage showed a substantial increase in average strain concentration and the gage at the edge also recorded a slight increase in average strain concentration. The strain behavior of the laminate tested at $0.1 \text{ } \epsilon/\text{min}$, as shown in Figure 4.23, was very similar to that at $0.0042 \text{ } \epsilon/\text{min}$.

Tests conducted at $2 \text{ } \epsilon/\text{min}$ for both tape layup and tow placed panels showed a peculiar strain distribution. The average strain distribution is shown in Figure 4.24. At 20% of the maximum stress, the strain concentrations recorded at the notch tip and middle gages were similar to that predicted by the analytical expression. However, the strain concentration at the third gage located at the edge of the panel was higher than the predicted value. This phenomenon was consistent for strain concentrations compiled for all the tests conducted at $2 \text{ } \epsilon/\text{min}$. It was also independent of specimen type.

The consistency of the strain gage recordings at the panels edge at $2 \text{ } \epsilon/\text{min}$ rule out experimental error or the existence of test artifacts. Also, the behavior cannot be attributed to the different specimen type: tape layup

and tow placed specimens behaved similarly. Upon reexamining the failed specimens, it was found that these gages had been attached to material damaged during specimen cutting. The top plies were badly split and delaminated for about 3 mm in from the cut edge and the gages had been attached to this damaged material. The results hint that edge effects may be strain rate dependent, but it is unclear if this effect contributes to specimen failure. It was observed in both the strain rate sensitive tape layup panels and the strain rate insensitive tow placed panels.

4.3.4 Mar-Lin Correlation of Notched Specimens

Failure stresses of the notched AS4/938 specimens were correlated to the Mar-Lin equation (2.2) and used to determine laminate fracture parameter. The value for the stress singularity (m) was set at 0.28. The laminate fracture parameter (H_C) was calculated individually for each specimen tested. The measured slit size was used in this calculation. The H_C values were then averaged for each strain rate and specimen type. The average fracture parameter for the AS4/938 notched tape layup and tow placed specimens is shown in Table 4.5. Mar-Lin curves relating failure stresses to slit length were plotted using these average values of H_C . Figure 4.25, Figure 4.26 and Figure 4.27 show the individual failure stresses of the tape layup and tow placed specimens plotted with the Mar-Lin curves at 0.0042 ϵ/min , 0.1 ϵ/min and 2 ϵ/min respectively. The measured slit lengths were used in these plots.

The laminate fracture parameter, H_C , is a measure of the damage tolerance of the specimens. The results showed good correlation between the experimentally obtained failure strengths and the Mar-Lin predictions. This correlation reinforces the previously noted result that although the

unnotched failure strengths are relatively independent of manufacturing techniques and strain rates, the damage tolerance is strongly dependent on both of these parameters.

Table 4.5 Average Mar-Lin Fracture Parameter (H_C) for AS4/938 specimens at Different Strain Rates

Strain Rate (ϵ/min)	H_C ($\text{MPa} \cdot \text{mm}^{0.28}$)	Coefficient of Variation
Tape Layup:		
0.0042	612	8.0%
0.1	610	12.4%
2	508	12.2%
Tow Placement:		
0.0042	840	5.1%
0.1	865	6.5%
2	783	7.5%

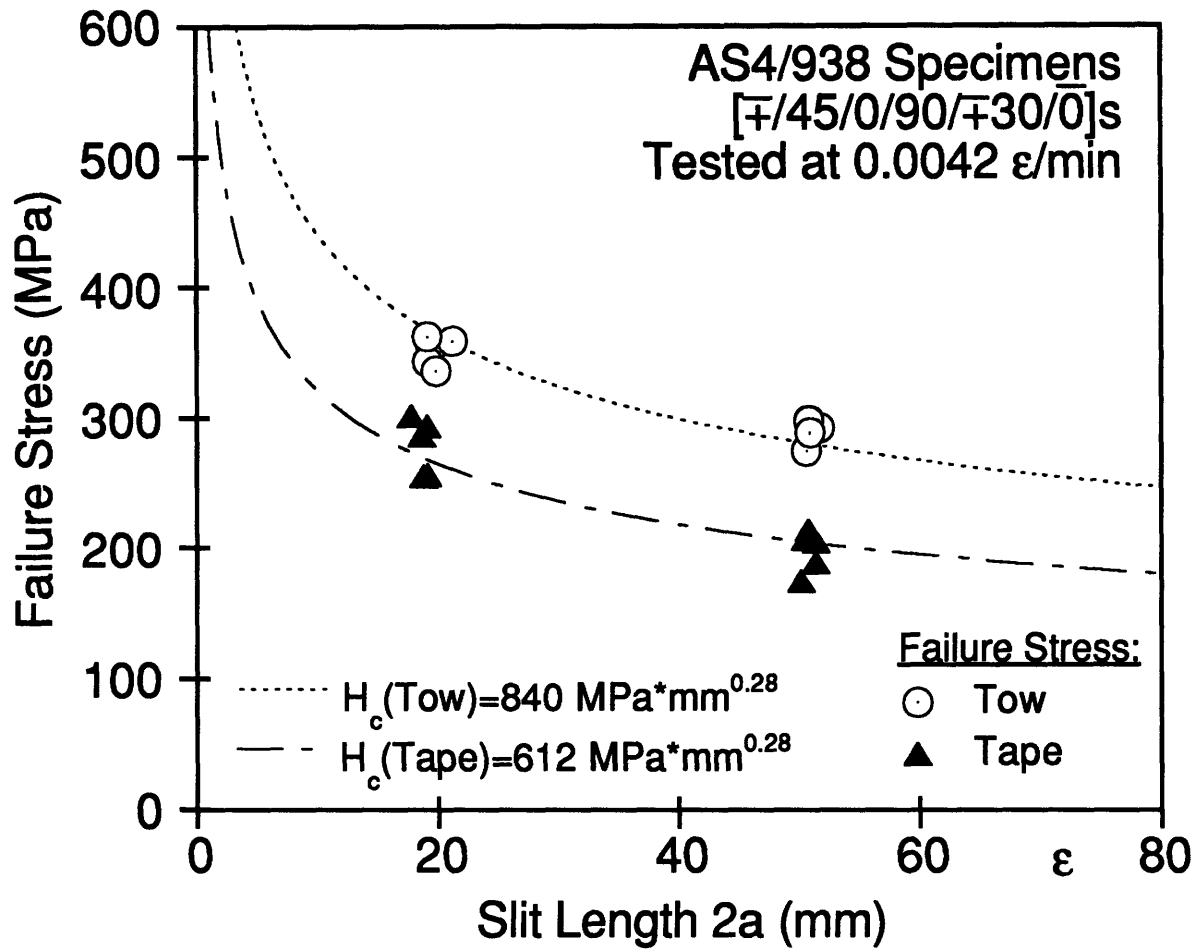


Figure 4.25 AS4/938 Notched Failure Stresses and Fracture Prediction Curve at $0.0042 \text{ } \epsilon/\text{min}$.

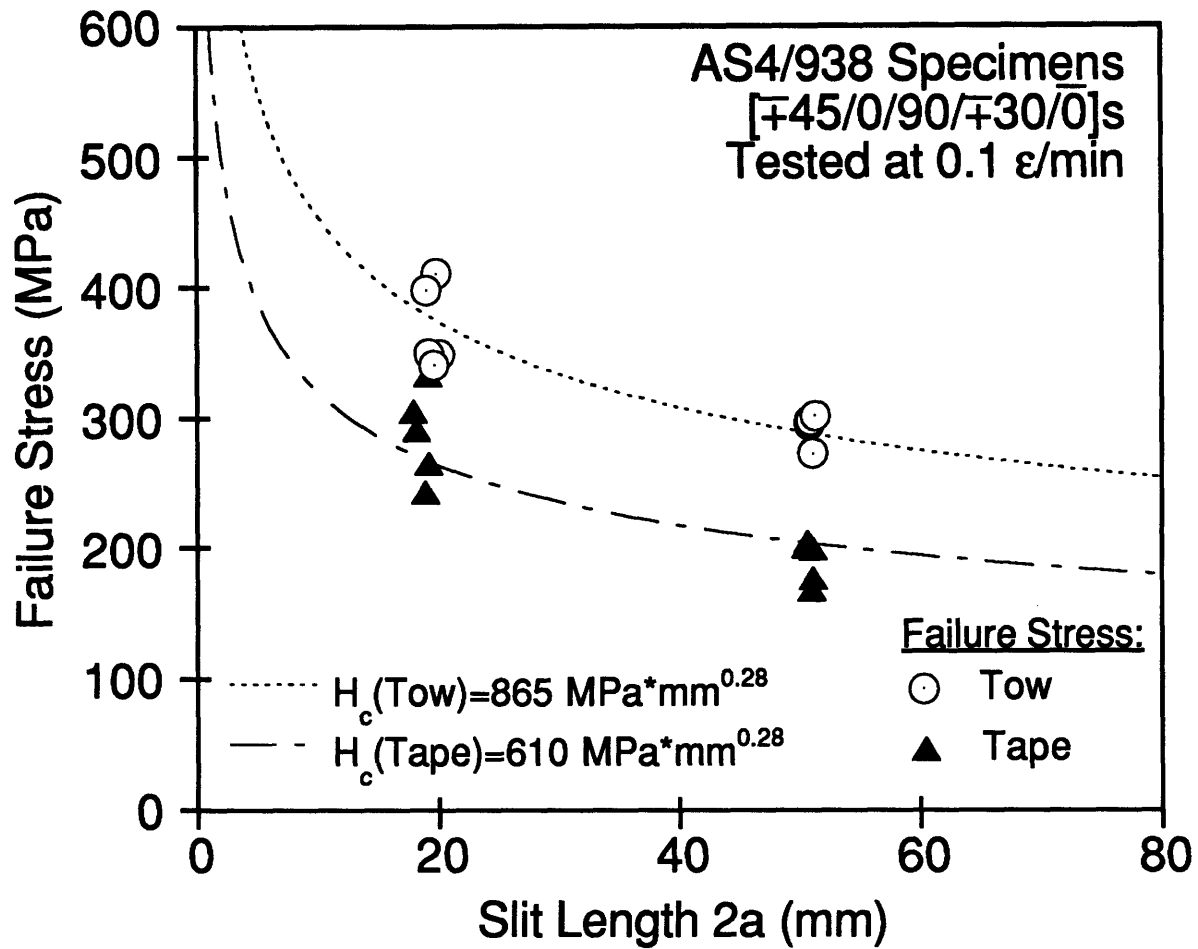


Figure 4.26 Notched AS4/938 Specimens Failure Stresses and Fracture Prediction Curve at $0.1 \epsilon/\text{min}$.

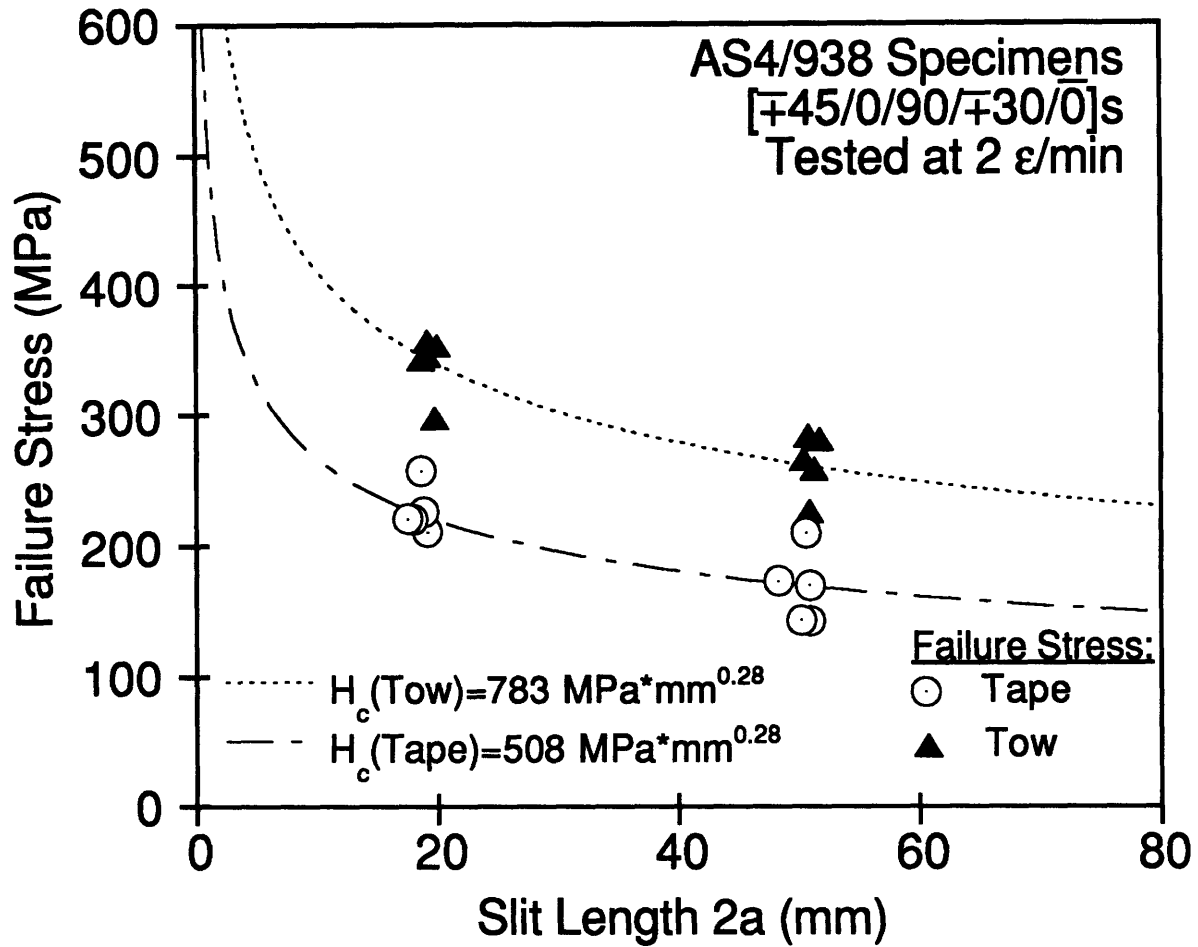


Figure 4.27 AS4/938 Notched Failure Stresses and Fracture Prediction Curve at 2 ε/min.

Chapter 5

DISCUSSION

In this chapter, a discussion of the experimental results is presented. Trends observed in the behavior of laminate failure under varying strain rates are identified and possible explanations proposed.

5.1 Strain Rate Effects on IM7/977-2 Specimens

The results of tests conducted on the IM7/977-2 unnotched and notched specimens are discussed below.

5.1.1 Unnotched Coupons

The failure modes, failure stresses, laminate longitudinal moduli and Poisson's ratios observed and measured for the IM7/977-2 unnotched coupons are insensitive to the range of strain rates tested.

The failure of the unnotched coupons is analyzed using a progressive failure model implemented as a computer code dubbed MCLAM. The model utilizes Tsai-Wu's stress quadratic interaction criterion [5]. Progressive failure in this analysis is achieved by reducing the transverse and shear moduli of failed plies by 0.5. The plies' longitudinal modulus and major Poisson's ratio remain unchanged. The predicted stress-strain behavior of the unnotched specimens is shown in Figure 5.1. The experimental stress-strain curves used in the plot are obtained from typical tests conducted at 0.005 ϵ /min and 0.5 ϵ /min. The prediction correlates well with the experimental results. Load drops in the experimental stress-strain curves and final failure of the coupons are fairly well predicted by the model. Load drops corresponding to failure of the $\pm 45^\circ$ plies are most

distinct in the experimental stress-strain curves. Audible clicks heard and recorded during the tests coincide with the observed load drops.

The layup of the IM7/977-2 specimens is fairly 'soft' compared to that of the AS4/938 specimens. The non-zero plies are oriented at 45°, 60° and 90°. Also, the resin type 977-2 is a 'toughened' resin. The layup softness and resin toughness combine to produce a progressive type of failure in these laminates.

5.1.2 Notched Panels

Failure stresses of the IM7/977-2 notched panels are insensitive to the range of strain rates tested. The average failure stress of the panels is about 45% of the unnotched failure stress. The IM7/977-2 tape layup panels are less notch sensitive than the AS4/983 tape layup panels.

Strain readings collected for a typical notched panel are shown in Figure 5.2. The curve representing the notch tip strain is fairly linear initially. At a modest fraction (less than 60%) of the final failure time, kinks start to appear and the curves become non-linear. The kinks in the curve are responses to a decrease in stiffness in the region near the strain gage due to damage beneath the gage. When these kinks occur in the readings from the gage situated closest to the notch tip, the onset of failure is implied. The applied load at which the kinks first occur is recorded and assumed to represent the failure initiation load.

The average far-field stresses at which the initiation of failure occurs in the notched panels are tabulated in Table 5.1. The recorded stresses are also normalized by the final failure stresses. Representative plots of the notch tip strain at the different strain rates are shown in Figure 5.3. The results show that the failure initiation stresses for the panels are similar at

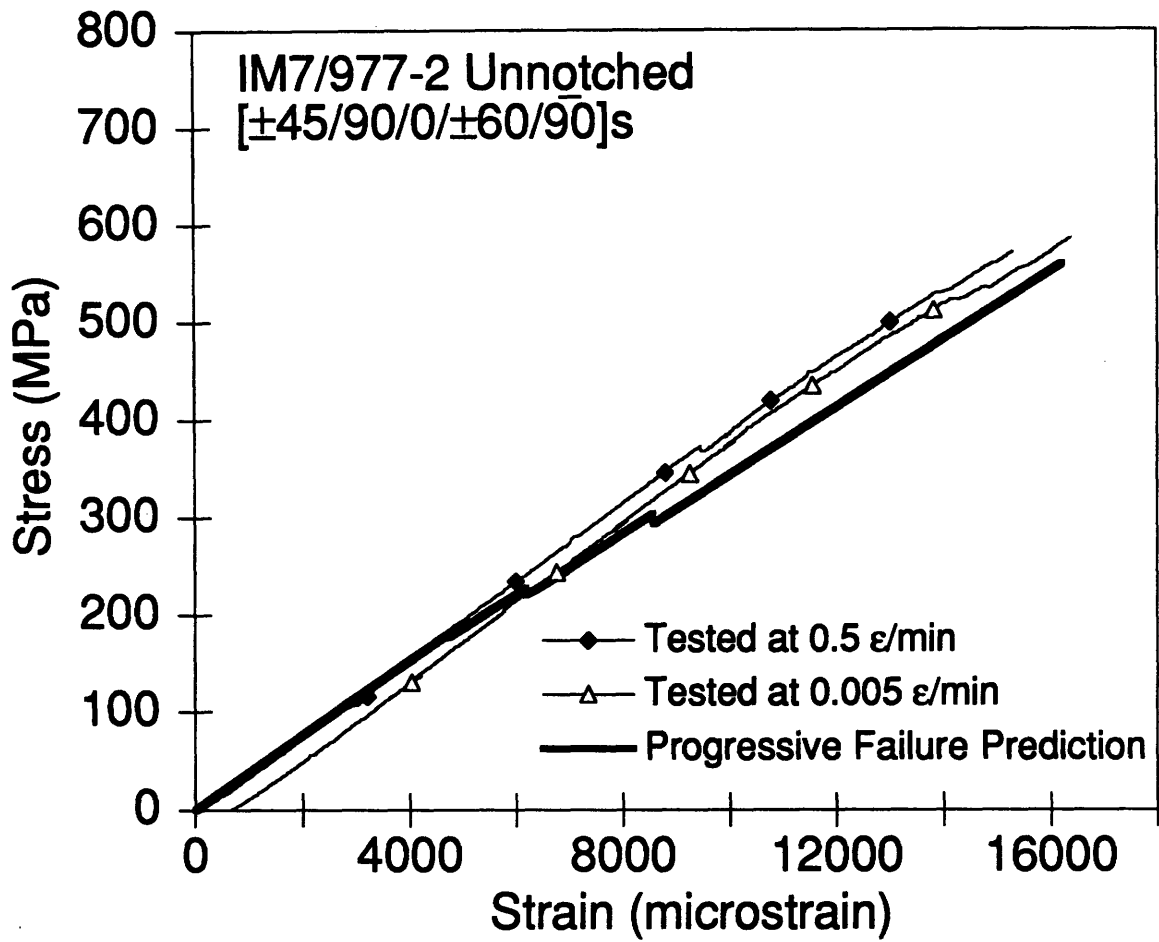


Figure 5.1 Experimental and Predicted Stress-Strain Curves of IM7/977-2 Unnotched Coupons.

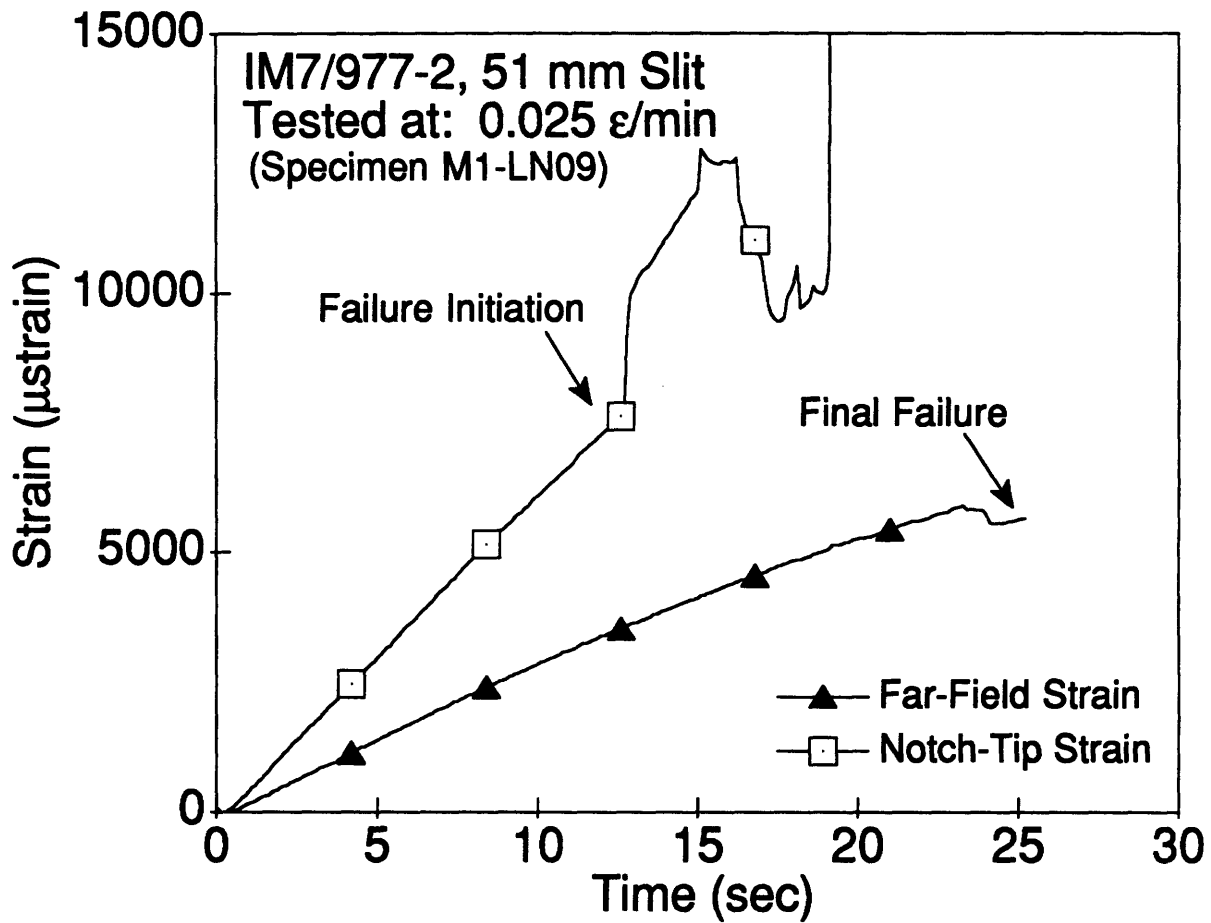


Figure 5.2 Strain Readings Collected of Typical IM7/977-2 Notched Panel.

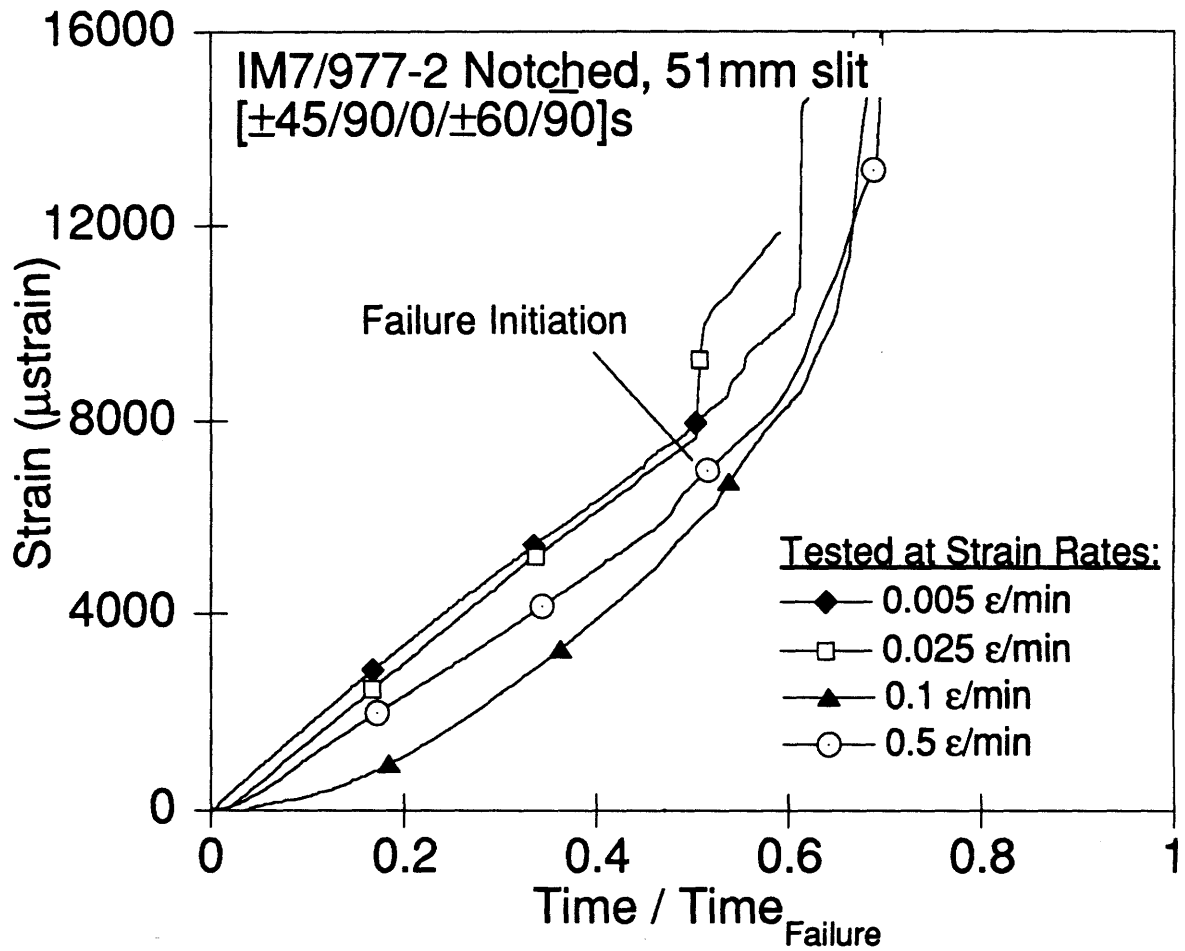


Figure 5.3 Plot of Notch Tip Strain versus Normalized Time of Representative IM7/977-2 Notched Specimens at Different Strain Rates.

Table 5.1 Average Stress at Failure Initiation and Ratio of Initiation Stress to Failure Stress for the IM7/977-2, 51 mm Notched Specimens

Strain Rate (ϵ/min)	Stress (MPa)	$\frac{\text{Stress}_{\text{initiation}}}{\text{Stress}_{\text{failure}}}$
0.005 ^a	147 (6.4%) ^c	0.56 (7.0%)
0.025 ^a	147 (3.9%)	0.56 (0.7%)
0.1 ^a	153 (4.1%)	0.59 (5.0%)
0.5 ^b	152 (4.0%)	0.59 (11.6%)

^a Data collected for 2 specimens

^b Data collected for 3 specimens

^c numbers in parentheses are coefficients of variation

all strain rates tested. Failure initiation in the IM7/977-2 notched panels is insensitive to strain rates.

The appearances of the failed notched specimens are different at different strain rates. The failure path at the slowest strain rate is straight and well defined. As the strain rate increases, the failure path becomes jagged, accompanied by severe matrix splitting on the outer plies.

Strain rate effects on the IM7/977-2 notched panels are only evident in the progression of final failure. The difference in failure modes observed is a post failure initiation phenomenon. Varying strain rates affect the path at which the final fracture propagates through the specimens and hence the appearance of the failed specimens. The duration of time for tests conducted at 0.5 ϵ /min is very short, the panels fail in 1.5 sec. Matrix splitting on the outer plies that accompanied failure propagation left strands of material that did not break completely. The strands are lifted from the surfaces and they continue to hold the panel together. Failure progression that results in a straight fracture path may be hindered. At the slower strain rates, failure progresses gradually. There is enough time for matrix splits to break cleanly and a straight fracture path to form.

5.2 Strain Rate Effects on AS4/938 Specimens

Discussion of results of tests conducted on the AS4/938 unnotched and notched specimens are presented below.

5.2.1 Unnotched Coupons

The failure stresses obtained for the tape layup and tow placed unnotched coupons show little sensitivity to strain rates. The average failure stress of the tape layup unnotched coupons decreases slightly (by

7%) when the strain rate is increased to 2 ϵ /min. The failure stresses of the tow placed unnotched coupons show no strain rate sensitivity.

The measured laminate longitudinal moduli and major Poisson's ratios of the two specimen types are similar and insensitive to strain rate. Also, these values agree with those calculated from CLPT. Failure modes of the AS4/938 tape layup and tow placed unnotched specimens are also similar and insensitive to strain rates.

The stress-strain behavior of the AS4/938 unnotched coupons are independent of strain rate and manufacturing technique. The progressive failure model, MCLAM, is used to analyze the failure of the AS4/938 unnotched coupons. The predicted stress-strain behavior is plotted with those typical of a tape layup and tow placed coupon. This is shown in Figure 5.4. The model over-predicts the failure strength of the unnotched coupons. The specimens tested fail at lower stresses and strains. On the prediction curve, distinct load drops are observed at about 600 MPa and 700 MPa, corresponding to failure of the 45° and 30° plies respectively. Predicted failure of the 45° plies coincided with final failure of the coupons tested. This implies that the AS4/938 unnotched coupons did not survive the failure of the $\pm 45^\circ$ plies.

The layup of the AS4/938 specimens is stronger than that of the IM7/977-2 specimens. The 60° plies are replaced by the 30° plies. Also, resin type 938 is an untoughened resin. The lack of load drops in the experimental stress-strain curves of the unnotched AS4/938 coupons indicates a less progressive type of failure. The curves behave almost linearly throughout the loading at all strain rates.

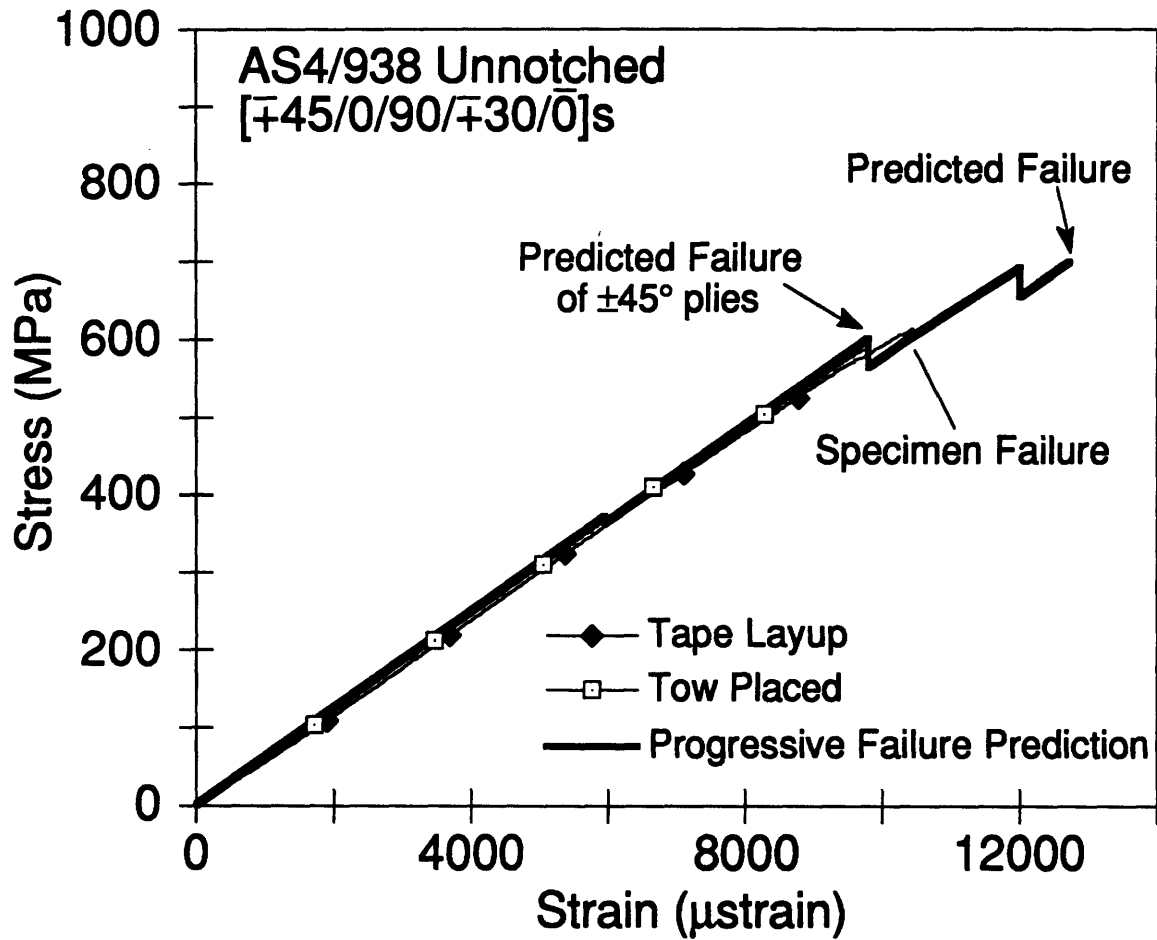


Figure 5.4 Experimental and Predicted Stress-Strain Curves of AS4/938 Unnotched Coupons.

5.2.2 Notched Specimens

Failure strengths of the AS4/938 tape layup notched specimens show significant dependency on strain rates while that of the tow placed specimens show less dependency on strain rates. The average failure strength of the tape layup specimens with the 19 mm slit decreases by 19% from the 'static' value at 2 ϵ /min; the average failure strength of the tow placed specimens shows no significant sensitivity at all strain rates. For specimens with the 51 mm slit, the average failure strength of the tape layup panels decreases by 15% from the 'static' value at 2 ϵ /min; the average failure strength of the tow placed panels decreases by 9% from the 'static' value at the same strain rate.

The failure strengths of the notched tow placed specimens with both slit sizes are higher than that for the corresponding tape layup specimens. This strength advantage is evident at all three strain rates. Tow placed specimens with the 19 mm slit are stronger than the tape layup specimens by about 25% at 0.0042 ϵ /min and 0.1 ϵ /min, and about 50% at 2 ϵ /min; tow placed specimens with the 51 mm slit are stronger than the tape layup specimens by about 50% at all strain rates.

Strain rate effects on the laminate longitudinal modulus and major Poisson's ratio of both specimen types are insignificant. Failure modes of the tape layup notched specimens are different from that of the tow placed specimens. The fracture path of the tape layup specimens is straight and relatively smooth. The failure path in the tow placed specimens is complicated by delaminations, with each ply failing at a separate location. This results in a jagged fracture path. The failure modes for each specimen type, however, are insensitive to strain rate.

The elastic responses of the AS4/938 tape layup and tow placed specimens are similar, and appear to be insensitive to strain rate. The AS4/948 unnotched coupons of both specimen types show identical stress-strain behavior at all strain rates. Their measured laminate properties are alike and insensitive to strain rates. The strain distributions of the AS4/938 notched panels of both types are also similar at low loads before the onset of damage. This elastic behavior is consistent at all strain rates.

Strain gage readings at the notch tip of the AS4/938 coupons and panels can be used to estimate the load at failure initiation. Strain readings collected for a typical notched panel are shown in Figure 5.5. Failure is assumed to initiate when the notch tip strain gage exhibits a major kink or other non-linear behavior. The average far-field stresses at which failure initiations occur are tabulated in Table 5.1 and Table 5.2 for the notched coupons and panels respectively. The recorded stresses are also normalized with the failure stresses.

Failure initiation stresses of the notched tape layup coupons and panels are only slightly lower than those of the tow placed specimens. These stresses appear to be slightly strain rate sensitive. The average failure initiation stress for the tape layup coupons decreases by about 7% at 2 ϵ /min. The average failure initiation stress of the tow placed specimens is insensitive to strain rate.

Failure initiation stresses are plotted along with the final failure stresses at different strain rates in Figure 5.6 and Figure 5.7 for the notched coupons and panels respectively. The distance between the initiation and final failure stresses indicates the nature of the progressive damage process for each type of specimen. A small separation indicates a 'brittle' failure with little load carrying capability beyond failure initiation. A large

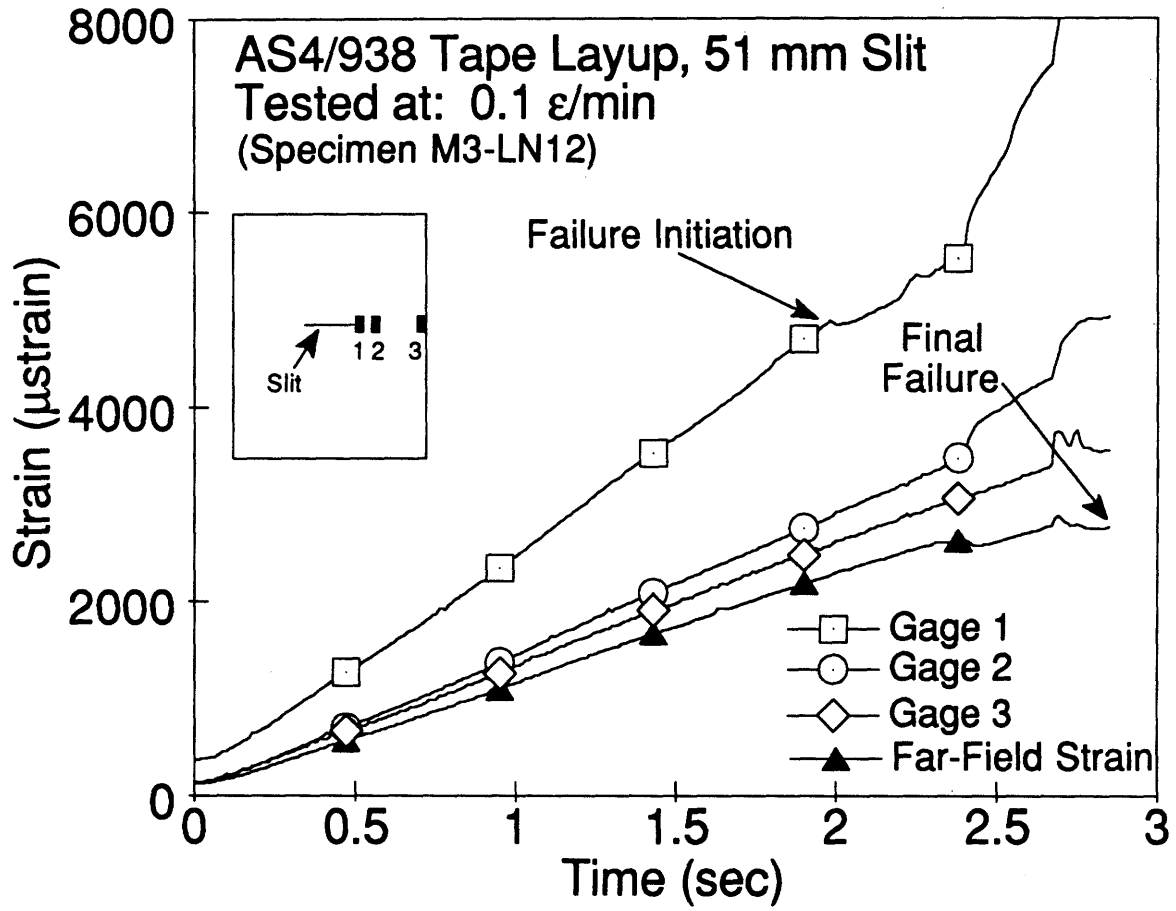


Figure 5.5 Strain Readings Collected of Typical IM7/977-2 Notched Panel.

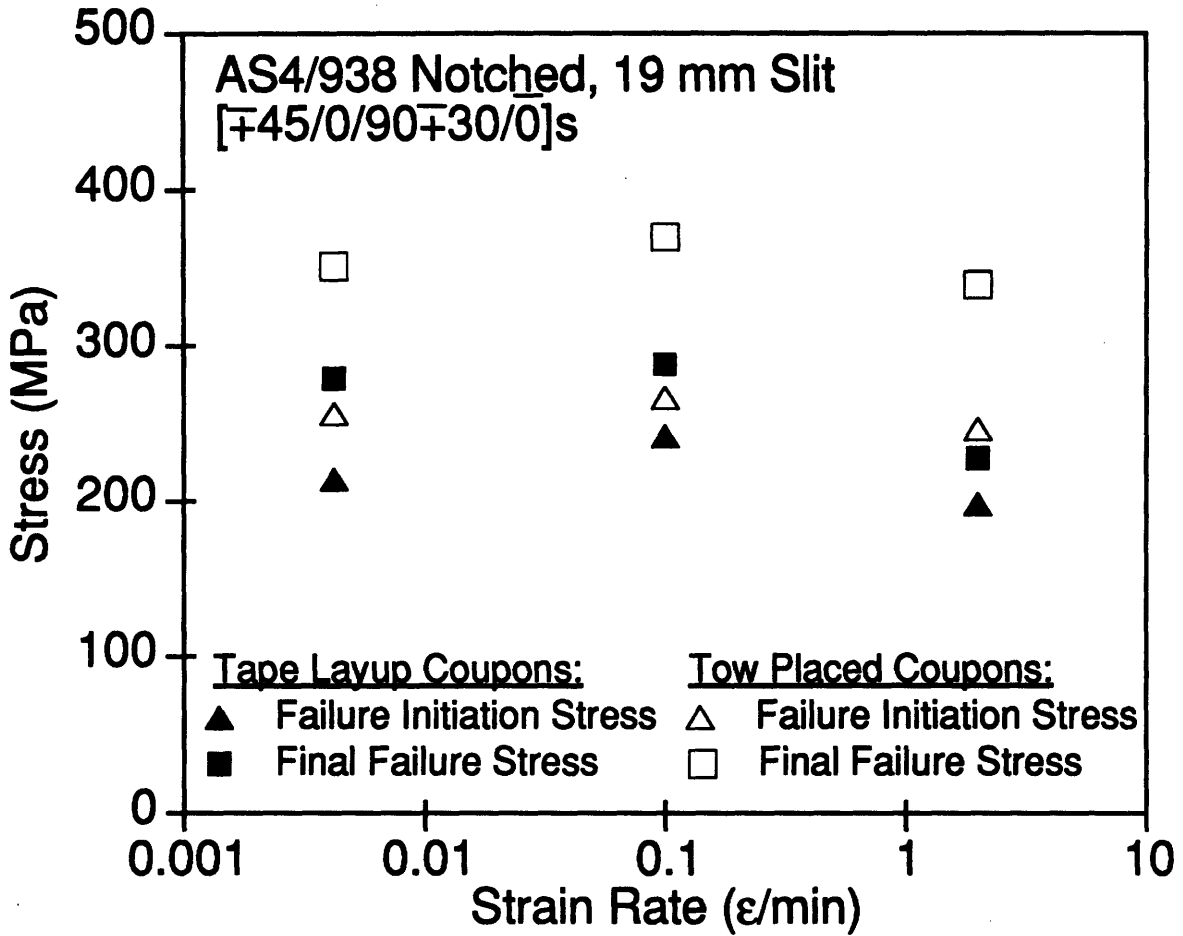


Figure 5.6 Failure Initiation Stress and Final Failure Stress of AS4/938 Notched Specimens, 19 mm Slit.

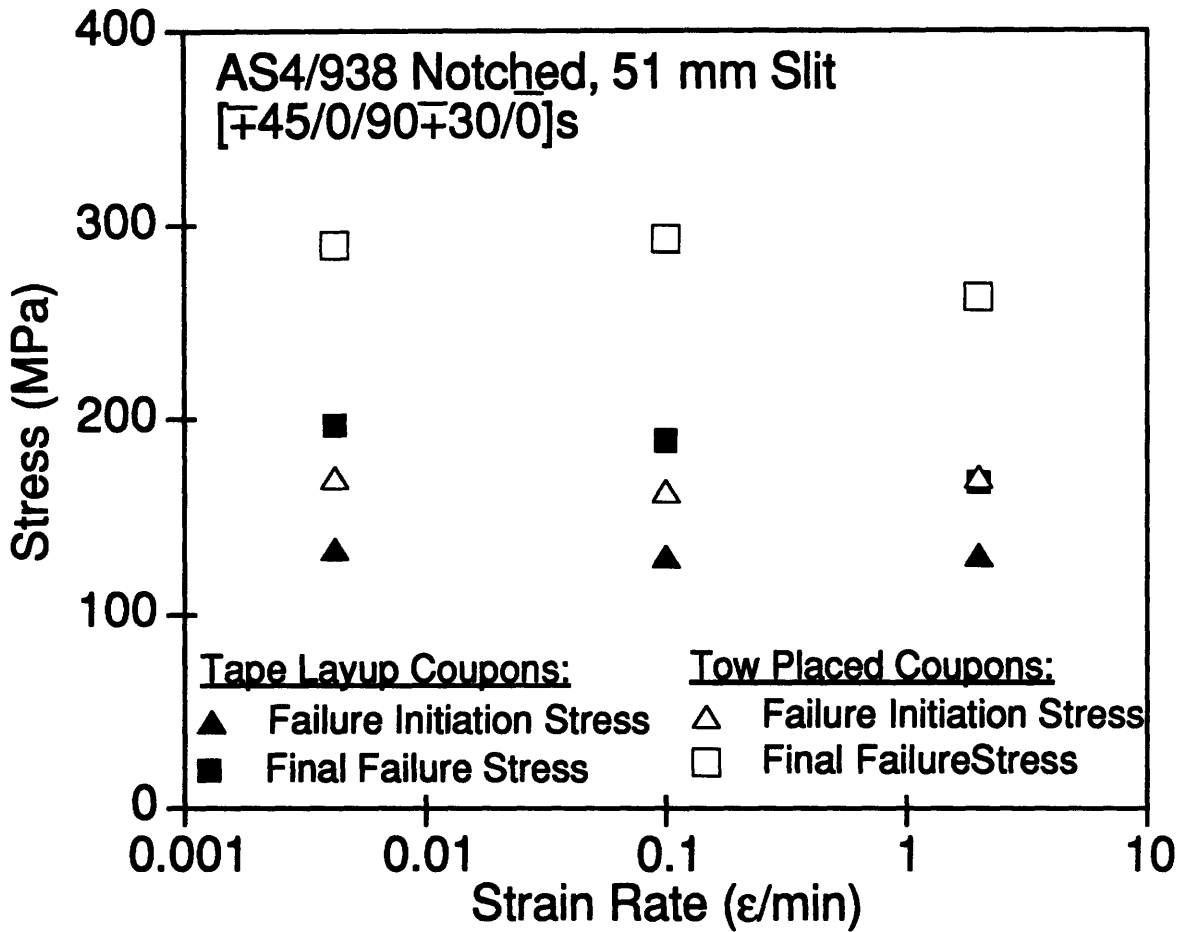


Figure 5.7 Failure Initiation Stress and Final Failure Stress of AS4/938 Notched Specimens, 19 mm Slit.

Table 5.2 Average Stress at Failure Initiation and Ratio of Initiation Stress to Failure Stress for the AS4/938, 19 mm Notched Specimens

Strain Rate (ϵ/min)	Stress (MPa)	$\frac{\text{Stress}_{\text{initiation}}}{\text{Stress}_{\text{failure}}}$
Tape Layup^a:		
0.0042	214 (17.7%) ^b	0.78 (22.0%)
0.1	241 (8.0%)	0.84 (6.96%)
2	198 (10.4%)	0.87 (11.0%)
Tow Placement^a:		
0.0042	256 (8.1%)	0.73 (10.7%)
0.1	266 (4.8%)	0.72 (10.1%)
2	246 (8.4%)	0.73 (15.4%)

^a Data collected for 5 specimens

^b numbers in parentheses are coefficients of variation

Table 5.3 Average Stress at Failure Initiation and Ratio of Initiation Stress to Failure Stress for the AS4/938, 51 mm Notched Specimens

Strain Rate (ϵ /min)	Stress (MPa)	$\frac{\text{Stress}_{\text{initiation}}}{\text{Stress}_{\text{failure}}}$
Tape Layup^a:		
0.0042	134 (7.2%) ^b	0.64 (4.2%)
0.1	130 (16.4%)	0.69 (8.1%)
2	131 (14.8%)	0.69 (0.1%)
Tow Placement^a:		
0.0042	170 (3.4%)	0.58 (2.0%)
0.1	163 (7.6%)	0.55 (8.3%)
2	171 (0.9%)	0.62 (3.7%)

a Data collected for 2 specimens

b numbers in parentheses are coefficients of variation

separation indicates a progressive failure. This may be a result of redistribution of stresses near the notch tip due to local damage.

Failure progression of the AS4/938 notched specimens appears to be dependent on both strain rate and manufacturing technique. For both slit sizes, failure progression is significantly more strain rate sensitive for the tape layup specimens than the tow placed specimens. As strain rate increases, failure progression is hastened in the tape layup specimens. On the other hand, failure progression of the tow placed specimens is strain rate insensitive for the slit size of 19 mm and only slightly strain rate sensitive for the slit size of 51 mm.

The different failure modes observed for both specimen types support this finding. The fracture path of the tape layup specimen is straight, implying that the specimen failed through the propagation of a macrocrack. This type of failure progression is faster at higher strain rates, resulting in lower failure strengths [43]. The fracture path of the tow-placed specimens is more jagged and rough. It does not cut through all the plies at the same location. Different sets of plies have their own distinct fracture path. Intuitively, this mode of failure will delay the progression to failure as higher loads are required to form the different fracture paths in the specimen.

In Section 4.3.4, the AS4/938 tow placed notched specimens were shown to have better damage tolerance than the tape layup specimens. This advantage extends over all three strain rates. As illustrated above, the failure mechanism for the tow placed and tape layup notched specimens is different. The AS4/938 tow placed specimens are slightly tougher than the tape layup specimens at all strain rates tested. This is indicated by the higher failure initiation stresses required for the tow placed specimens.

However, once failure begins, the tow placed specimens behave in the 'softer' manner. They are able to redistribute or absorb stresses better than the tape layup specimens. This finding is consistent with results obtained by other researchers [46]. They found intraply resin rich zones in the tow placed specimens that enhance the splitting mechanism along the loading axis.

The AS4/938 tape layup notched specimens exhibit brittle failure that is common with graphite/epoxy composite systems. The 'brittleness' of this material increases with increasing strain rates, resulting in lower failure strengths. The overall effect on these specimens is a decreasing ability to tolerate damage as strain rate increases. Previous work on interlaminar fracture toughness showed strain rate sensitivity in the same regime of strain rates [40, 41]. In those experiments, the material used was AS4/3501-6, whose material properties are very similar to that of AS4/938. However, as mentioned in Section 2.2, the results obtained were contradictory. Nonetheless, they show that the toughness and damage mechanism of this type material system are strain rate sensitive. The results obtained here are consistent, in a general way, with the previous finding.

Chapter 6

CONCLUSIONS AND RECOMMENDATIONS

The conclusions and recommendations presented in this chapter are a result of the experimental work and subsequent analysis conducted in the course of this investigation and presented in the previous chapters.

6.1 Conclusions

The primary finding of this work is that the damage tolerance and progressive failure mechanisms of graphite/epoxy laminates are dependent on strain rate and manufacturing technique.

The elastic behavior of these laminates was not dependent on these factors. The measured elastic properties and elastic strain distributions showed no such dependencies. They agreed very well with existing theories. The failure loads of the unflawed specimens also showed no strain rate or manufacturing technique sensitivities. In the notched panels, the load at which evidence of failure was first detected was also only weakly dependent on these factors.

However, the progression from initial failure to final failure in notched specimens is clearly strain rate and manufacturing technique dependent. Specimens made of a soft layup of toughened IM7/977-2 material showed no sensitivity to strain rate in their final failure loads. However, the appearance of the failed specimens differed after tests at different strain rates. This indicates the final progress of the failure after peak load was reached was strain rate dependent.

Notched specimens made from a 'harder' layup of AS4/938 material showed strong dependence of the final failure load on both strain rates and manufacturing technique. Tape layup specimens acted in a brittle fashion, failing soon after failure initiation. This problem worsened at higher strain rates. The tow placed specimens failed at loads much higher than the loads at which failure initiated. Their failure appearance gives further evidence that they failed by a complex, progressive mechanism.

6.2 Recommendations

Further work is already in progress to identify the effects of other parameters, such as different material systems and layups, on this problem. It is recommended that materials under consideration for use in composite aircraft structure (e.g., new toughened matrix composites) be tested for strain rate sensitivity. It is also recommended that the strain rates used be adjusted as necessary to reflect realistic loading scenarios.

Work that could contribute to the better understanding of the mechanisms of progressive damage in composite materials is also recommended. Specimens partially damaged by loading to a level between initiation and final failure loads can be inspected to observe the progress of damage. The interaction of these mechanisms with other damage mechanisms such as fatigue and impact should also be studied through combined tests. Finally, these additional studies should be carried out with a view of either supporting or disproving proposed damage mechanisms. The long term goal of this work should be the development of sufficient understanding of damage mechanisms in composite materials to allow confident analysis of these materials, and structures made of them.

REFERENCES

- 1 Nahas, M.H., "Survey of Failure and Post-Failure Theories of Laminated Fiber-Reinforced Composites", *Journal of Composites Technology and Research*, Vol. 8, No. 4, 1986, pp. 138-153.
- 2 Snell, M.B., "Strength and Elastic Response of Symmetric Angle-Ply CFRP", *Composites*, July 1978, pp. 167-176.
- 3 Hill, R., *The Mathematical Theory of Plasticity*, Oxford University Press, 1950.
- 4 Hoffman, O., "The Brittle Strength of Orthotropic Materials", *Journal of Composite Materials*, Vol. 1, 1967, pp. 200-206.
- 5 Tsai, S.W., and Wu, E.M., "A Generalized Theory of Strength for Anisotropic Materials", *Journal of Composite Materials*, Vol. 5, 1971, pp. 58-80.
- 6 Gol'denblat, I.I., and Kopnov, V.A., "Strength of Glass-Reinforced Plastics in the Complex Stress State", *Polymer Mechanics*, (translation of Mekhanika Polimerov), Vol. 1, 1966, pp. 54-59.
- 7 Puppo, A.H., and Evensen, H.A., "Strength of Anisotropic Materials Under Combined Stresses", *AIAA Journal*, Vol. 10, April 1972, pp. 468-474.
- 8 Jones, R.M., *Mechanics of Composite Materials*, Hemisphere Publishing Corporation, U.S.A., 1975.
- 9 Hahn, H.T., and Tsai, S.W., "On the Behavior of Composite Laminates After Initial Failures", *Journal of Composite Materials*, Vol. 8, July 1974, pp. 208-305.
- 10 Chou, Shun-Chin, Orringer, O., and Rainey, J.H., "Post-Failure Behavior of Laminates I - No Stress Concentration", *Journal of Composite Materials*, Vol. 10, 1976, pp. 371-381.

- 11 Petit, P.H., and Waddoups, M.E., "A Method of Predicting the Nonlinear Behavior of Laminated Composites", *Journal of Composite Materials*, Vol. 3, 1969, pp. 2-19.
- 12 Tsai, S.W., "A survey of Macroscopic Failure Criteria for Composite Materials", *Journal of reinforced Plastics and Composites*, Vol. 3, January 1984, pp. 40-62.
- 13 Irwin, G.R., "Fracture Behavior of Composite Materials", *Composite Materials Workshop*, Ed. by S.W. Tsai, J.C. Halpin, and N.J. Pagano, Technomic Publications, 1968, pp. 9-19.
- 14 Awerbach, J., and Madhukar, M.S., "Notched Strength of Composite Laminates Predictions and Experiments - A Review", *Journal of Reinforced Plastics and Composites*, Vol. 4, January 1985, pp. 3-159.
- 15 Mar, James W., and Lin, Kuen Y., "Fracture of Boron/Aluminum Composites with Discontinuities", *Journal of Composite Materials*, Vol. 11, 1977, pp. 405-421.
- 16 Lagace, Paul A., "Notch Sensitivity and Stacking Sequence of Laminated Composites", *Composite Materials Testing and Design*, ASTM STP 893, American Society for Testing and Materials, 1986, pp. 161-176.
- 17 Fenner, D.N., "Stress Singularities in Composite Materials with an Arbitrarily Oriented Crack Meeting an Interface", *International Journal of Fractures*, Vol. 12, 1975, pp. 705-721.
- 18 Awerbuch, J., and Hahn, H.T., "Crack-Tip Damage and Fracture Toughness of Boron/Aluminum Composites", *Journal of Composite Materials*, Vol. 13, 1979, pp. 82-107.
- 19 Mar, J.W., and Lin, K.Y., "Fracture Mechanics Correlation for Tensile Failure of Filamentary Composites with Holes", *Journal of Aircraft*, Vol. 14, 1977, pp. 703-704.

- 20 Lagace, Paul A., "Static Tensile Fracture of Graphite/Epoxy", M.I.T. Department of Aeronautics and Astronautics, Ph.D. Thesis, April 1982.
- 21 Nuismer, R.J., and Whitney, J.M., "Uniaxial Failure of Composite Laminates Containing Stress Concentrations", *Fracture Mechanics of Composites*, ASTM STP 593, American Society for Testing and Materials, 1975, pp. 117-142.
- 22 Whitney, J.M., and Nuismer, R.J., "Stress Fracture Criteria for Laminated Composites Containing Stress Concentrations", *Journal of Composite Materials*, Vol. 8, 1974, pp. 253-265.
- 23 Nuismer, R.J., and Whitney, J.M., "Uniaxial Failure of Composite Materials Containing Stress Concentrations", *Fracture Mechanics of Composites*, ASTM 593, American Society for Testing and Materials, 1975, pp. 117-142.
- 24 Lagace, Paul A., "Notch Sensitivity and Stacking Sequence of Laminated Composites", *Composite Materials Testing and Design*, ASTM STP 893, American Society for Testing and Materials, 1986, pp. 161-176.
- 25 Waddoups, M.E., Eisenmann, J.R., and Kaminski, B.E., "Macroscopic Fracture Mechanics of Advanced Composite Materials", *Journal of Composite Materials*, Vol. 5, 1971, pp. 446-454.
- 26 Chang, F.K., and Chang, K.Y., "A Progressive Damage Model for Laminated Composites Containing Stress Concentrations", *Journal of Composite Materials*, Vol. 21, September 1987, pp. 834-855.
- 27 Daniel, I.M., "High Strain Rate Properties of Unidirectional Composites", NASA Contractor Report 189083, December 1991.
- 28 Lindholm, U.S., "Dynamic Deformation of Metals", *Behavior of Materials Under Dynamic Loading*, edited by N.J. Huffington, Jr., American Society of Mechanical Engineers, 1965.

- 29 Zukas, J. (ed.), *Impact Dynamics*, John Wiley and Sons, New York, N.Y., 1982.
- 30 Lifshitz, J.M., "Time-Dependent Fracture of Fibrous Composites", *Composite Materials*, Vol. 5, Chap. 6, pp. 249-311.
- 31 Daniel, I.M., and Hamilton, W.G. and Labedz, R.H., "Strain Rate Characterization of Unidirectional Graphite/Epoxy Composite", *Composite Materials: Testing and Design*, ASTM STP 787, 1982, pp. 393-413.
- 32 Harding, J., and Welsh, L.M., "Tensile Testing Technique for Fiber-Reinforced Composites at Impact Rates of Strain", *Journal of Materials Science*, Vol. 18, No. 6, June 1983, pp. 1810-1826.
- 33 Armenakas, A.E., and Sciammarella, C.A., "Response of Glass Fiber Reinforced Epoxy Specimens to High Rates of Tensile Loading", *Experimental Mechanics*, Vol. 13, No. 10, October 1973, pp. 433-440.
- 34 Daniel, I.M., and Liber, T., "Testing of Fiber Composites at High Strain Rates", Proceedings of the 2nd International Conference on Composite Materials, ICCM/2, Toronto, April 1978, pp. 1003-1018.
- 35 Al-Salehi, F.A.R., Al-Hassani, S.T.S., and Hinton, M.J., "Experimental Investigation into the Strength of Angle Ply GRP Tubes under High Rate of Loading", *Journal of Composite Materials*, No. 23, No. 3, March 1989, pp. 288-305.
- 36 Rotem, A., and Lifshitz, J.M., "Longitudinal strength of Unidirectional Fibrous Composite Under High Rate of Loading", Proceedings of the 26th Annual Technical Conference, Reinforced Plastics/Composites Division, The Society of Plastics Industry, Sec. 10-G, Feb., 1971.
- 37 Sierakowski, R.L., Nevill, G.E., Ross, C.A., and Jones, E.R., "Dynamic Compressive Strength and Failure of Steel reinforced Epoxy Composites", *Journal of Composite Materials*, Vol. 5, July 1971, pp. 362-377.

- 38 Frey, T.J., and Vinson, J.R., "High Strain Rate Mechanical Properties of Glass/Polyester and Carbon/Aluminum Composite Materials", Proceedings of the 32nd AIAA/ASME/ASCE/AHS/ASC Structures, Structural Dynamics and Materials Conference, April, 1991
- 39 Mall, S., Law, G.E., and Katouzian, M., "Loading Rate Effect on Interlaminar Fracture Toughness of a Thermoplastic Composite", *Journal of Composite Materials*, Vol. 21, June 1987, pp. 569-579.
- 40 Smiley, A.J., and Pipes, R.B., "Rate Effects on Mode I Interlaminar Fracture Toughness in Composite Materials", *Journal of Composite Materials*, Vol. 21, July 1987, pp. 670-687.
- 41 Aliyu, A.A., and Daniel, I.M., "Effects of Strain Rate on Delamination Fracture Toughness of Graphite/Epoxy", *Delamination and Debonding of Materials*, ASTM STP 876, edited by W.S. Johnson, American Society for Testing and Materials, Philadelphia, 1985, pp. 336-348.
- 42 Mullin, J., Berry, J.M., and Gatti, A., "Some Fundamental Fracture Mechanisms Applicable to Advanced Filament Reinforced Composites", *Journal of Composite Materials*, Vol. 2, No. 1, January 1968, pp. 82-103.
- 43 Suvorova, J.V., "The Influence of Time and Temperature on the Reinforced Plastic Strength", *Handbook of Composites*, Vol. 3 - Failure Mechanics of Composites, edited by G.C. Sih and A.M. Skudra, 1985, pp. 177-213
- 44 Strong, B., *Fundamentals of Composite Manufacturing: Materials, Methods and Applications*, Society of Manufacturing Engineers, Dearborn, Michigan, 1989.
- 45 William, P.B., and Reynolds, B., "Materials Considerations for Automated Fiber Placement", Society of Manufacturing Engineers Technical Paper, August 1991.

- 46 Walker, T.H., Avery W.B., Ilcewicz, L.B., Poe, Jr. C.C., and Harris, C.E., "Tension Fracture of Laminates for Transportation Fuselage. Part 1: Material Screening", To be published in the 9th DOD/NASA/FAA Conference on Fibrous Composites and Structural Design, November 1991.
- 47 Lagace, Paul A., Brewer, J.C. and Varnerin, C.F., "TELAC Manufacturing Course Class Notes", TELAC Report 88-4, M.I.T. Department of Aeronautics and Astronautics, May 1988
- 48 Sawicki, A.J., "Damage Tolerance of Integrally Stiffened Composite Plates and Cylinders", M.I.T. Department of Aeronautics and Astronautics, Master's Thesis, August 1988.
- 49 Pemberton, R., "Behavior of Wide Graphite/Epoxy Plates with Notches", Internal TELAC Document, May 1989.
- 50 National Instruments, "LabVIEW2 Data Acquisition VI Library Reference Manual", Part Number 320249-01, September 1991 Edition.
- 51 Vizzini, A.J., "An Efficient Algorithm to Characterize Stress-Stain Data Using Piecewise Linear Curves", *Journal of Testing and Evaluation*, Vol. 20, No. 2, March 1992, pp. 126-131.
- 52 Lekhnitskii, S.G., *Anisotropic Plates*, S.W. Tsai and T. Cheron, Trans., Gordon and Breach Science Publishers, 1968.
- 53 Brown, W.F., and Srawley, J.E., "Plane Strain Crack Toughness Testing of High Strength Metallic Materials", ASTM STP 410, American Society of Testing and Materials, 1965, pp. 30-83.

APPENDIX A

Table A.1 IM7/977-2 Unnotched Coupon Parameters

Specimen	Average Width [mm]	Average Thickness [mm]	Strain Rate Tested [ε/min]
M1-SU01	51.1	2.44	0.025
M1-SU02	51.3	2.45	0.025
M1-SU03	51.4	2.44	0.005
M1-SU04	47.2	2.45	0.005
M1-SU05	51.2	2.45	0.1
M1-SU06	51.6	2.46	0.5
M1-SU07	51.2	2.46	0.5
M1-SU08	47.2	2.46	0.1

Table A.2 IM7/977-2 Notched Panel Parameters

Specimen	Average Width [mm]	Average Thickness [mm]	Measured Slit Size [mm]	Strain Rate Tested [ε/min]
M1-LN01	206.0	2.47	50.2	0.005
M1-LN02	206.0	2.43	51.6	0.5
M1-LN03	206.0	2.47	51.4	0.125
M1-LN04	205.9	2.46	51.7	0.0125 ^a
M1-LN05	205.9	2.49	50.2	0.5
M1-LN06	205.9	2.45	50.8	0.125
M1-LN07	205.1	2.5	52.0	0.025
M1-LN08	205.2	2.48	50.7	0.005
M1-LN09	205.1	2.46	51.3	0.025
M1-LN10	205.3	2.43	51.7	0.125
M1-LN11	205.2	2.47	50.9	0.005
M1-LN12	205.1	2.47	50.2	0.5

^a Incorrect stroke rate used during test

Table A.3 IM7/977-2 Unnotched Coupon Failure and Stiffness Data

Measured Strain Rate [ϵ/min]	Failure Stress [MPa]	Failure Strain [μstrain]	Laminate Longitudinal Modulus [GPa]	Laminate Major Poisson's Ratio
0.004	579	15720	35.6	0.26
0.004	509	14870	38.5	0.26
0.020	534	16300	39.0	0.26
0.020	586	16390	40.3	0.27
0.08	518	14900	38.2	0.27
0.08	502	15250	37.4	0.27
0.4	572	15300	39.0	0.27
0.4	558	14720	39.2	0.26

Table A.4 IM7/977-2 Notched Panels Failure Data

Measured Strain Rate [ϵ/min]	Failure Stress [MPa]	Failure Strain [μstrain]
0.004	254	5950
0.004	257	6050
0.004	267	6200
0.009 ^a	262	5960
0.018	259	5910
0.018	260	5650
0.090	266	6140
0.080	256	6200
0.083	263	6070
0.34	246	5910
0.32	260	5880
0.30	269	6010

^a Incorrect stroke rate used during test

APPENDIX B

Table B.1 AS4/938 Tape Layup Unnotched Coupon Parameters

Specimen	Average Width [mm]	Average Thickness [mm]	Strain Rate Tested [ϵ /min]
M3-SU01	77.0	2.52	0.1
M3-SU02	77.1	2.46	0.0042
M3-SU03	77.1	2.50	0.0042
M3-SU04	77.0	2.47	0.0042
M3-SU05	77.1	2.45	0.0042
M3-SU06	77.1	2.42	0.0042
M3-SU07	77.0	2.43	0.1
M3-SU08	76.7	2.45	0.1
M3-SU09	76.9	2.46	0.1
M3-SU10	77.1	2.46	0.1
M3-SU11	77.1	2.42	2
M3-SU12 ^a	76.9	2.45	2
M3-SU13 ^a	77.1	2.44	2
M3-SU14	77.0	2.45	2
M3-SU15	77.2	2.47	2
M3-SU16	76.7	2.44	2
M3-SU17	76.8	2.44	2

^a Data lost during test

Table B.2 AS4/938 Tow Placed Unnotched Coupon Parameters

Specimen	Average Width [mm]	Average Thickness [mm]	Strain Rate Tested [ϵ/min]
M2-SU01	76.3	2.52	0.0042
M2-SU02	76.1	2.53	0.1
M2-SU03	76.2	2.53	0.1
M2-SU04	76.2	2.42	2
M2-SU05	76.1	2.52	0.0042
M2-SU06	76.1	2.52	0.0042
M2-SU07	76.1	2.52	0.0042
M2-SU08	76.1	2.52	0.1
M2-SU09	77.3	2.51	0.1
M2-SU10	77.4	2.52	2
M2-SU11	76.1	2.52	2
M2-SU12	76.1	2.50	2
M2-SU13	76.9	2.52	0.1
M2-SU14	76.2	2.51	0.0042
M2-SU15	76.2	2.53	2

Table B.3 AS4/938 Tape Layup Notched Coupon Parameters

Specimen	Average Width [mm]	Average Thickness [mm]	Measured Slit Size [mm]	Strain Rate Tested [ε/min]
M3-SN01	76.9	2.48	- a	0.0042
M3-SN02	77.1	2.45	19.1	0.0042
M3-SN03	77.1	2.43	18.8	0.0042
M3-SN04	77.1	2.46	17.7	0.0042
M3-SN05	76.9	2.44	18.6	0.0042
M3-SN06	77.2	2.45	18.9	0.1
M3-SN07	77.1	2.47	18.2	0.1
M3-SN08	76.7	2.44	17.9	0.1
M3-SN09	77.2	2.44	19.2	0.1
M3-SN10	77.1	2.44	18.6	2
M3-SN11	77.1	2.39	19.1	2
M3-SN12	77.0	2.47	18.8	2
M3-SN13 ^b	77.0	2.48	18.6	2
M3-SN14	77.1	2.48	17.9	2
M3-SN15	76.9	2.38	17.5	2
M3-SN16	76.4	2.40	19.1	0.1

a Slit size not measured prior to test

b Data lost during test

Table B.4 AS4/938 Tow Placed Notched Coupon Parameters

Specimen	Average Width [mm]	Average Thickness [mm]	Measured Slit Size [mm]	Strain Rate Tested [ϵ/min]
M2-SN01	76.4	2.52	19.4	0.0042
M2-SN02	76.2	2.54	18.6	2
M2-SN03	76.2	2.55	19.8	0.1
M2-SN04	76.1	2.52	19.1	2
M2-SN05	76.1	2.51	21.2	0.0042
M2-SN06	77.4	2.51	19.0	0.1
M2-SN07	76.1	2.52	20.1	0.1
M2-SN08	76.1	2.49	19.1	0.0042
M2-SN09	76.1	2.50	19.7	2
M2-SN10	76.1	2.51	19.2	0.1
M2-SN11	76.1	2.51	19.8	0.0042
M2-SN12	77.4	2.51	19.9	2
M2-SN13	76.1	2.51	19.6	0.1
M2-SN14	75.9	2.52	19.1	0.0042
M2-SN15	76.0	2.51	19.1	2

Table B.5 AS4/938 Tape Layup Notched Panel Parameters

Specimen	Average Width [mm]	Average Thickness [mm]	Measured Slit Size [mm]	Strain Rate Tested [ϵ/min]
M3-LN01	204.3	2.43	50.9	2
M3-LN03	204.4	2.46	50.5	0.1
M3-LN04	204.4	2.44	- a	0.0042
M3-LN05	204.6	2.47	51.4	0.0042
M3-LN06	204.8	2.41	50.7	0.1
M3-LN07	204.6	2.46	50.9	2
M3-LN08	204.8	2.46	51.0	0.1
M3-LN09	204.8	2.42	50.5	0.0042
M3-LN10	204.8	2.47	50.6	2
M3-LN11	204.9	2.47	48.3	2
M3-LN12	204.3	2.42	51.1	0.1
M3-LN13	205.0	2.43	51.4	0.0042
M3-LN14	203.7	2.43	50.2	2
M3-LN15	204.4	2.43	50.2	0.0042
M3-LN16	204.7	2.40	51.1	0.1

^a Slit size not measured prior to test

Table B.6 AS4/938 Tow Placed Notched Panel Parameters

Specimen	Average Width [mm]	Average Thickness [mm]	Measured Slit Size [mm]	Strain Rate Tested [ε/min]
M2-LN01	203.2	2.52	50.6	0.0042
M2-LN02	203.3	2.50	50.4	2
M2-LN03	203.3	2.46	51.7	0.0042
M2-LN04	205.5	2.50	50.8	0.1
M2-LN05	203.6	2.52	50.8	0.0042
M2-LN06	203.6	2.53	51.7	2
M2-LN07	204.1	2.51	50.8	0.0042
M2-LN08	203.7	2.53	50.8	0.1
M2-LN09	204.0	2.51	50.9	0.1
M2-LN10	203.6	2.52	50.9	0.0042
M2-LN11	204.0	2.53	50.8	2
M2-LN12	203.8	2.50	51.3	2
M2-LN13	204.2	2.51	51.3	0.1
M2-LN14	204.4	2.52	50.9	2
M2-LN15	204.1	2.52	51.1	0.1

Table B.7 AS4/938 Tape Layup Unnotched Coupon Failure and Stiffness

Measured Strain Rate [ϵ/min]	Failure Stress [MPa]	Failure Strain [μstrain]	Data Laminate Longitudinal Modulus [GPa]	Laminate Major Poisson's Ratio
0.003	634	10540	61.2	0.48
0.003	614	10170	61.3	0.48
0.003	589	9850	60.6	0.49
0.003	631	9970	62.9	0.46
0.003	572	10054	57.6	0.49
0.084	606	10280	58.9	0.45
0.084	575	10150	56.8	0.48
0.080	585	9880	60.8	0.48
0.082	612	10040	61.0	0.46
0.079	610	10010	60.6	0.47
1.51	525	9260	57.6	0.52
1.51	577	9680	63.1	0.50
1.47	568	9320	62.6	0.50
1.47	563	9480	61.6	0.49
1.53	592	9590	63.4	0.48

Table B.8 AS4/938 Tow Placed Unnotched Coupon Failure and Stiffness Data

Measured Strain Rate [ϵ/min]	Failure Stress [MPa]	Failure Strain [μstrain]	Laminate Longitudinal Modulus [GPa]	Laminate Major Poisson's Ratio
0.003	589	10410	60.6	0.48
0.003	614	10450	62.1	0.47
0.003	574	9450	60.7	0.52
0.003	584	10240	59.0	0.44
0.003	585	9783	60.5	0.50
0.079	602	9760	63.1	0.53
0.080	619	10090	63.9	0.54
0.080	606	10120	60.6	0.49
0.081	588	9750	62.1	0.47
0.083	612	10210	61.5	0.51
1.42	579	9090	65.7	0.52
1.45	584	9720	62.0	0.47
1.43	589	9750	61.6	0.49
1.46	578	9590	60.4	0.49
1.51	579	9920	59.6	0.46

Table B.9 AS4/938 Tape Layup Notched Specimens Failure Data

Notched Coupon (19mm Slit)			Notched Panel (50.8mm Slit)		
Measured Strain Rate [ϵ/min]	Failure Stress [MPa]	Failure Strain [μstrain]	Measured Strain Rate [ϵ/min]	Failure Stress [MPa]	Failure Strain [μstrain]
0.003	294	4600	0.003	213	2890
0.003	256	4000	0.003	204	2664
0.003	255	3320	0.003	206	3180
0.003	302	4440	0.003	188	2800
0.003	287	4770	0.003	174	2640
0.074	243	4040	0.068	200	2880
0.076	291	4300	0.067	204	3100
0.075	305	4700	0.069	168	2597
0.073	265	4110	0.068	199	2760
0.072	333	4820	0.068	176	2590
1.31	257	3840	1.07	170	2460
1.30	211	3210	1.13	142	2300
1.30	226	3390	1.09	210	3080
1.30	221	3290	1.16	173	2630
1.35	221	3510	1.15	143	2050

Table B.10 AS4/938 Tow Placed Notched Specimens Failure Data

Notched Coupon (19mm Slit)			Notched Panel (51mm Slit)		
Measured Strain Rate [ε/min]	Failure Stress [MPa]	Failure Strain [μstrain]	Measured Strain Rate [ε/min]	Failure Stress [MPa]	Failure Strain [μstrain]
0.003	354	5290	0.003	274	4010
0.003	359	4760	0.003	292	4320
0.003	343	5190	0.003	298	3880
0.003	336	5000	0.003	297	4130
0.003	362	5200	0.004	288	4030
0.074	411	5860	0.064	294	3760
0.073	398	5530	0.071	297	4470
0.074	349	5120	0.068	298	4090
0.074	350	5030	0.068	301	4360
0.073	341	5140	0.071	273	3650
1.30	343	5280	1.13	266	3640
1.26	357	4680	1.09	280	3720
1.20	297	3600	1.14	283	3970
1.33	353	5320	1.20	259	3800
1.34	345	5120	1.20	226	3380

APPENDIX C

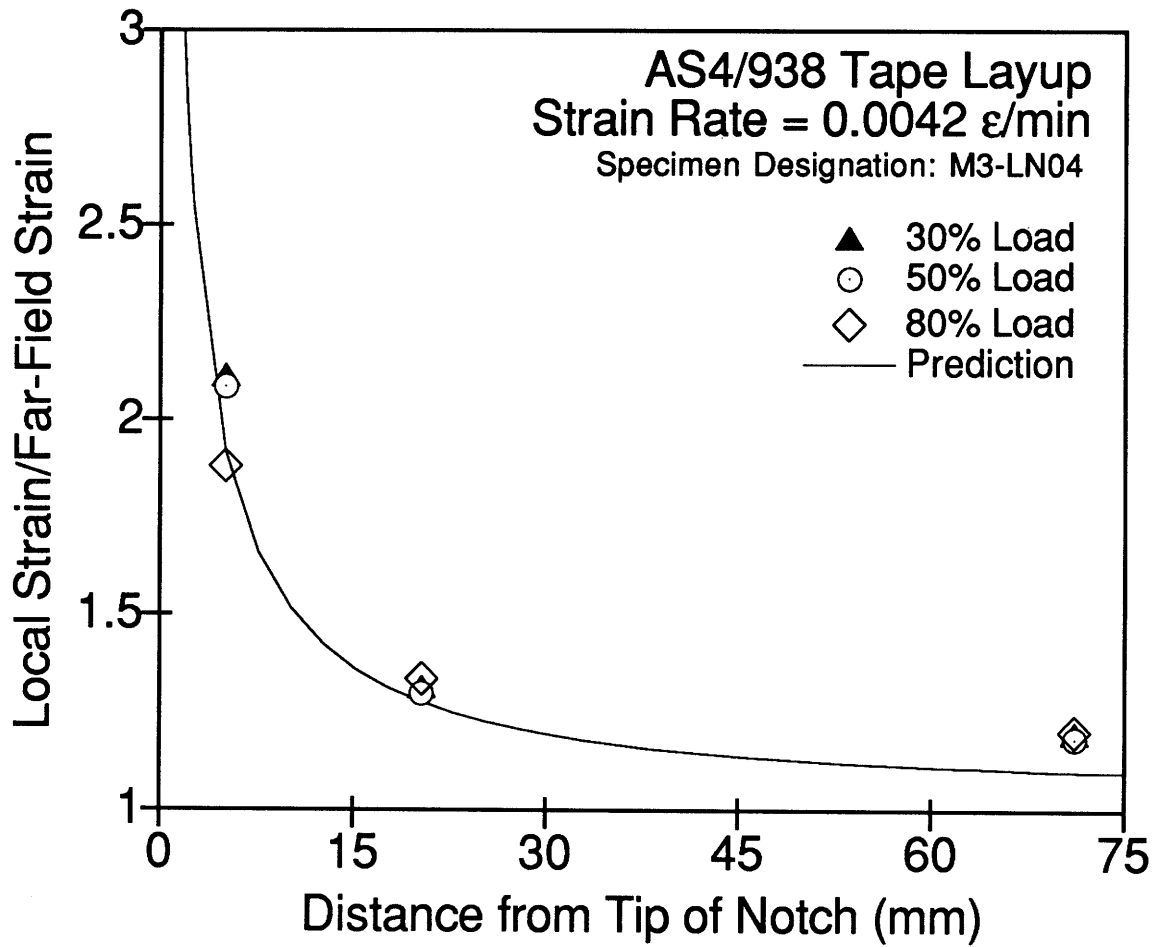


Figure C.1 Strain Distribution of AS4/938 Tape Layup Notched Specimen M3-LN04 at 0.0042 ϵ /min.

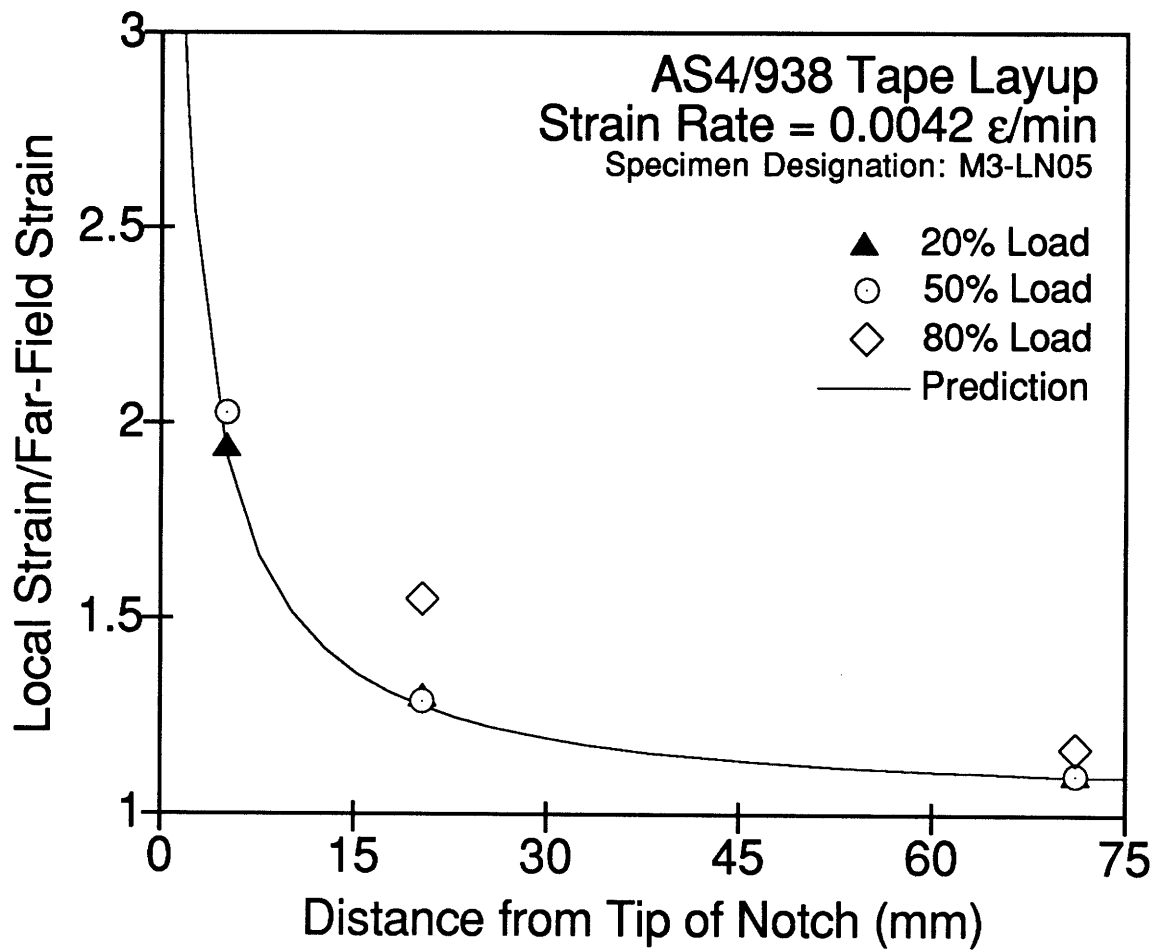


Figure C.2 Strain Distribution of AS4/938 Tape Layup Notched Specimen M3-LN05 at 0.0042 ϵ /min.

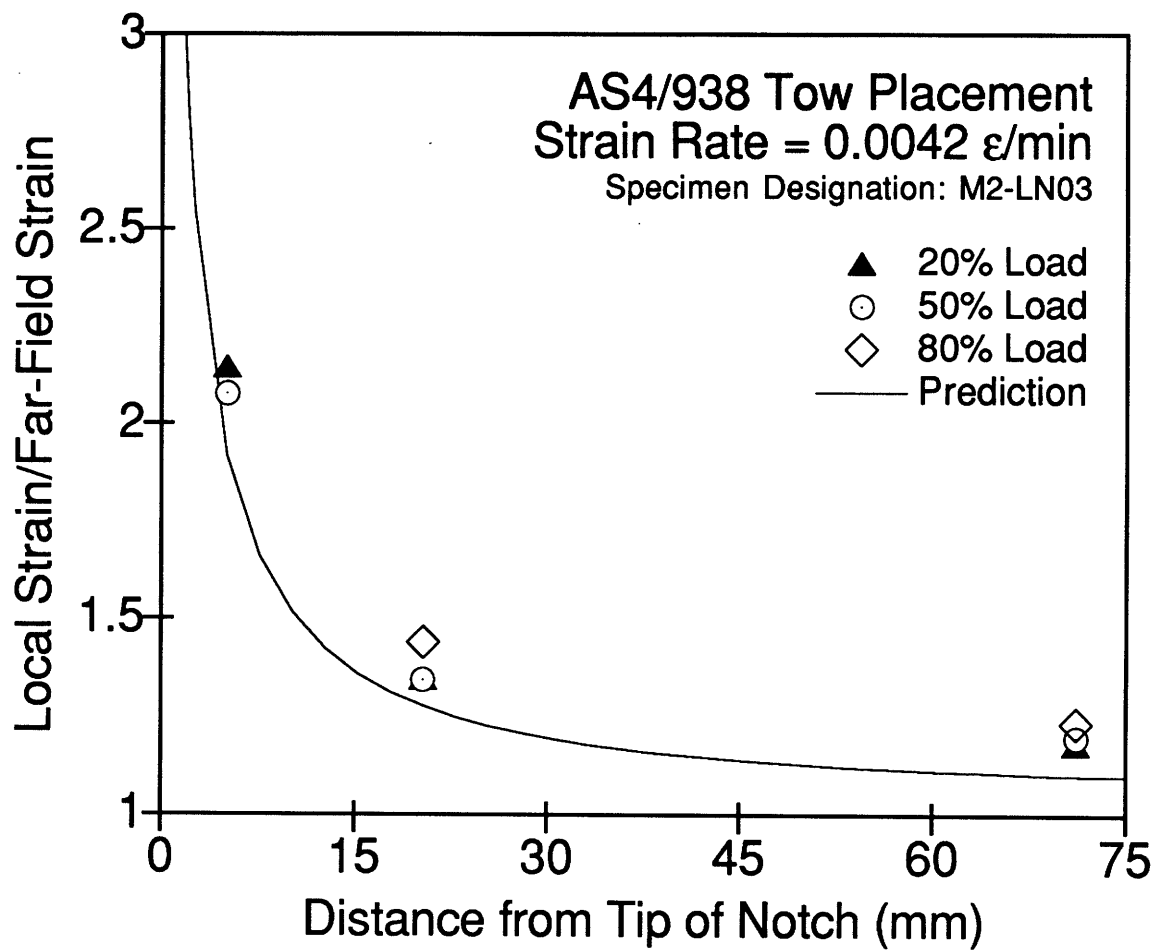


Figure C.3 Strain Distribution of AS4/938 Tow Placed Notched Specimen M2-LN03 at 0.0042 ϵ /min.

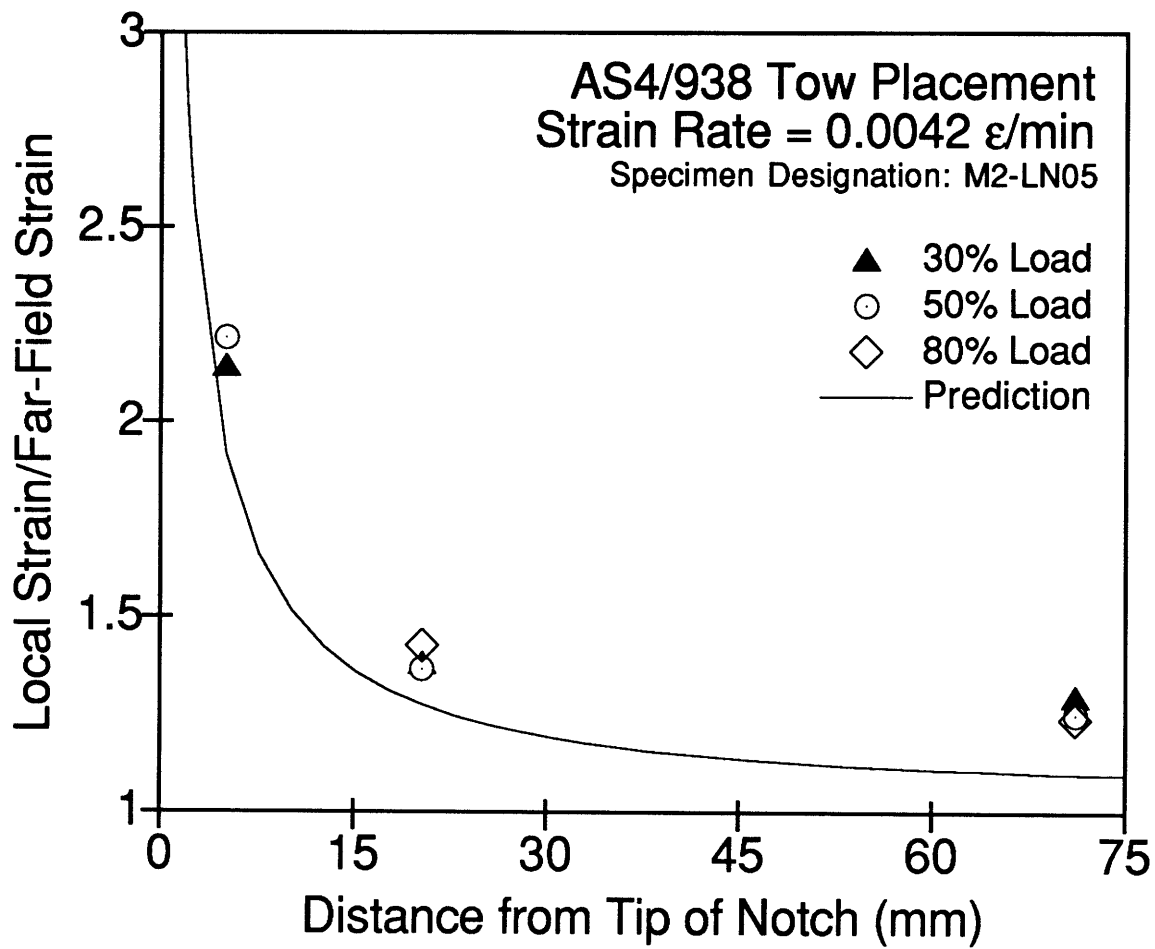


Figure C.4 Strain Distribution of AS4/938 Tow Placed Notched Specimen M2-LN05 at 0.0042 ϵ /min.

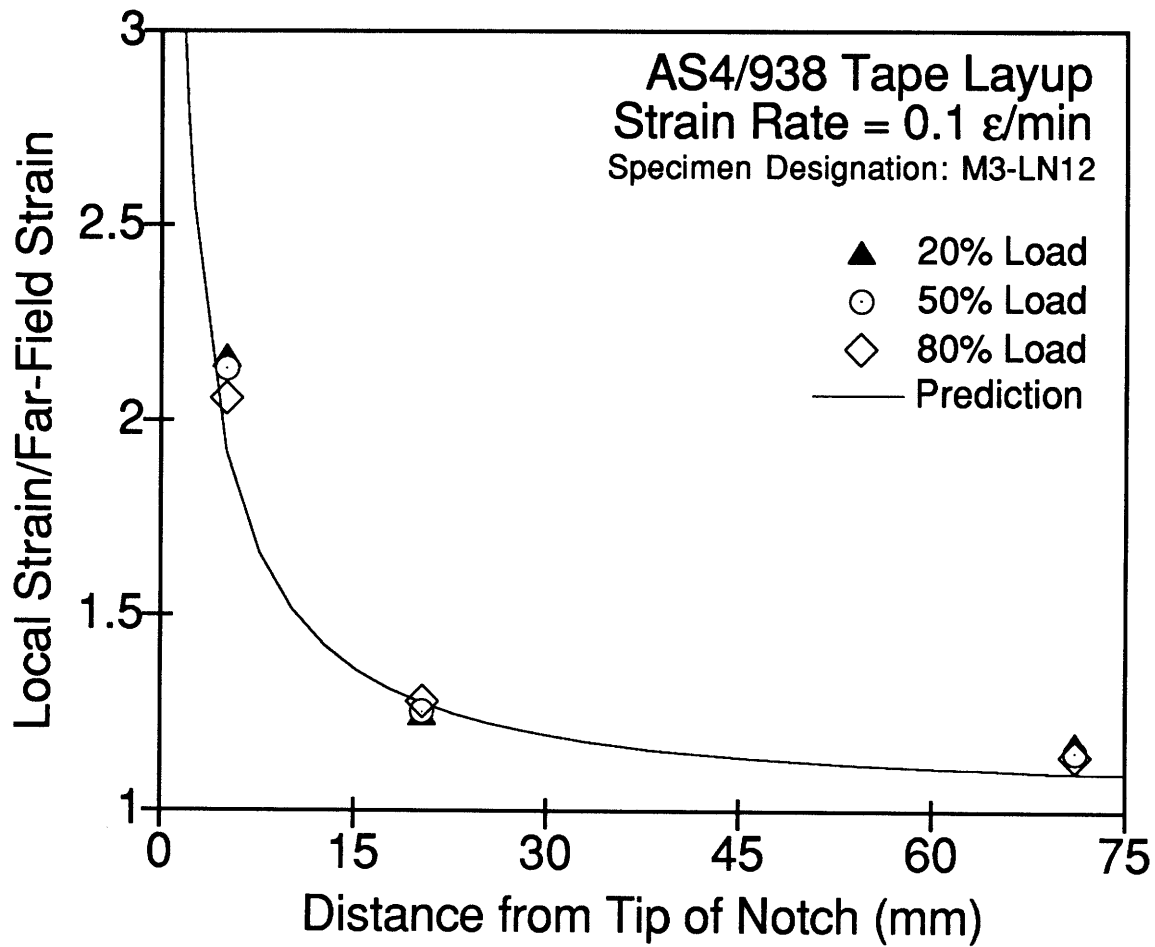


Figure C.5 Strain Distribution of AS4/938 Tape Layup Notched Specimen M3-LN12 at 0.1 ϵ /min.

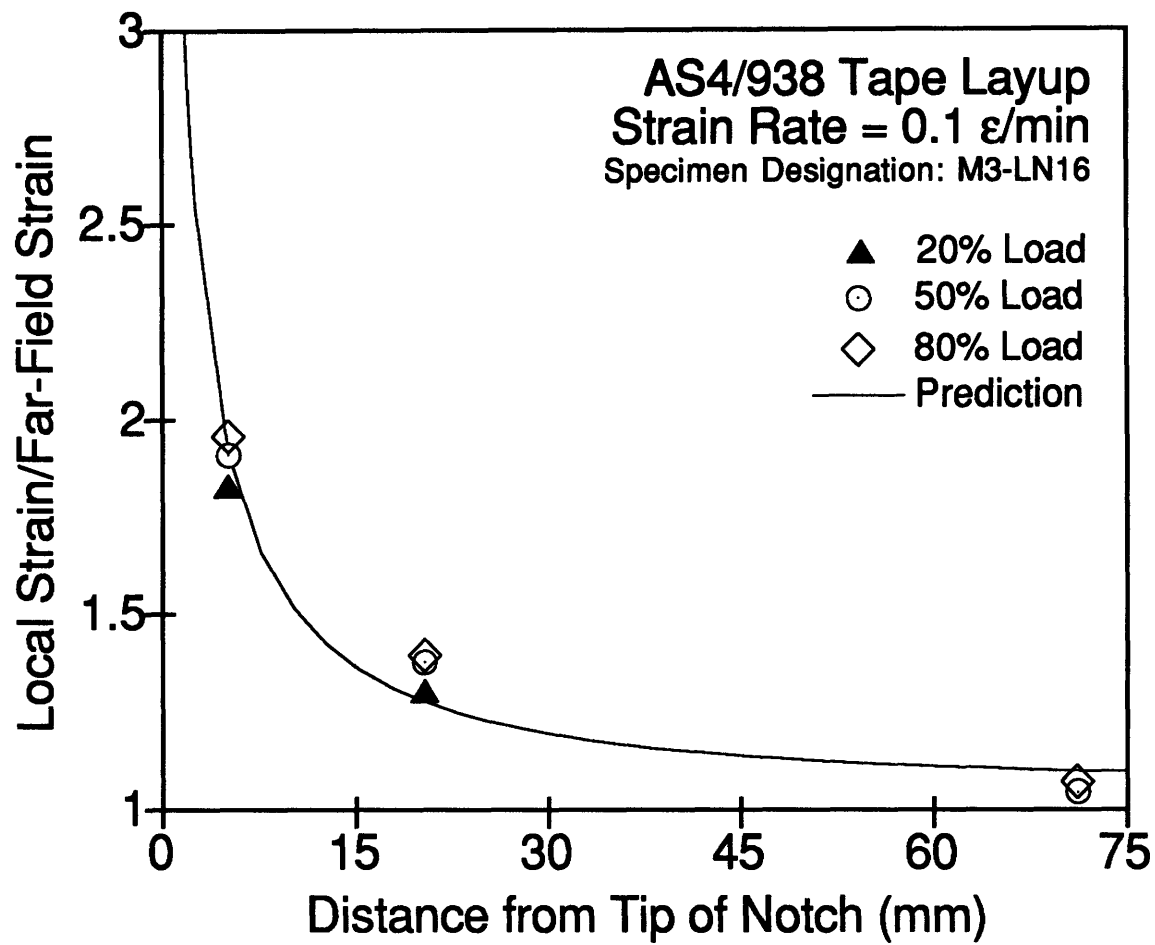


Figure C.6 Strain Distribution of AS4/938 Tape Layup Notched Specimen M3-LN16 at 0.1 ϵ /min.

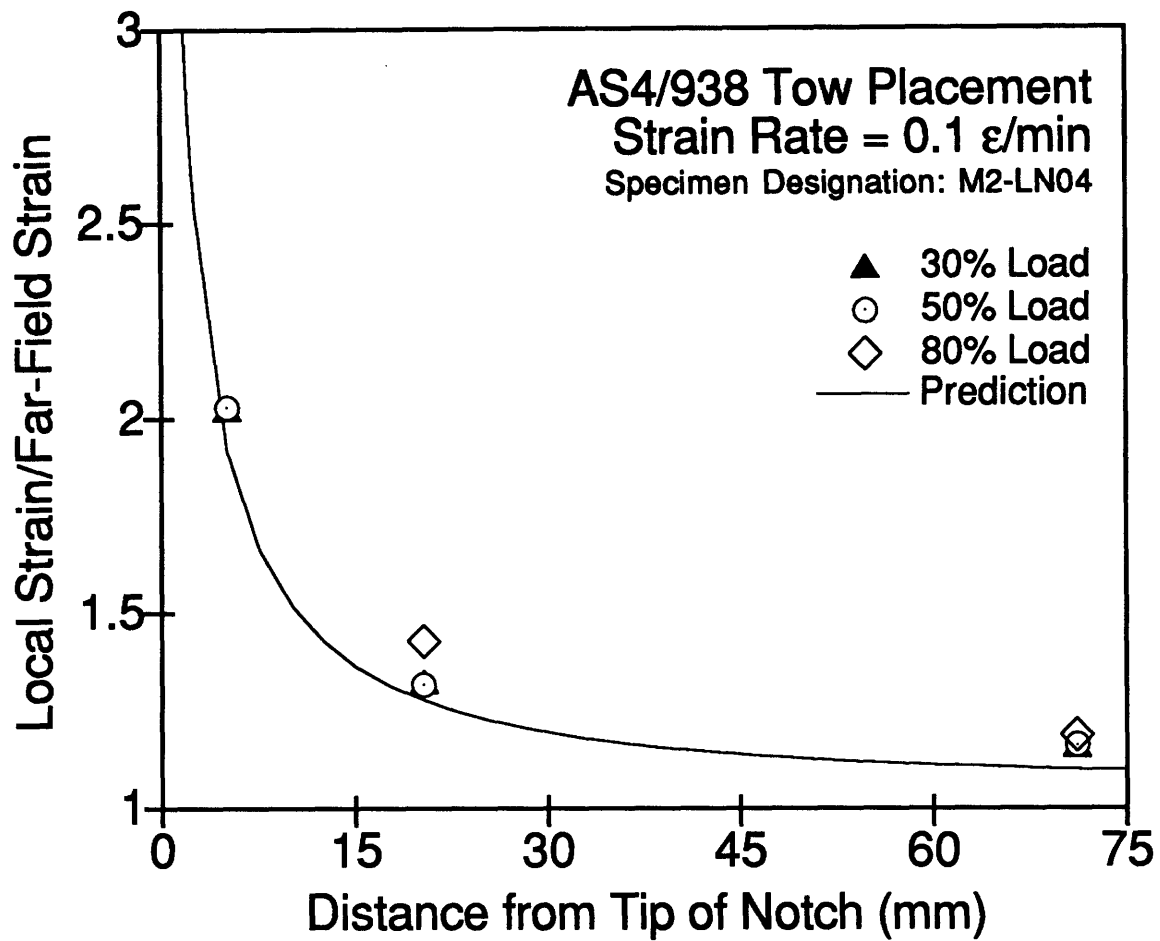


Figure C.7 Strain Distribution of AS4/938 Tow Placed Notched Specimen M2-LN04 at 0.1 ϵ /min.

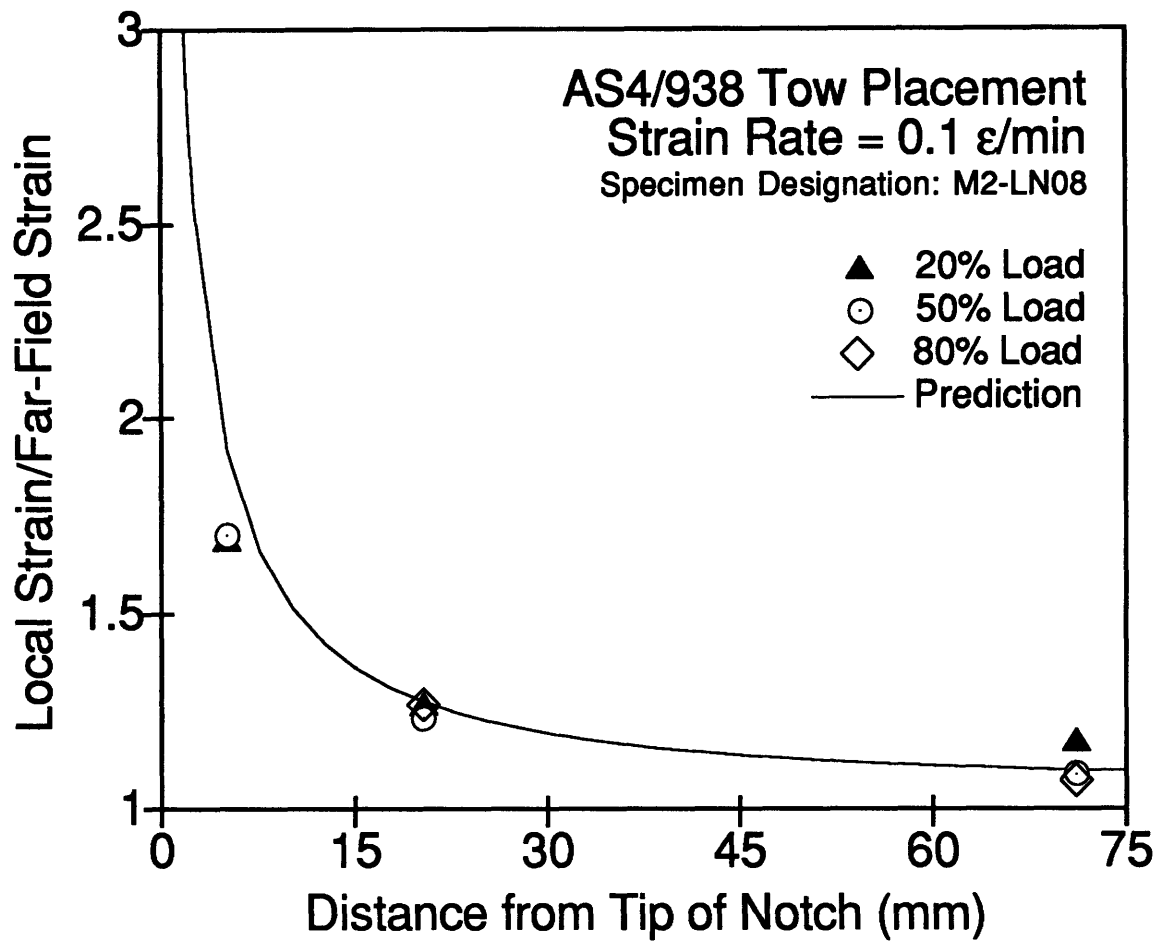


Figure C.8 Strain Distribution of AS4/938 Tow Placed Notched Specimen M2-LN08 at 0.1 ϵ /min.

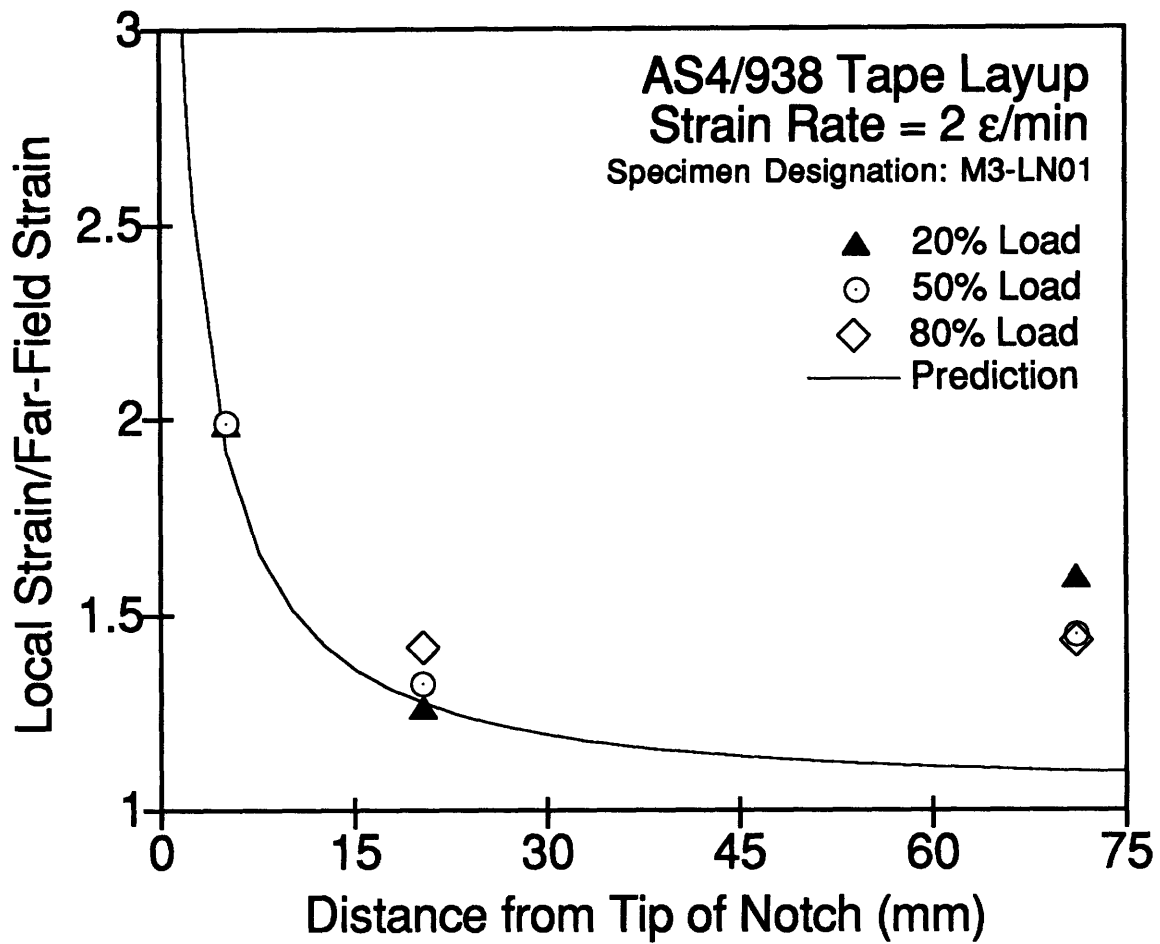


Figure C.9 Strain Distribution of AS4/938 Tape Layup Notched Specimen M3-LN01 at 2 ϵ /min.

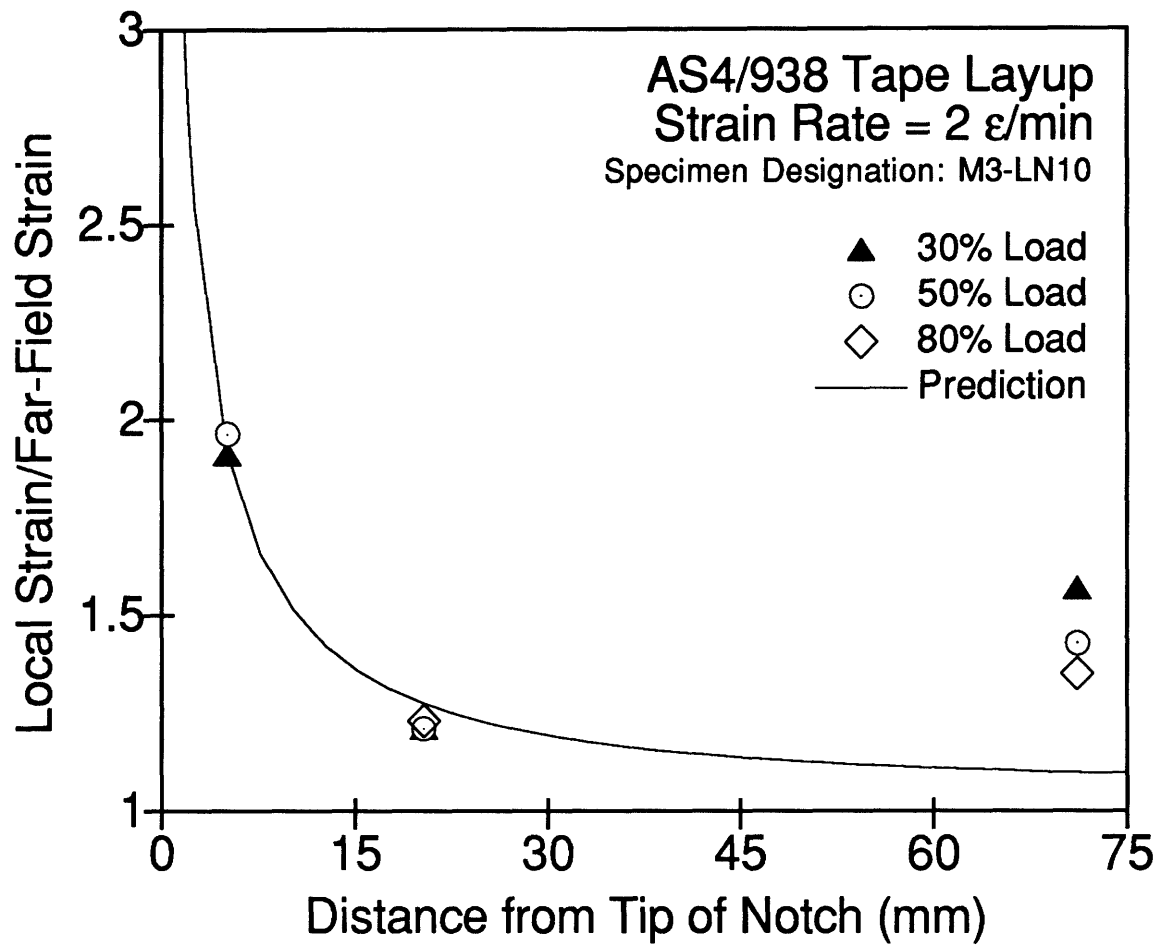


Figure C.10 Strain Distribution of AS4/938 Tape Layup Notched Specimen M3-LN10 at 2 ϵ /min.

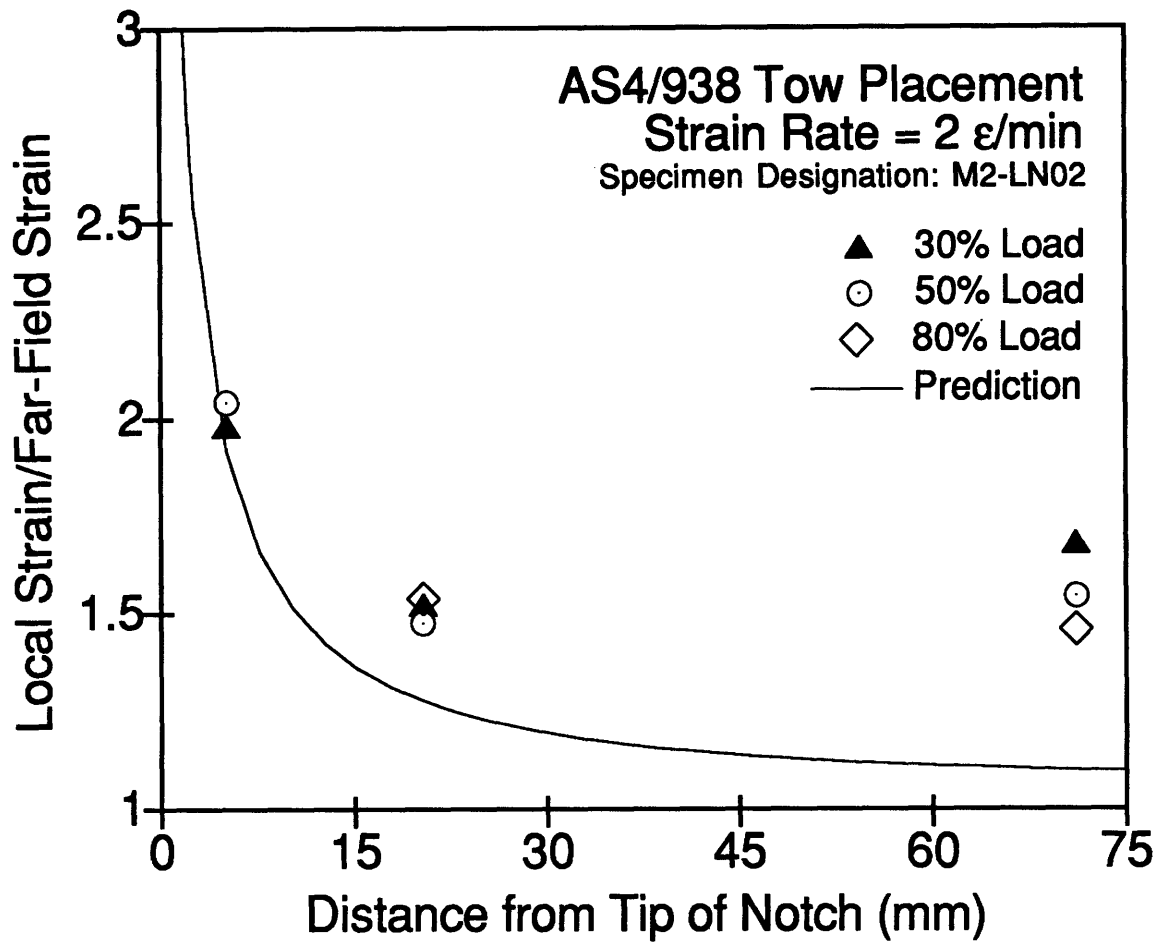


Figure C.11 Strain Distribution of AS4/938 Tow Placed Notched Specimen M2-LN02 at 2 ϵ /min.

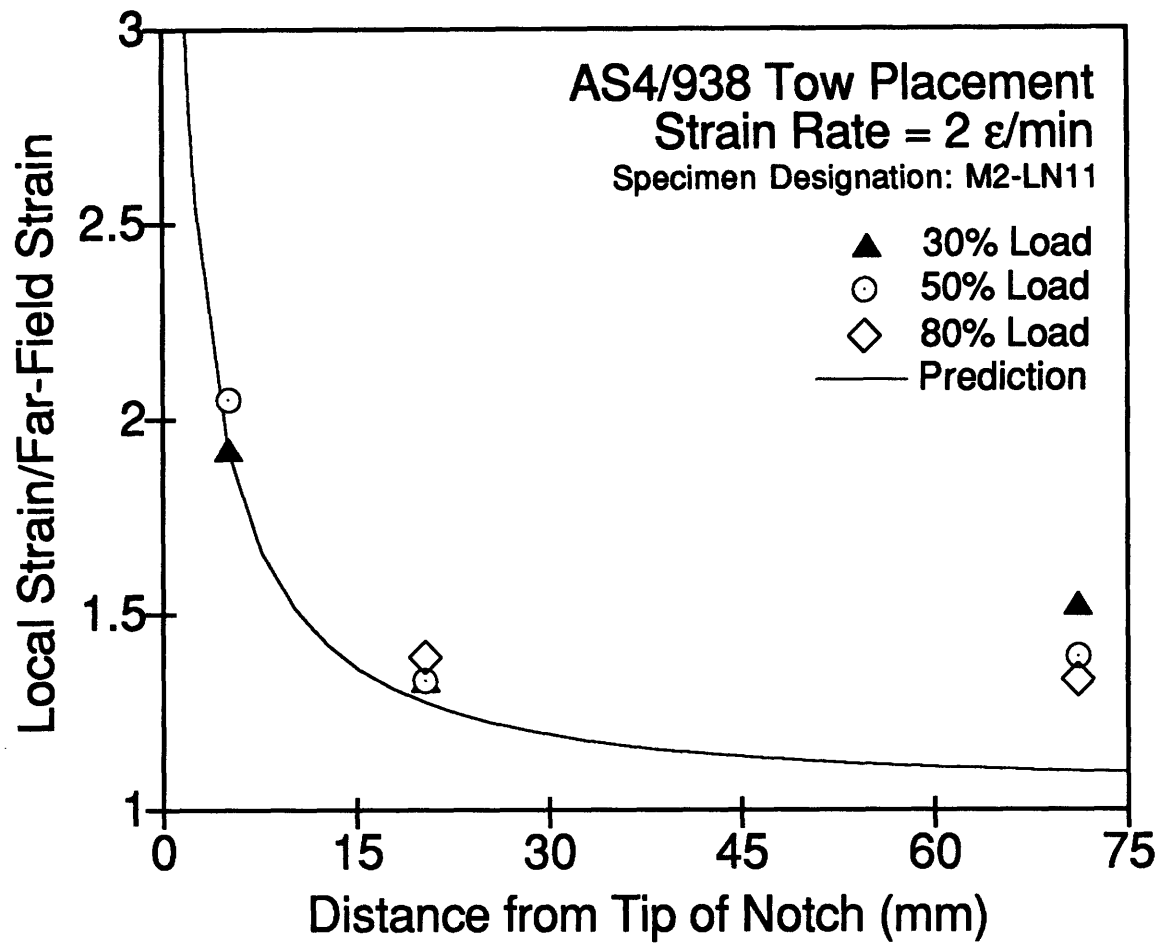


Figure C.12 Strain Distribution of AS4/938 Tow Placed Notched Specimen M2-LN11 at 2 ϵ /min.

APPENDIX D

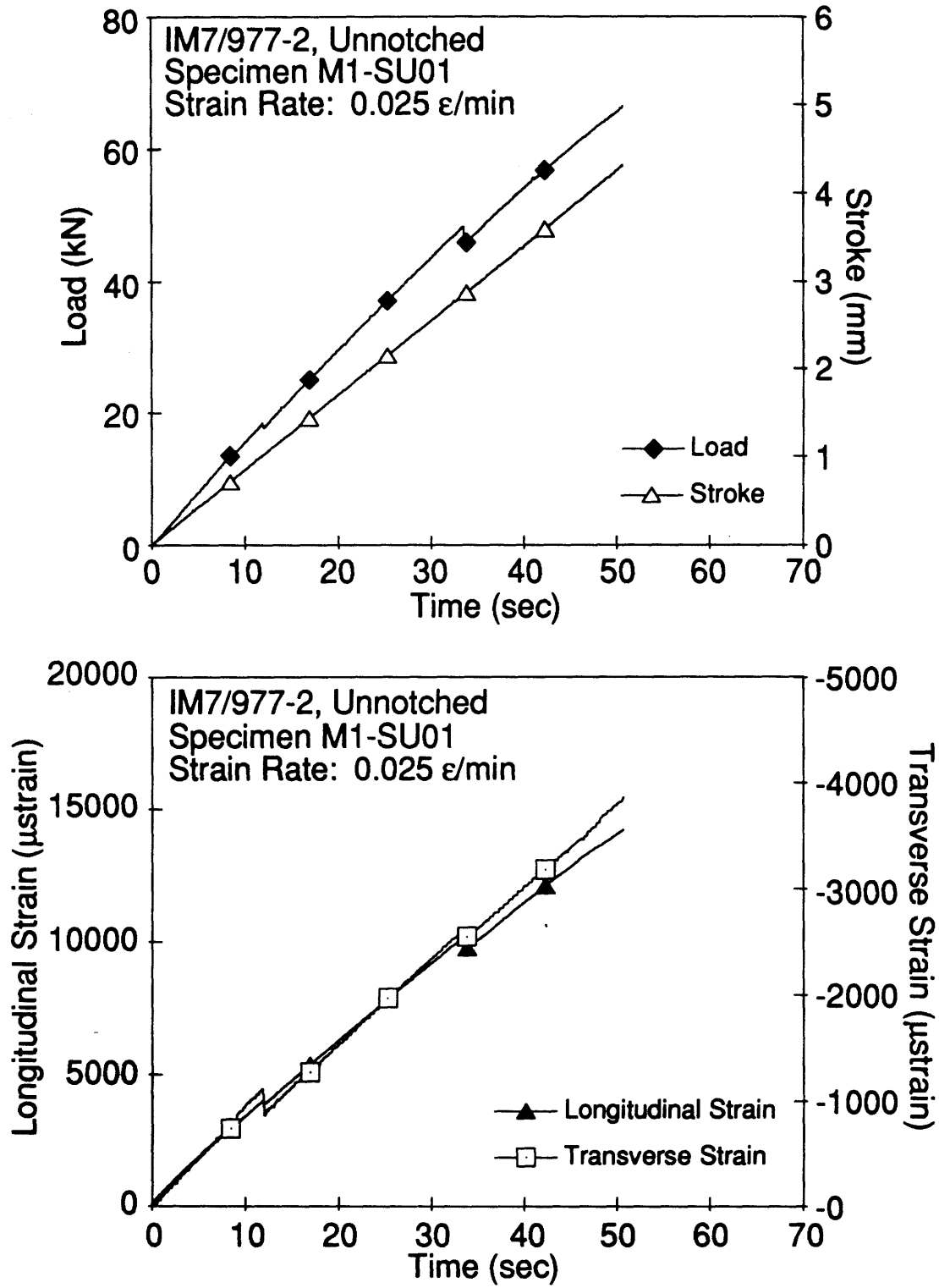


Figure D.1 Plots of Load, Stroke, Longitudinal Strain and Transverse Strain versus Time for Specimen M1-SU01.

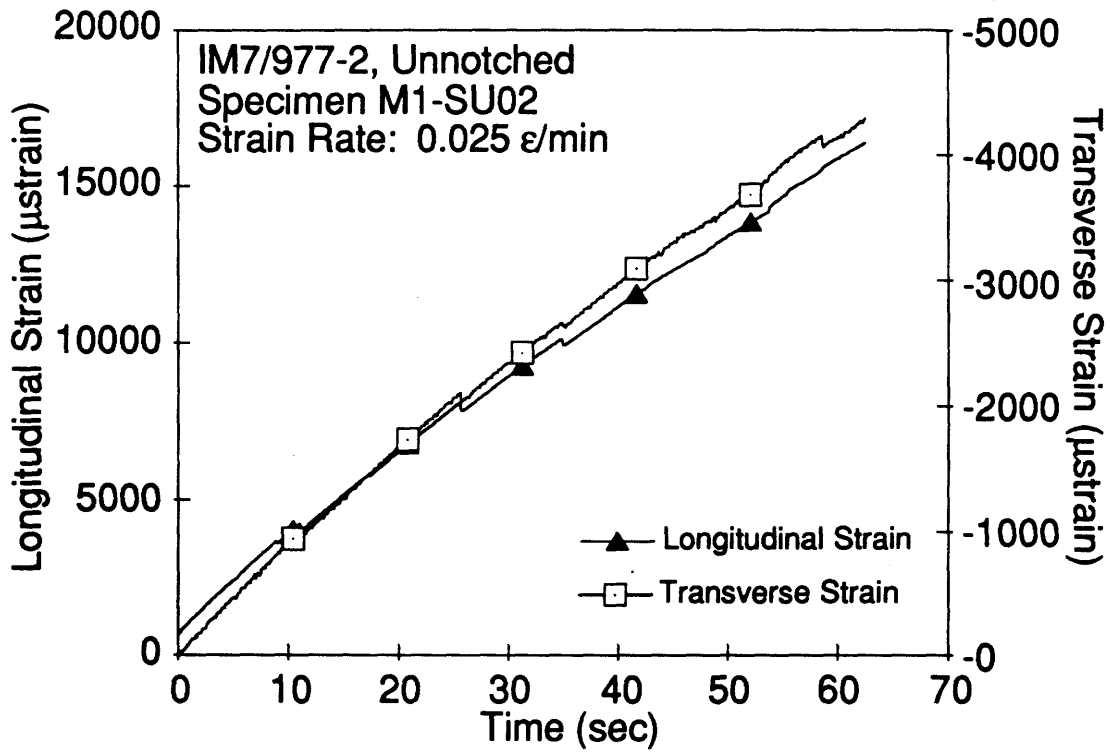
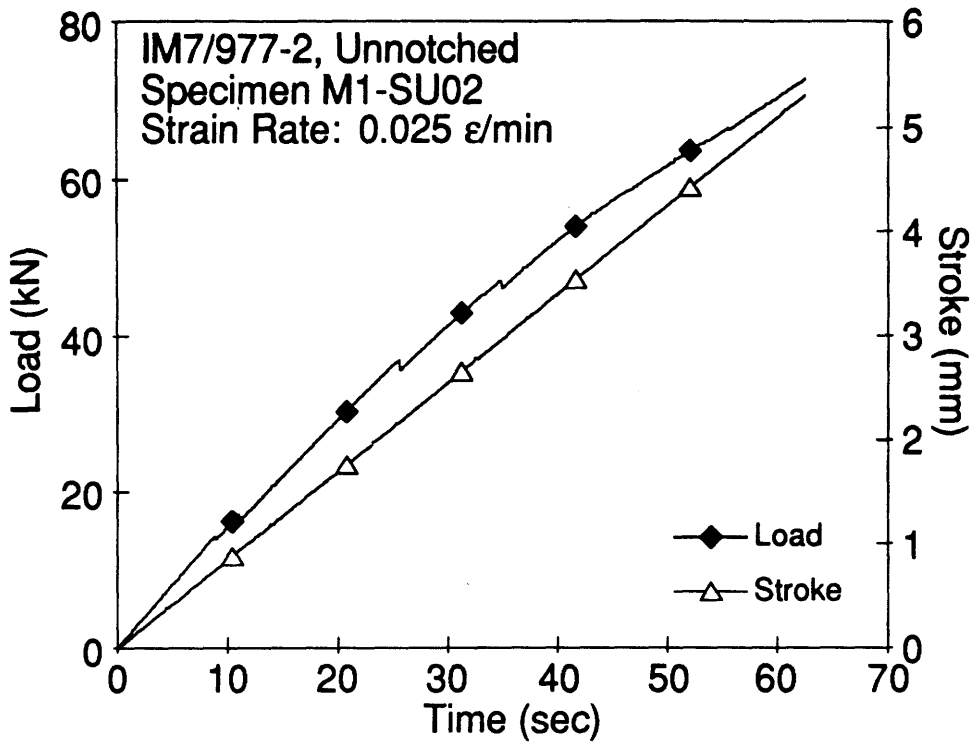


Figure D.2 Plots of Load, Stroke, Longitudinal Strain and Transverse Strain versus Time for Specimen M1-SU02.

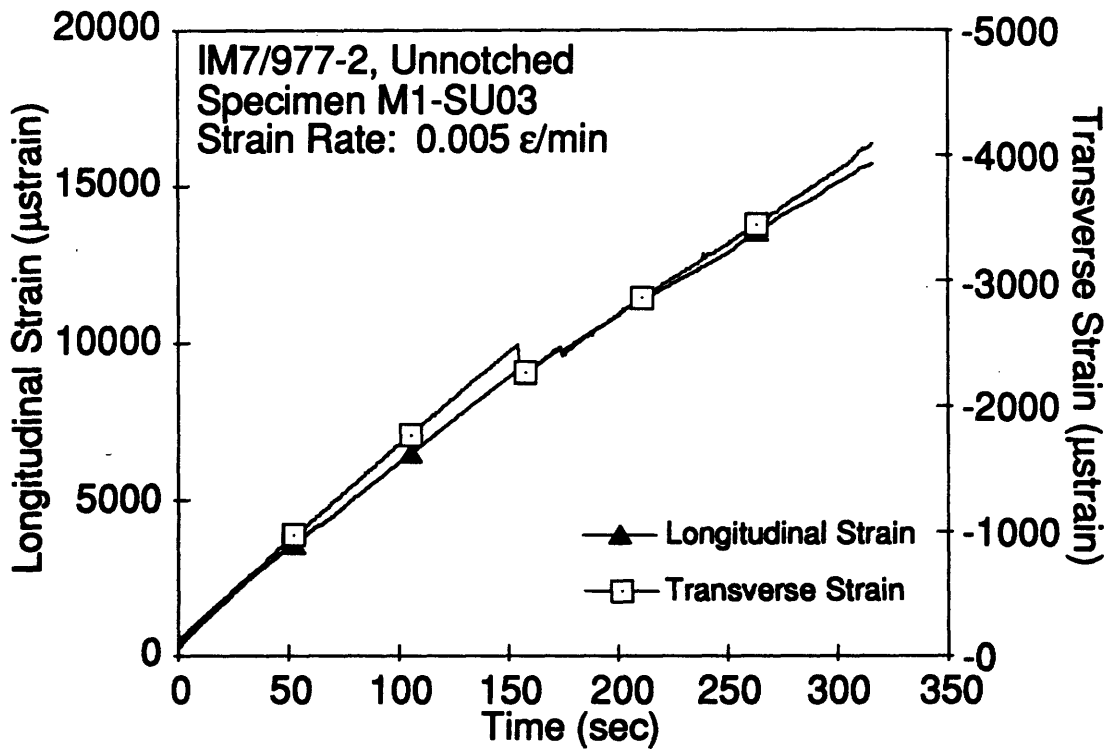
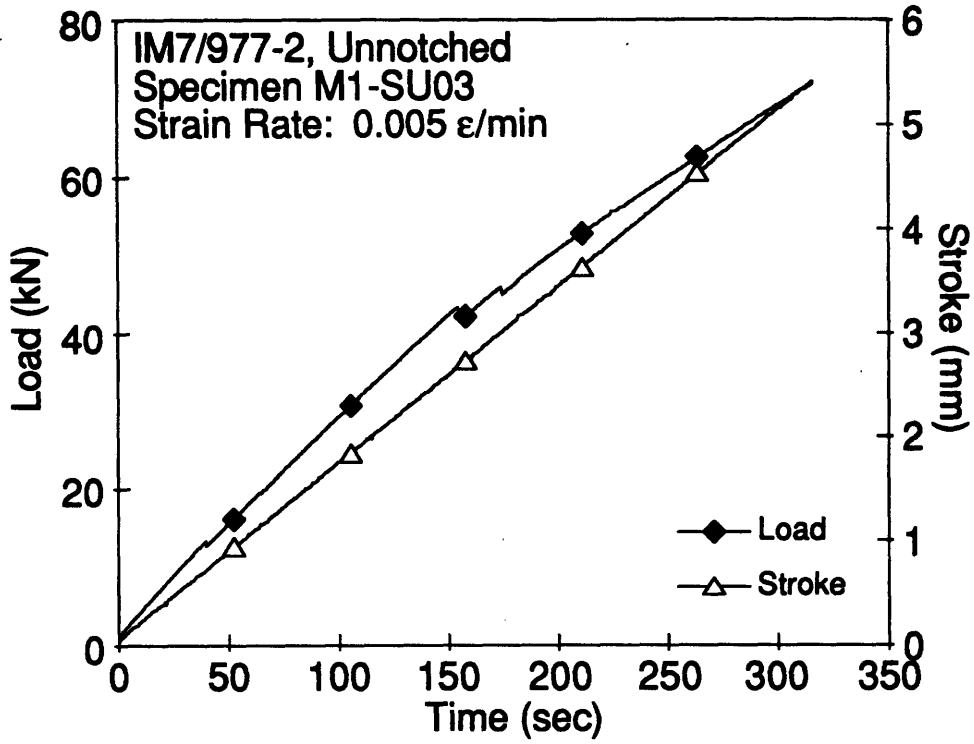


Figure D.3 Plots of Load, Stroke, Longitudinal Strain and Transverse Strain versus Time for Specimen M1-SU03.

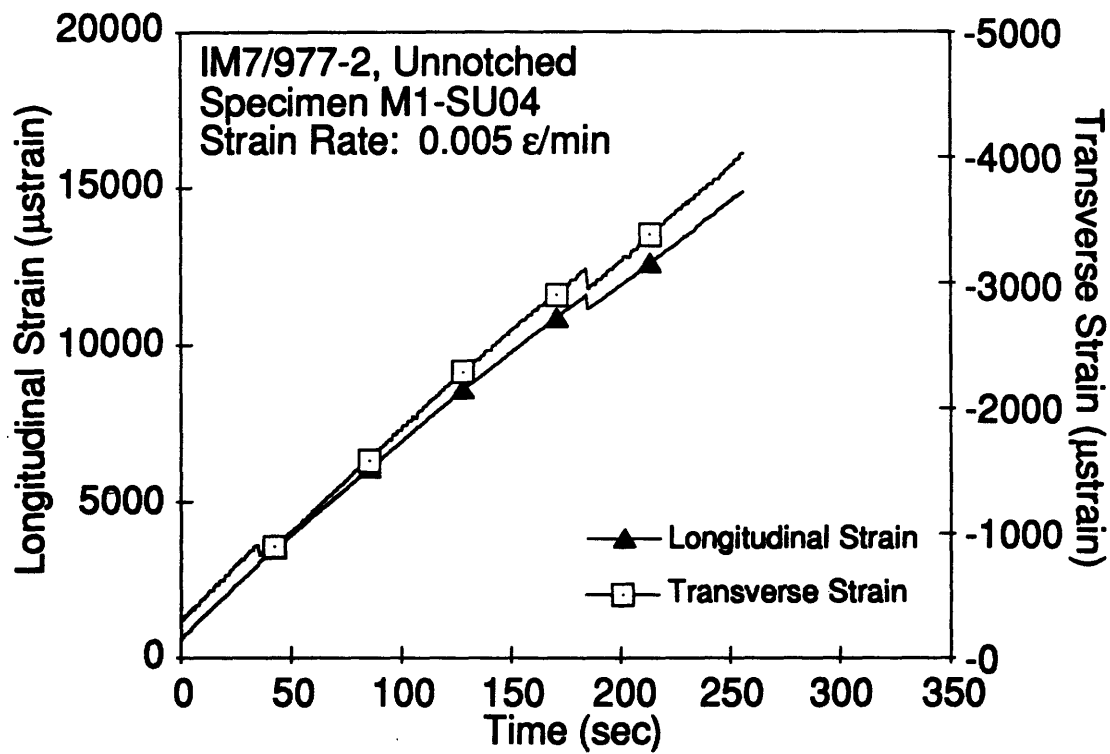
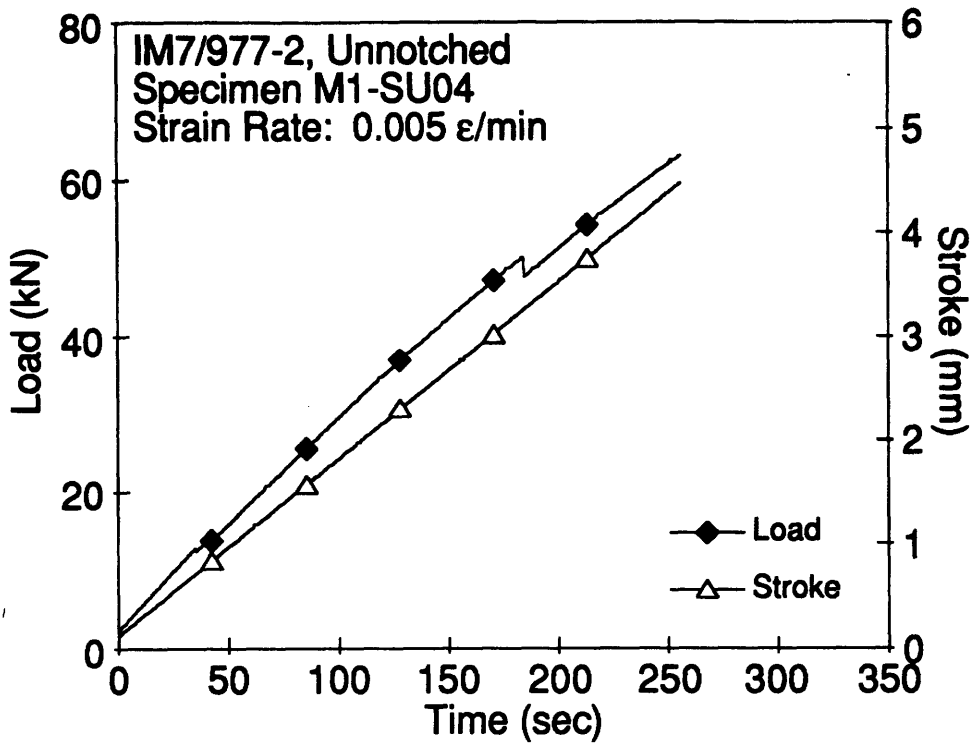


Figure D.4 Plots of Load, Stroke, Longitudinal Strain and Transverse Strain versus Time for Specimen M1-SU04.

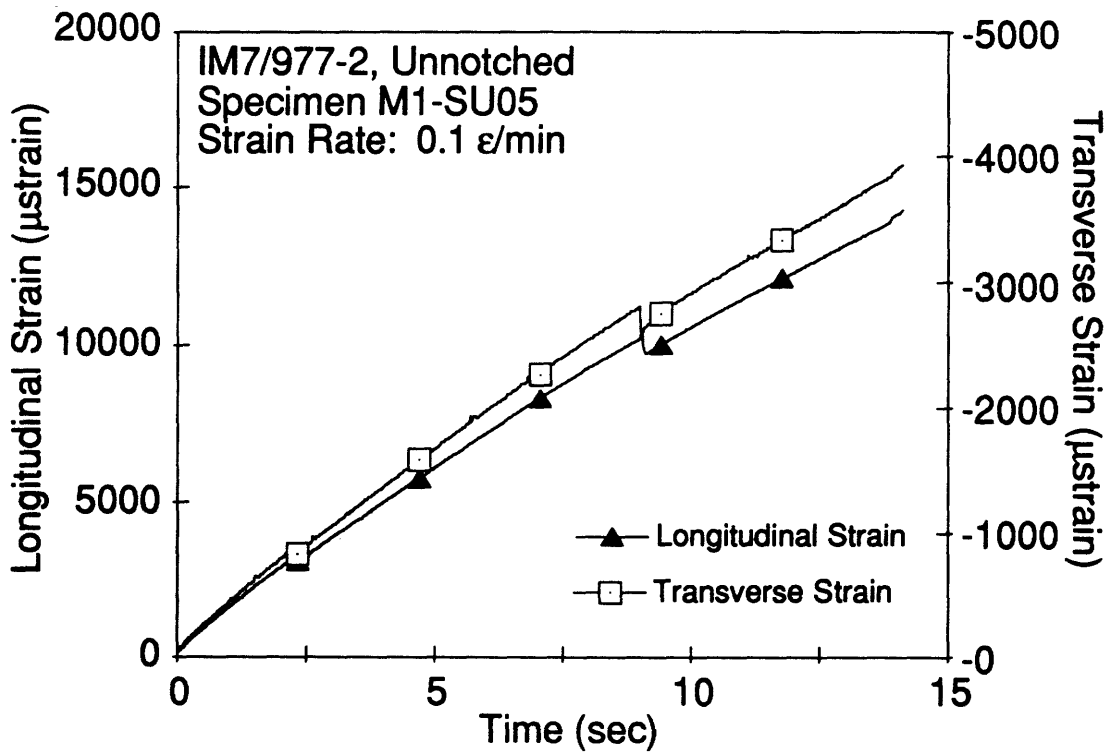
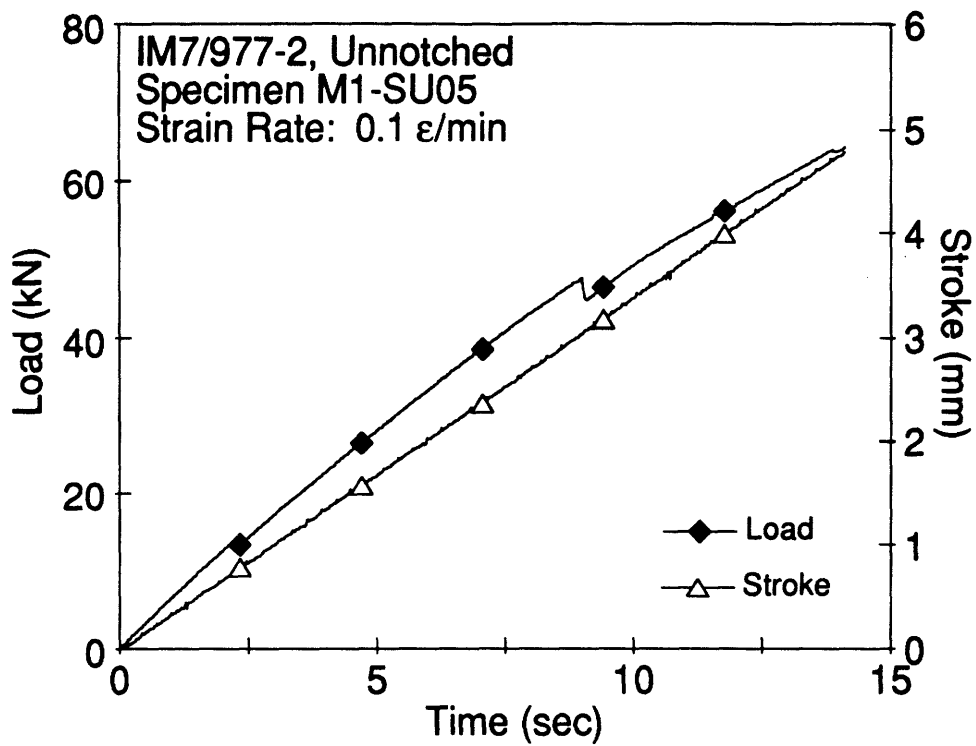


Figure D.5 Plots of Load, Stroke, Longitudinal Strain and Transverse Strain versus Time for Specimen M1-SU05.

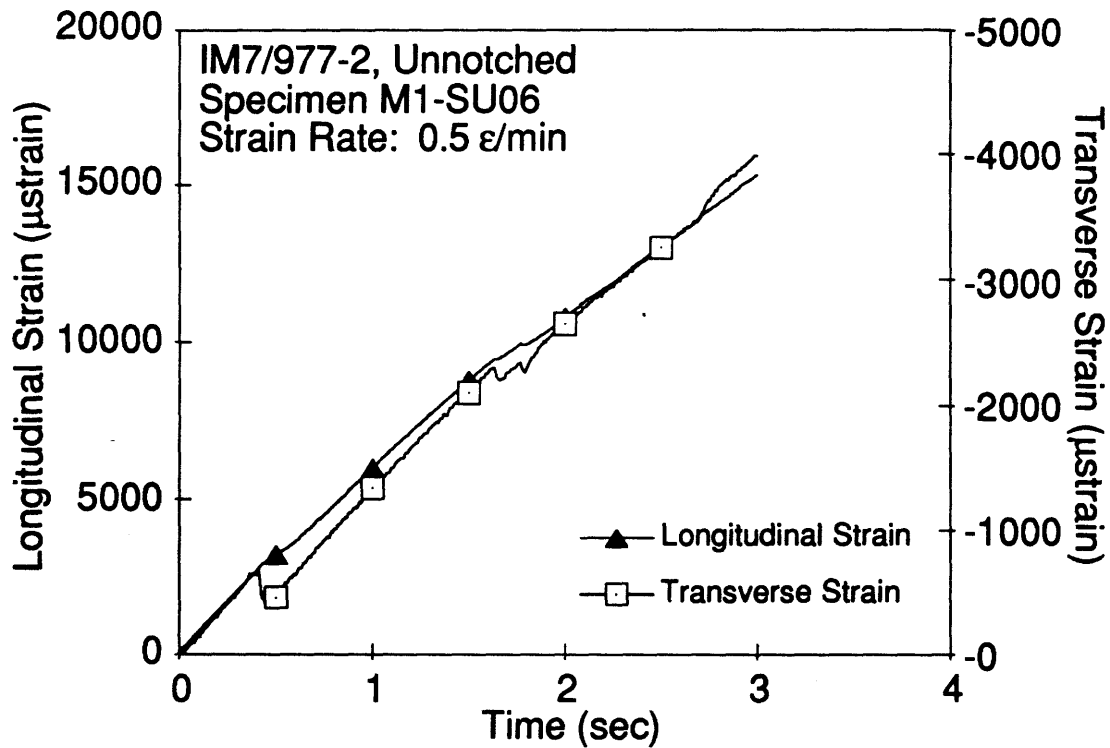
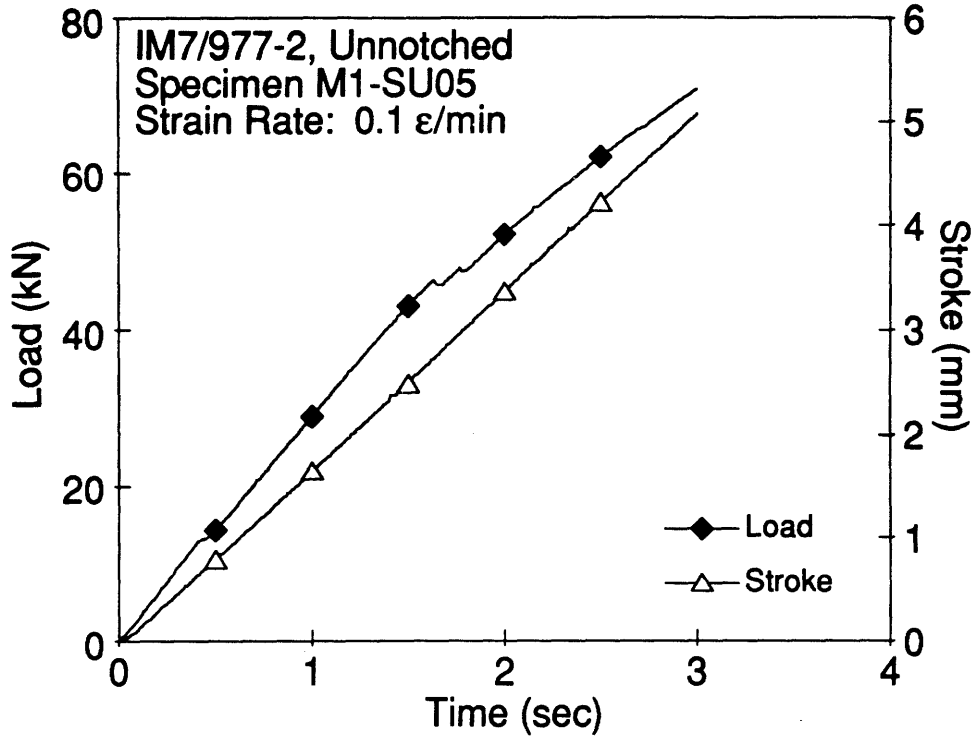


Figure D.6 Plots of Load, Stroke, Longitudinal Strain and Transverse Strain versus Time for Specimen M1-SU06.

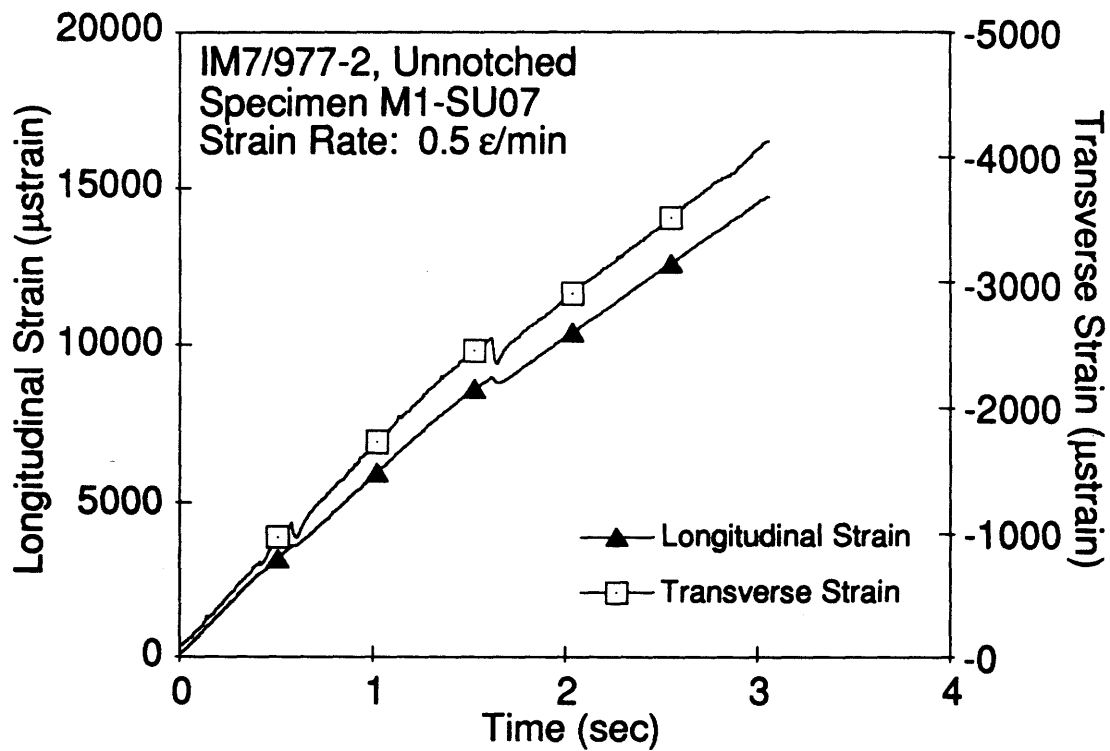
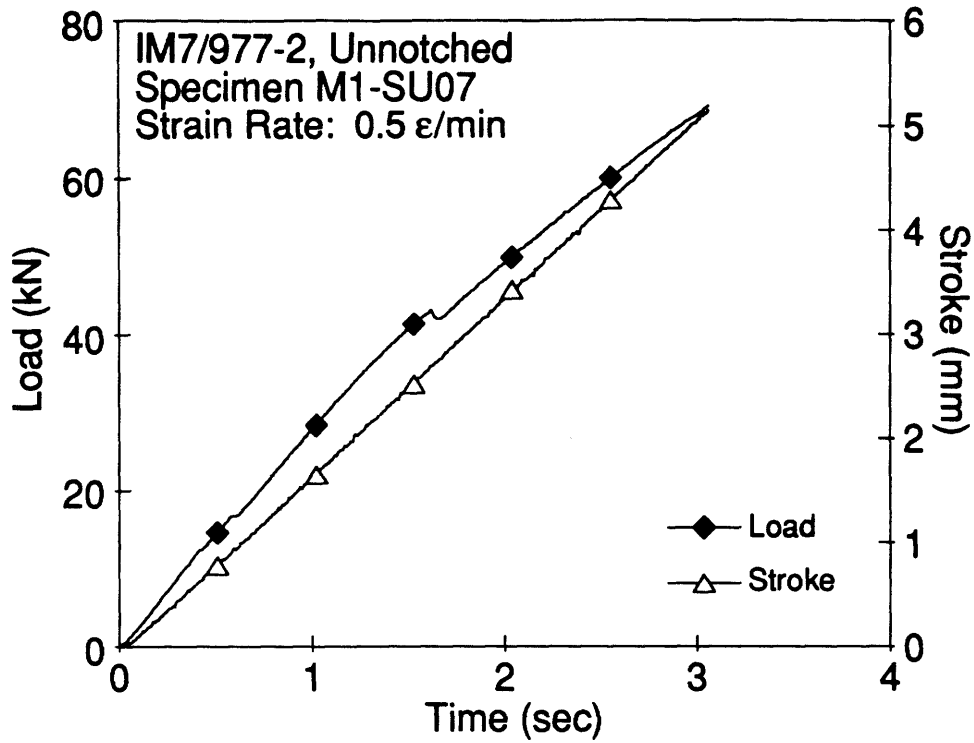


Figure D.7 Plots of Load, Stroke, Longitudinal Strain and Transverse Strain versus Time for Specimen M1-SU07.

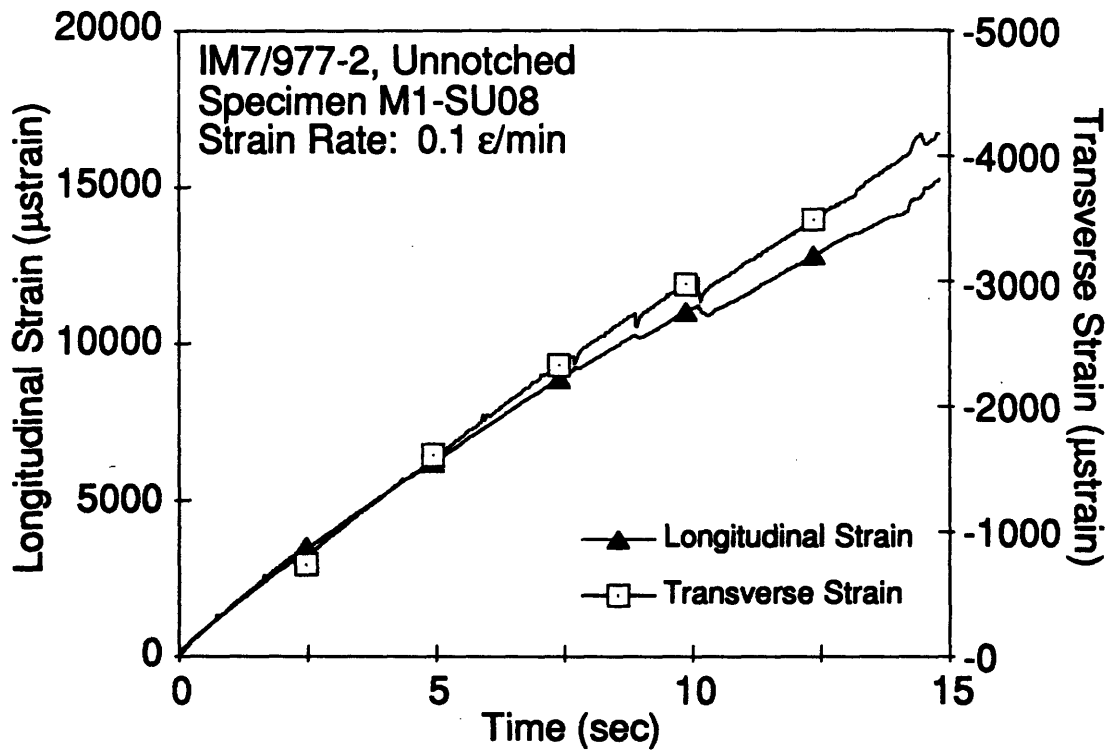
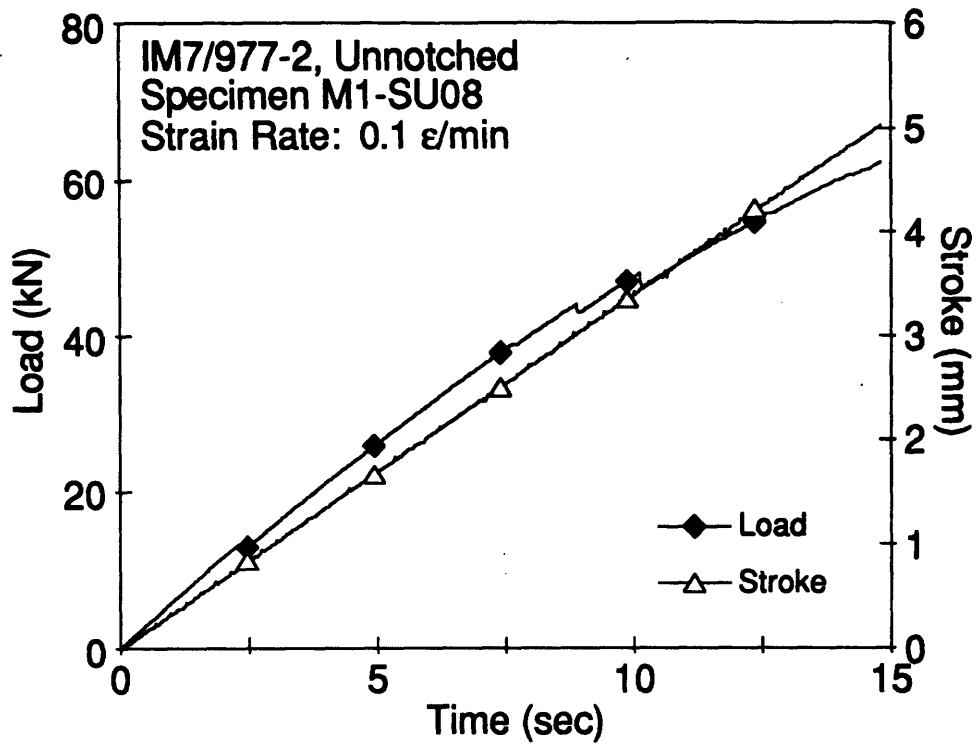


Figure D.8 Plots of Load, Stroke, Longitudinal Strain and Transverse Strain versus Time for Specimen M1-SU08.

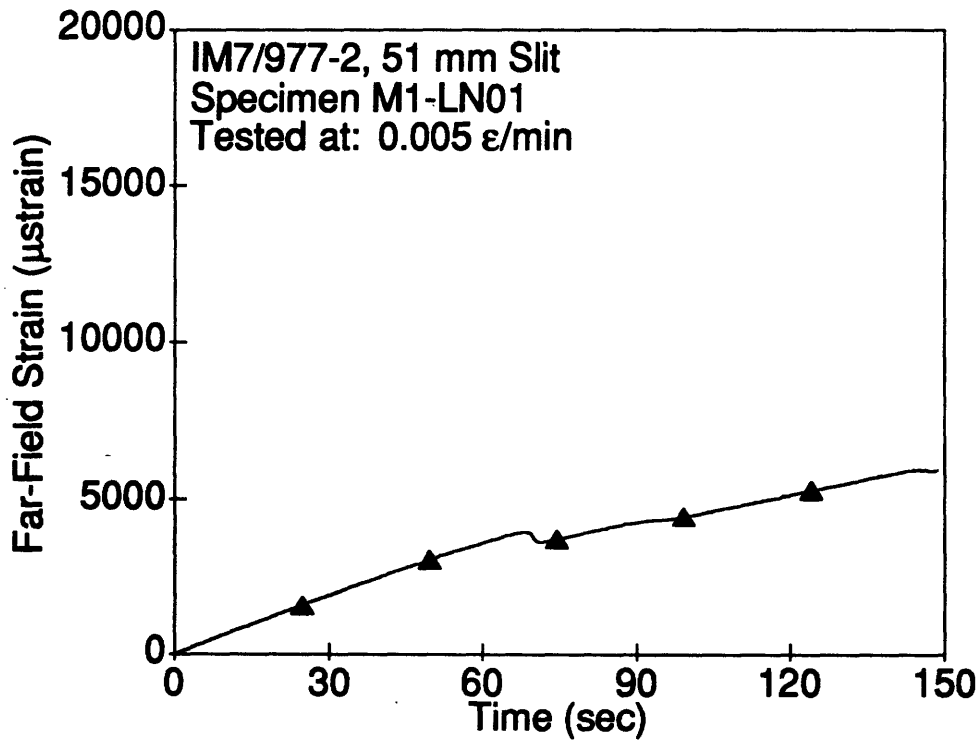
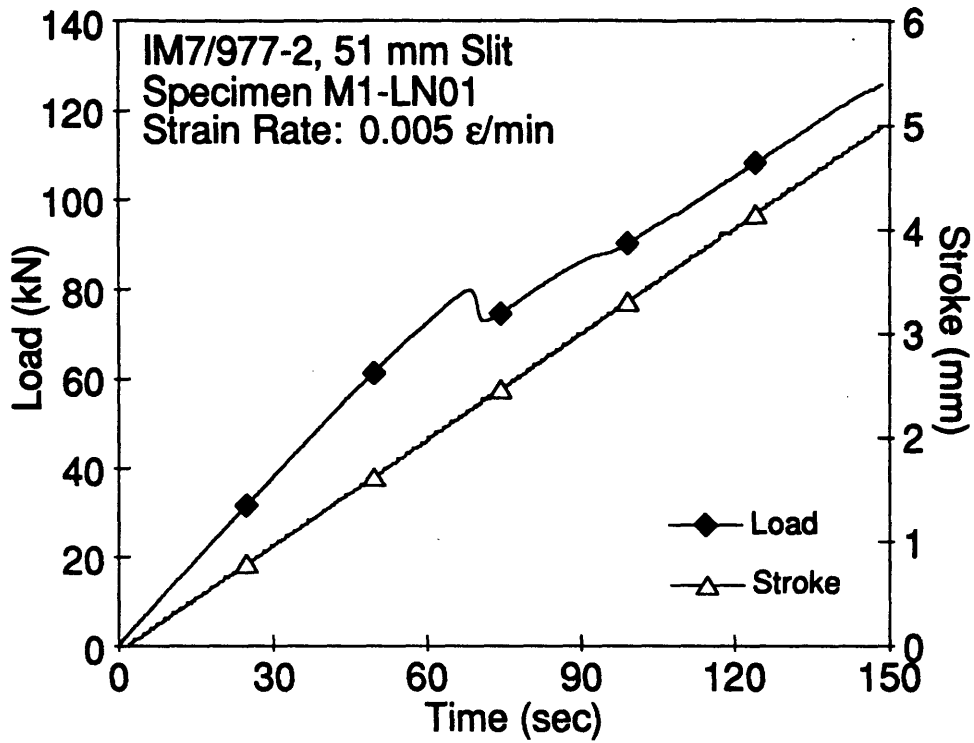


Figure D.9 Plots of Load, Stroke and Far-Field Strain versus Time for Specimen M1-LN01.

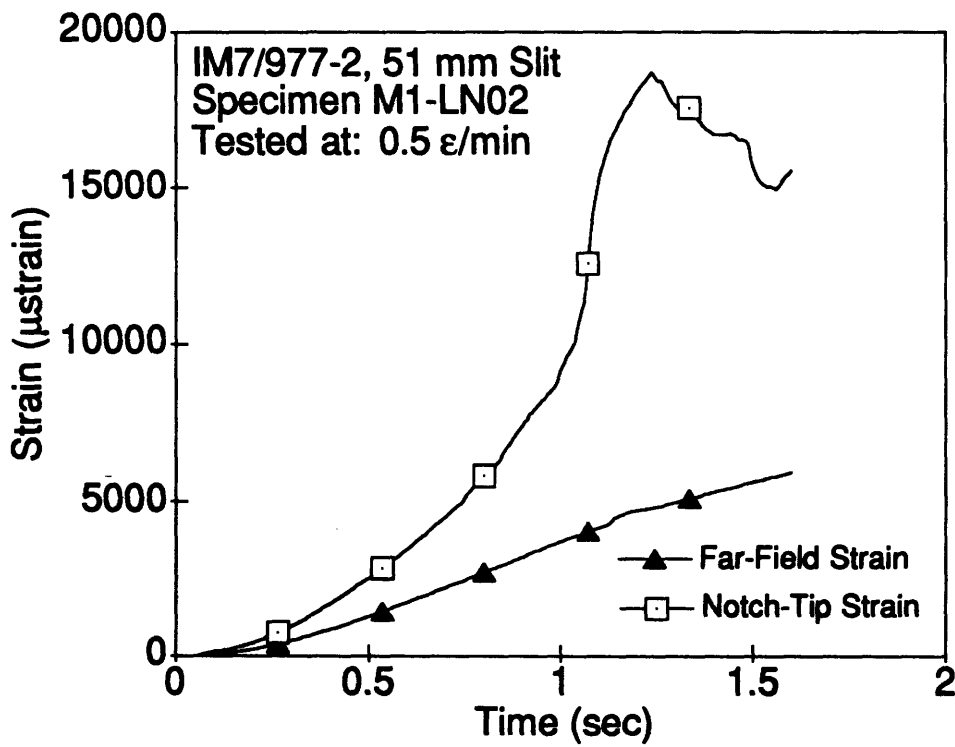
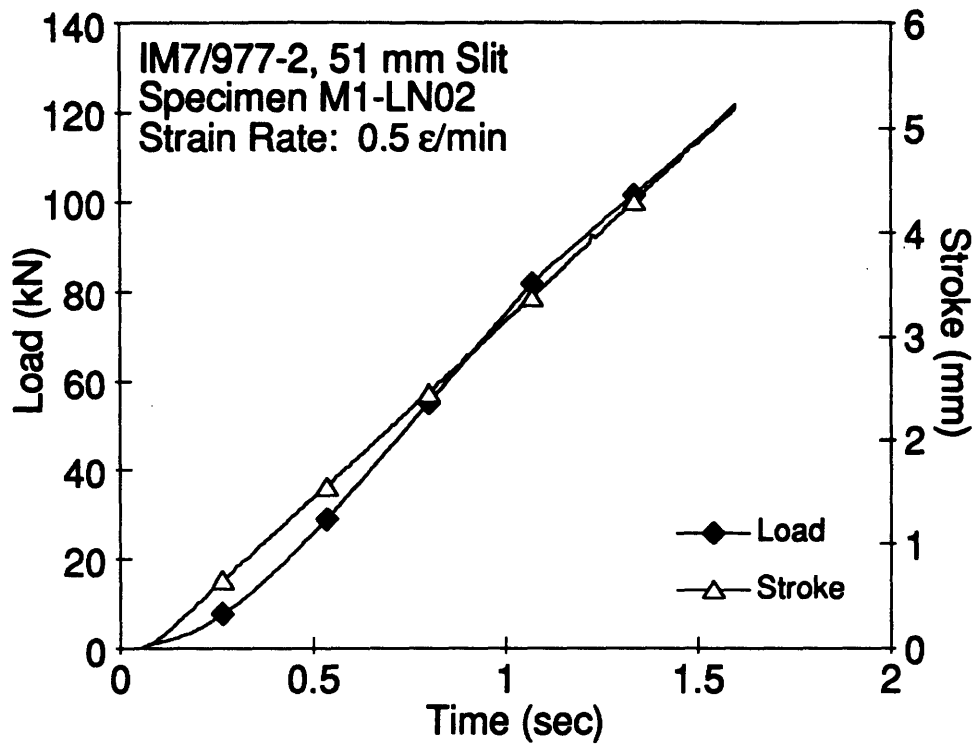


Figure D.10 Plots of Load, Stroke, Far-Field Strain and Notch-Tip Strain versus Time for Specimen M1-LN02.

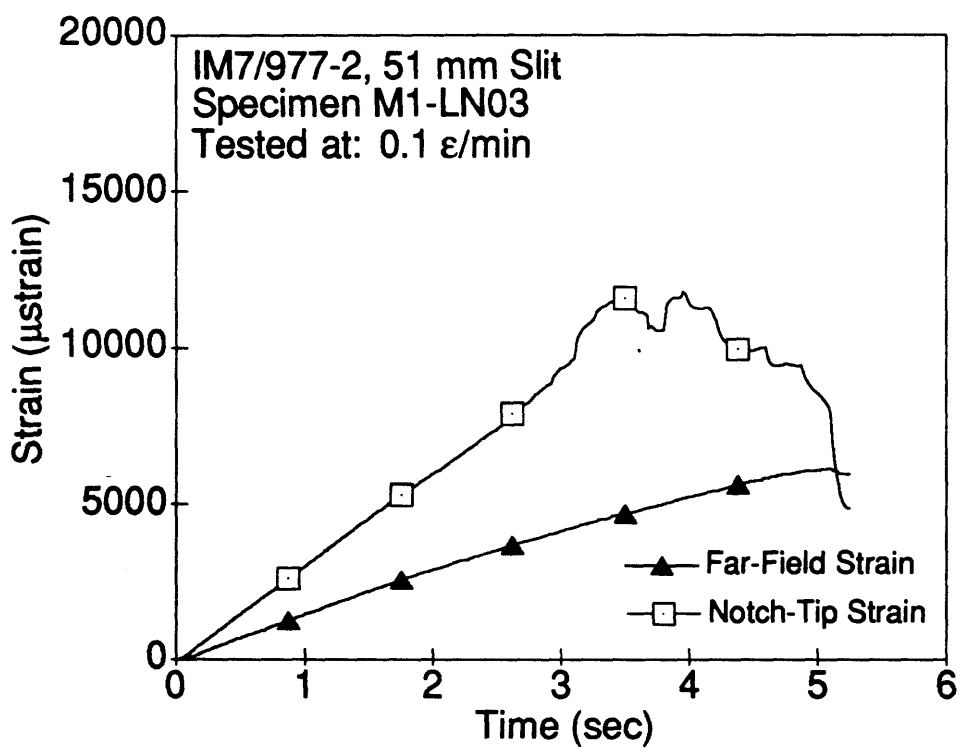
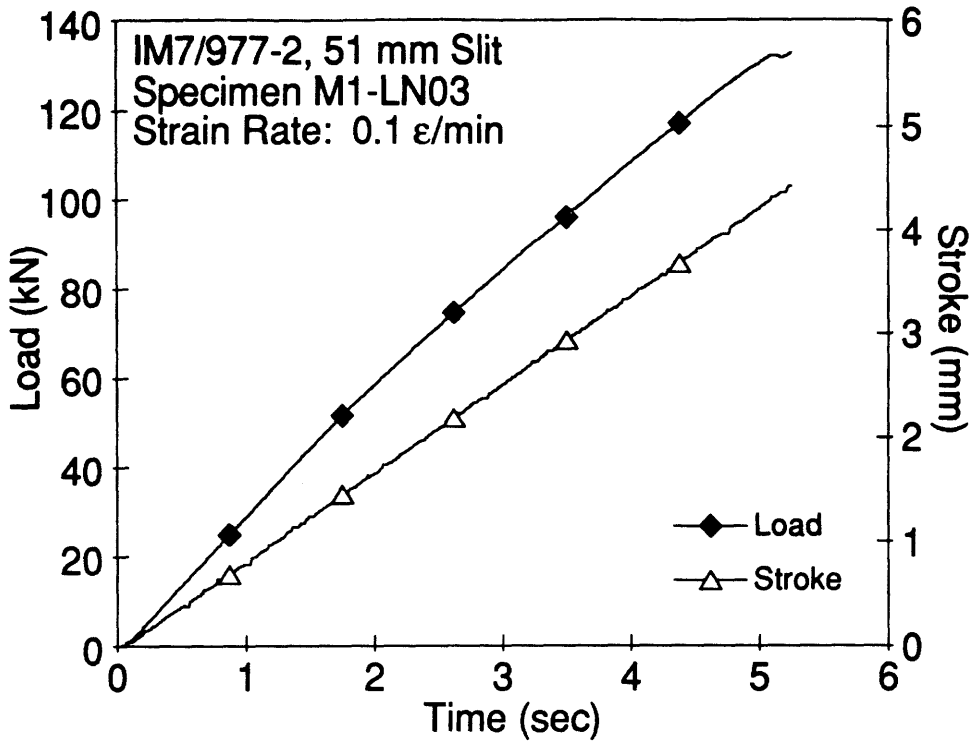


Figure D.11 Plots of Load, Stroke, Far-Field Strain and Notch-Tip Strain versus Time for Specimen M1-LN03.

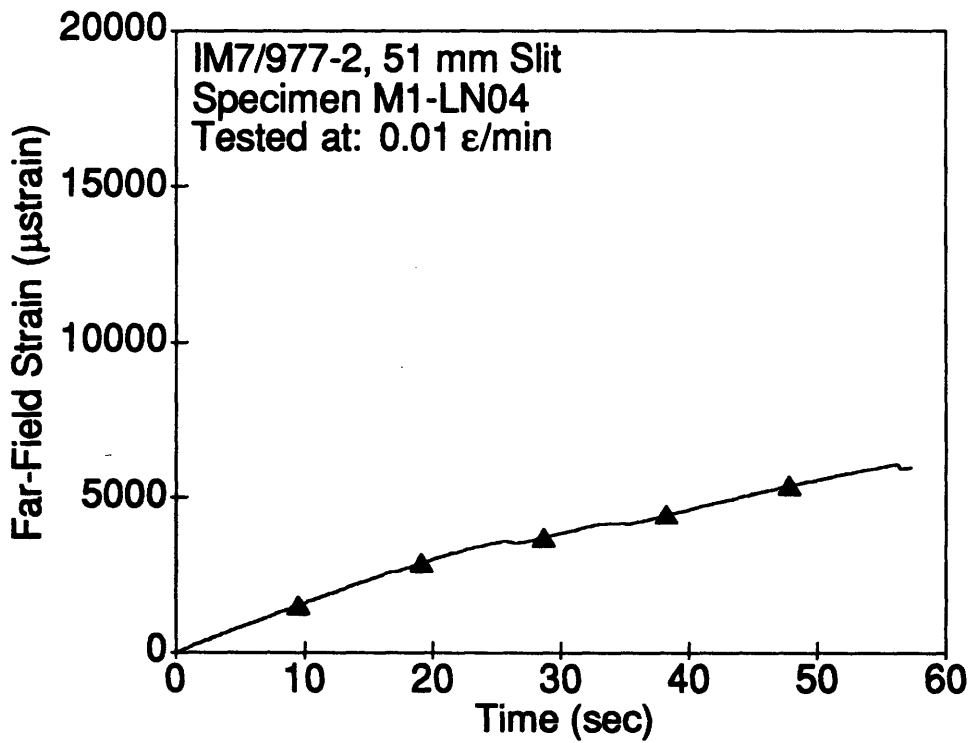
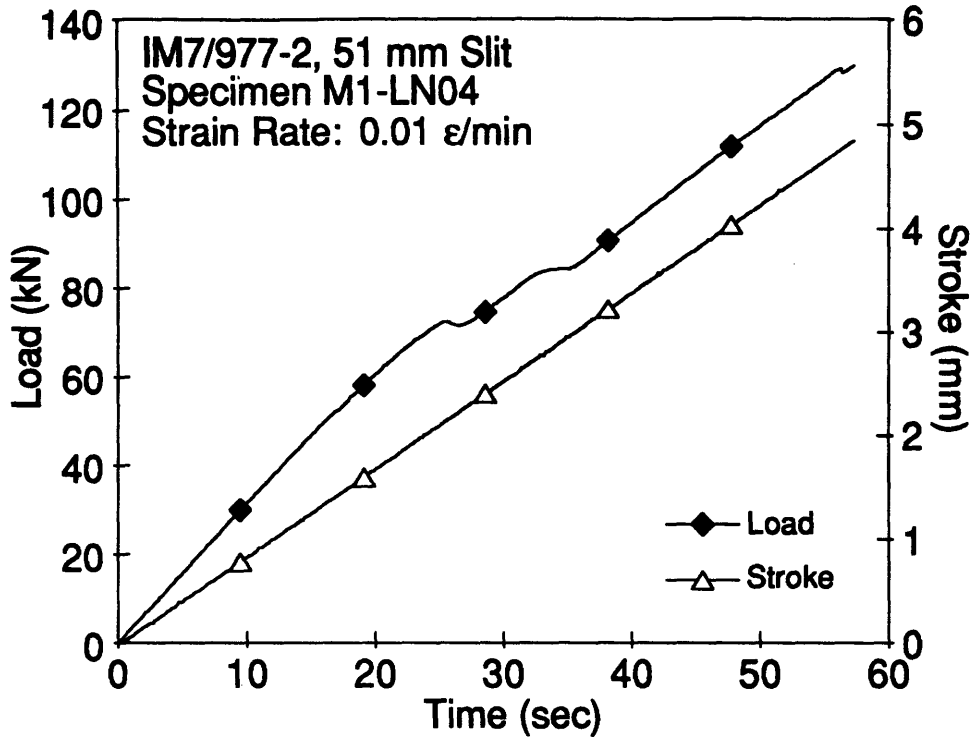


Figure D.12 Plots of Load, Stroke and Far-Field Strain versus Time for Specimen M1-LN04.

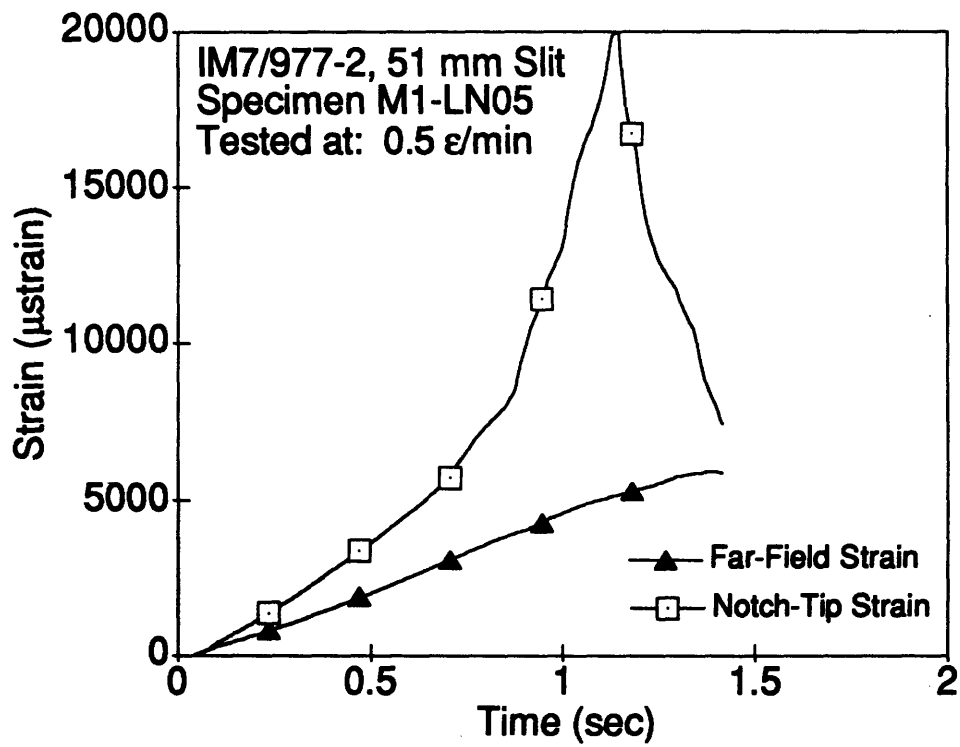
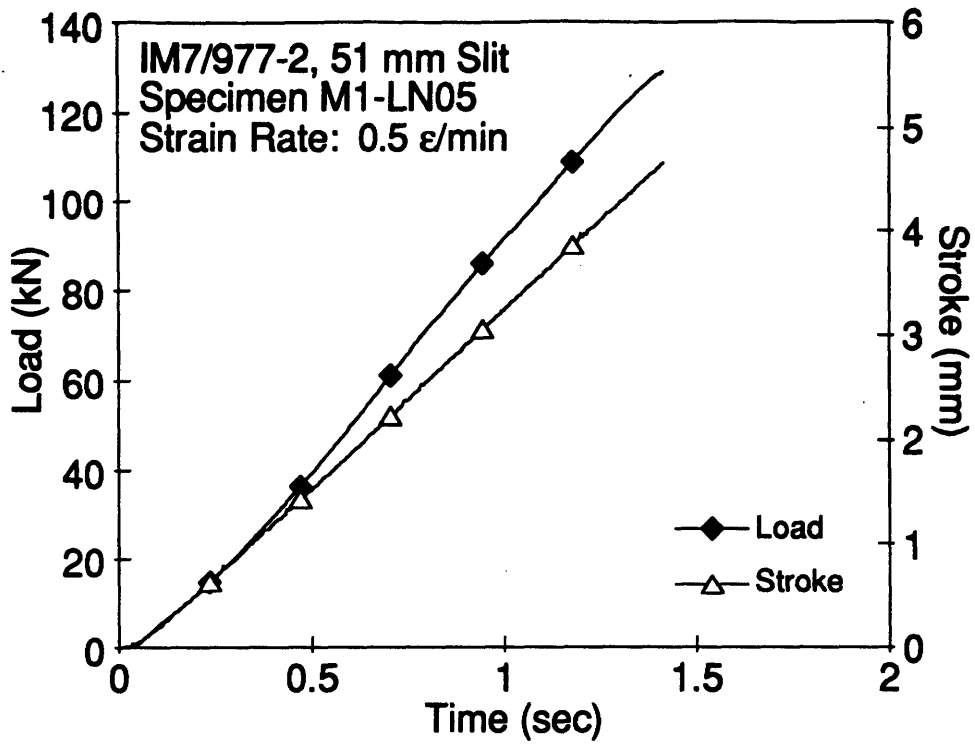


Figure D.13 Plots of Load, Stroke, Far-Field Strain and Notch-Tip Strain versus Time for Specimen M1-LN05.

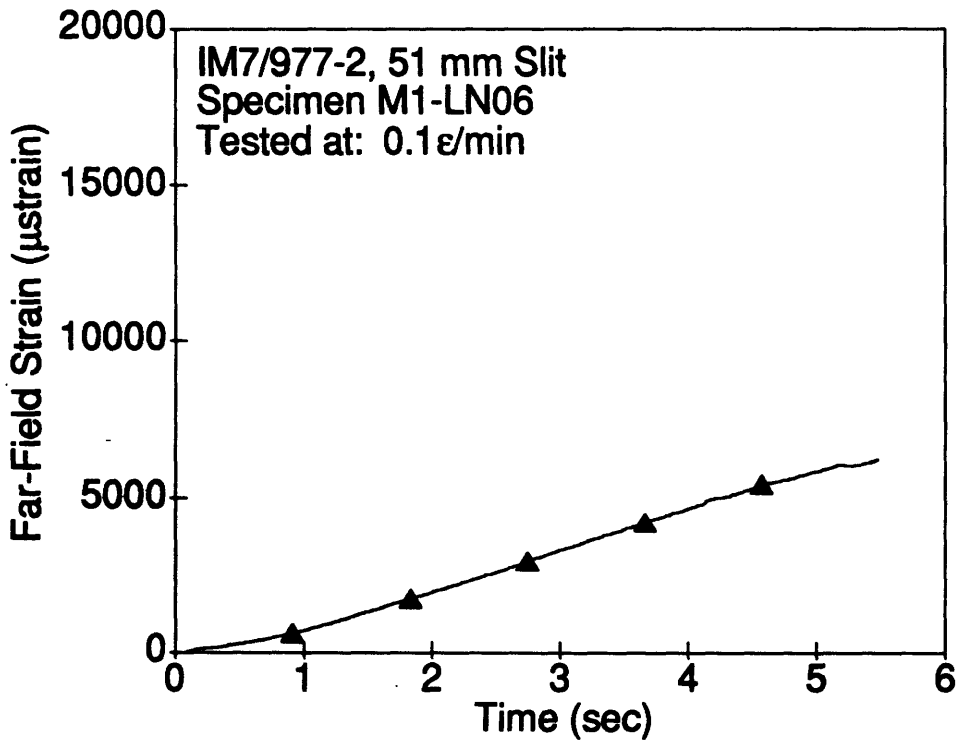
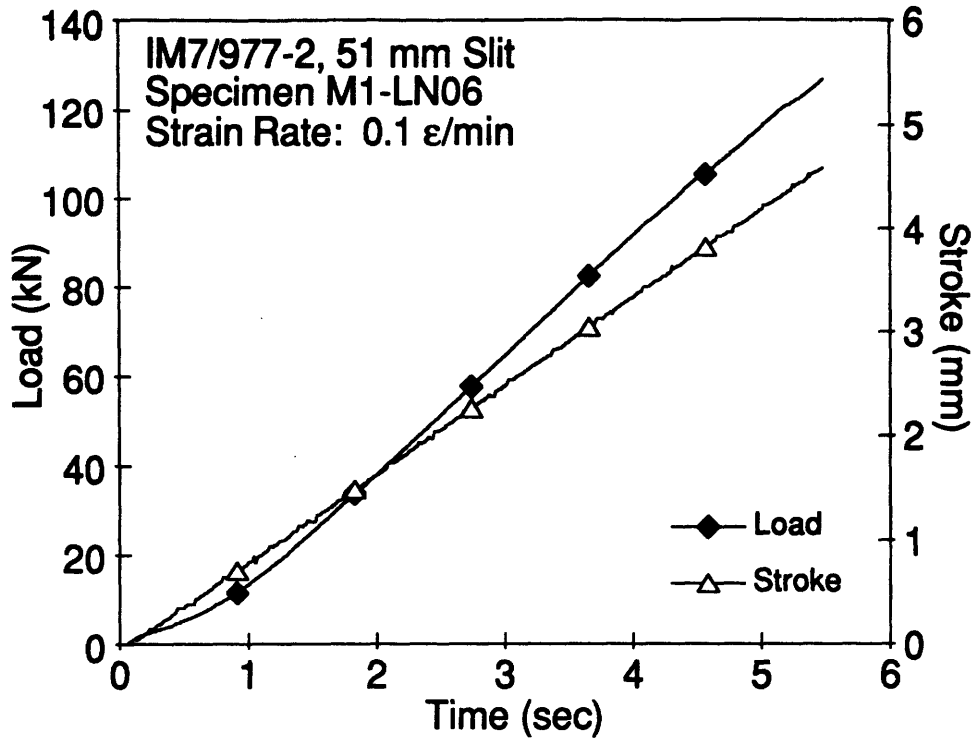


Figure D.14 Plots of Load, Stroke and Far-Field Strain versus Time for Specimen M1-LN06.

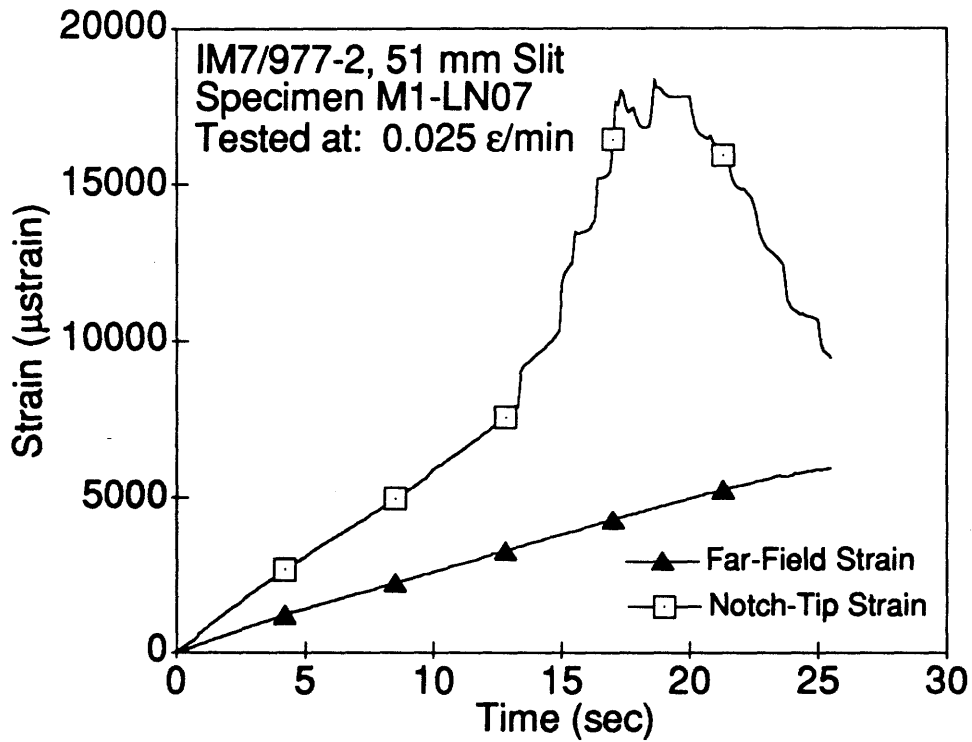
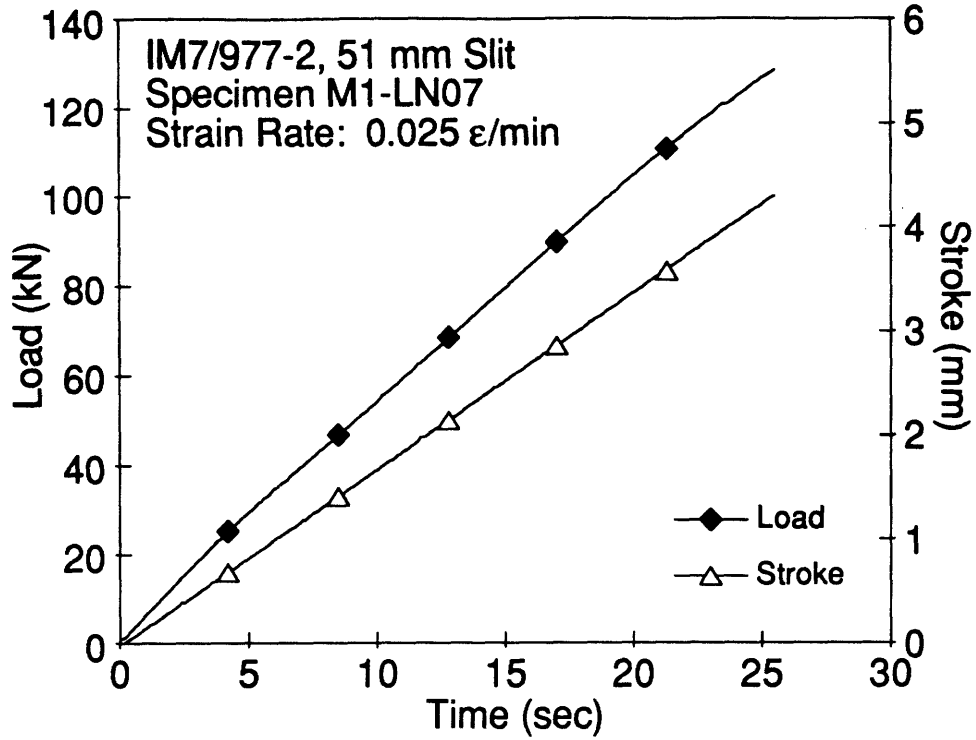


Figure D.15 Plots of Load, Stroke, Far-Field Strain and Notch-Tip Strain versus Time for Specimen M1-LN07.

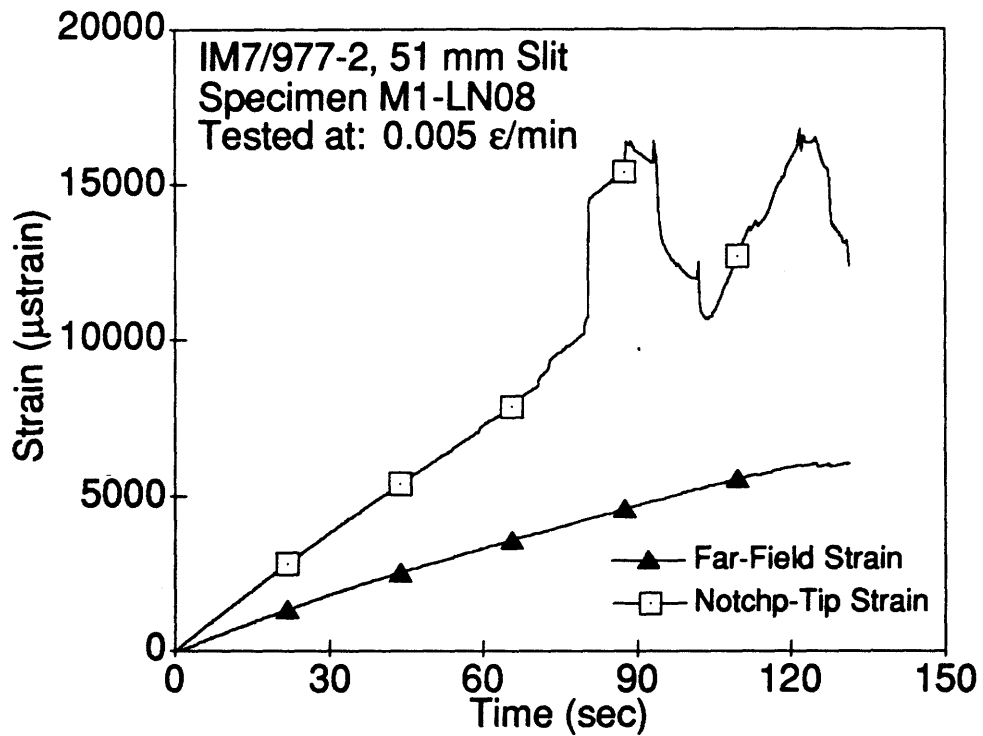
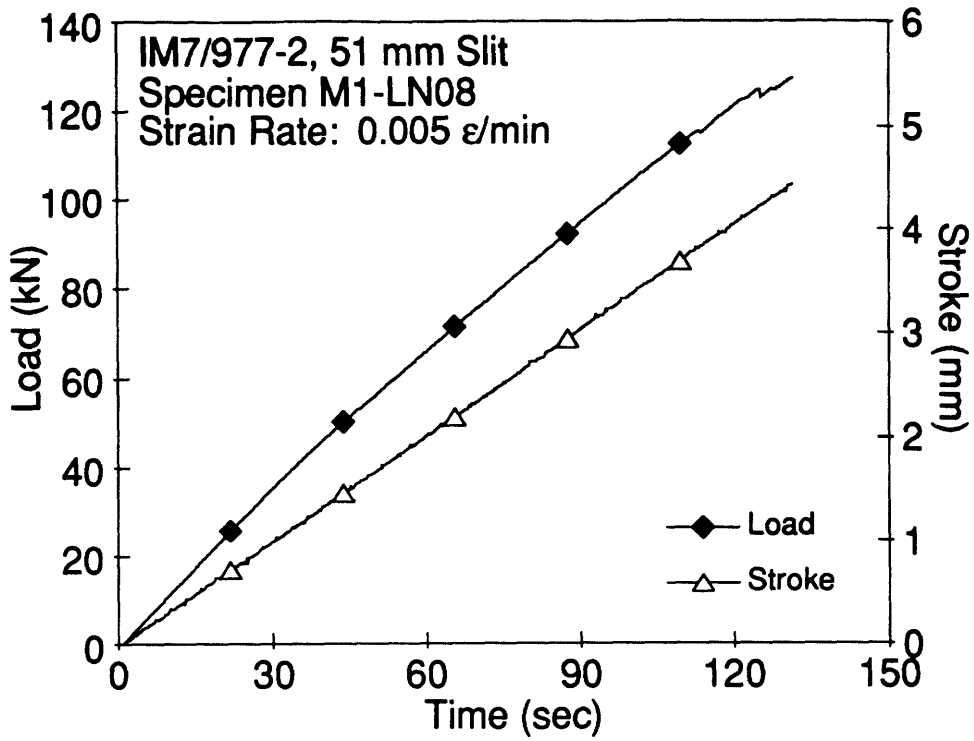


Figure D.16 Plots of Load, Stroke, Far-Field Strain and Notch-Tip Strain versus Time for Specimen M1-LN08.

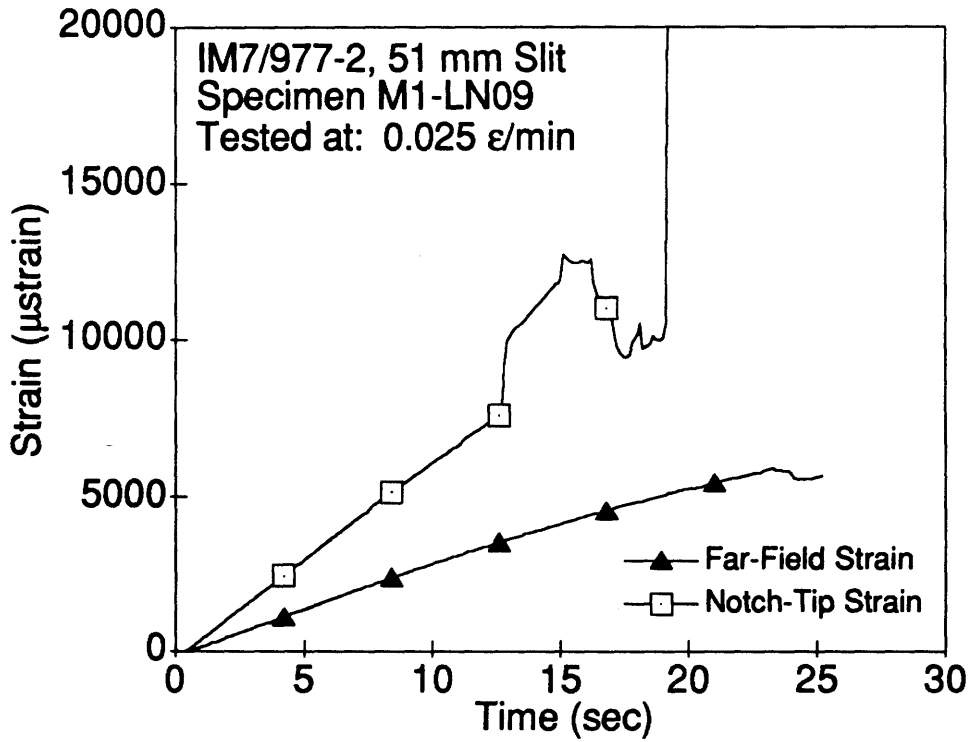
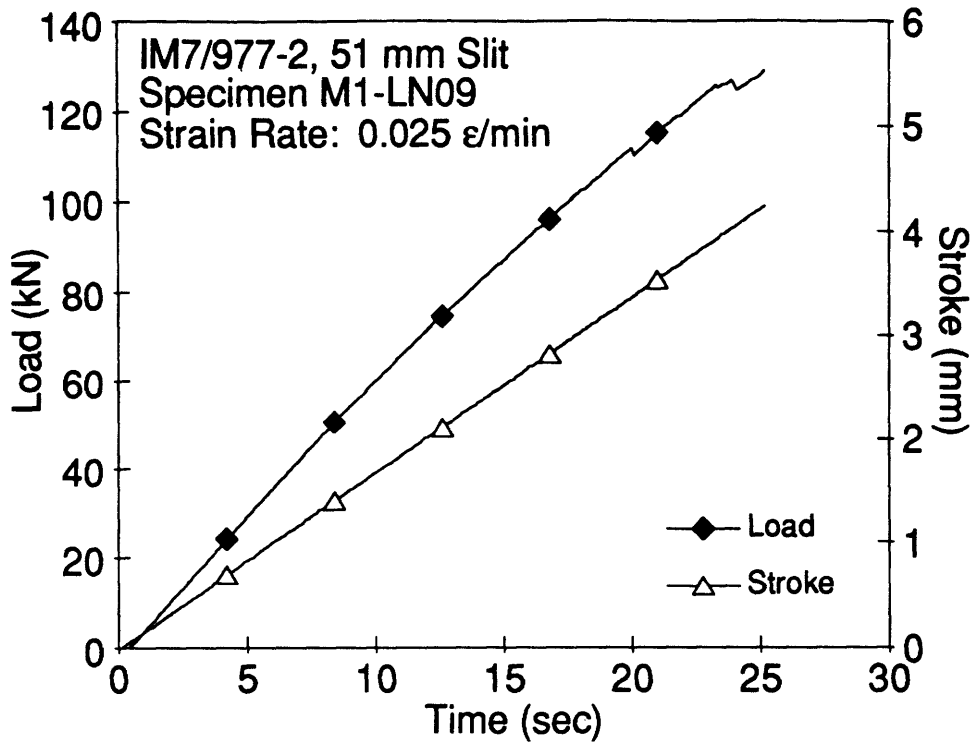


Figure D.17 Plots of Load, Stroke, Far-Field Strain and Notch-Tip Strain versus Time for Specimen M1-LN09.

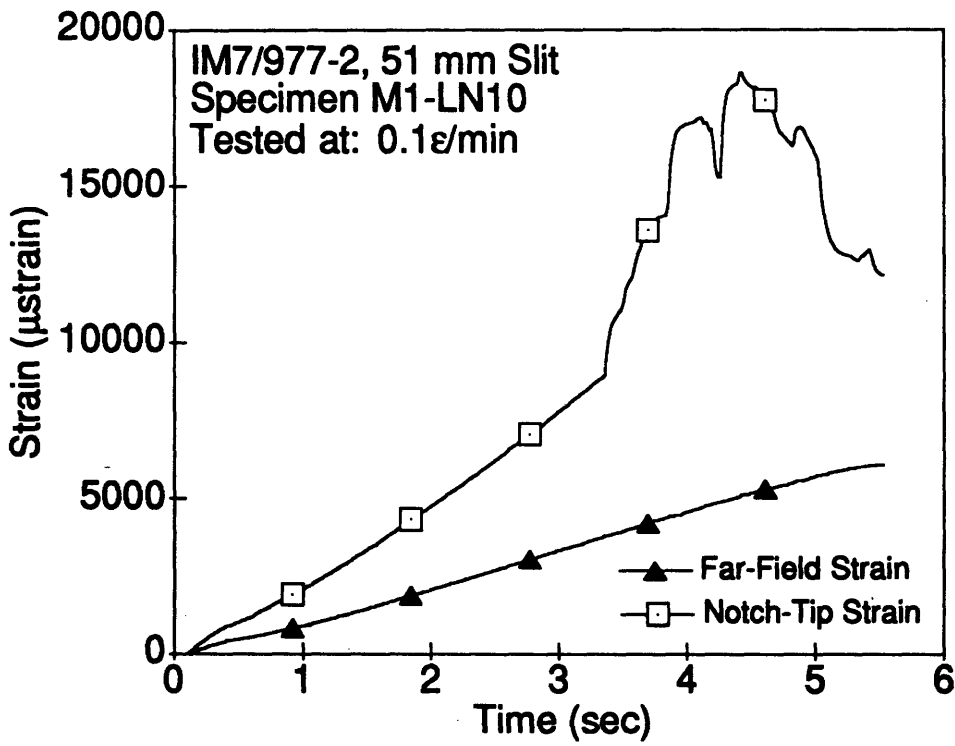
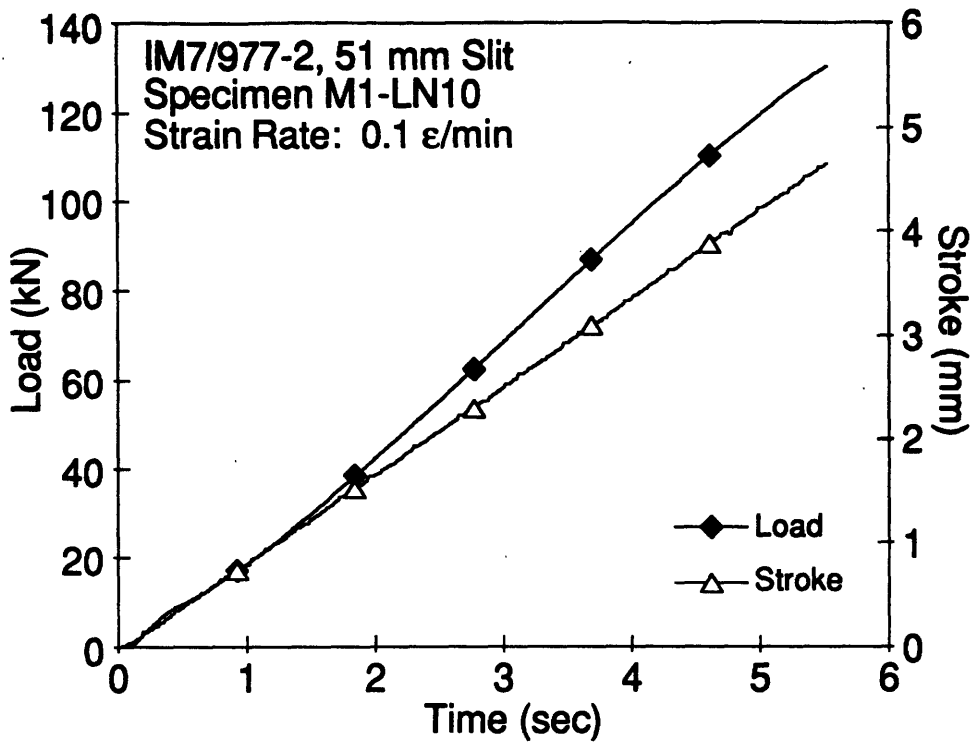


Figure D.18 Plots of Load, Stroke, Far-Field Strain and Notch-Tip Strain versus Time for Specimen M1-LN10.

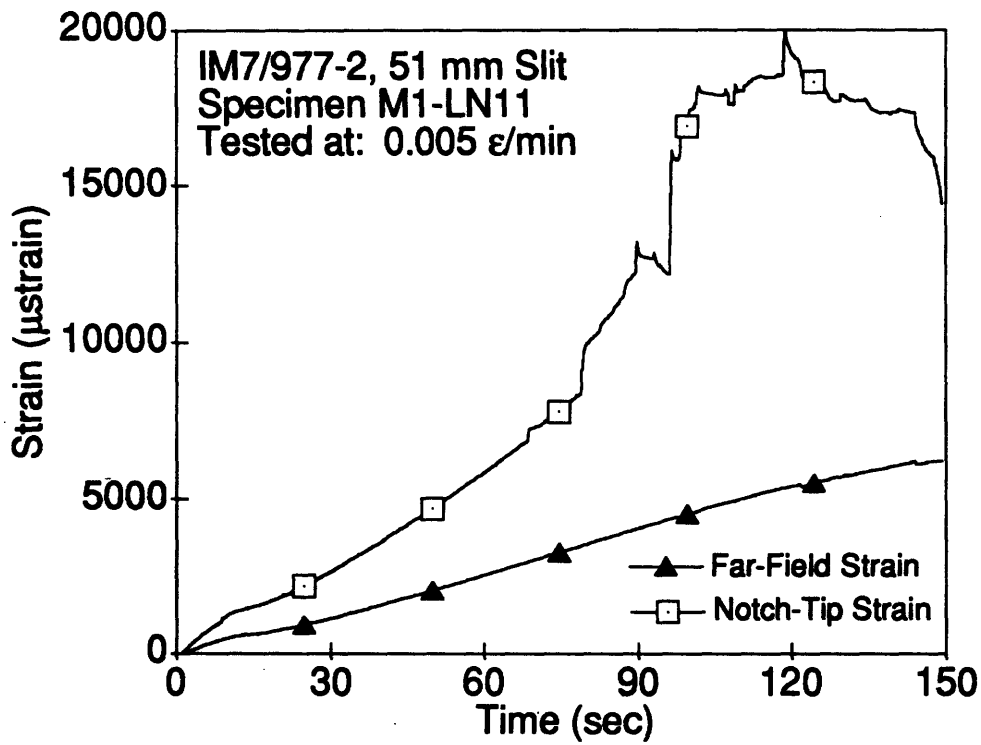
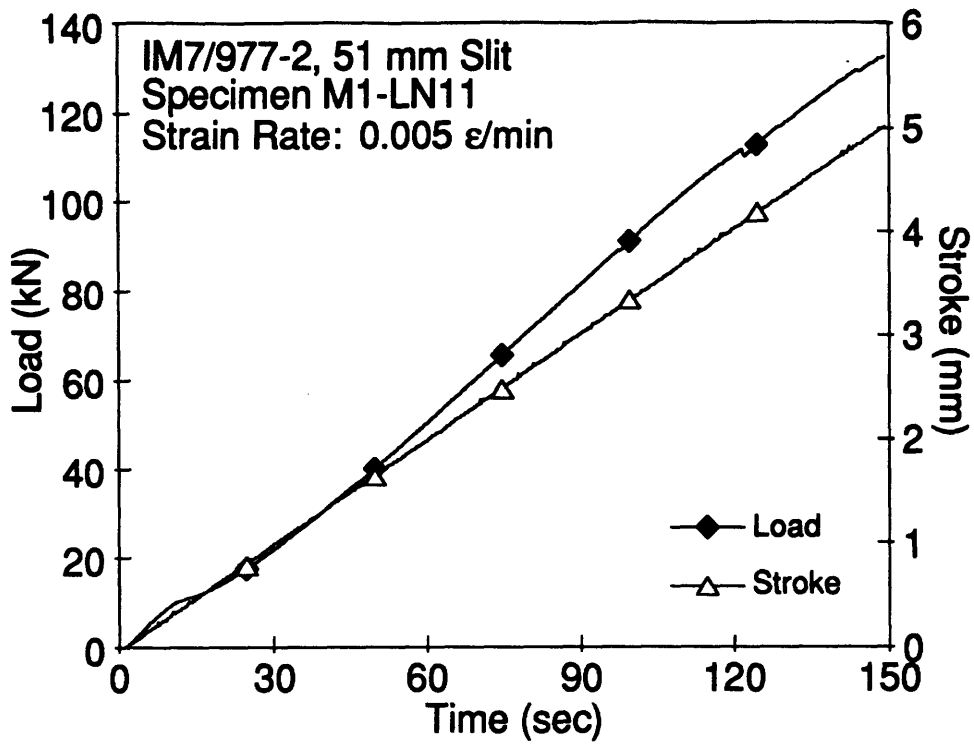


Figure D.19 Plots of Load, Stroke, Far-Field Strain and Notch-Tip Strain versus Time for Specimen M1-LN11.

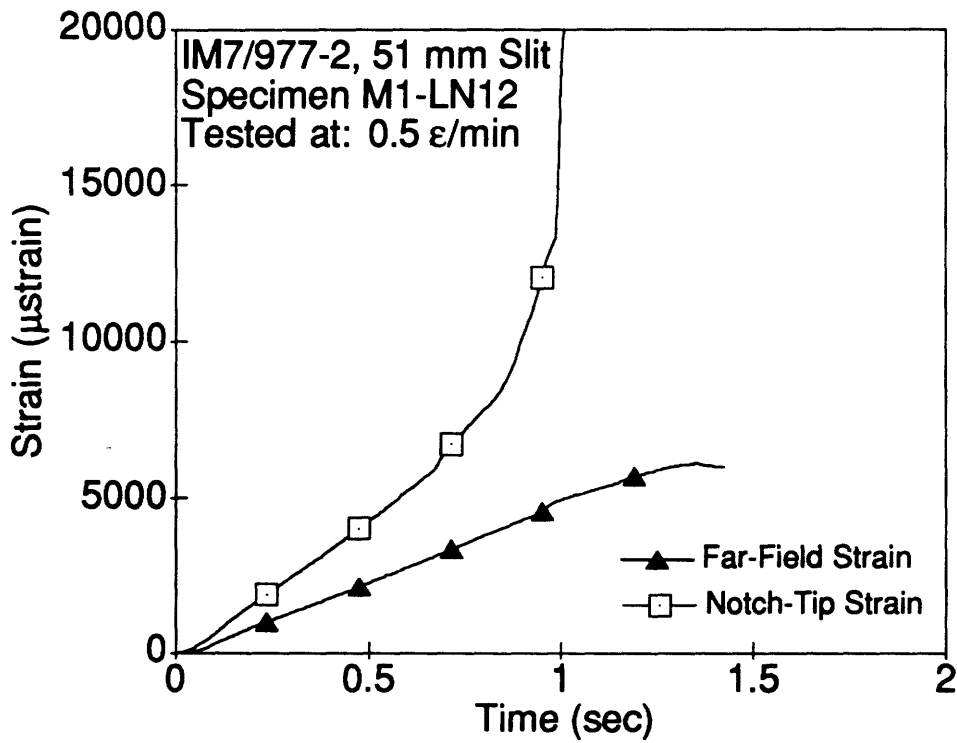
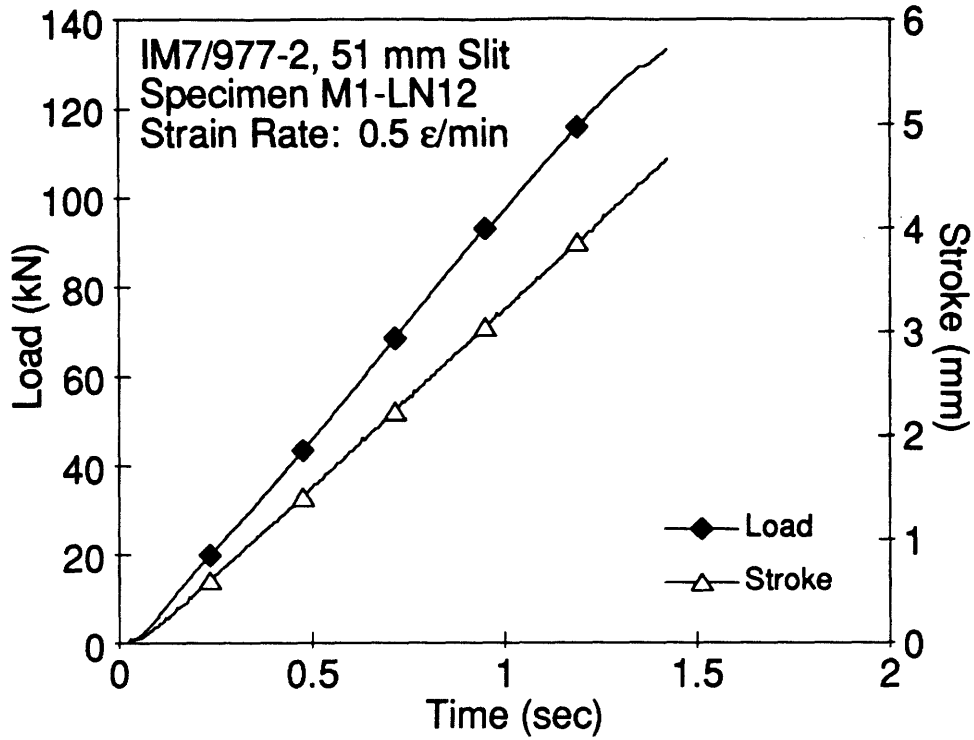


Figure D.20 Plots of Load, Stroke, Far-Field Strain and Notch-Tip Strain versus Time for Specimen M1-LN12.

APPENDIX E

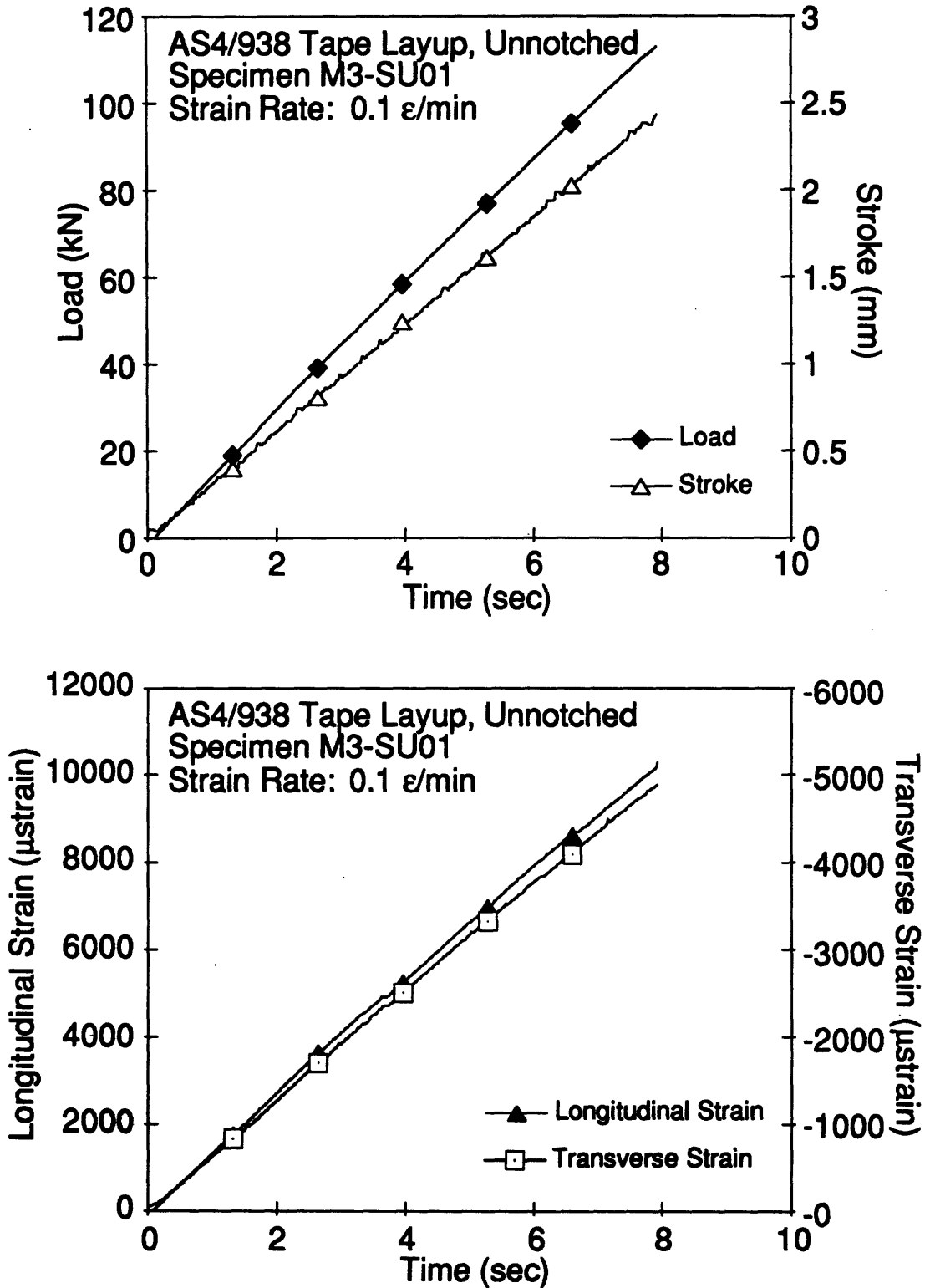


Figure E.1 Plots of Load, Stroke, Longitudinal Strain and Transverse Strain versus Time for Specimen M3-SU01.

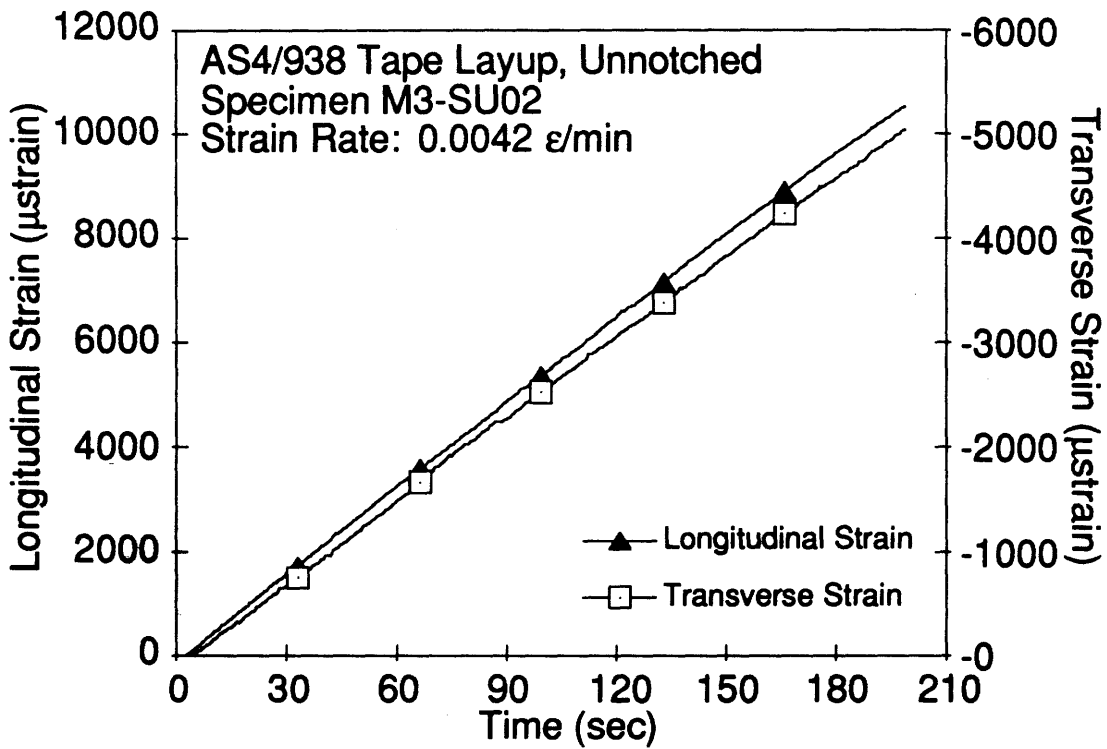
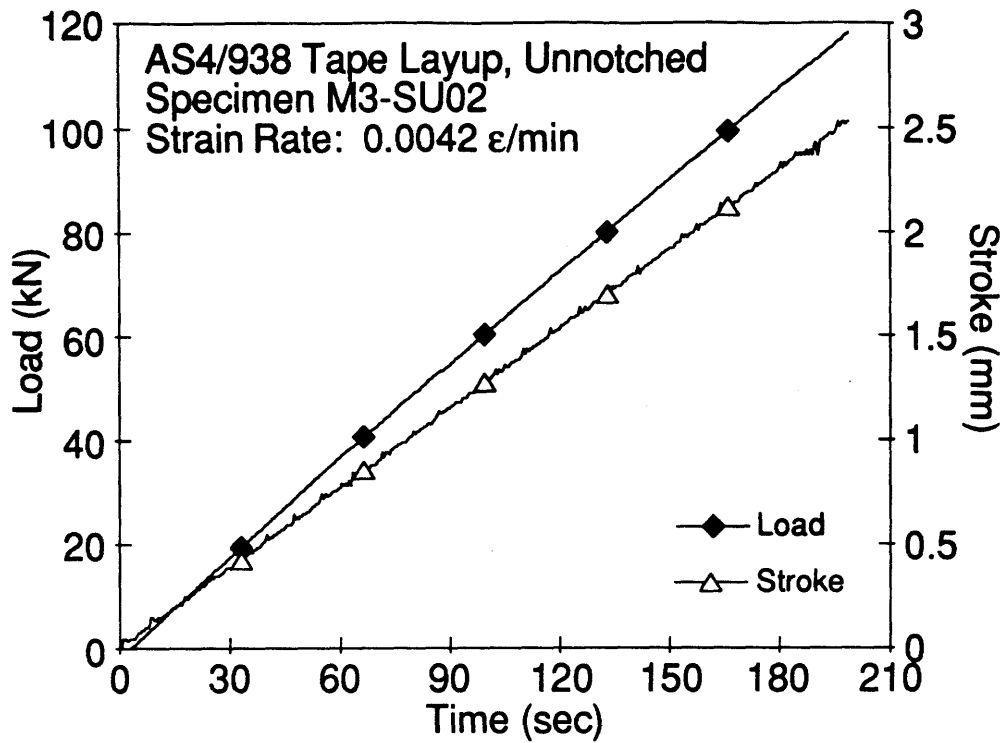


Figure E.2 Plots of Load, Stroke, Longitudinal Strain and Transverse Strain versus Time for Specimen M3-SU02.

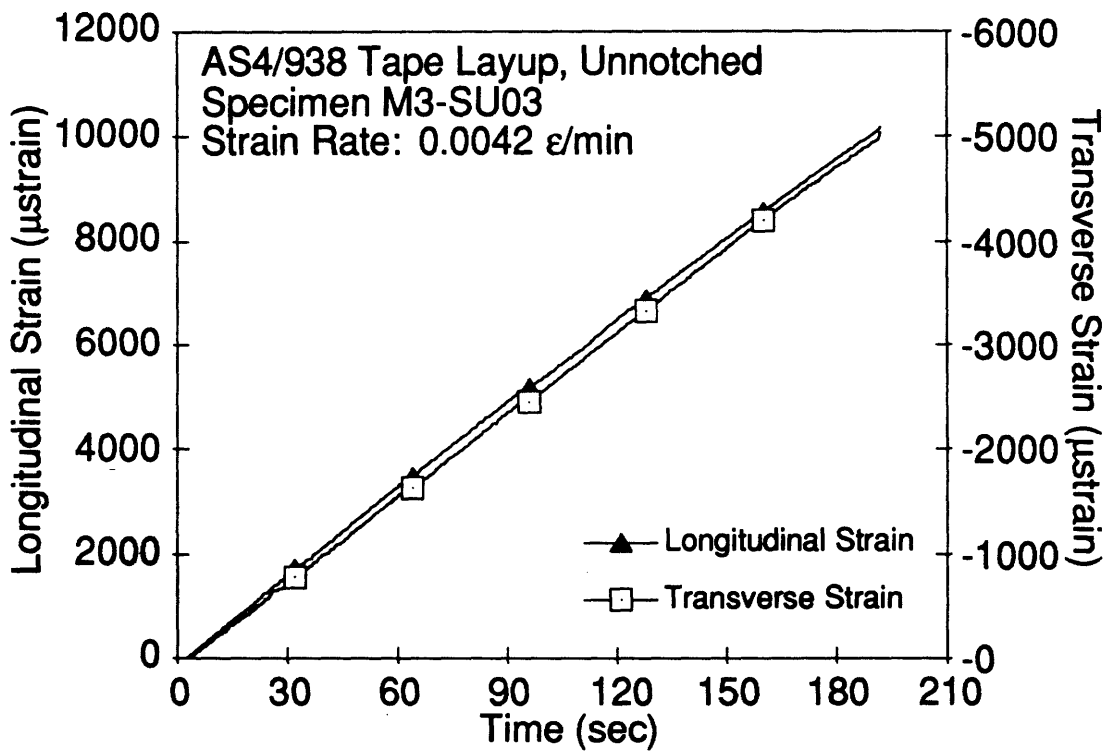
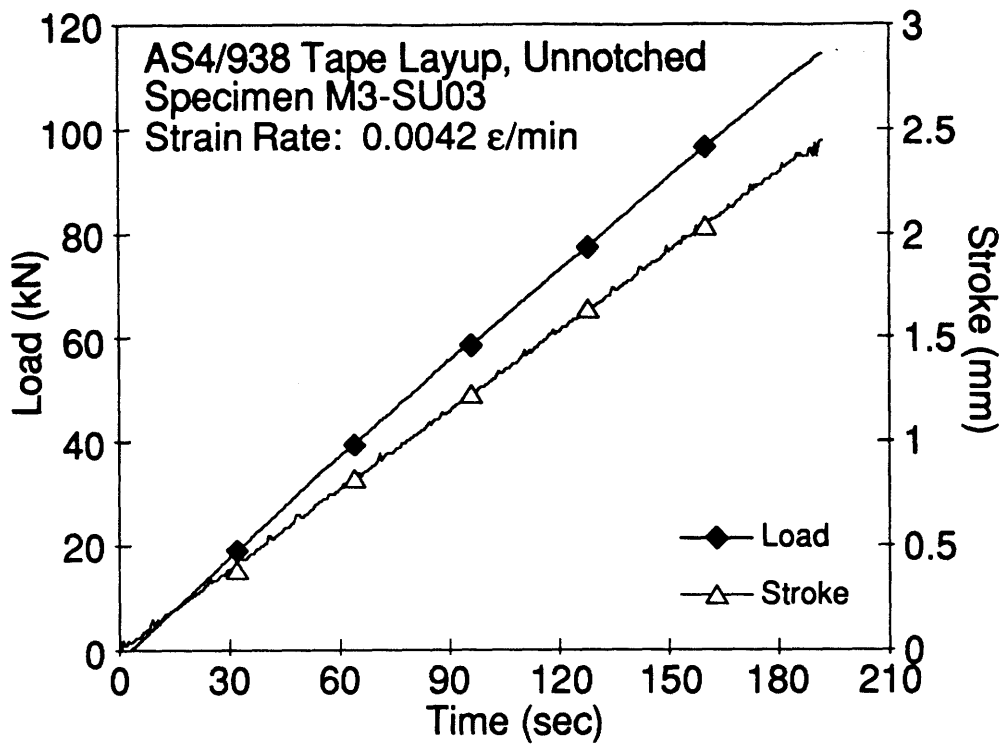


Figure E.3 Plots of Load, Stroke, Longitudinal Strain and Transverse Strain versus Time for Specimen M3-SU03.

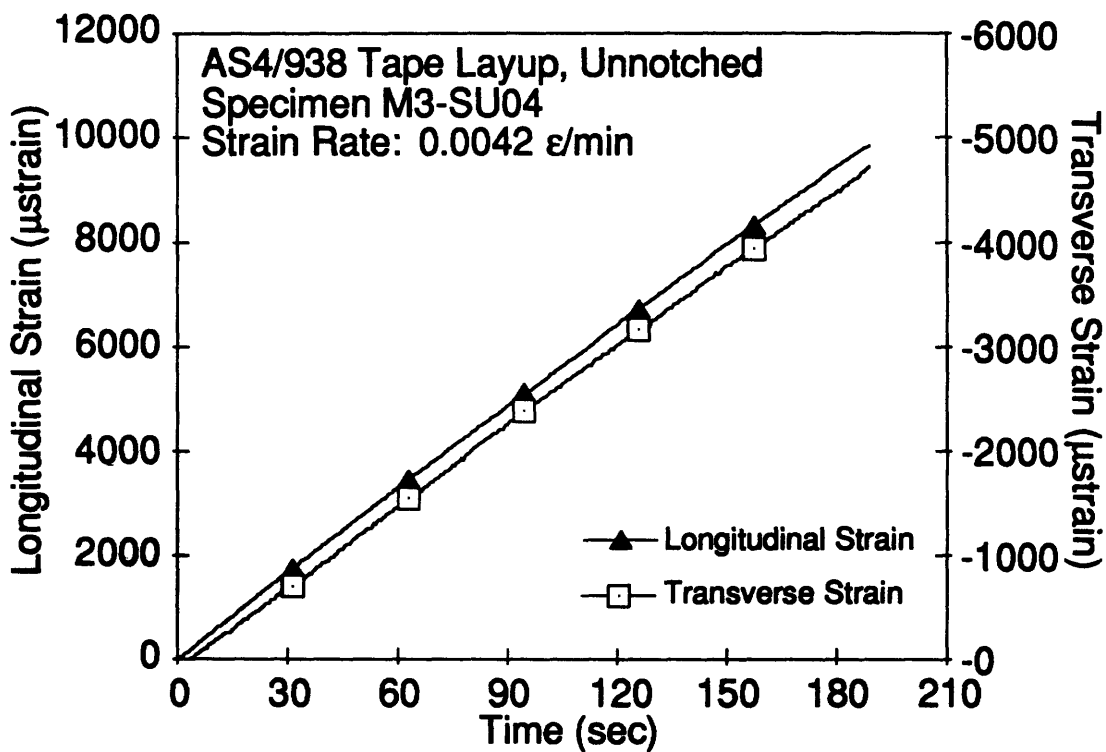
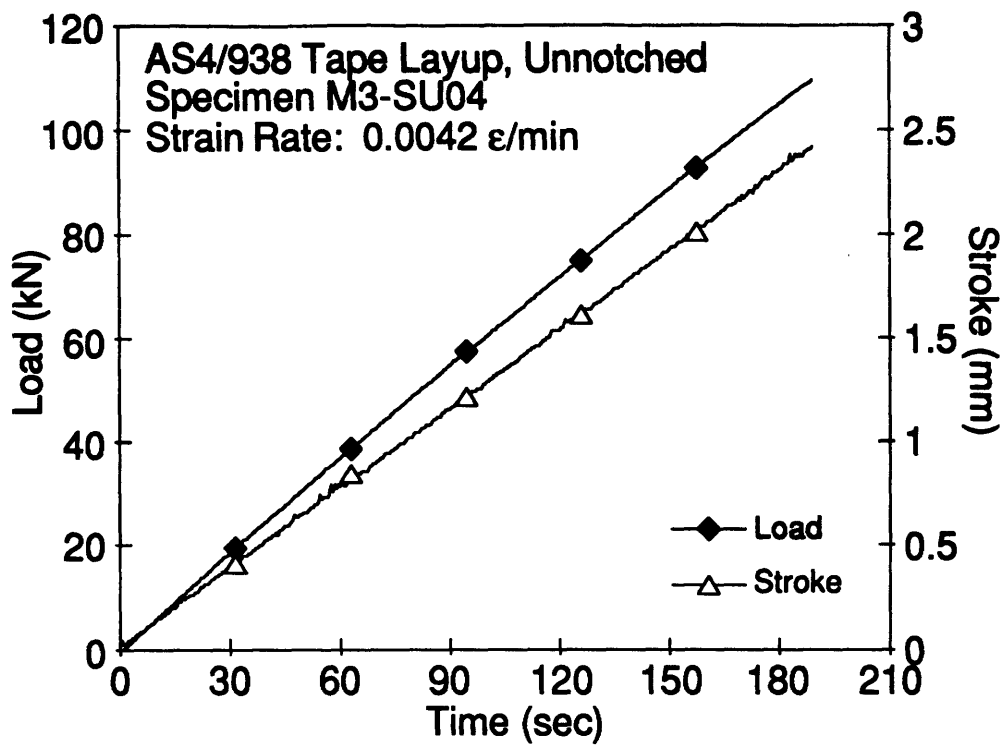


Figure E.4 Plots of Load, Stroke, Longitudinal Strain and Transverse Strain versus Time for Specimen M3-SU04.

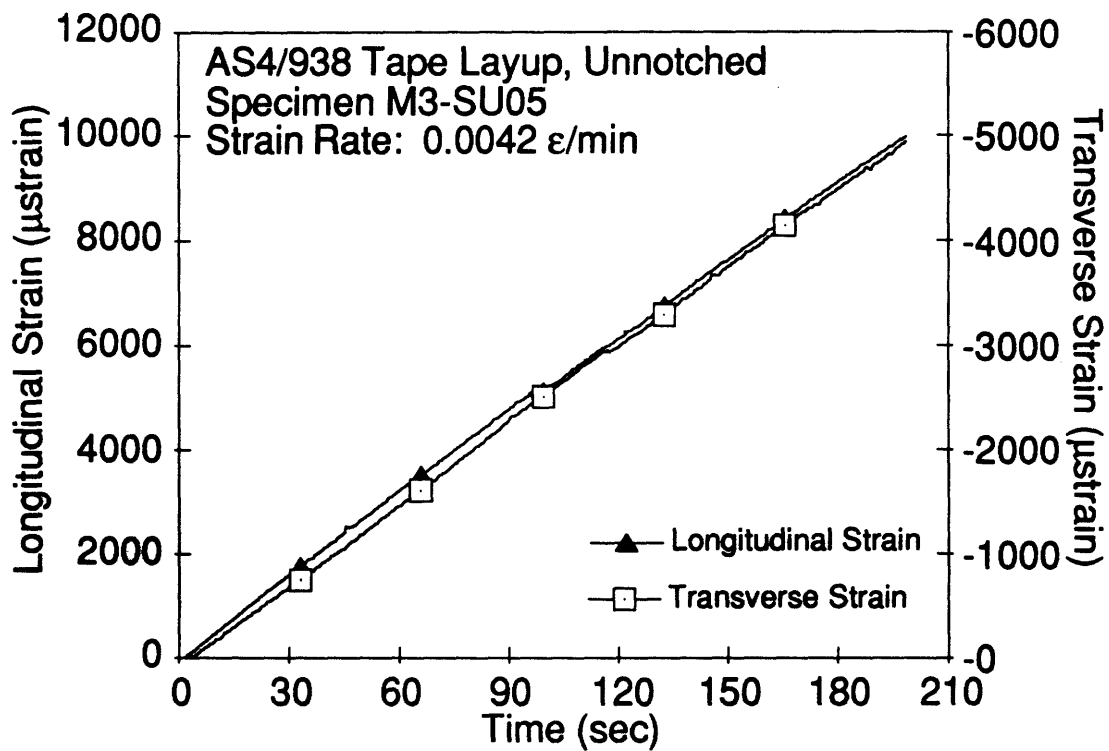
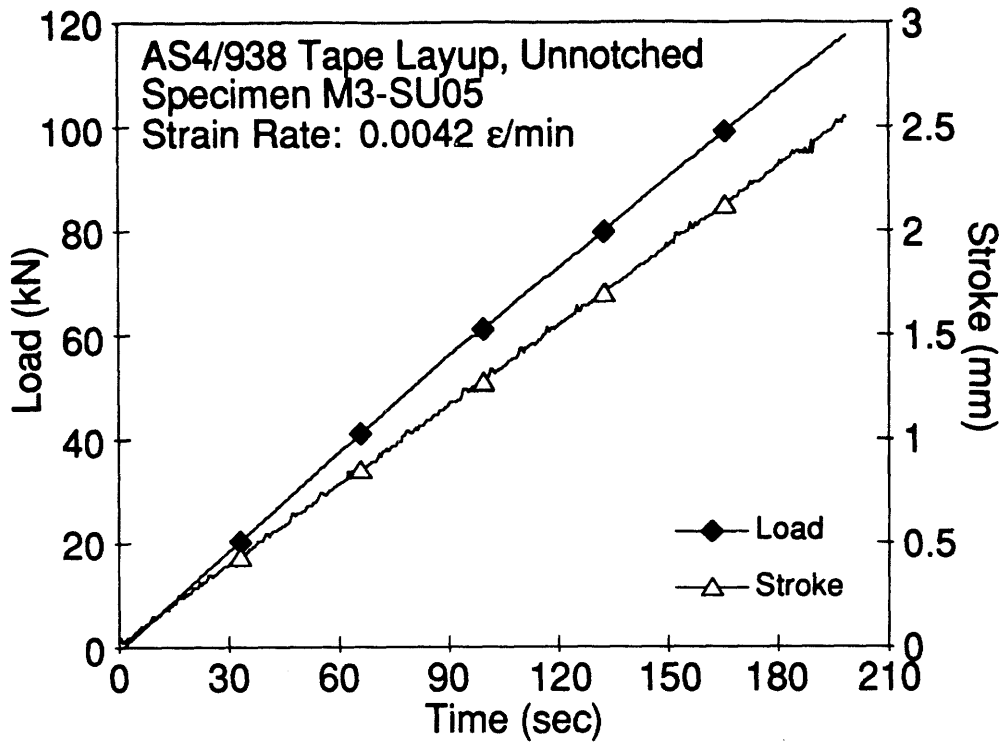


Figure E.5 Plots of Load, Stroke, Longitudinal Strain and Transverse Strain versus Time for Specimen M3-SU05.

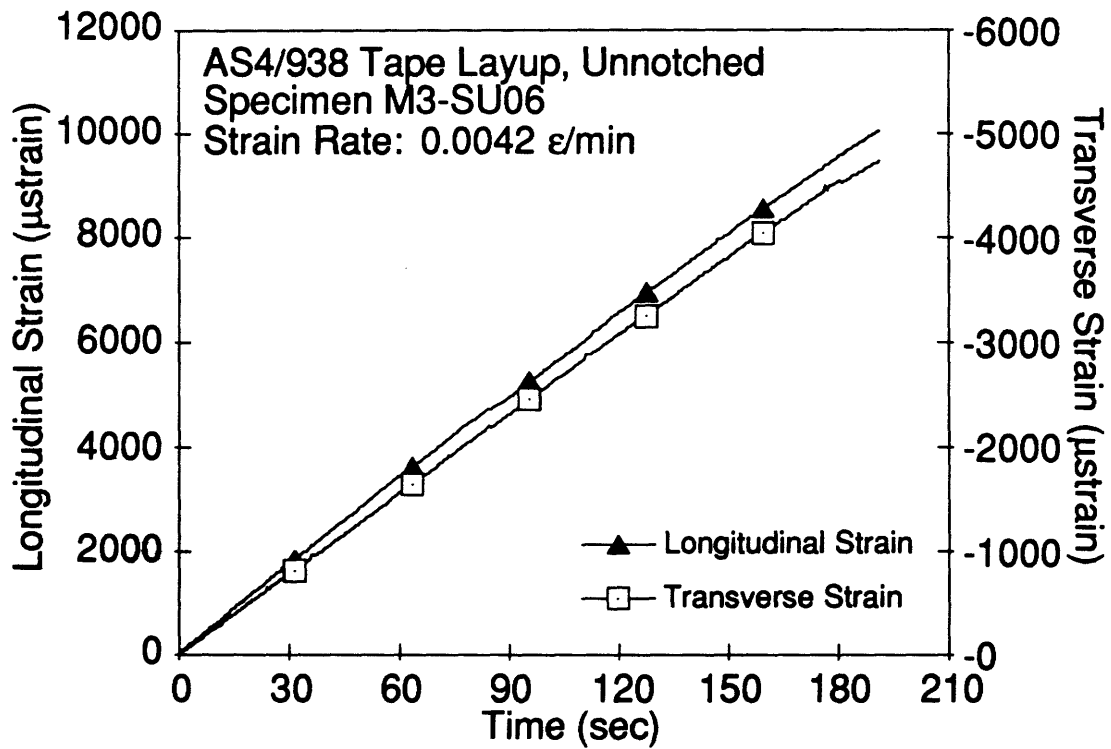
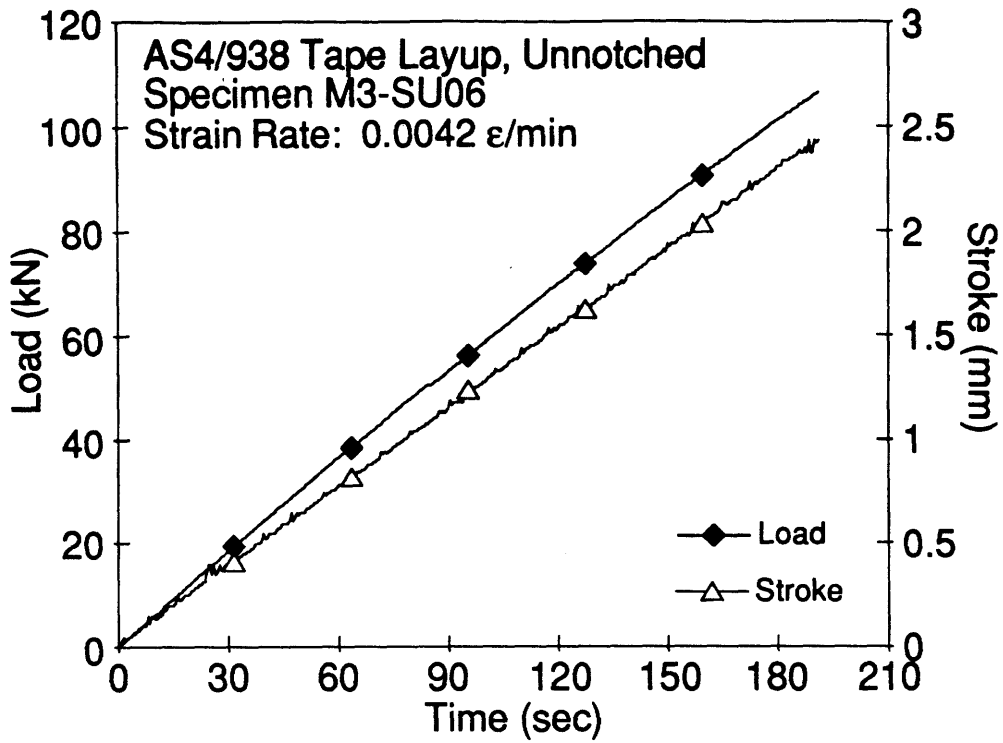


Figure E.6 Plots of Load, Stroke, Longitudinal Strain and Transverse Strain versus Time for Specimen M3-SU06.

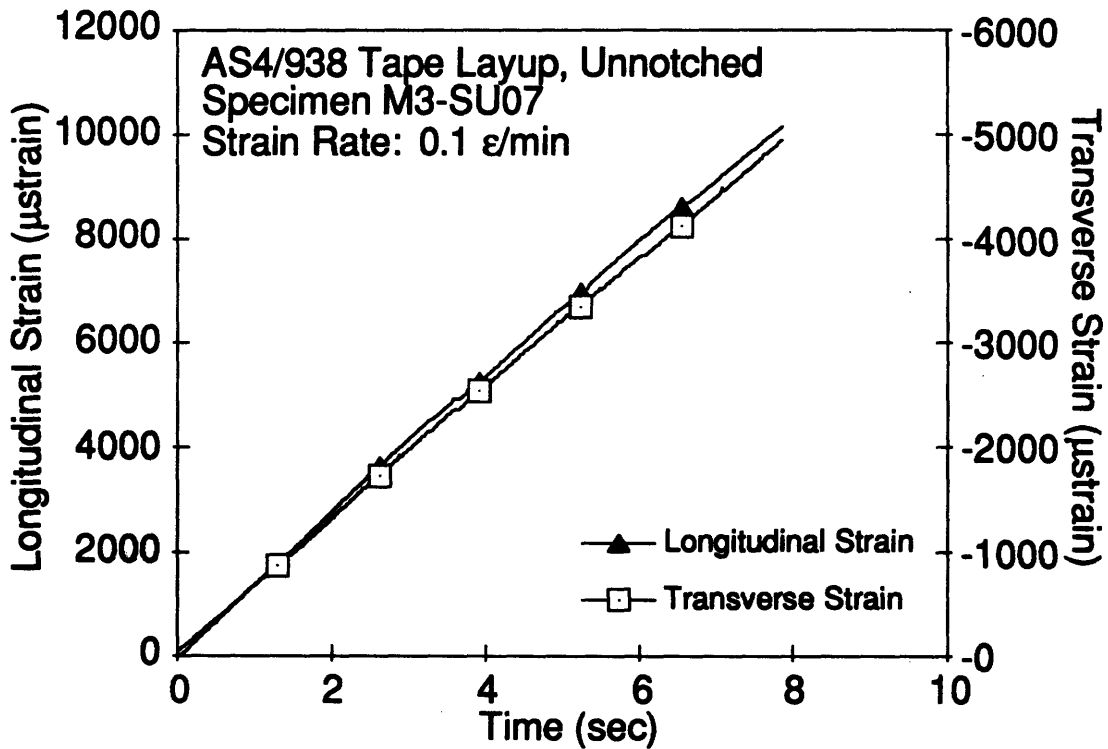
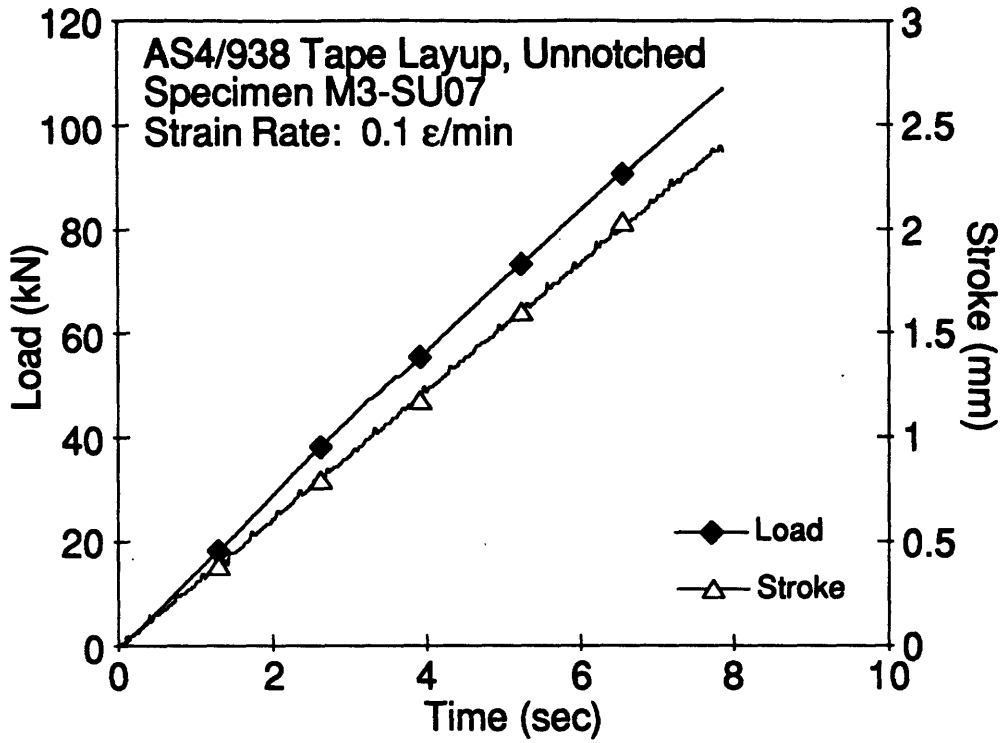


Figure E.7 Plots of Load, Stroke, Longitudinal Strain and Transverse Strain versus Time for Specimen M3-SU07.

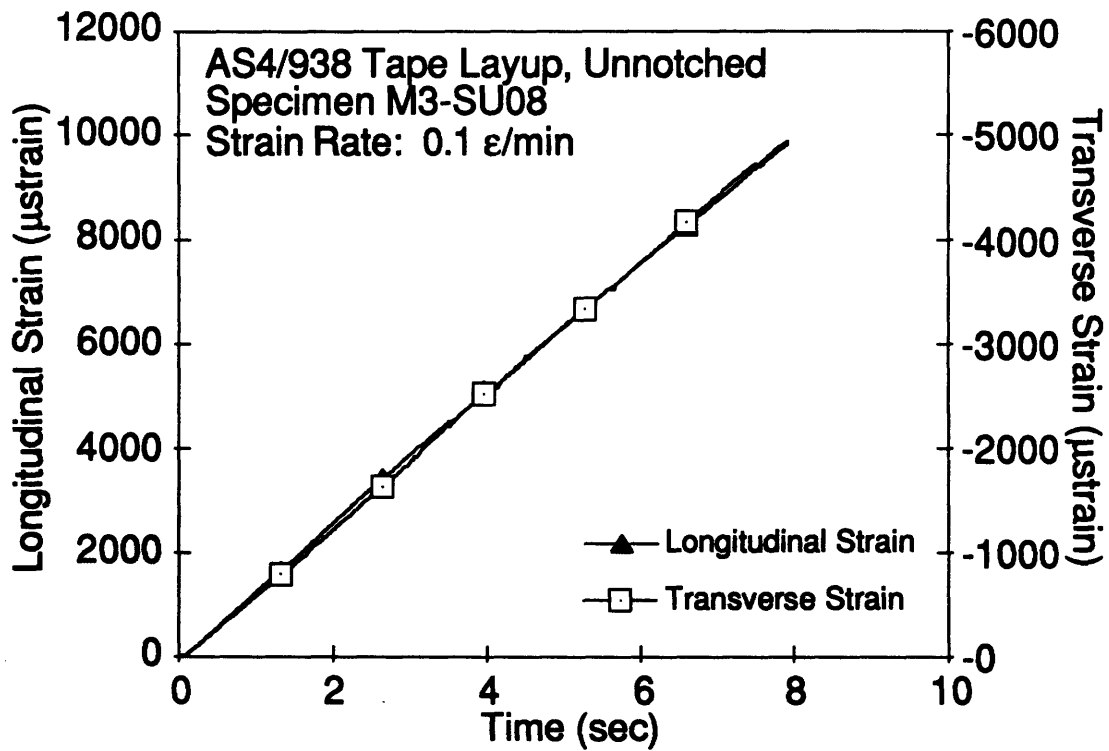
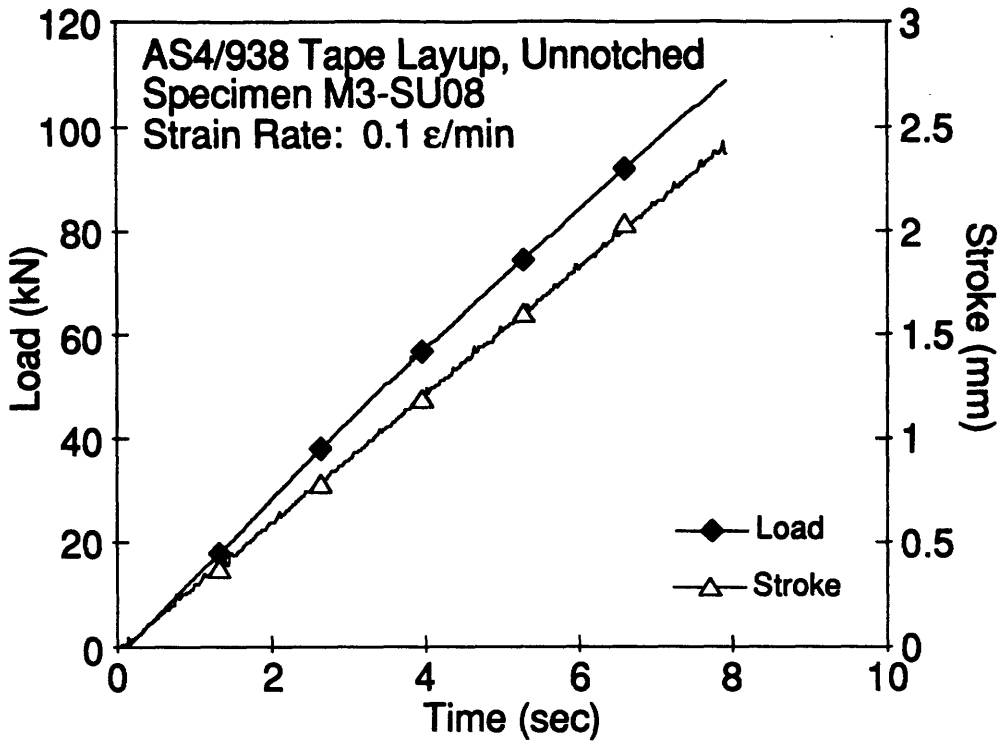


Figure E.8 Plots of Load, Stroke, Longitudinal Strain and Transverse Strain versus Time for Specimen M3-SU08.

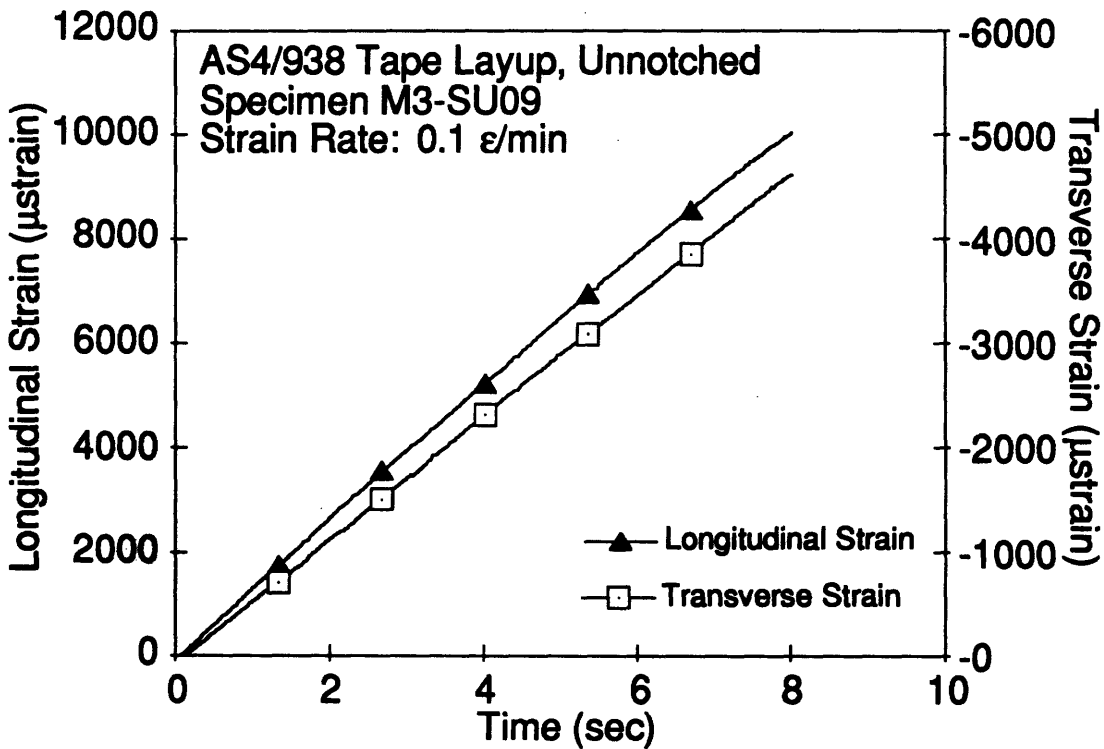
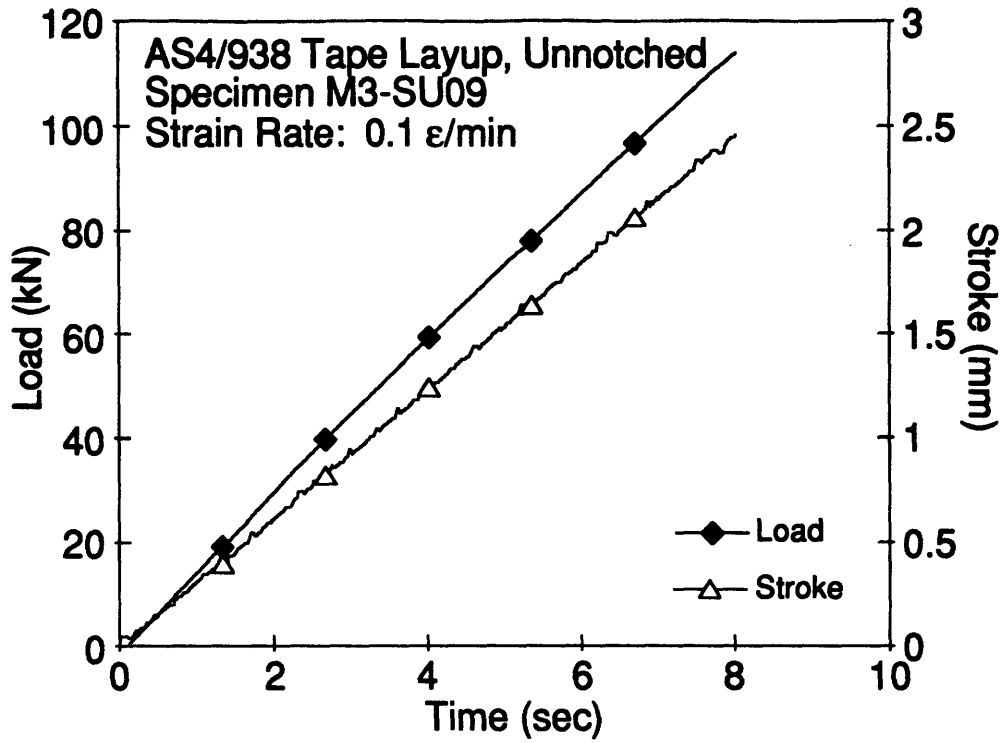


Figure E.9 Plots of Load, Stroke, Longitudinal Strain and Transverse Strain versus Time for Specimen M3-SU09.

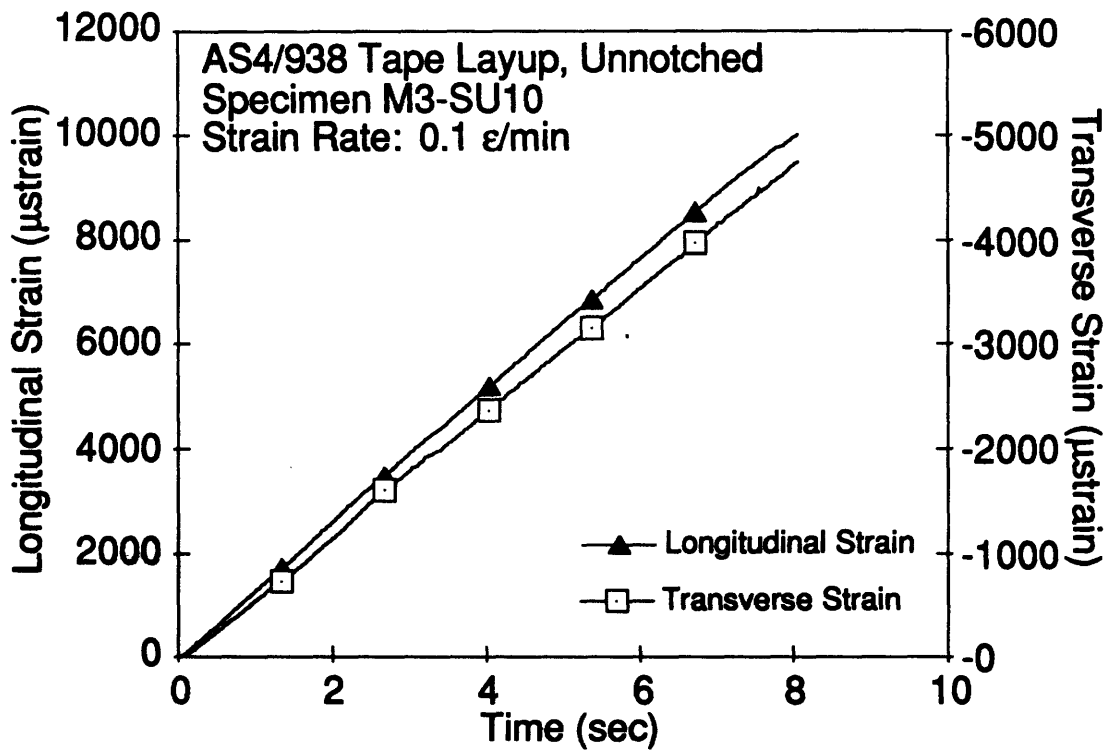
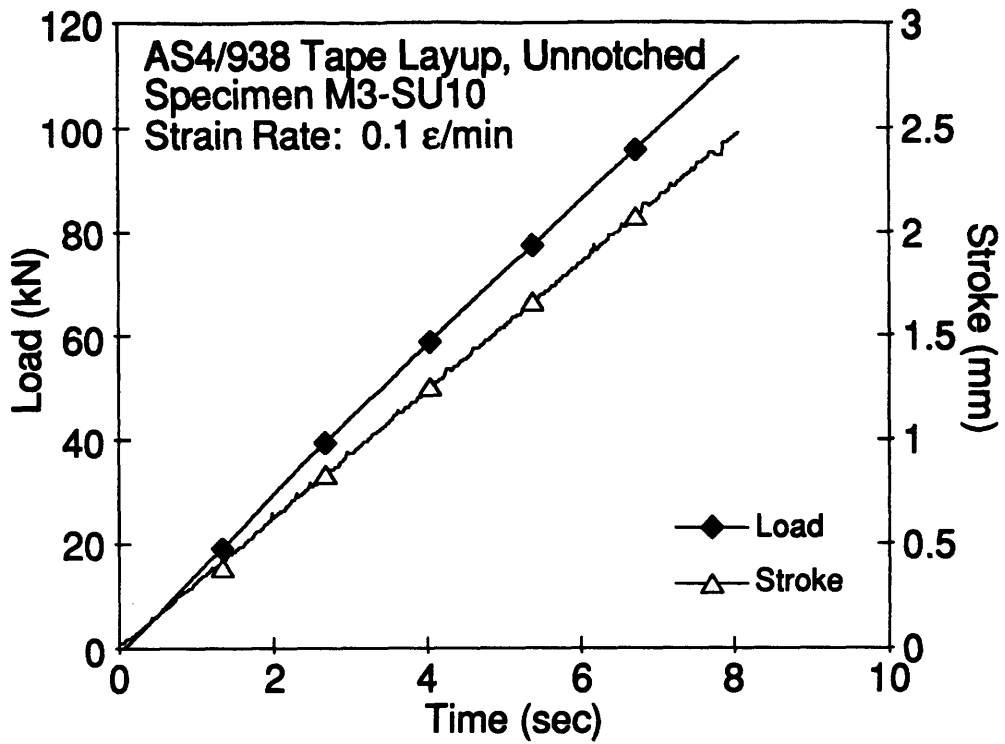


Figure E.10 Plots of Load, Stroke, Longitudinal Strain and Transverse Strain versus Time for Specimen M3-SU10.

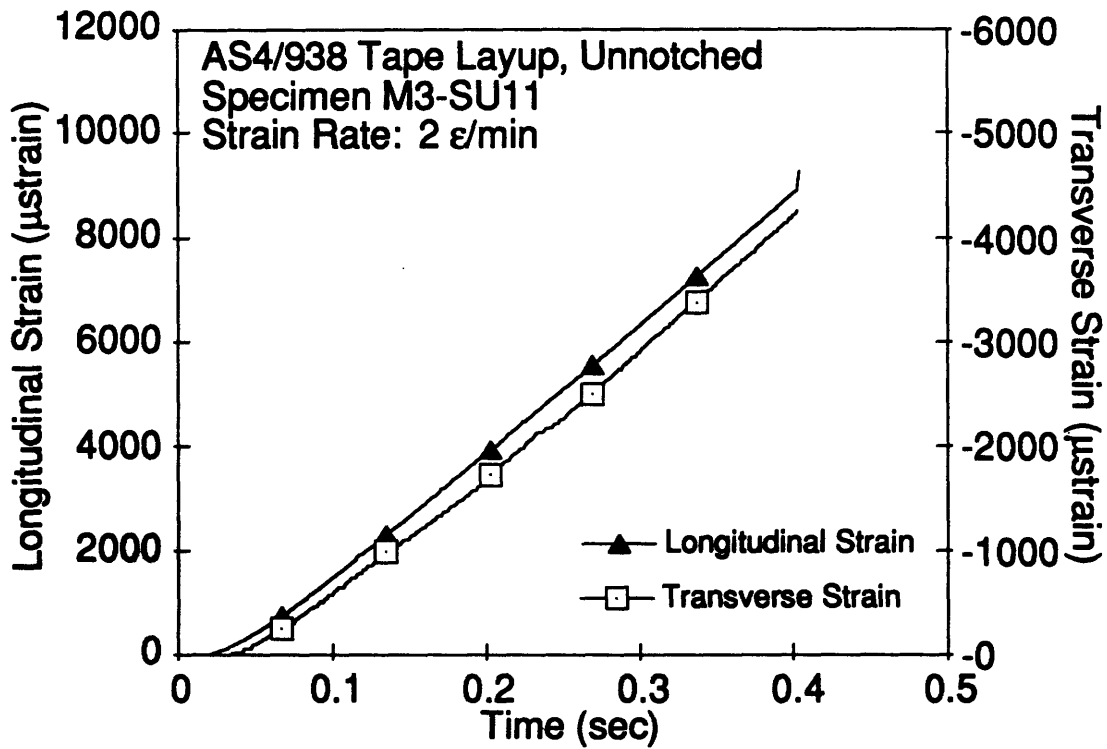
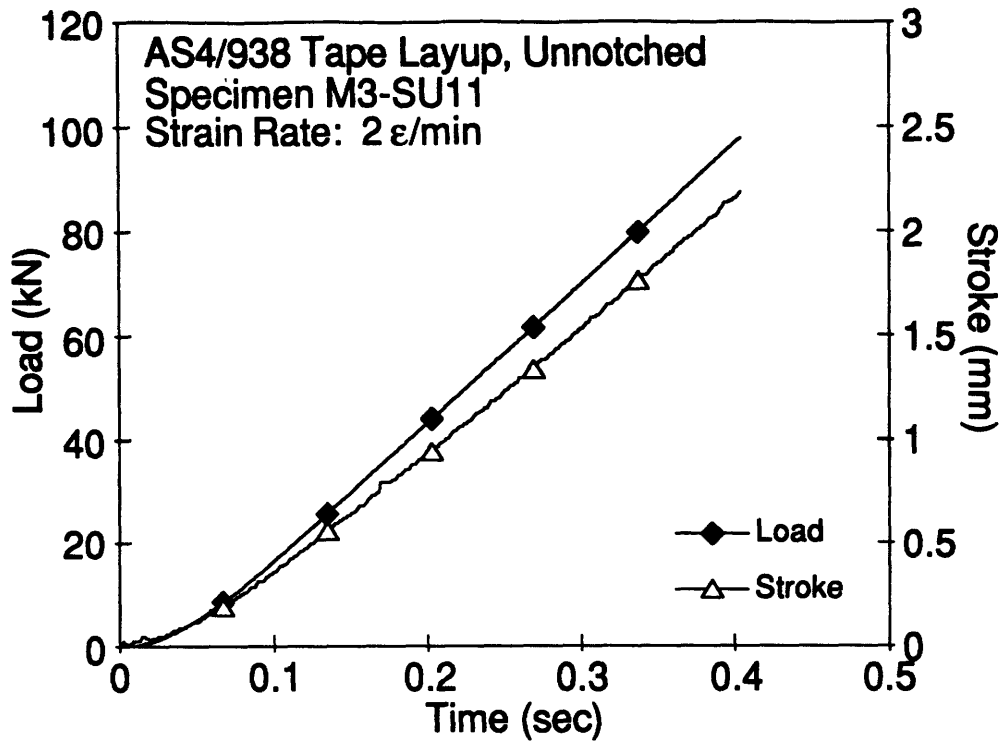


Figure E.11 Plots of Load, Stroke, Longitudinal Strain and Transverse Strain versus Time for Specimen M3-SU11.

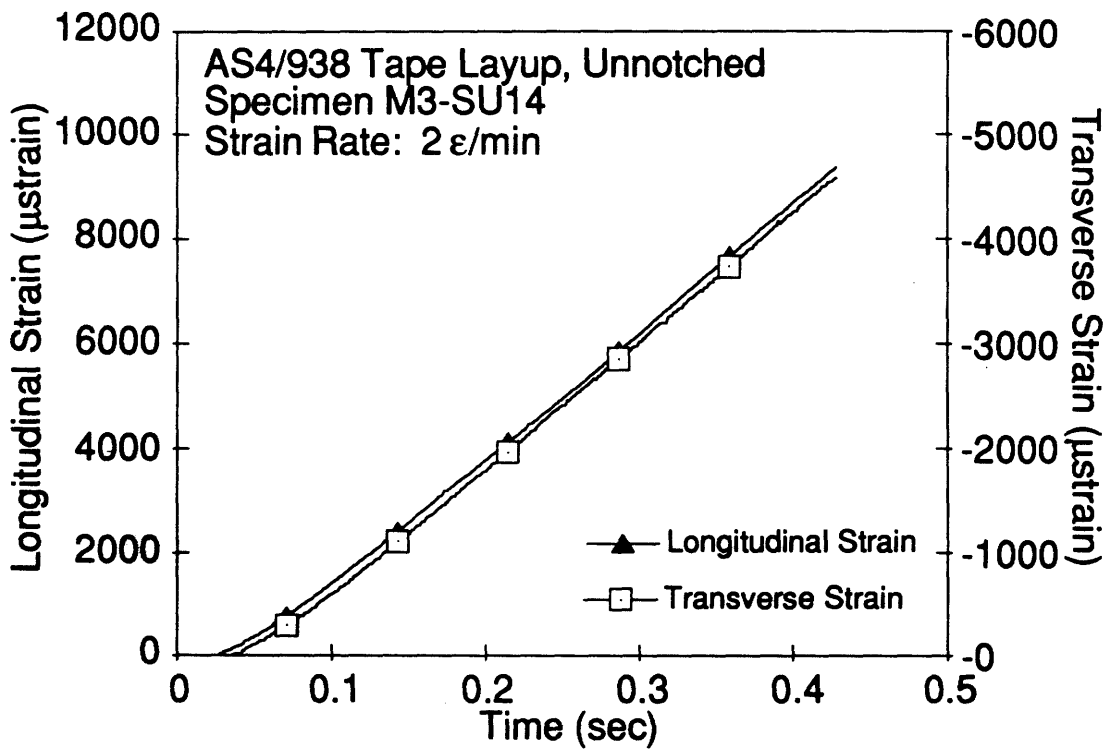
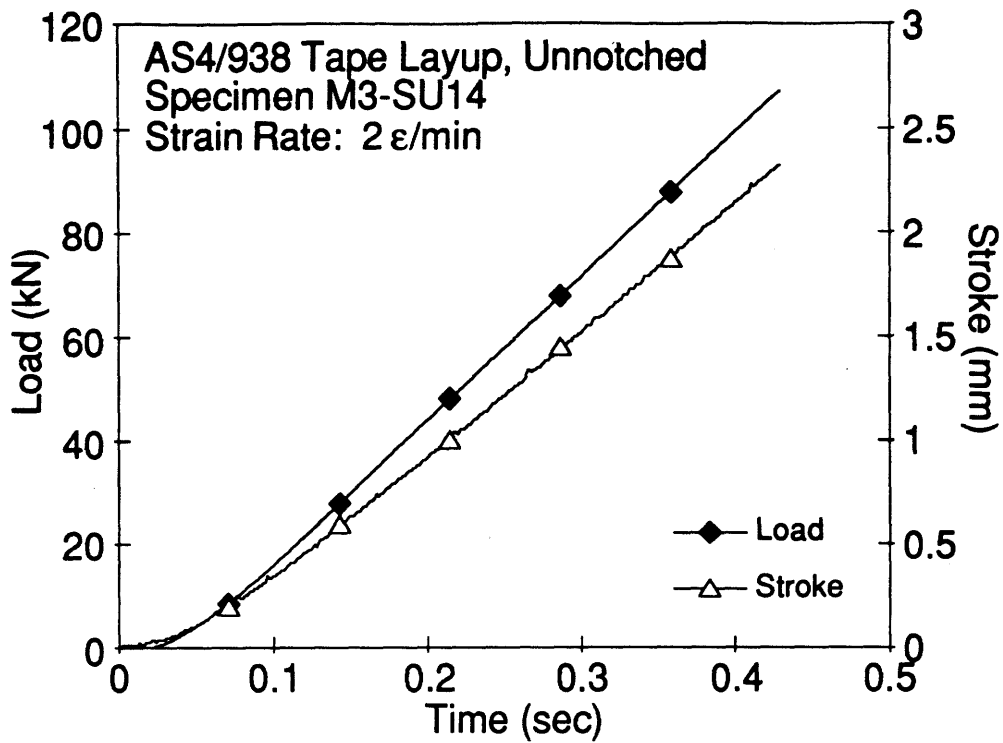


Figure E.12 Plots of Load, Stroke, Longitudinal Strain and Transverse Strain versus Time for Specimen M3-SU14.

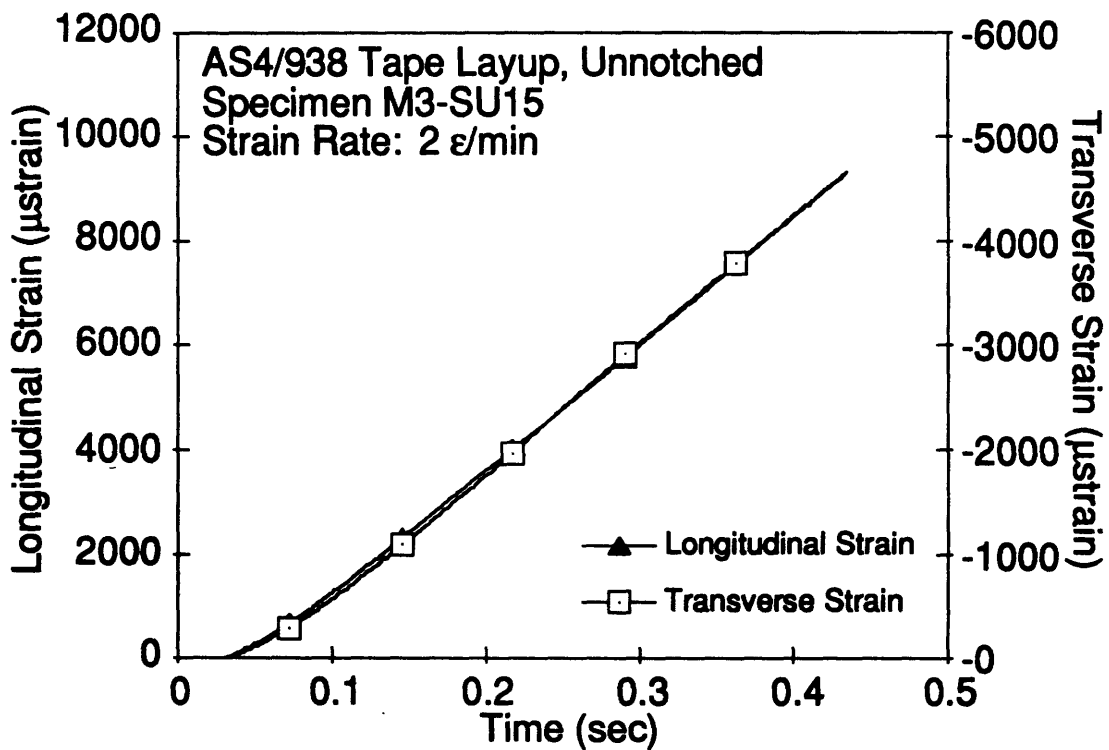
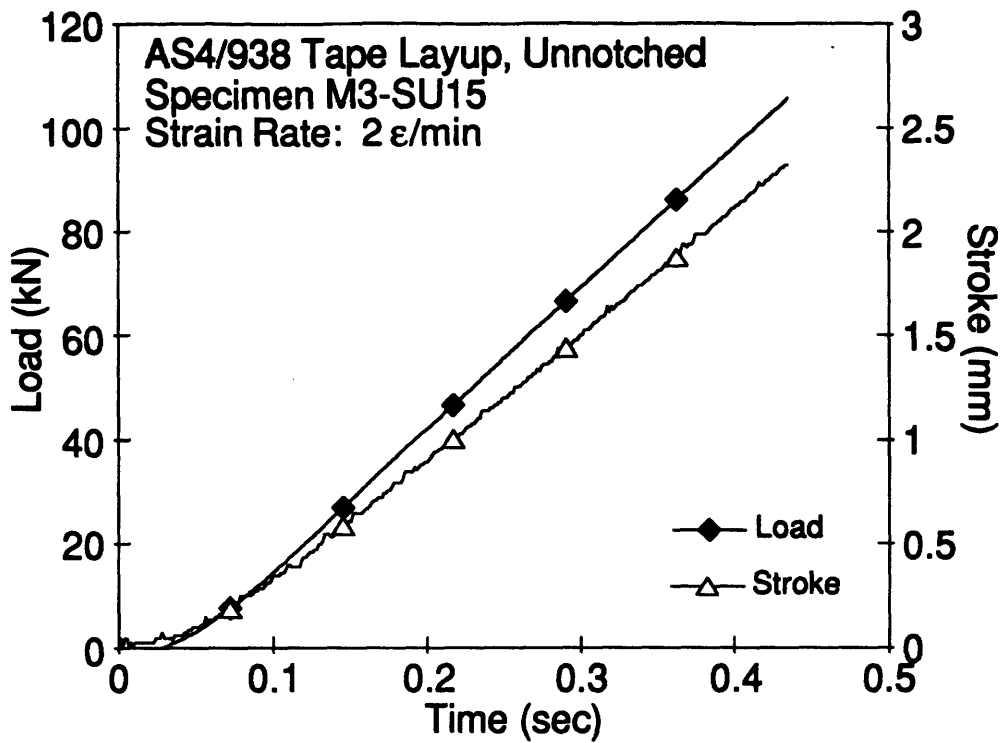


Figure E.13 Plots of Load, Stroke, Longitudinal Strain and Transverse Strain versus Time for Specimen M3-SU15.

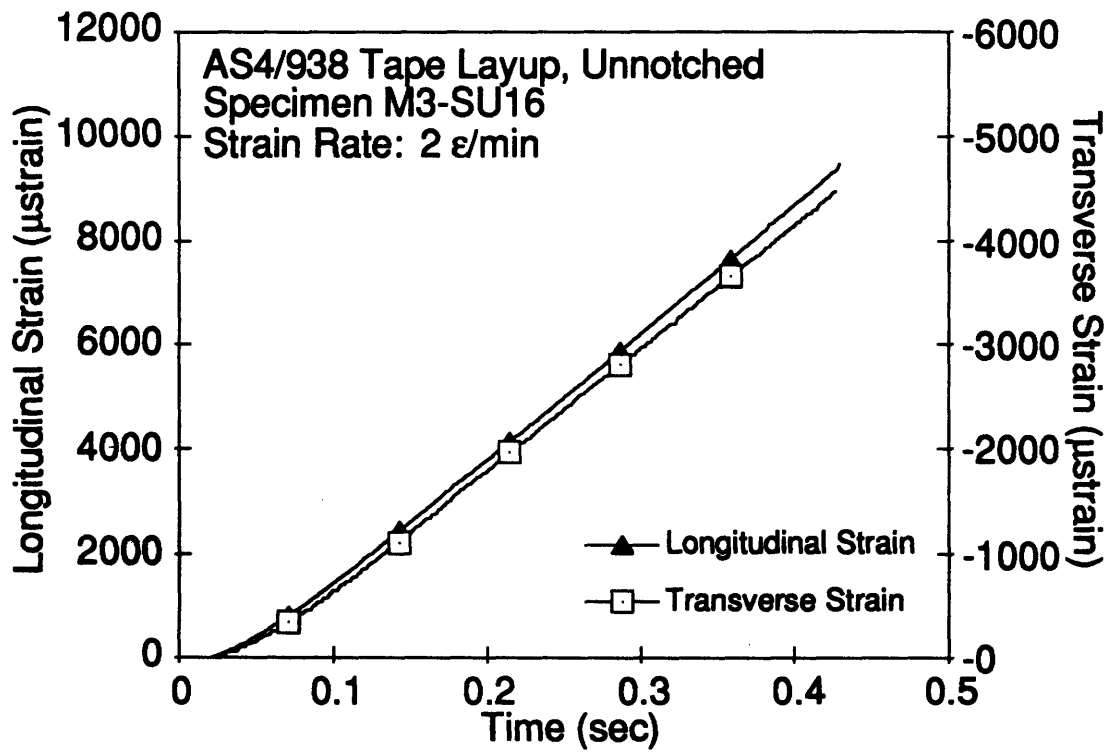
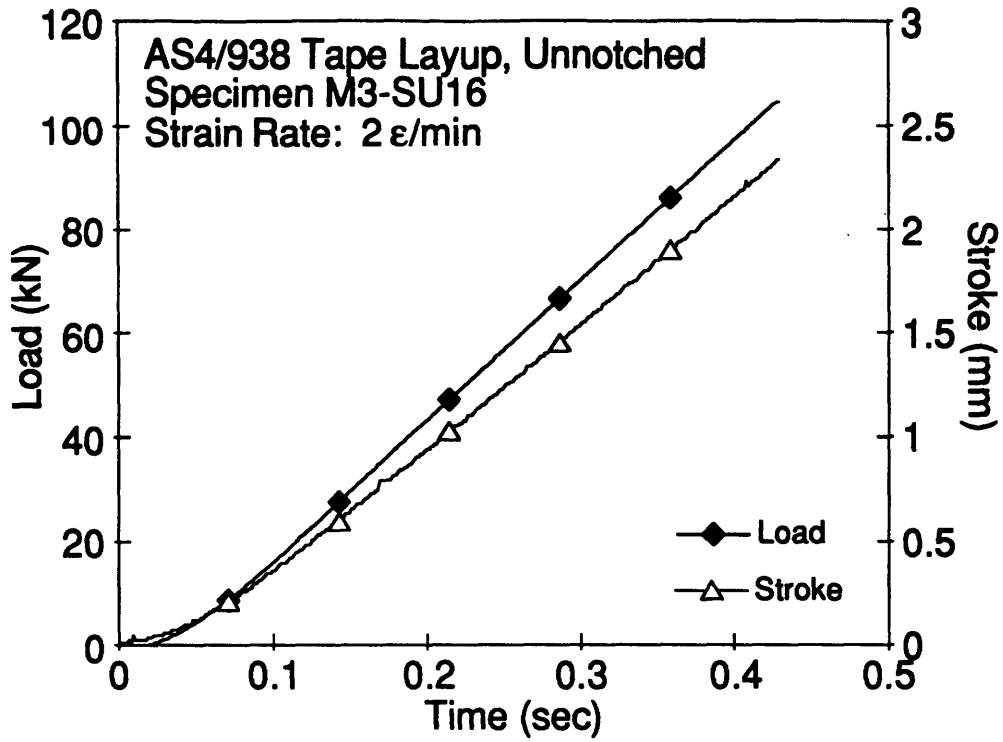


Figure E.14 Plots of Load, Stroke, Longitudinal Strain and Transverse Strain versus Time for Specimen M3-SU16.

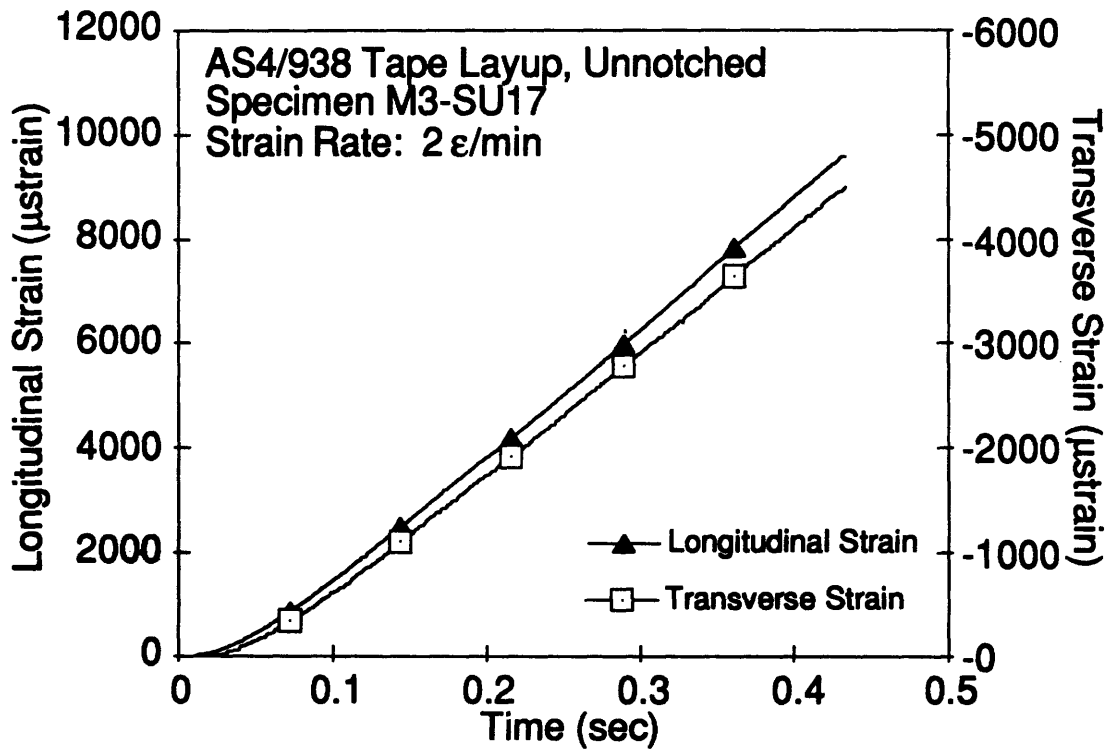
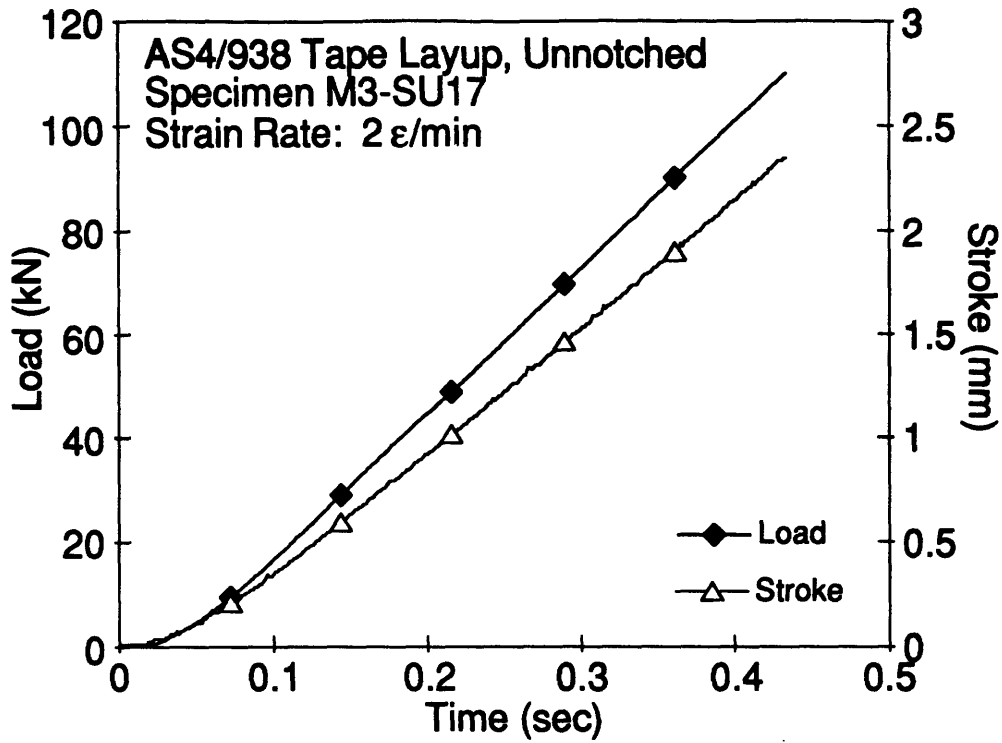


Figure E.15 Plots of Load, Stroke, Longitudinal Strain and Transverse Strain versus Time for Specimen M3-SU17.

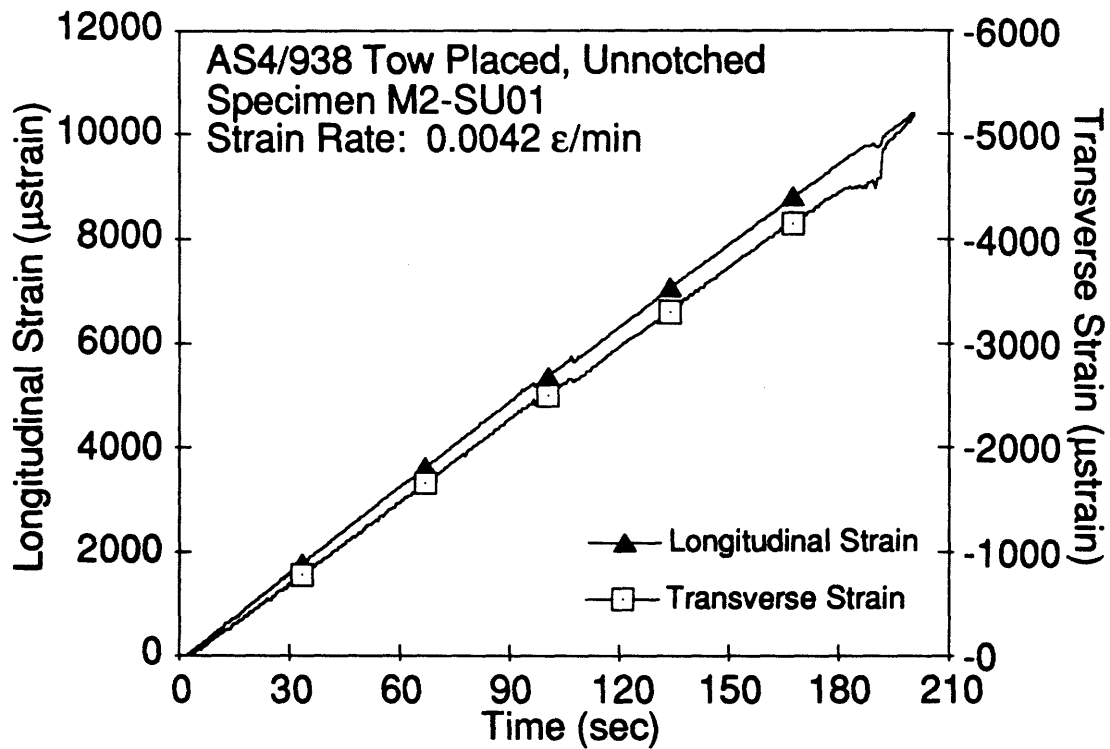
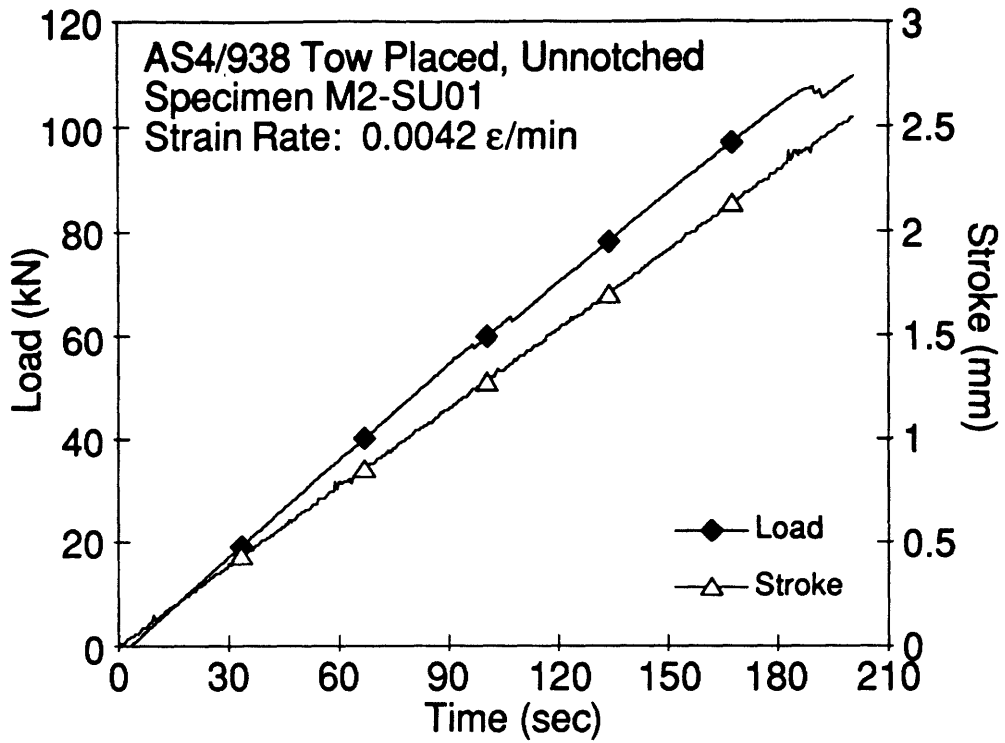


Figure E.16 Plots of Load, Stroke, Longitudinal Strain and Transverse Strain versus Time for Specimen M2-SU01.

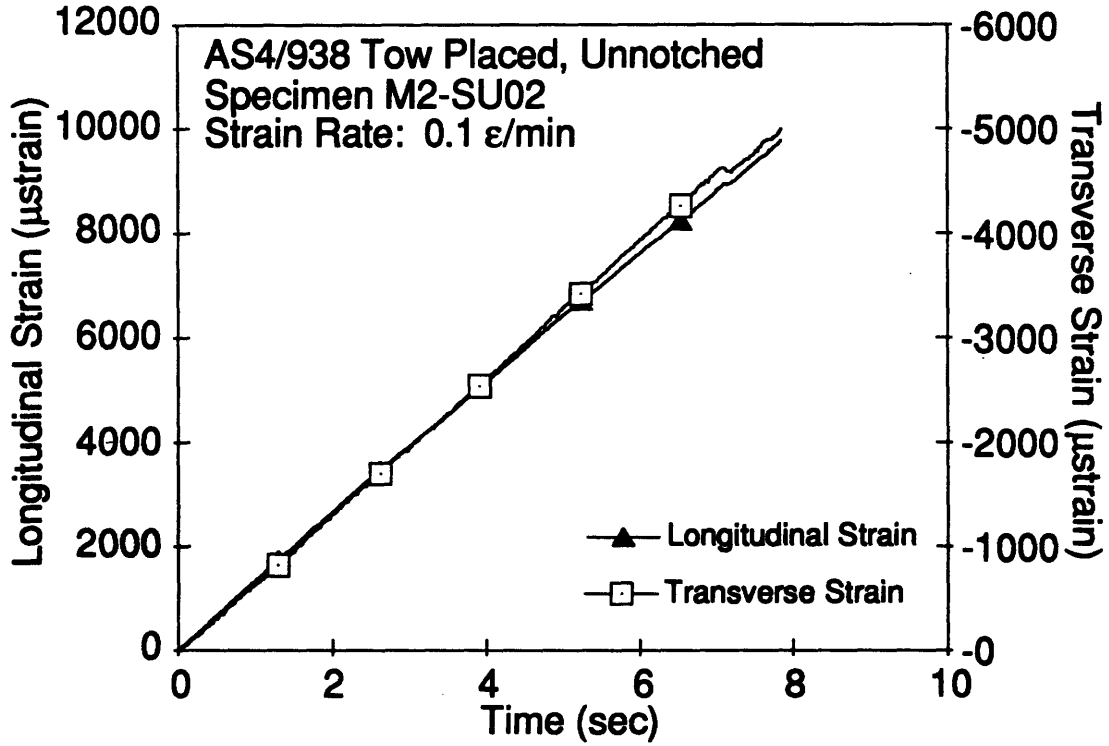
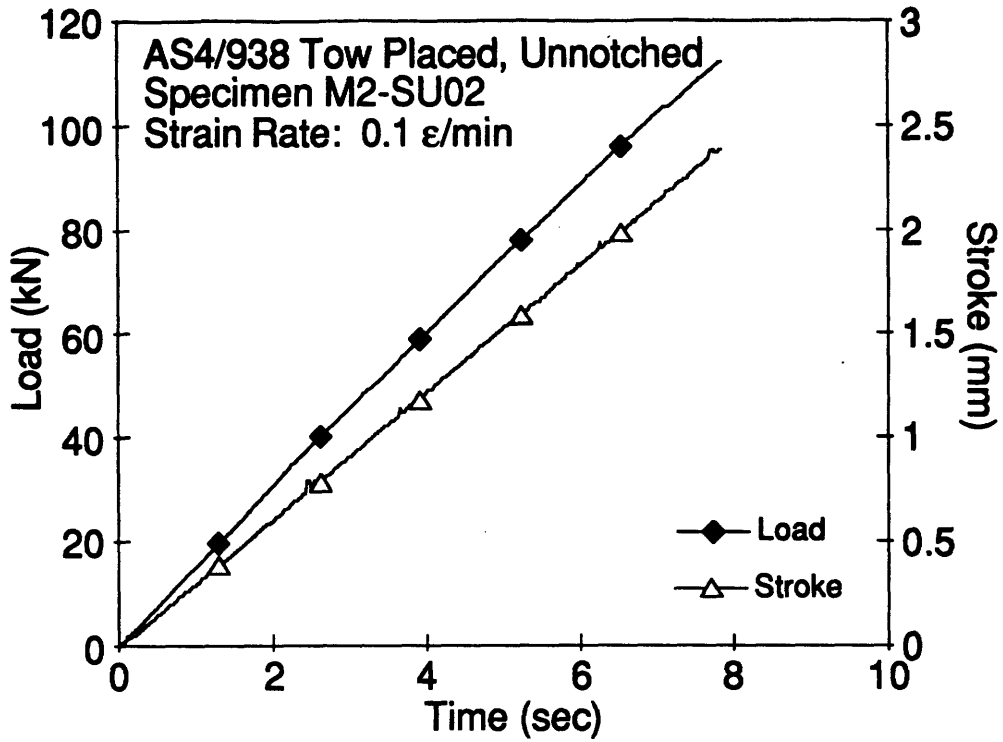


Figure E.17 Plots of Load, Stroke, Longitudinal Strain and Transverse Strain versus Time for Specimen M2-SU02.

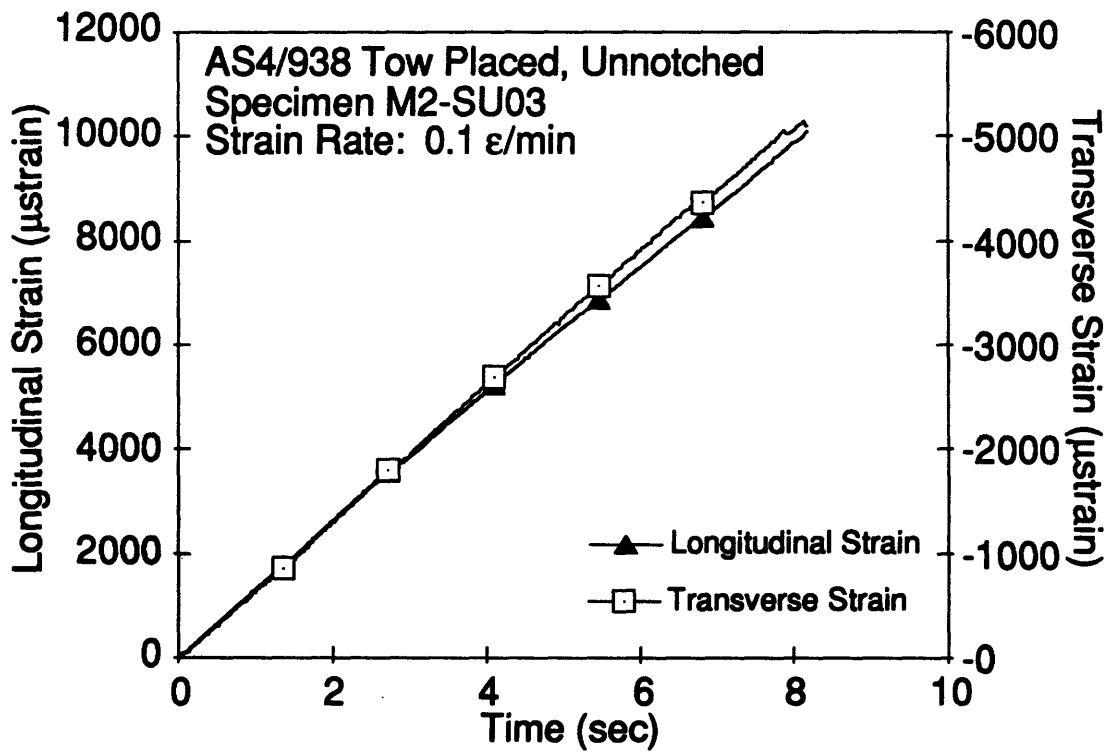
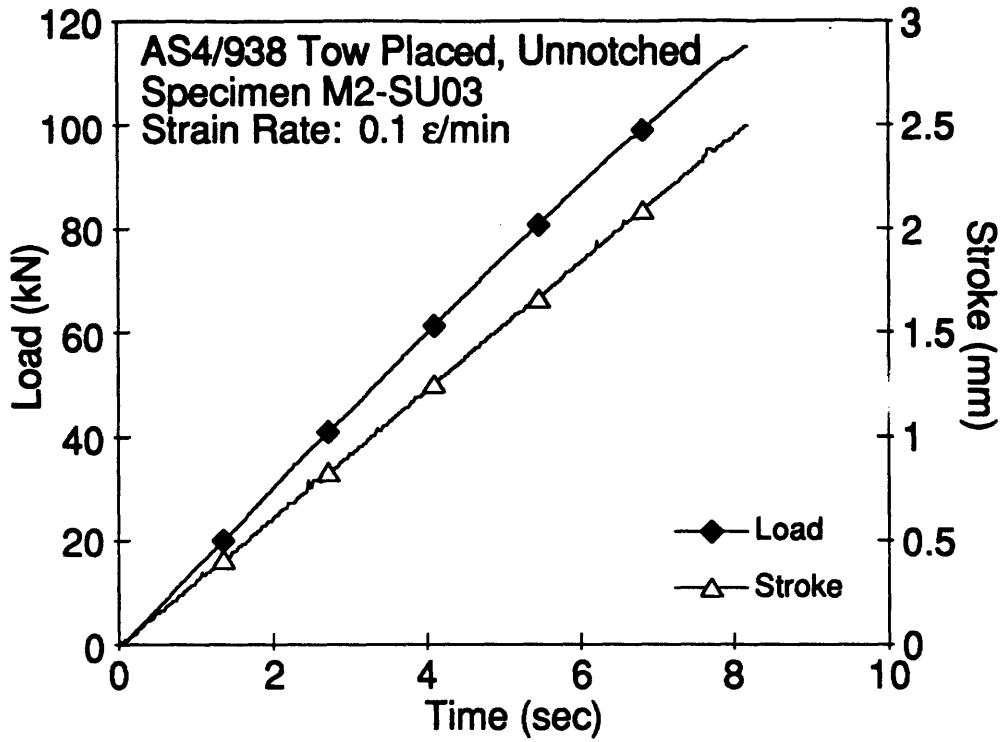


Figure E.18 Plots of Load, Stroke, Longitudinal Strain and Transverse Strain versus Time for Specimen M2-SU03.

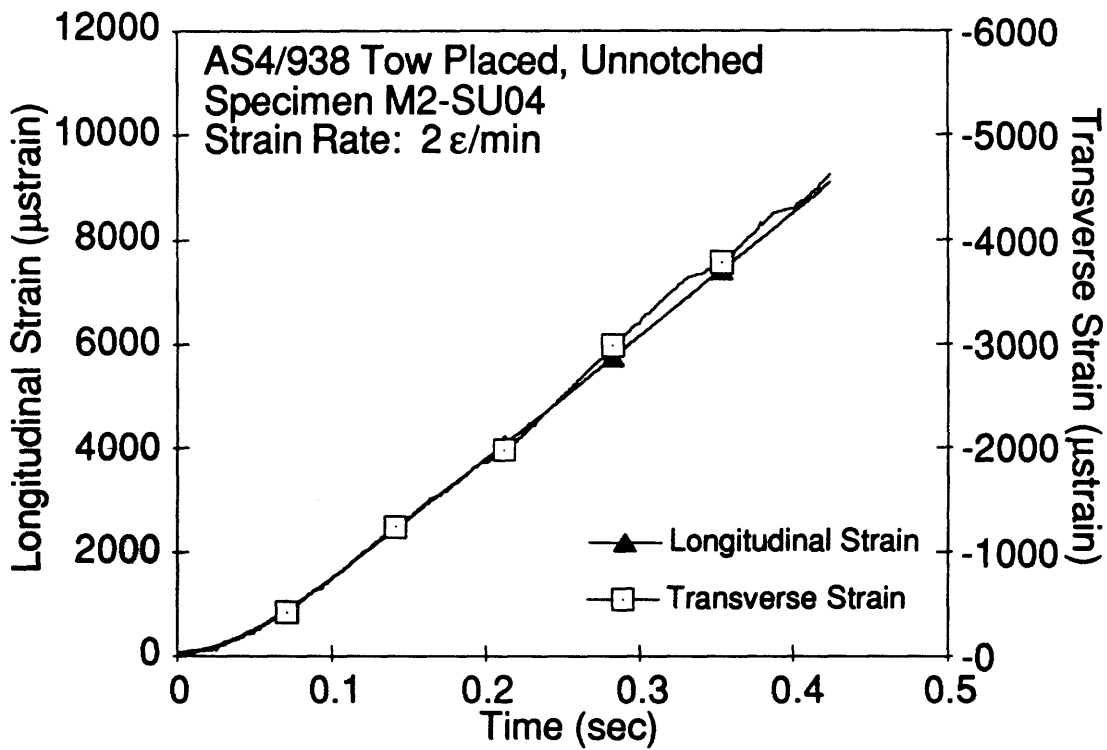
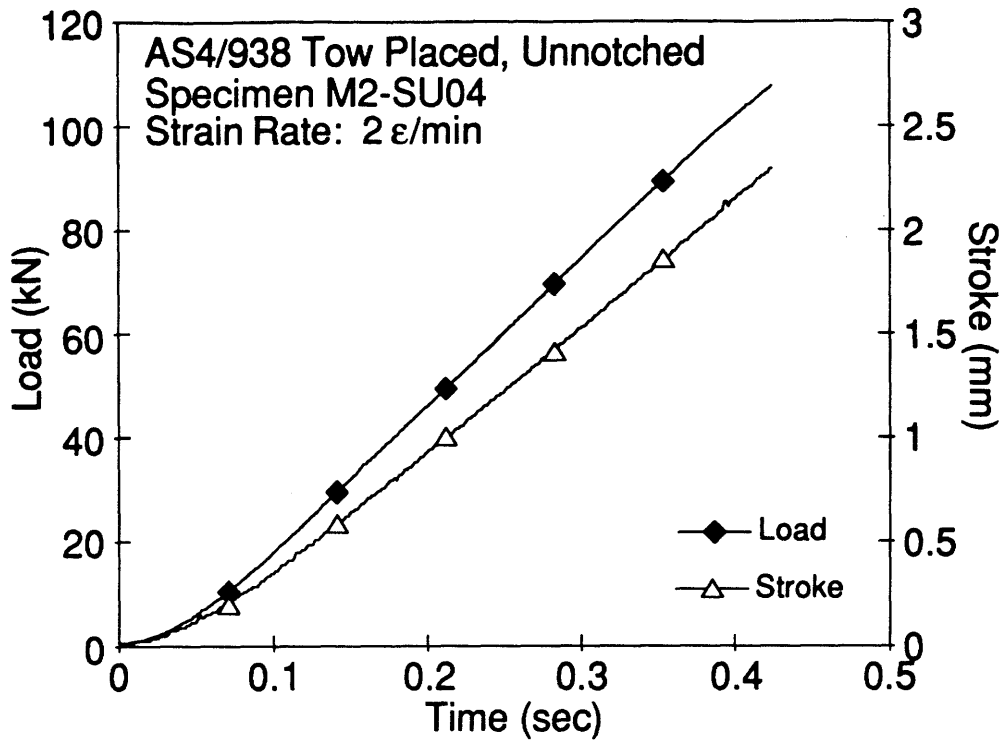


Figure E.19 Plots of Load, Stroke, Longitudinal Strain and Transverse Strain versus Time for Specimen M2-SU04.

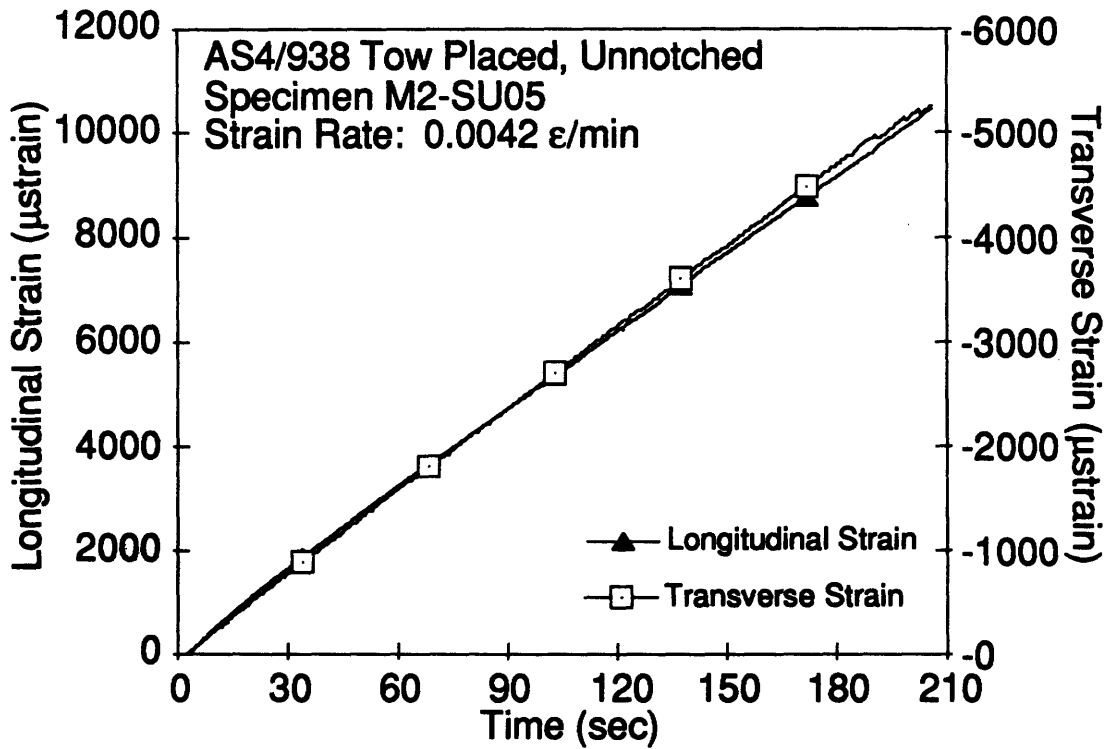
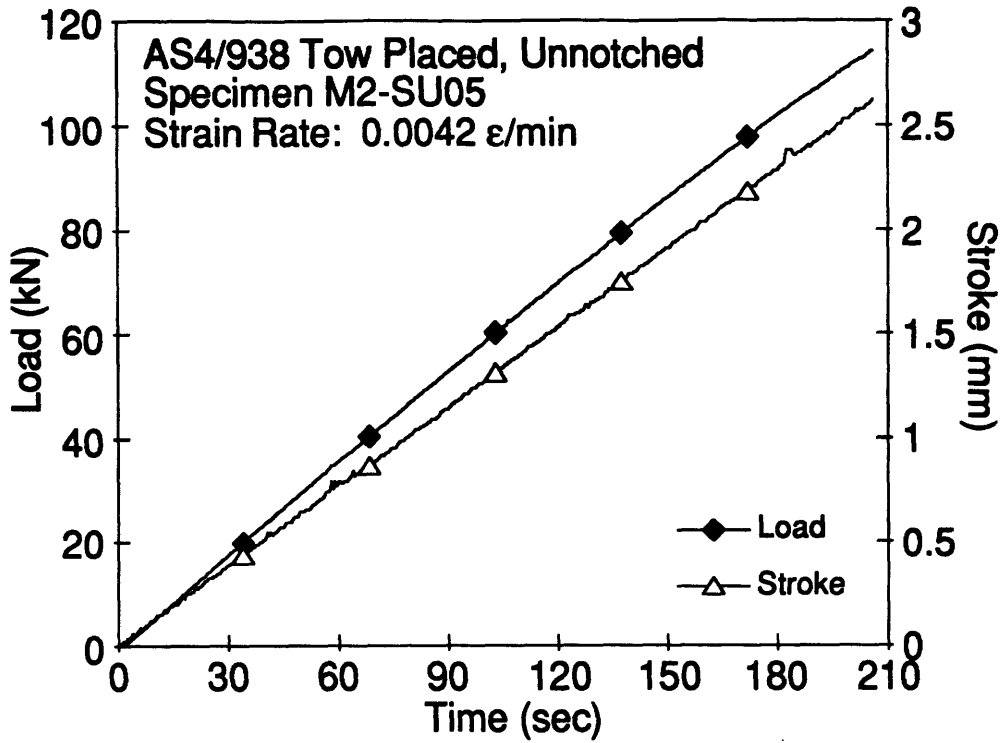


Figure E.20 Plots of Load, Stroke, Longitudinal Strain and Transverse Strain versus Time for Specimen M2-SU05.

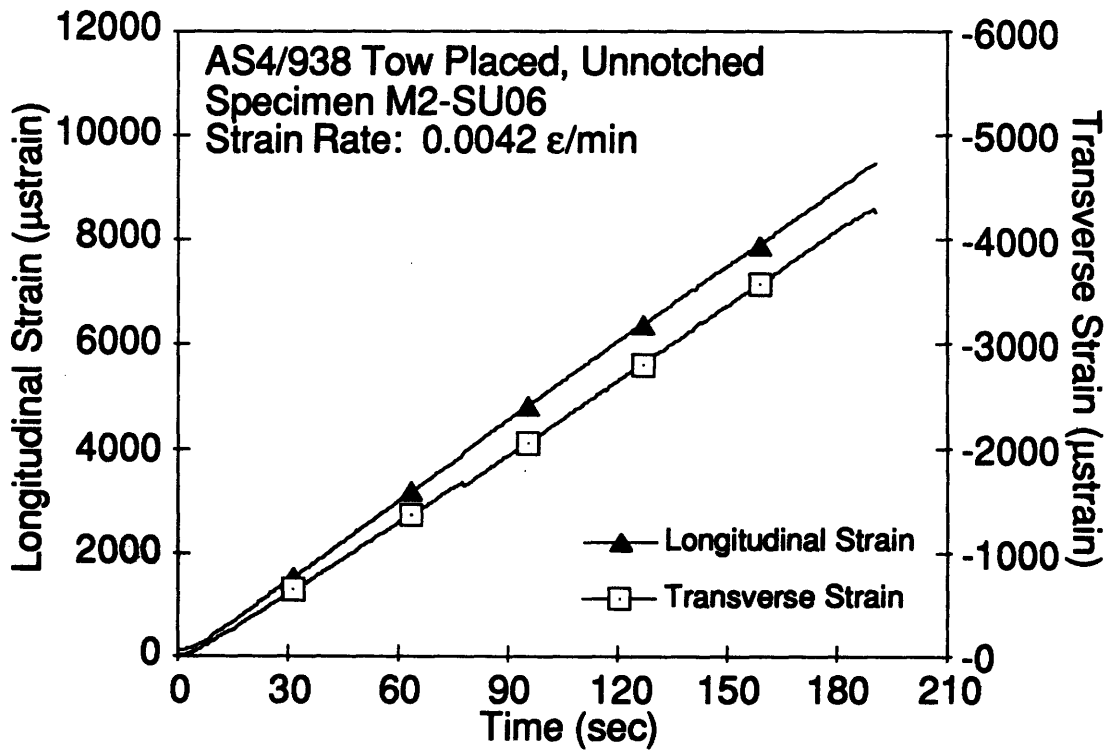
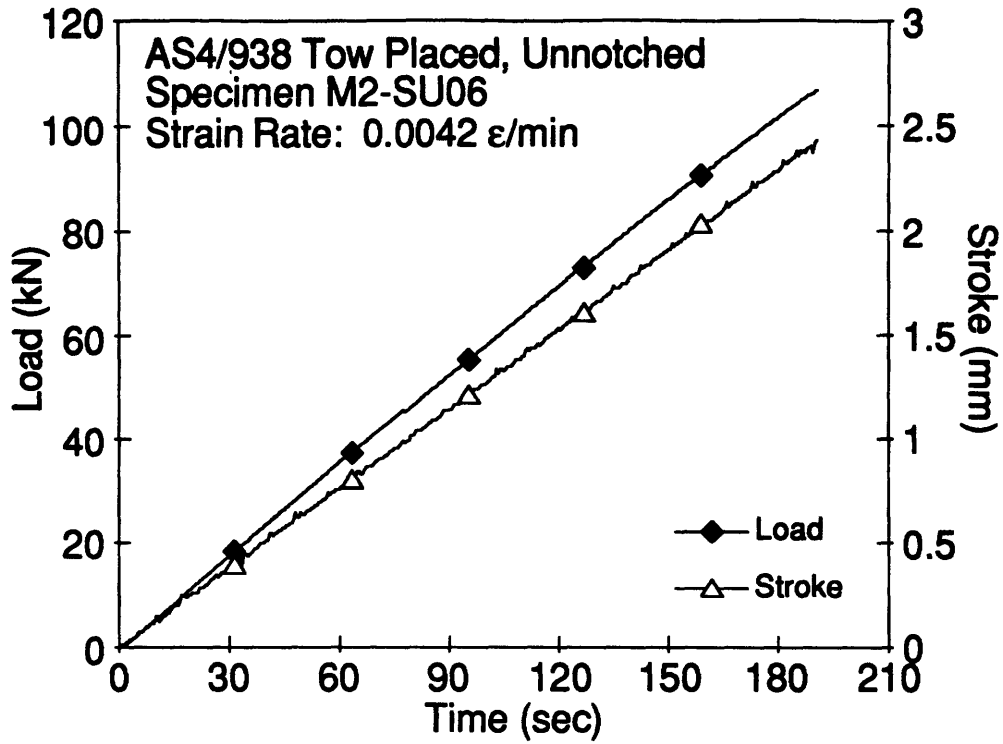


Figure E.21 Plots of Load, Stroke, Longitudinal Strain and Transverse Strain versus Time for Specimen M2-SU06.

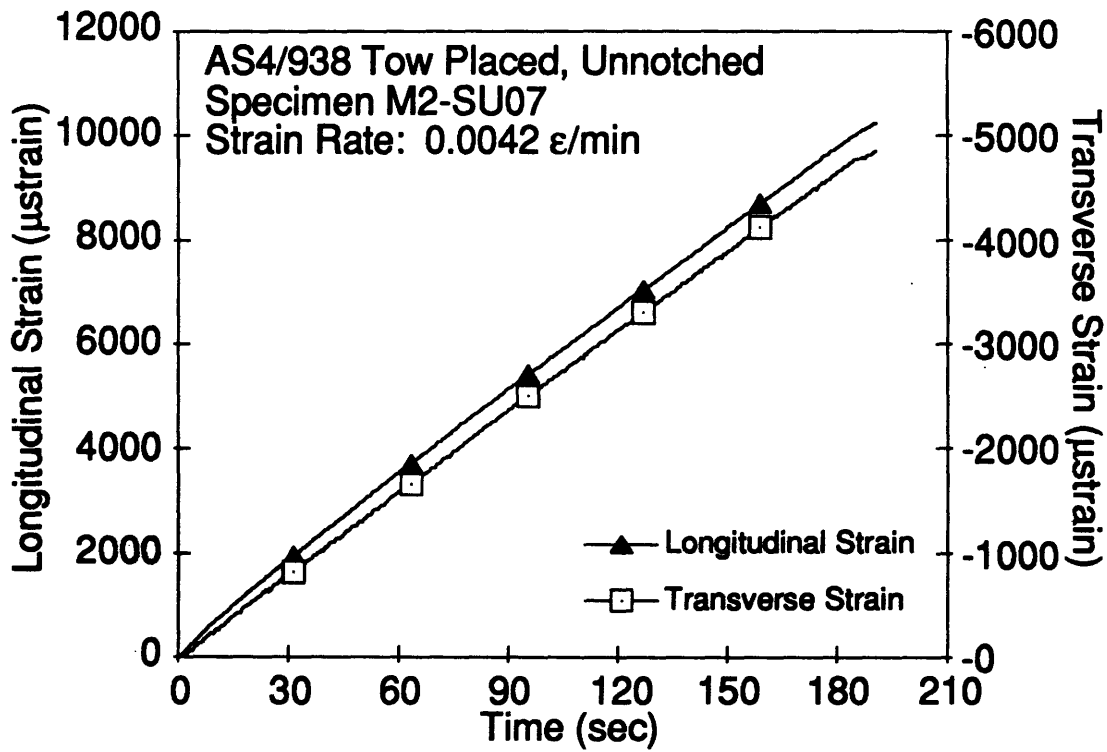
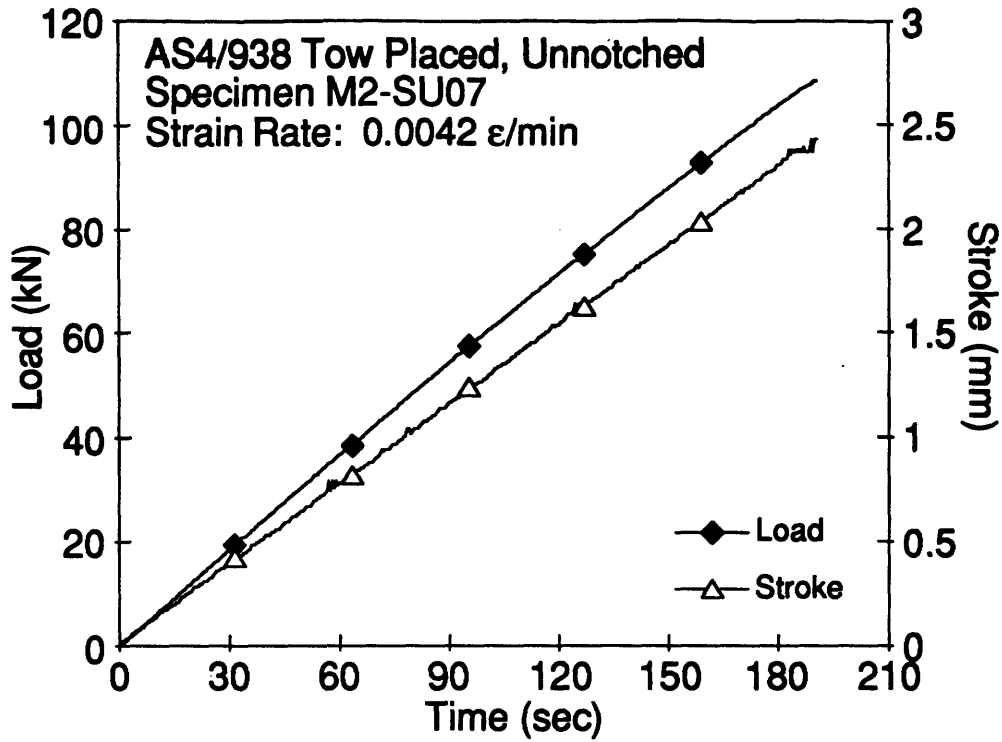


Figure E.22 Plots of Load, Stroke, Longitudinal Strain and Transverse Strain versus Time for Specimen M2-SU07.

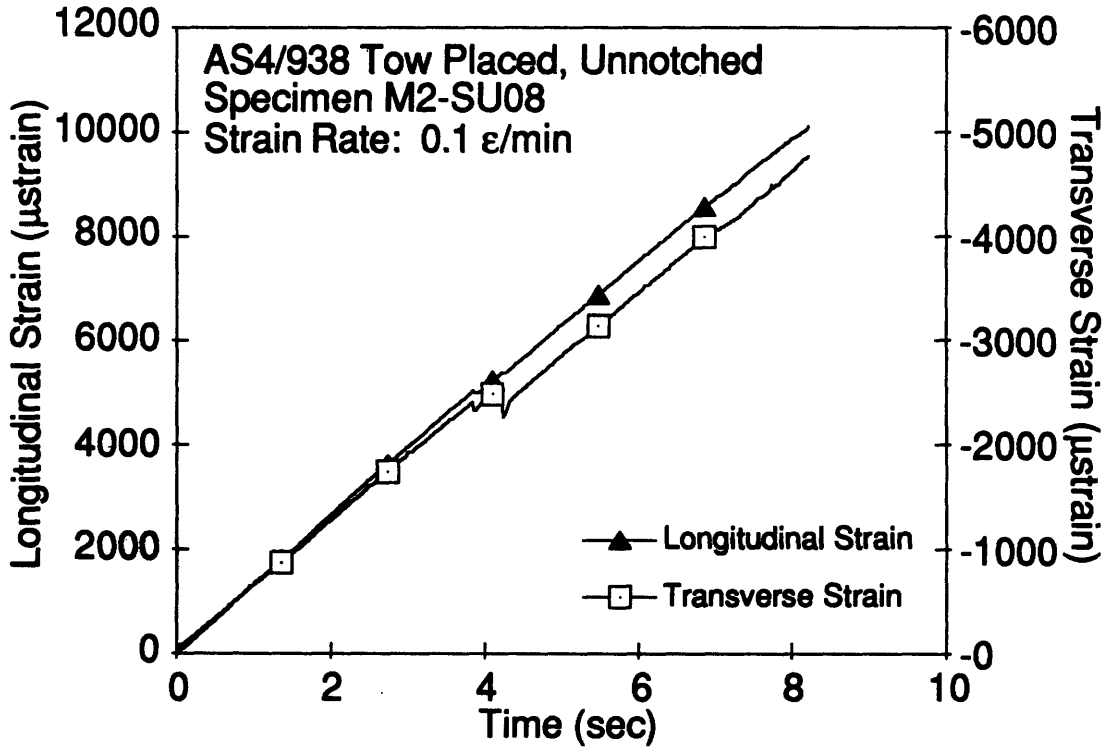
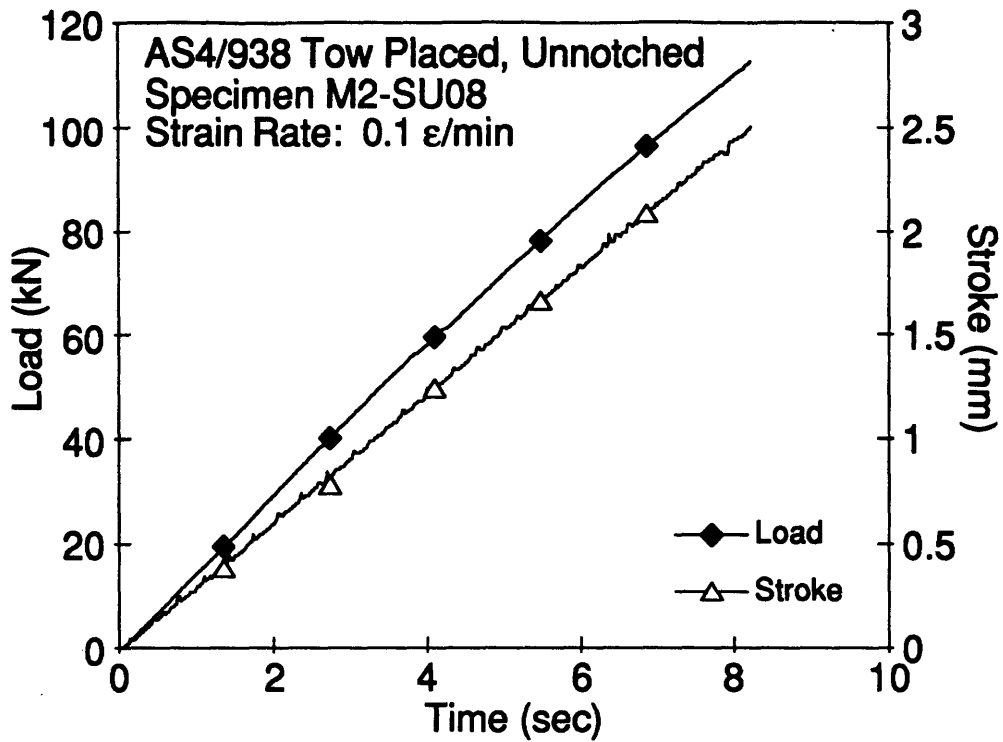


Figure E.23 Plots of Load, Stroke, Longitudinal Strain and Transverse Strain versus Time for Specimen M2-SU08.

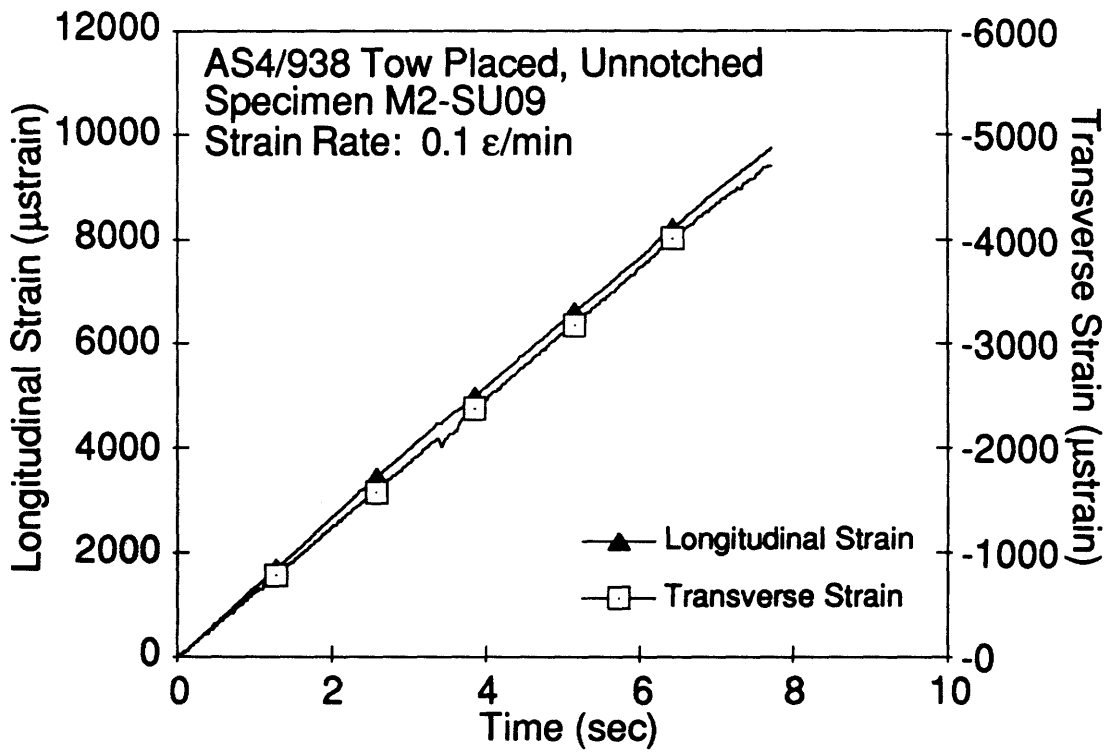
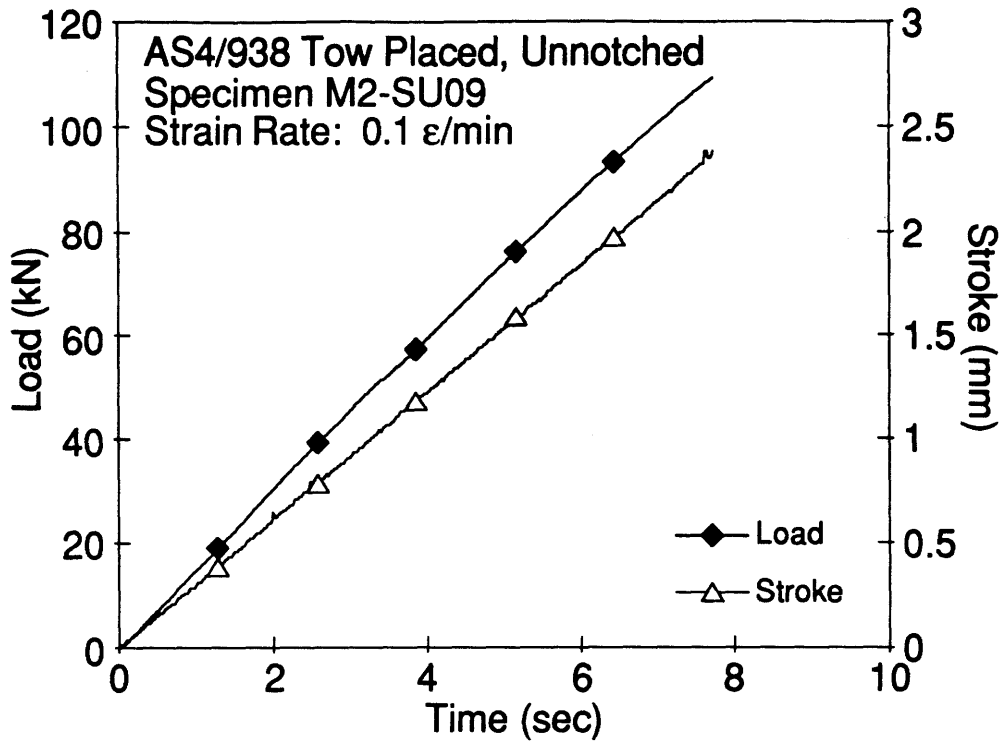


Figure E.24 Plots of Load, Stroke, Longitudinal Strain and Transverse Strain versus Time for Specimen M2-SU09.

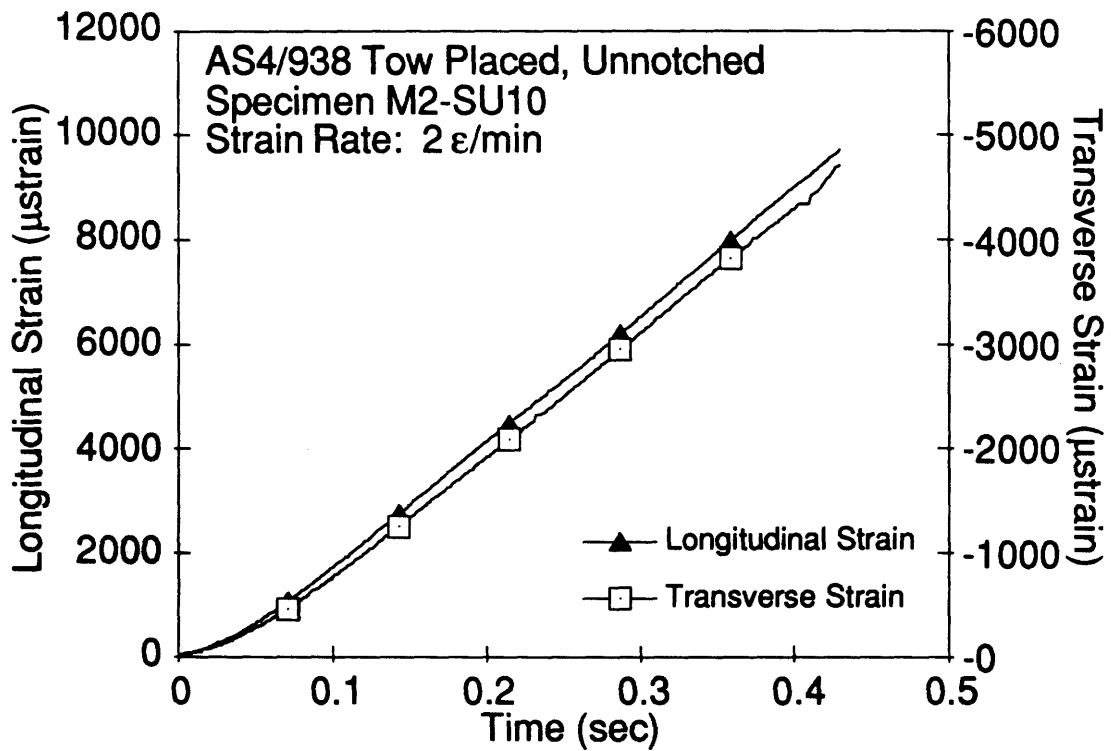
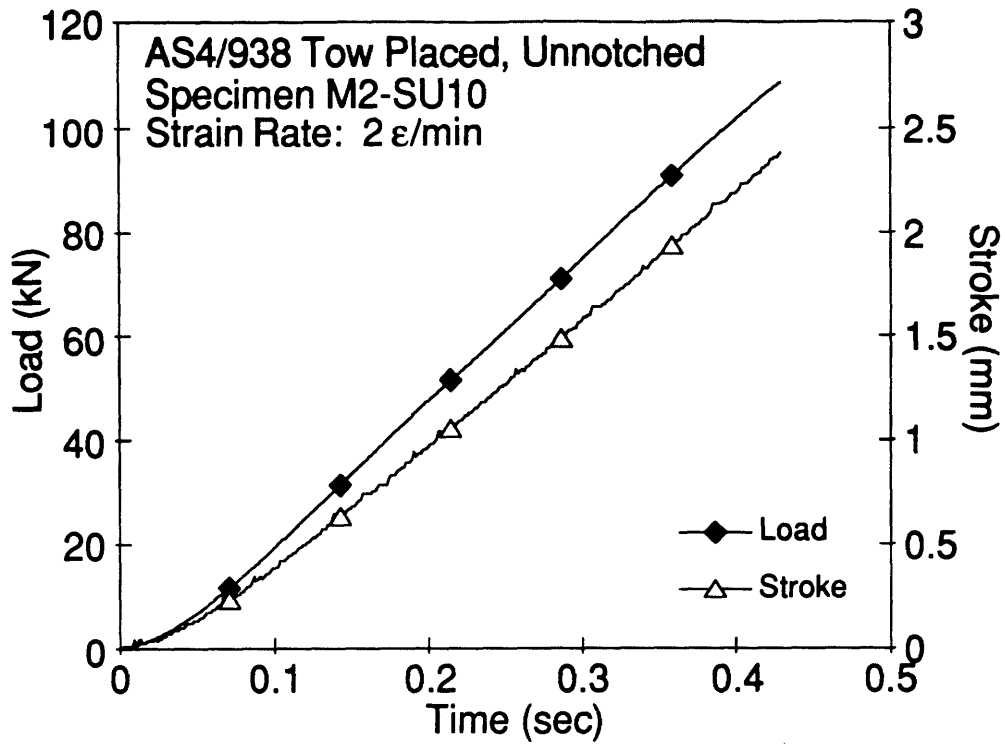


Figure E.25 Plots of Load, Stroke, Longitudinal Strain and Transverse Strain versus Time for Specimen M2-SU10.

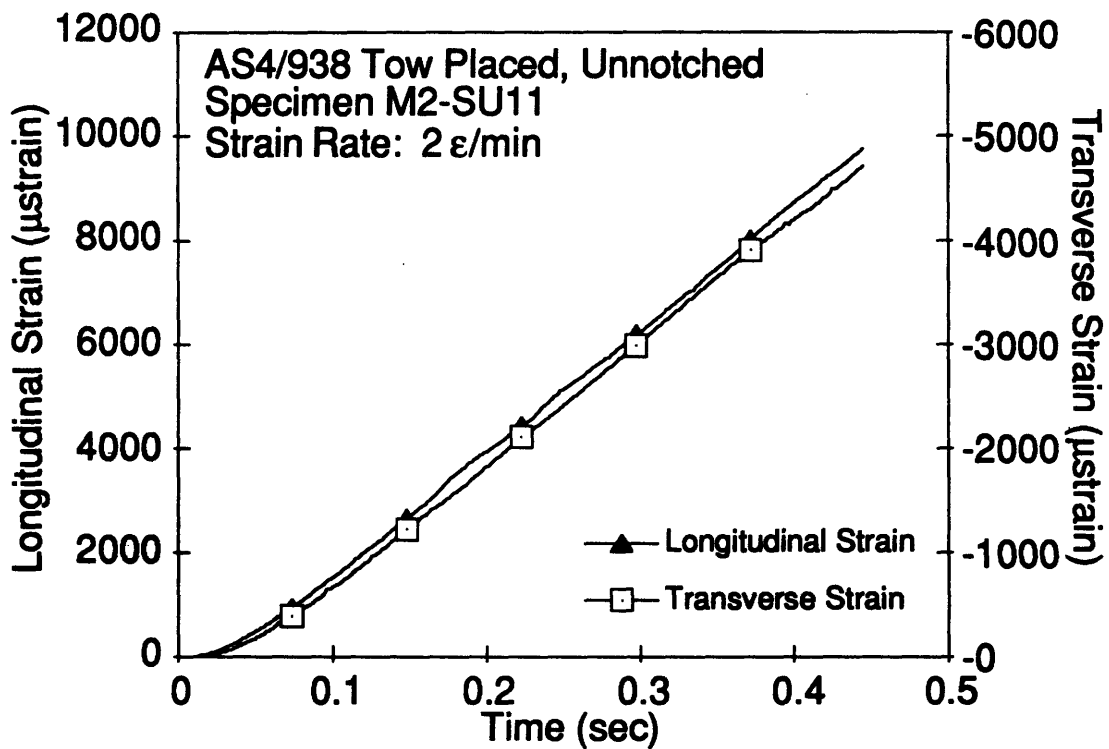
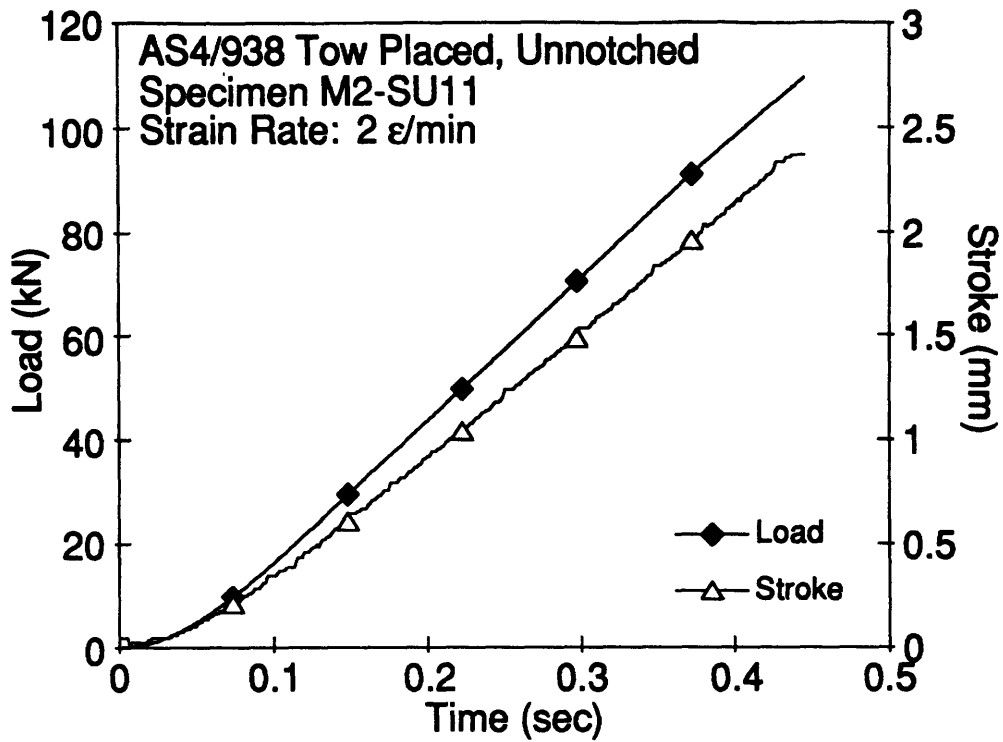


Figure E.26 Plots of Load, Stroke, Longitudinal Strain and Transverse Strain versus Time for Specimen M2-SU11.

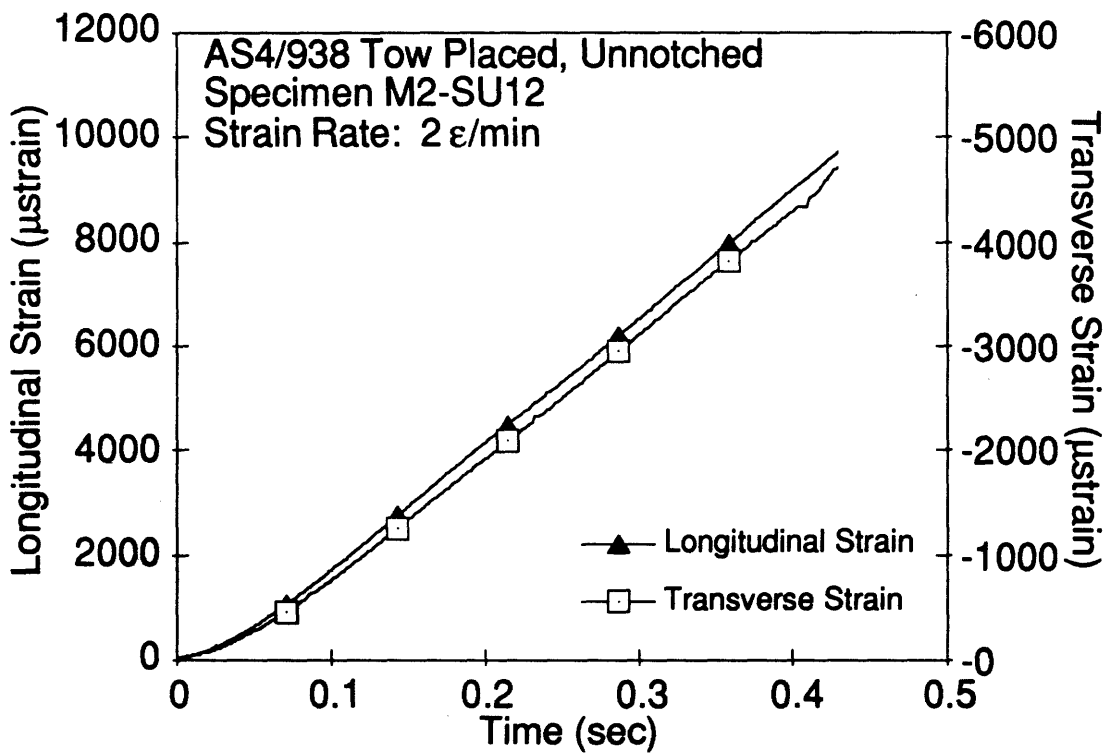
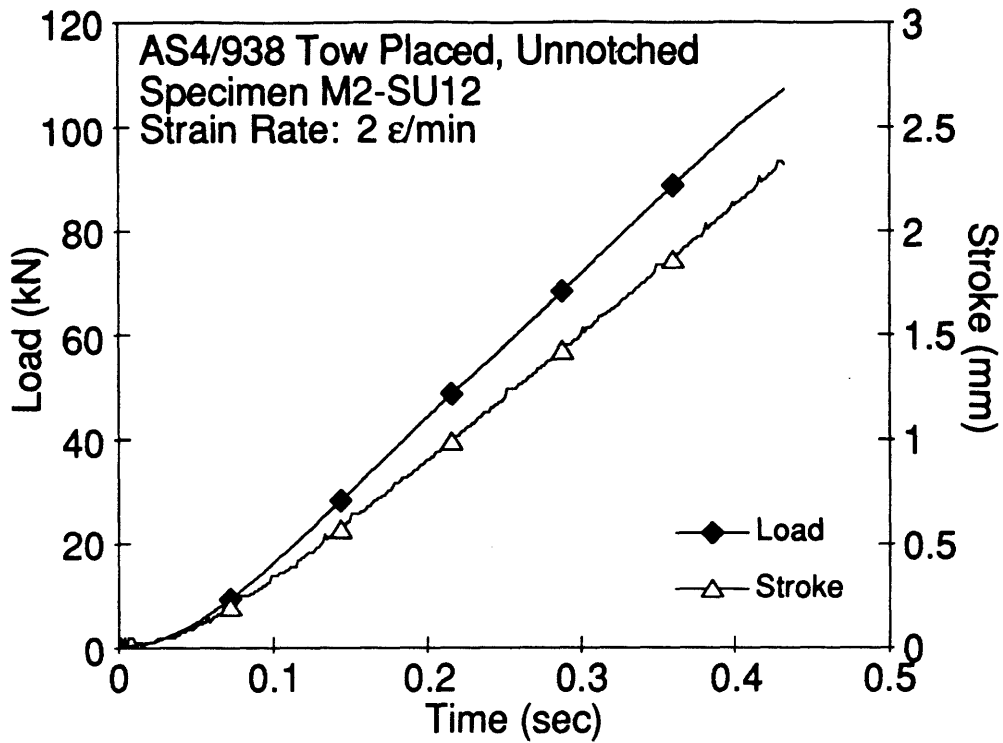


Figure E.27 Plots of Load, Stroke, Longitudinal Strain and Transverse Strain versus Time for Specimen M2-SU12.

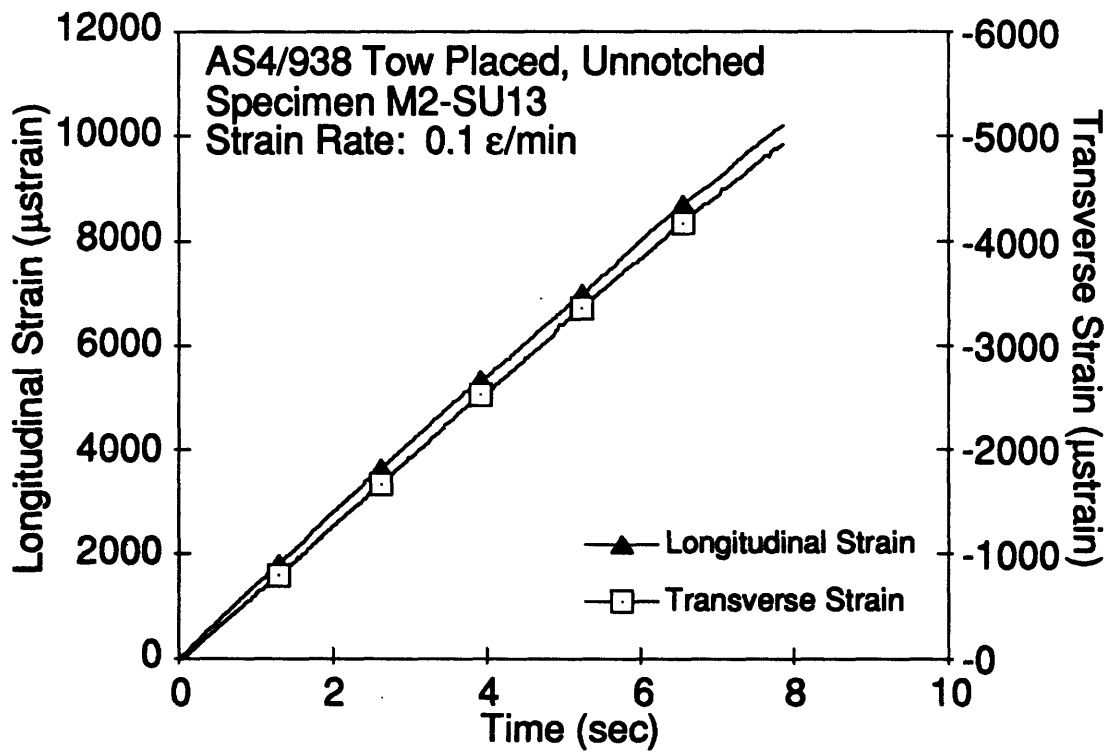
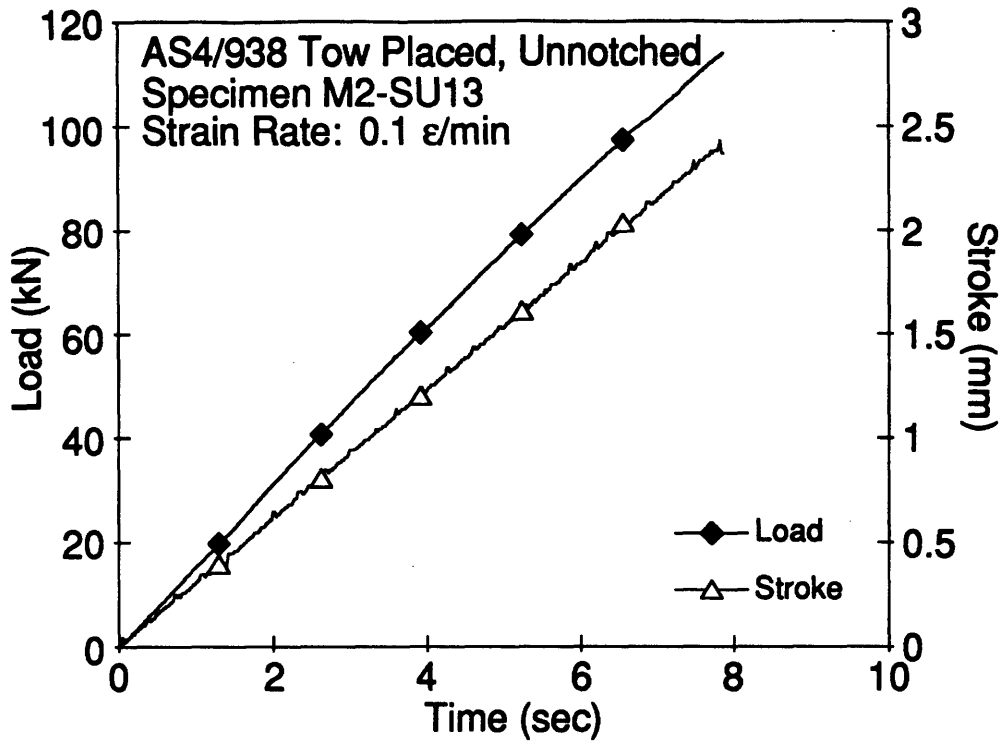


Figure E.28 Plots of Load, Stroke, Longitudinal Strain and Transverse Strain versus Time for Specimen M2-SU13.

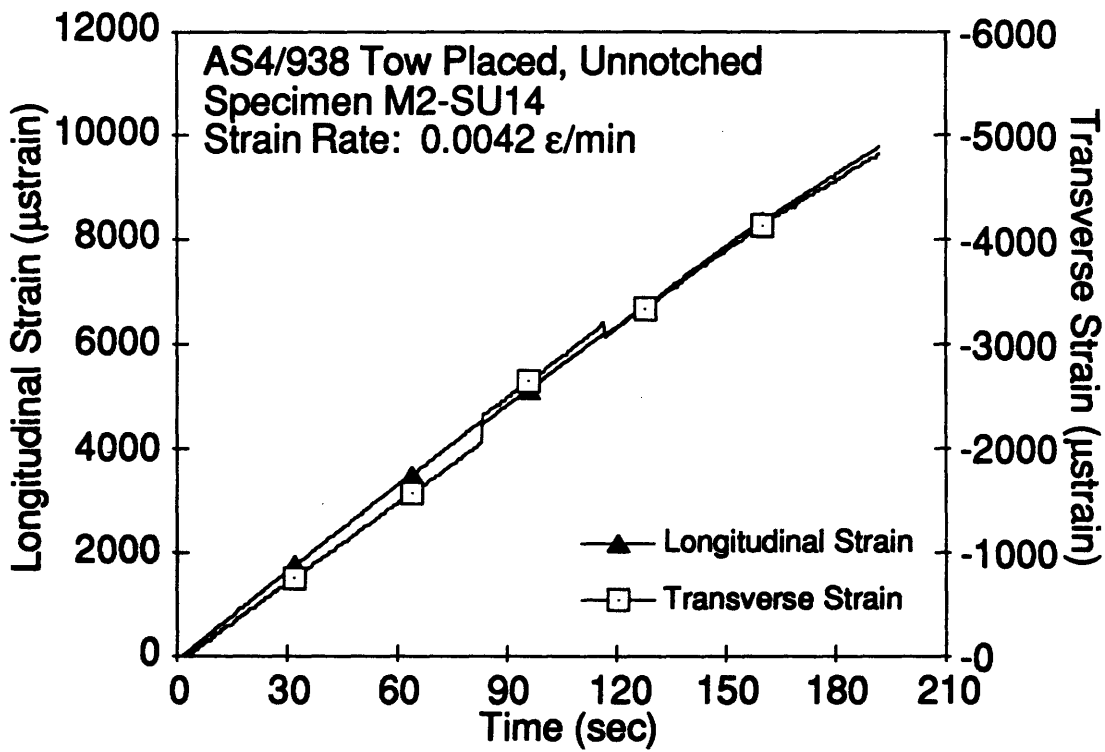
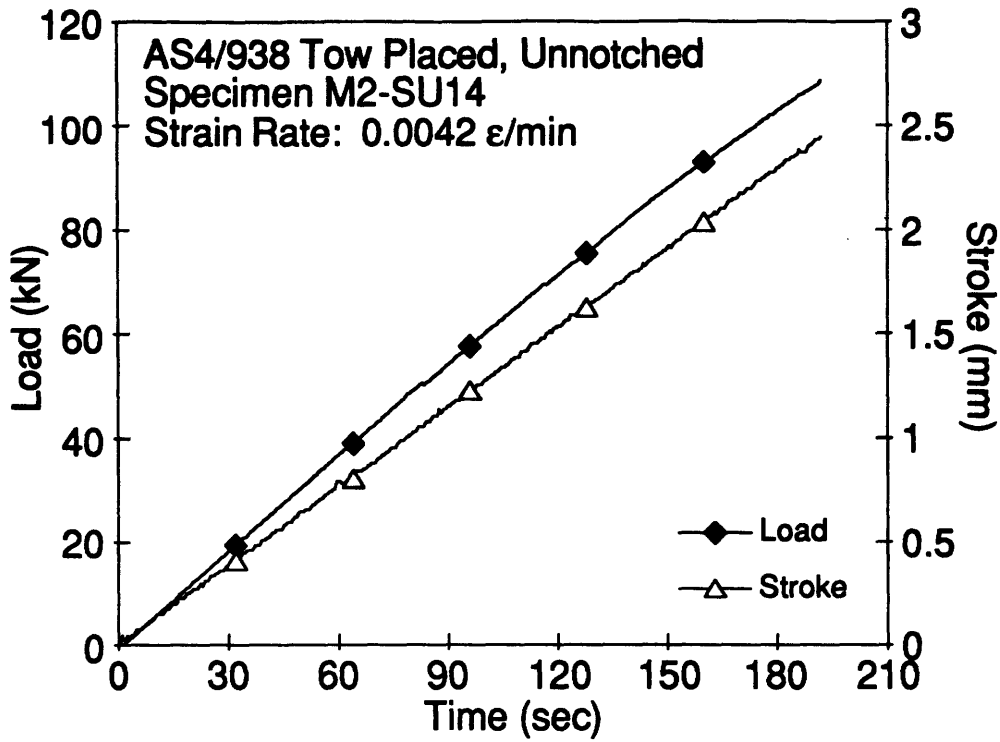


Figure E.29 Plots of Load, Stroke, Longitudinal Strain and Transverse Strain versus Time for Specimen M2-SU14.

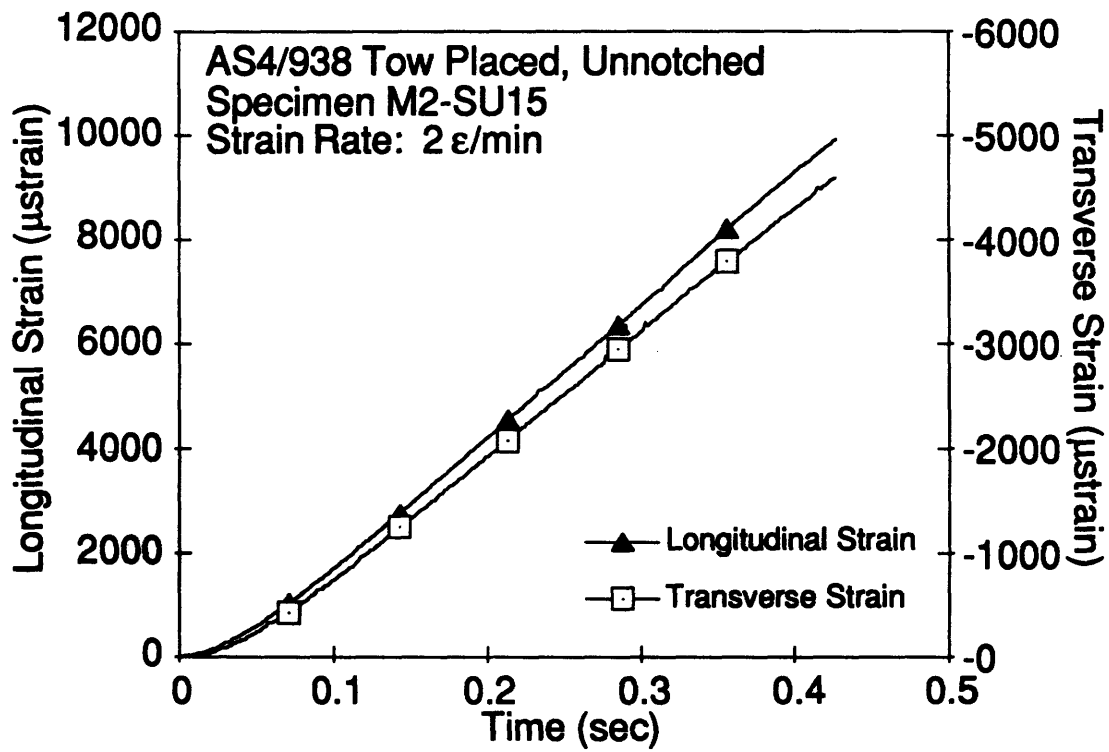
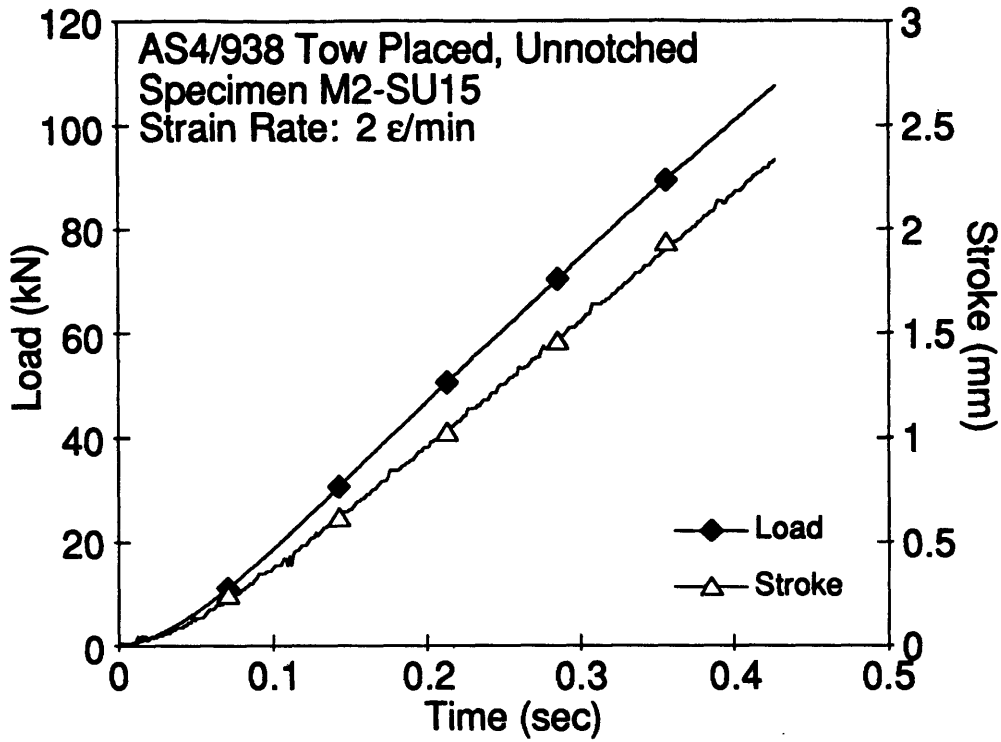


Figure E.30 Plots of Load, Stroke, Longitudinal Strain and Transverse Strain versus Time for Specimen M2-SU15.

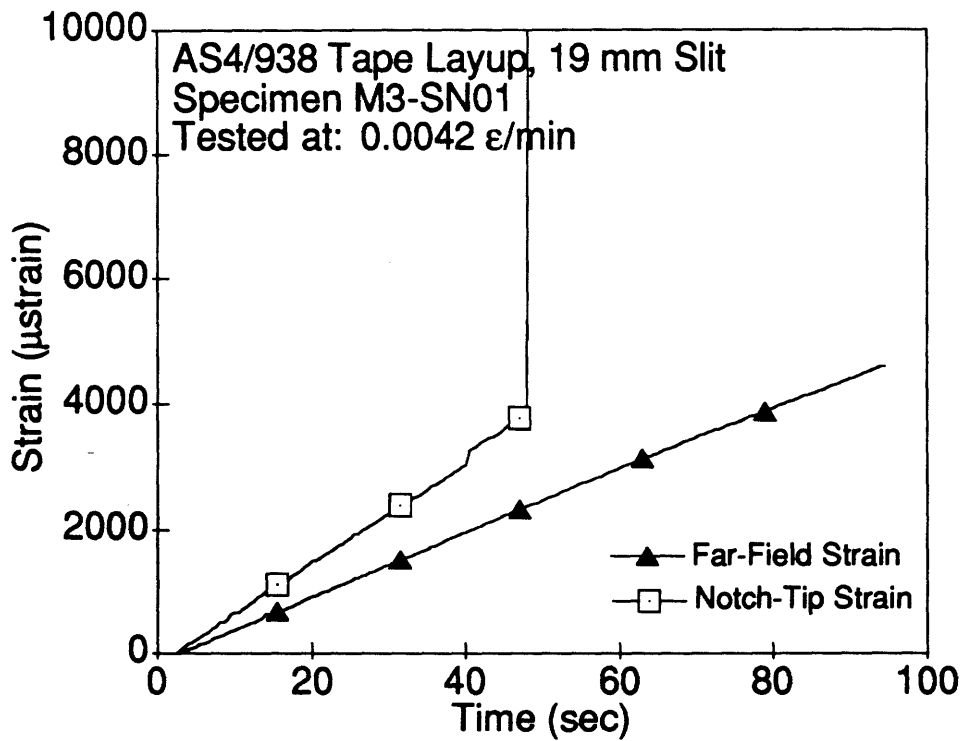
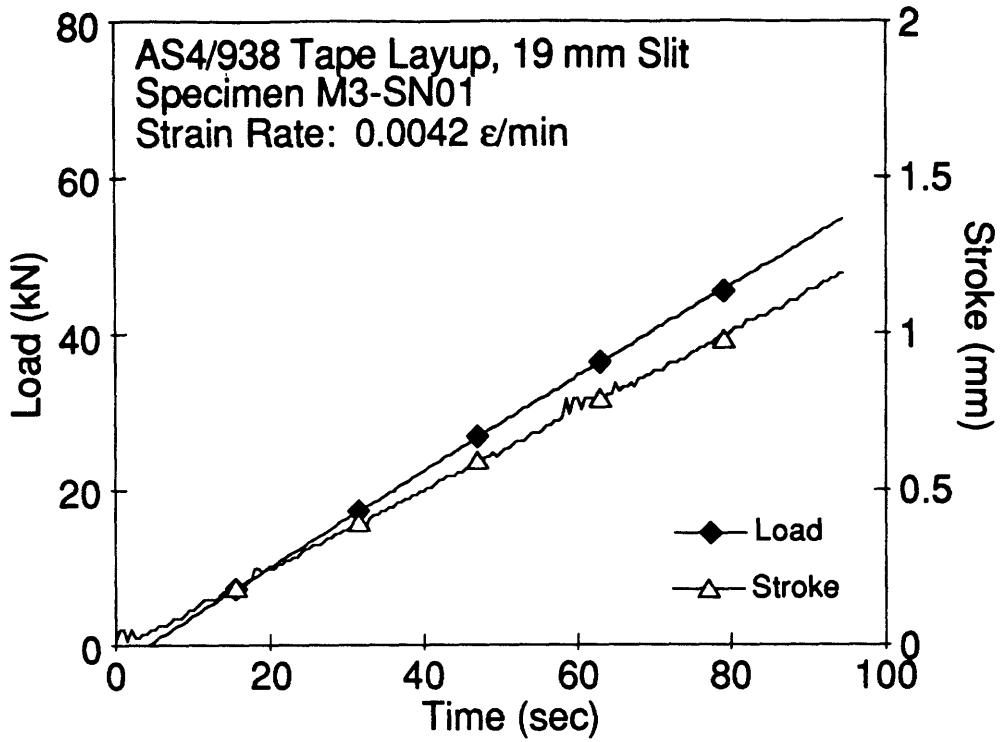


Figure E.31 Plots of Load, Stroke, Far-Field Strain and Notch-Tip Strain versus Time for Specimen M3-SN01.

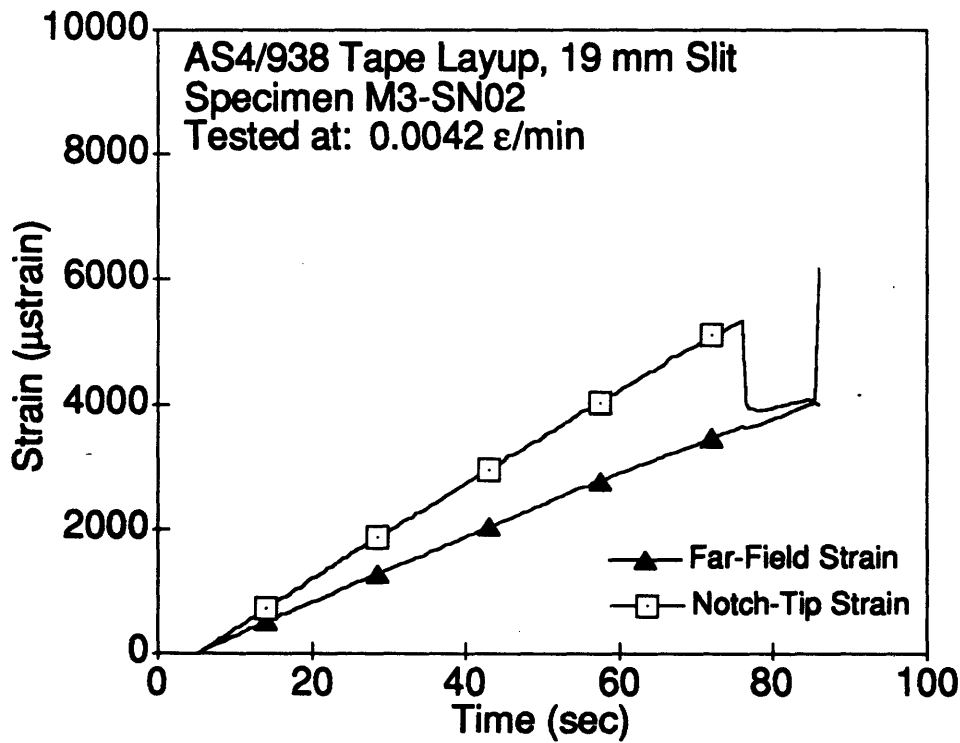
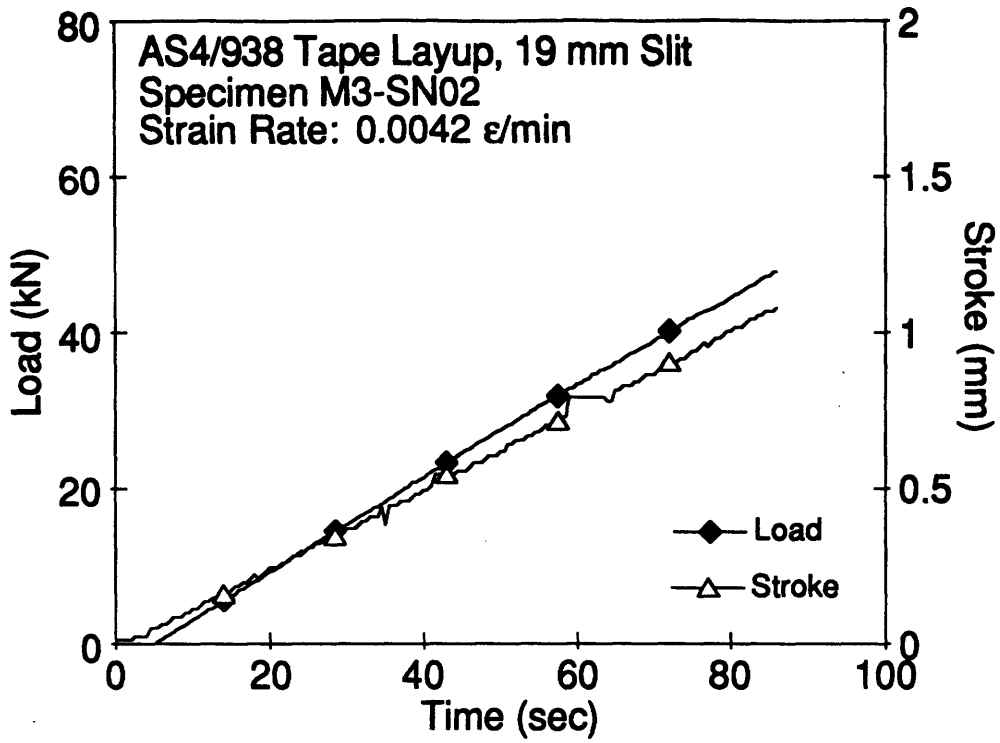


Figure E.32 Plots of Load, Stroke, Far-Field Strain and Notch-Tip Strain versus Time for Specimen M3-SN02.

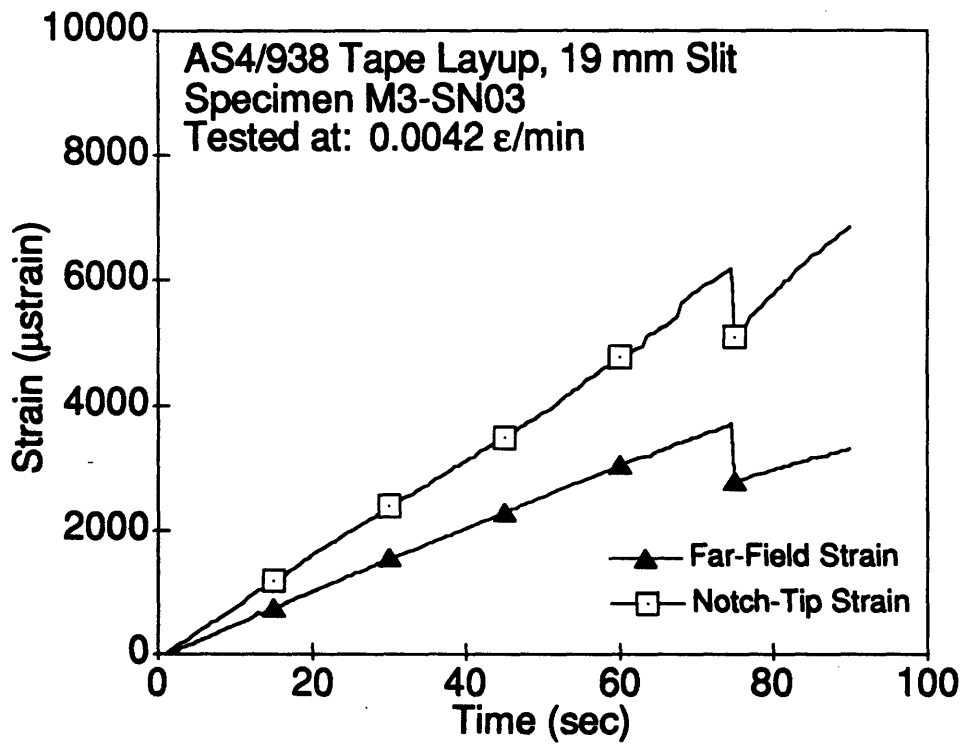
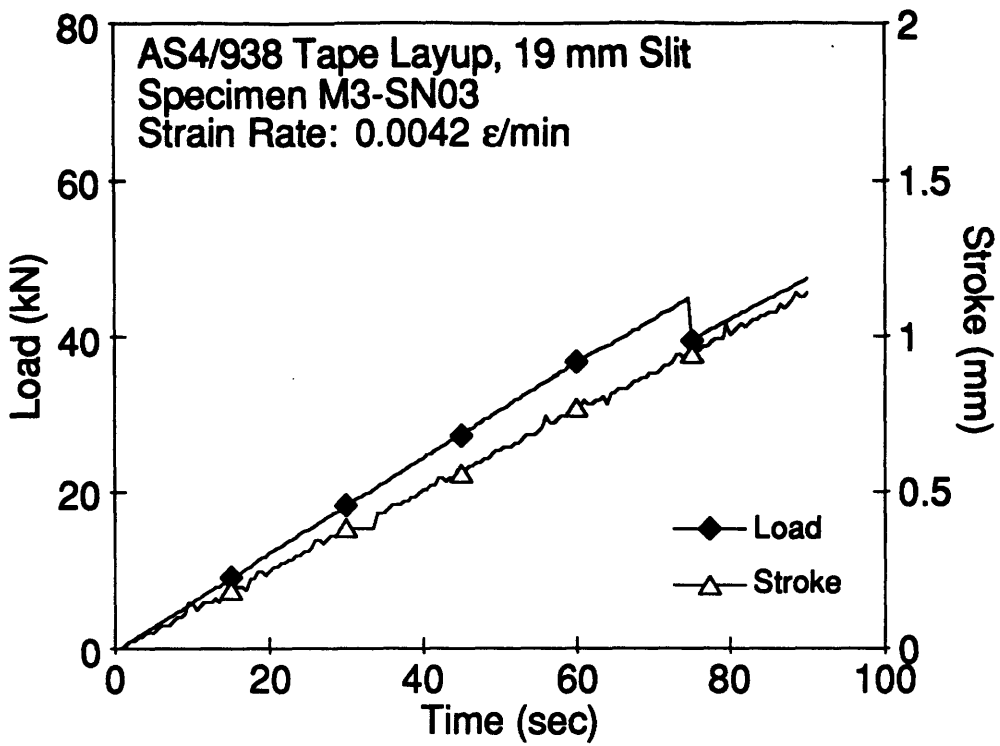


Figure E.33 Plots of Load, Stroke, Far-Field Strain and Notch-Tip Strain versus Time for Specimen M3-SN03.

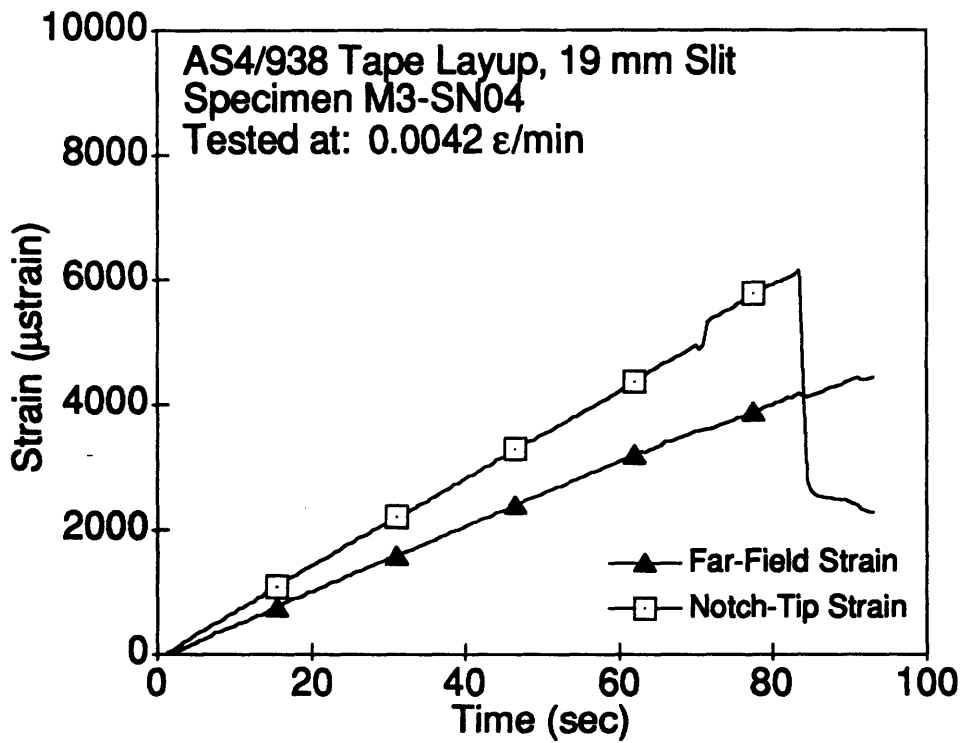
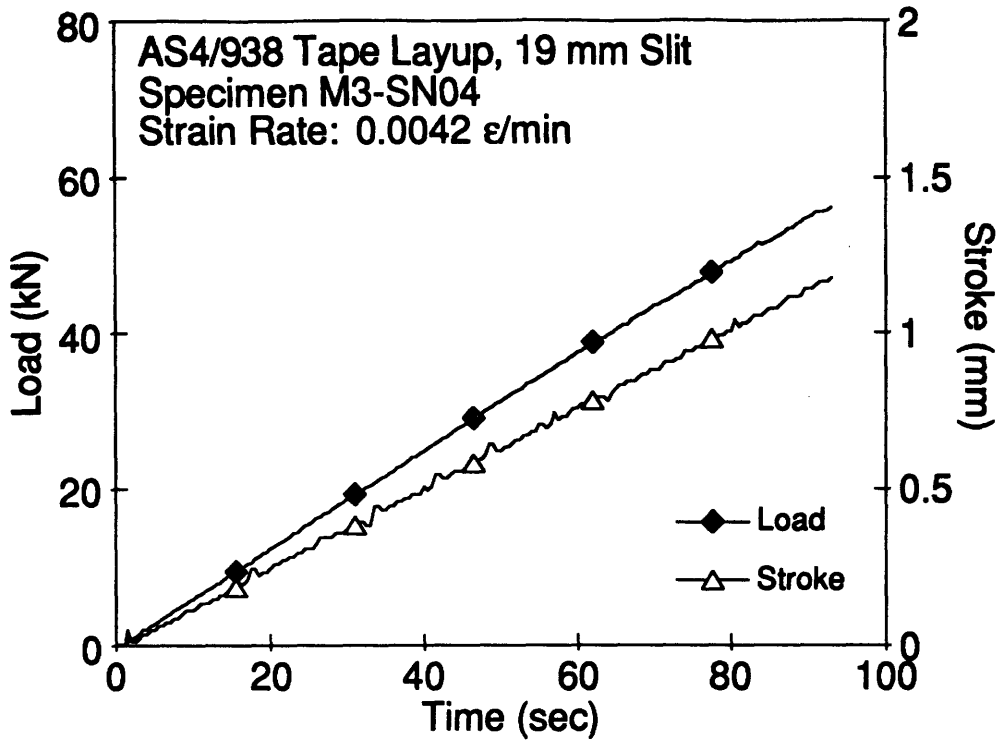


Figure E.34 Plots of Load, Stroke, Far-Field Strain and Notch-Tip Strain versus Time for Specimen M3-SN04.

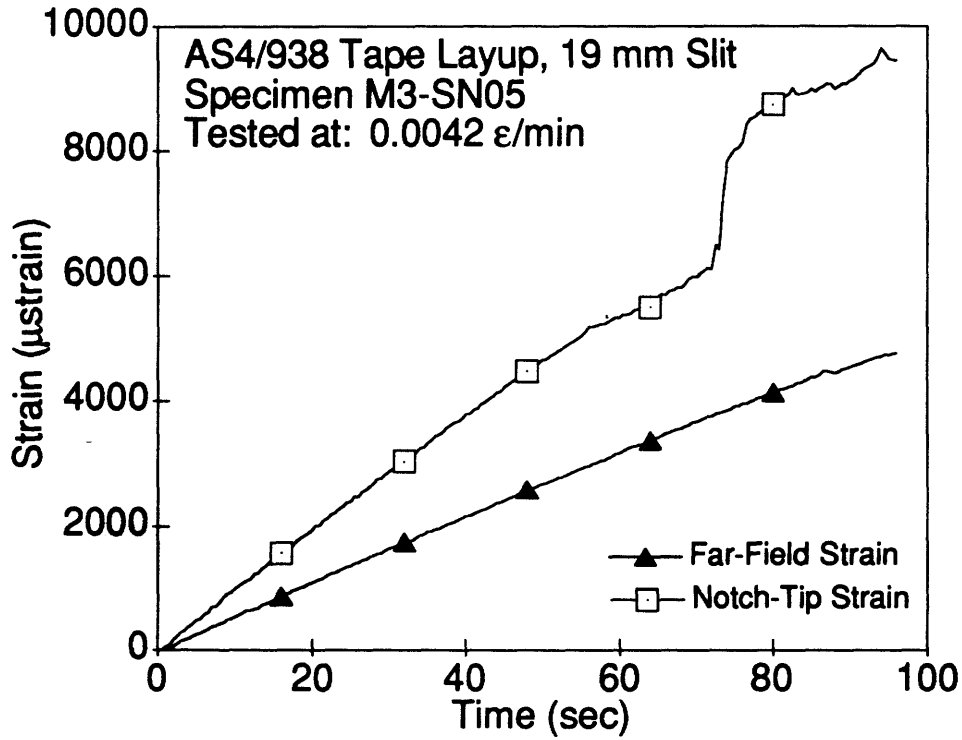
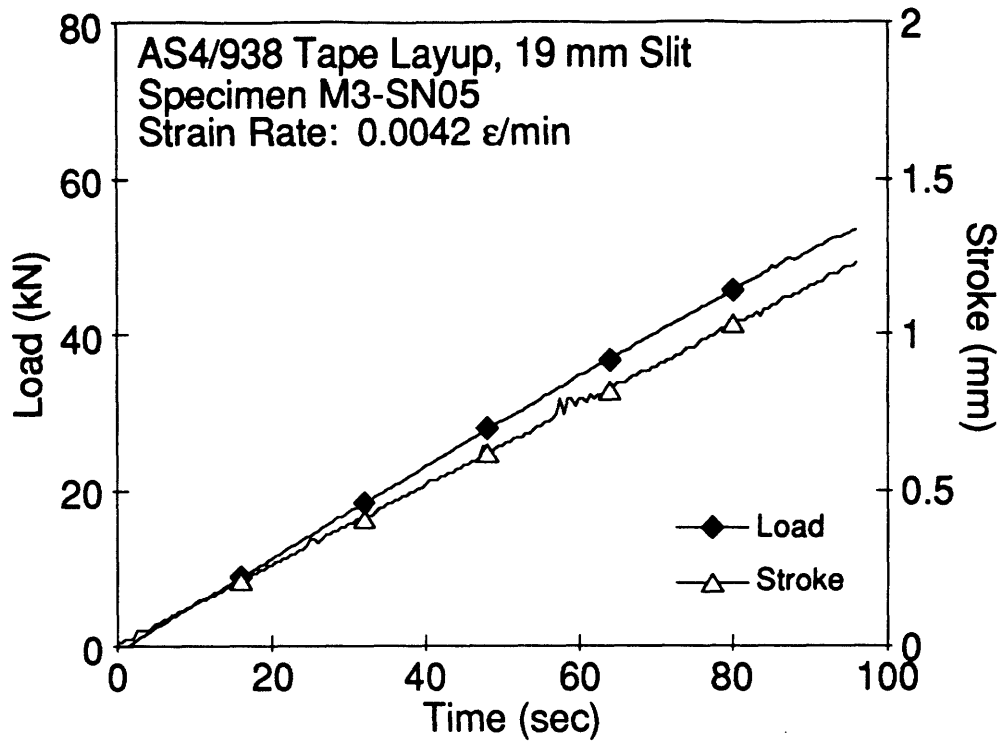


Figure E.35 Plots of Load, Stroke, Far-Field Strain and Notch-Tip Strain versus Time for Specimen M3-SN05.

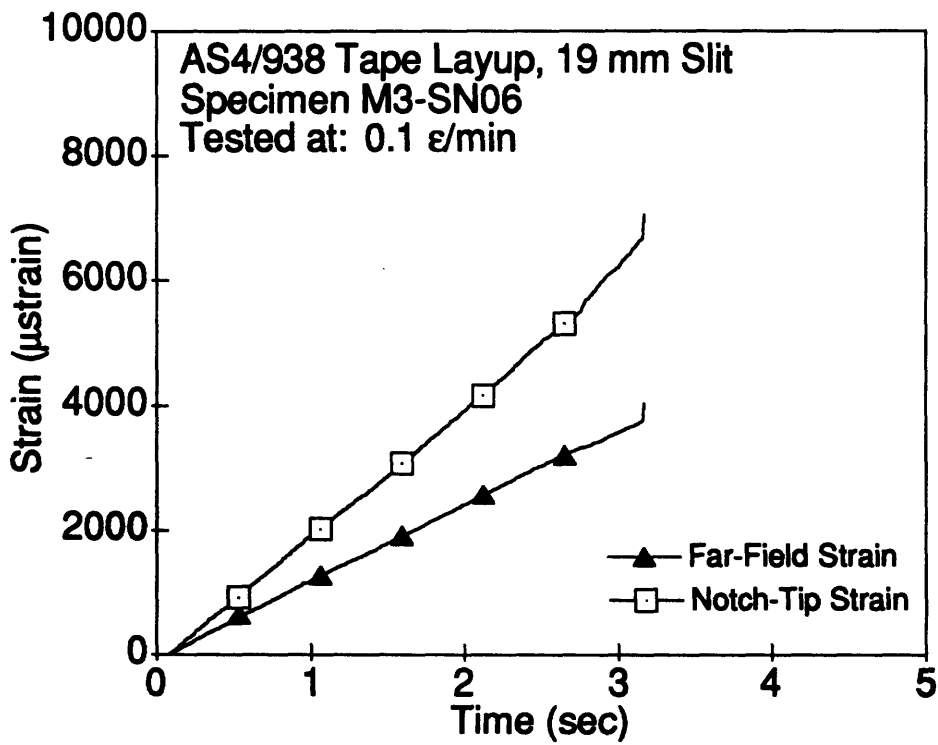
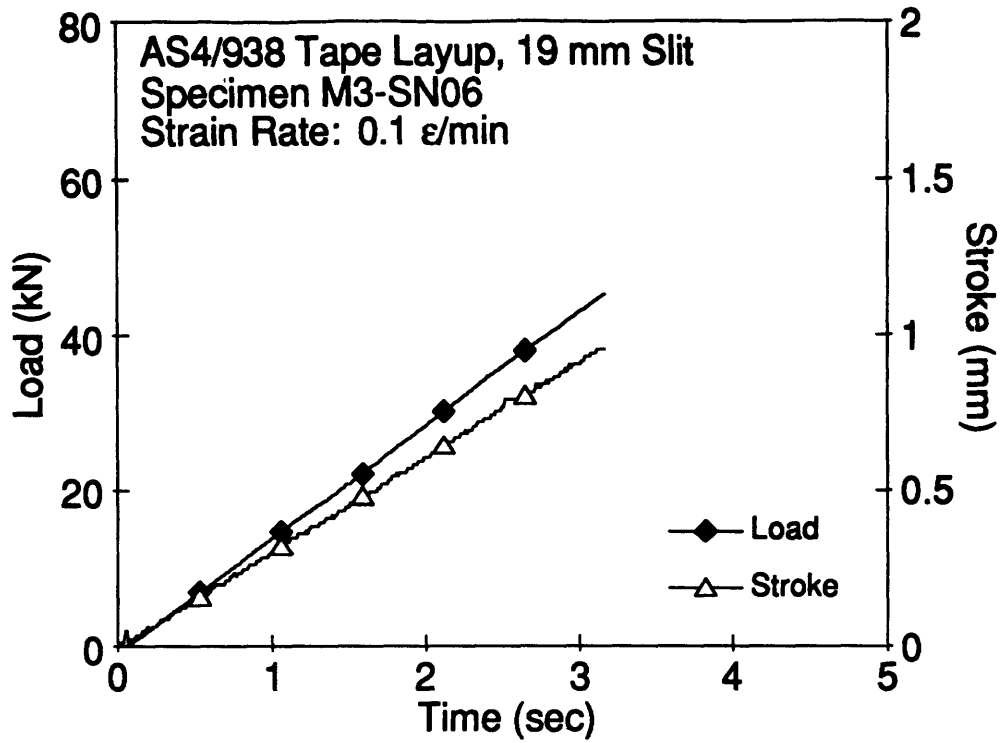


Figure E.36 Plots of Load, Stroke, Far-Field Strain and Notch-Tip Strain versus Time for Specimen M3-SN06.

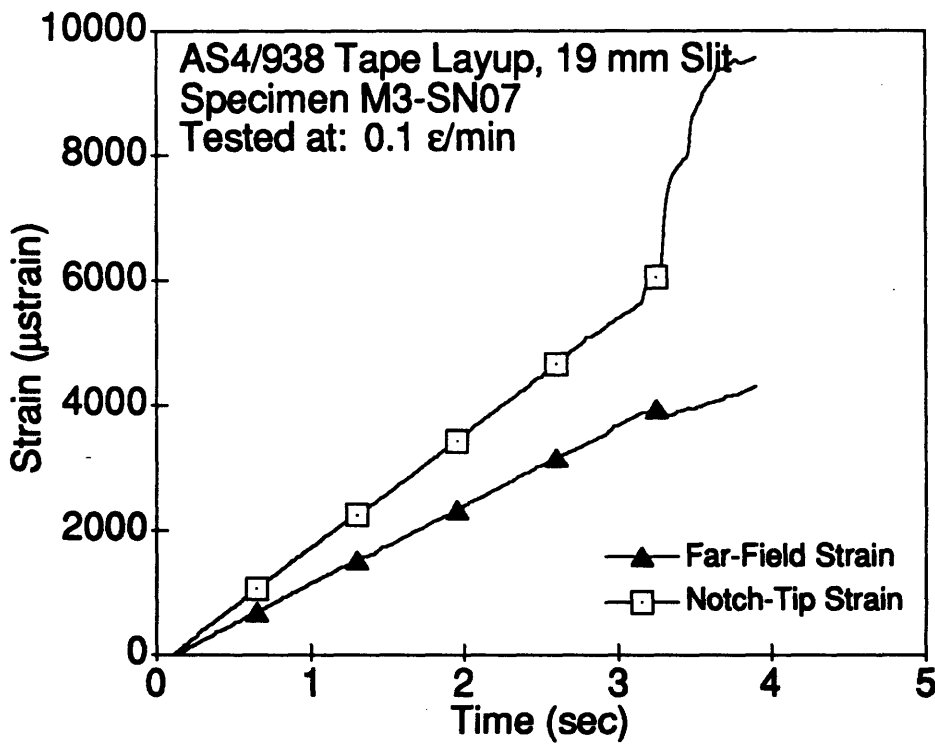
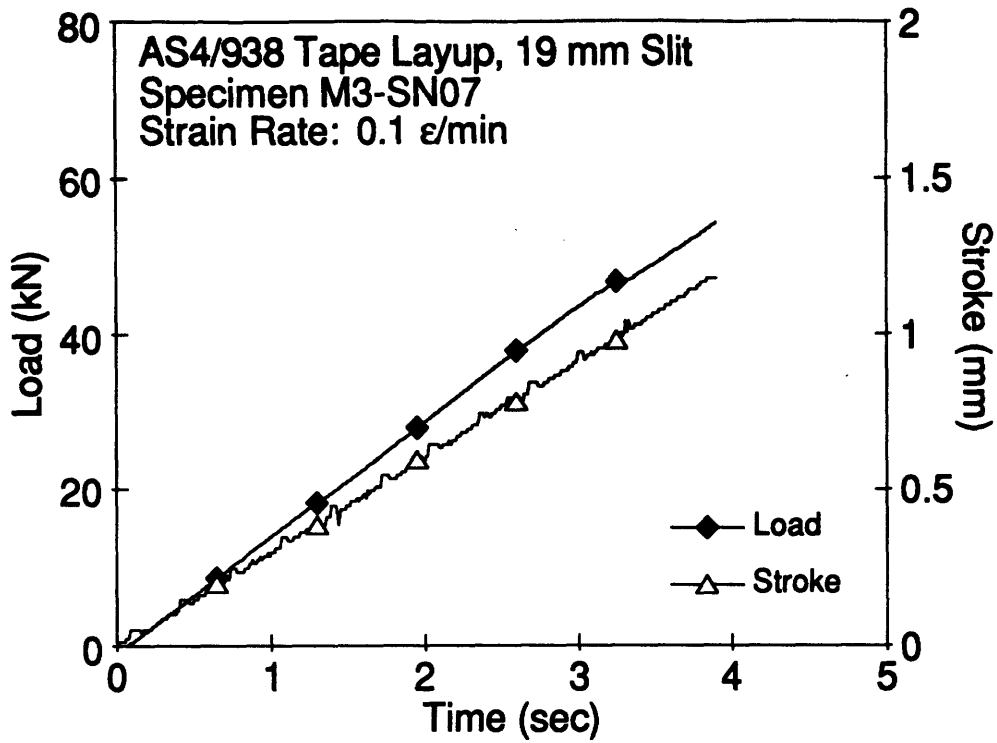


Figure E.37 Plots of Load, Stroke, Far-Field Strain and Notch-Tip Strain versus Time for Specimen M3-SN07.

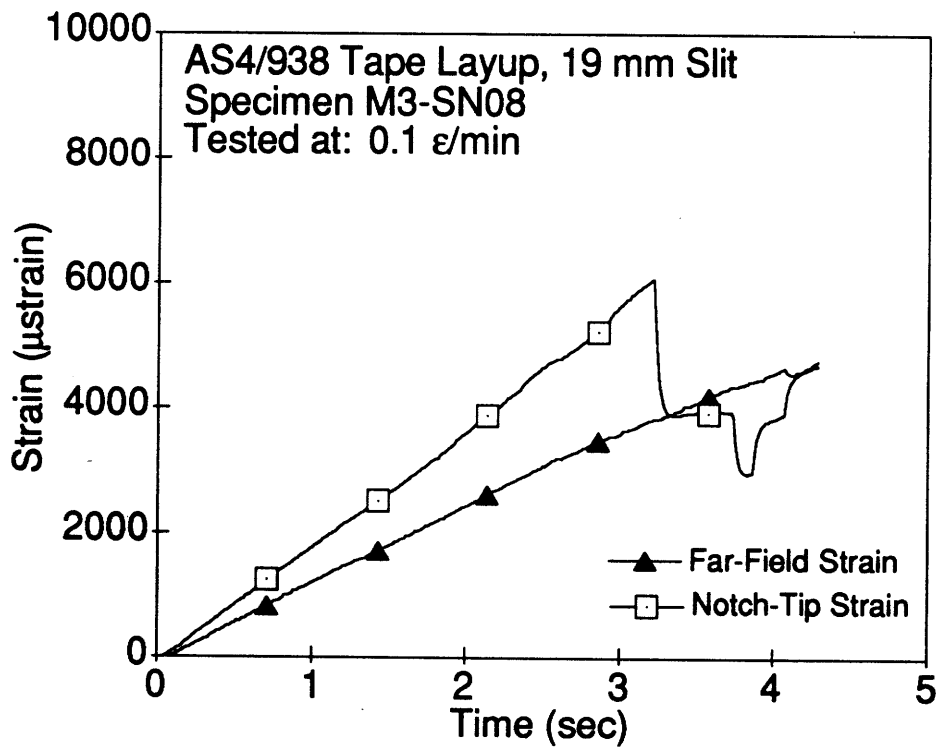
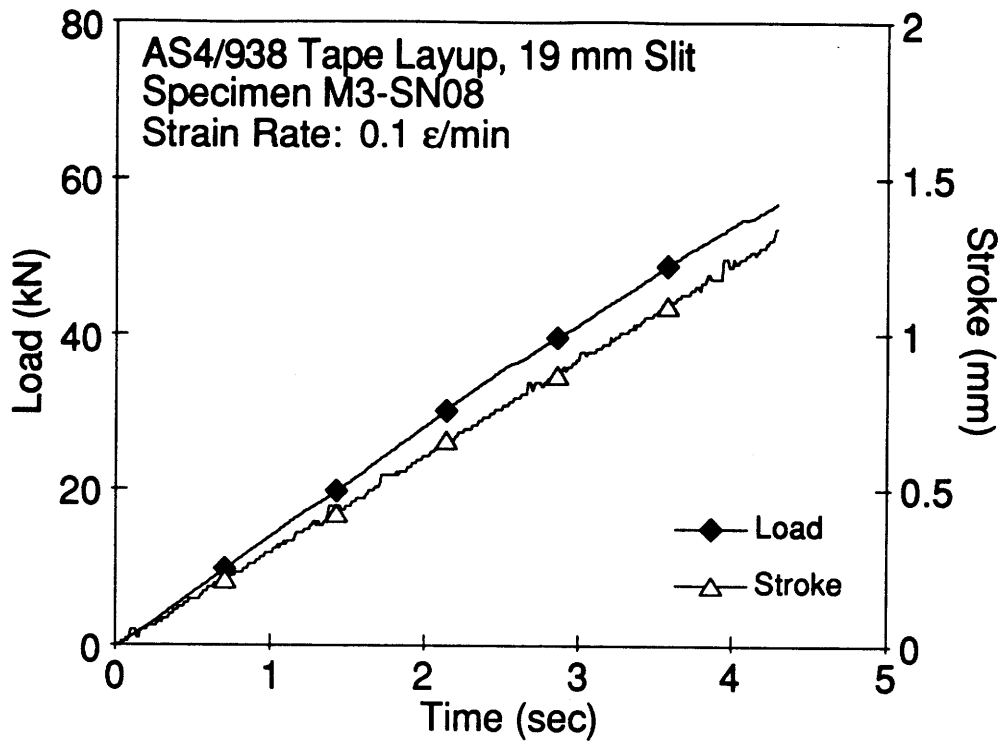


Figure E.38 Plots of Load, Stroke, Far-Field Strain and Notch-Tip Strain versus Time for Specimen M3-SN08.

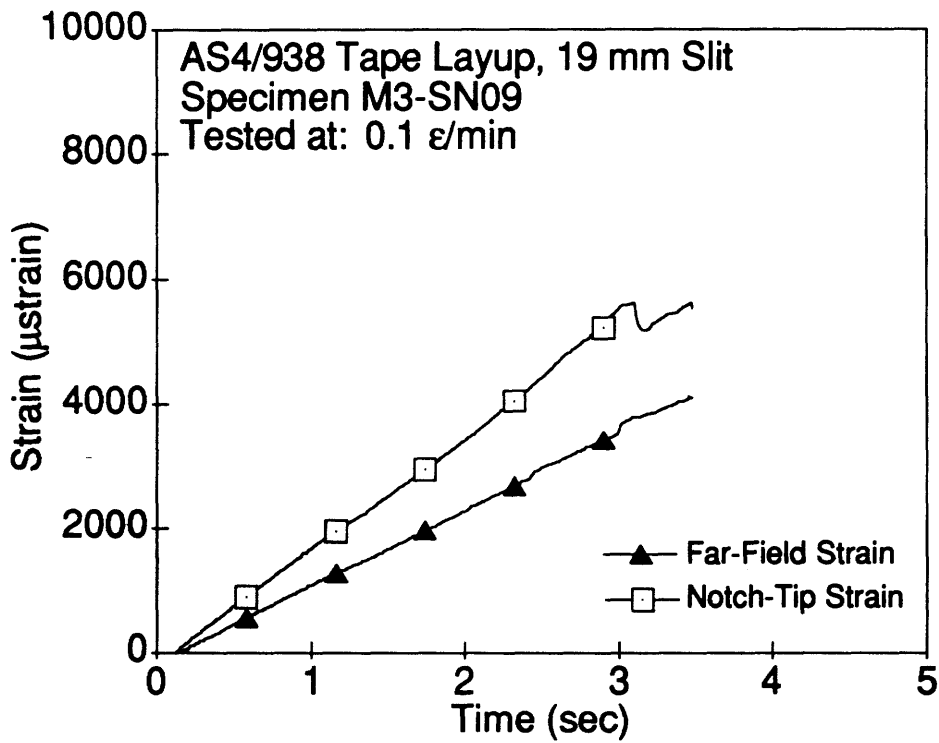
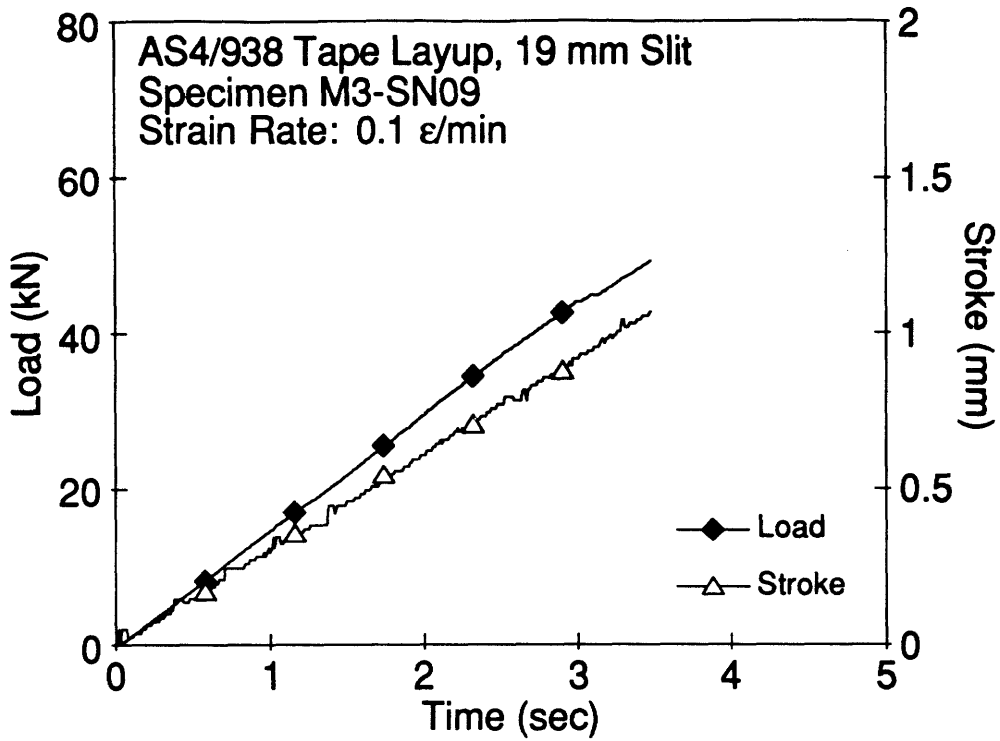


Figure E.39 Plots of Load, Stroke, Far-Field Strain and Notch-Tip Strain versus Time for Specimen M3-SN09.

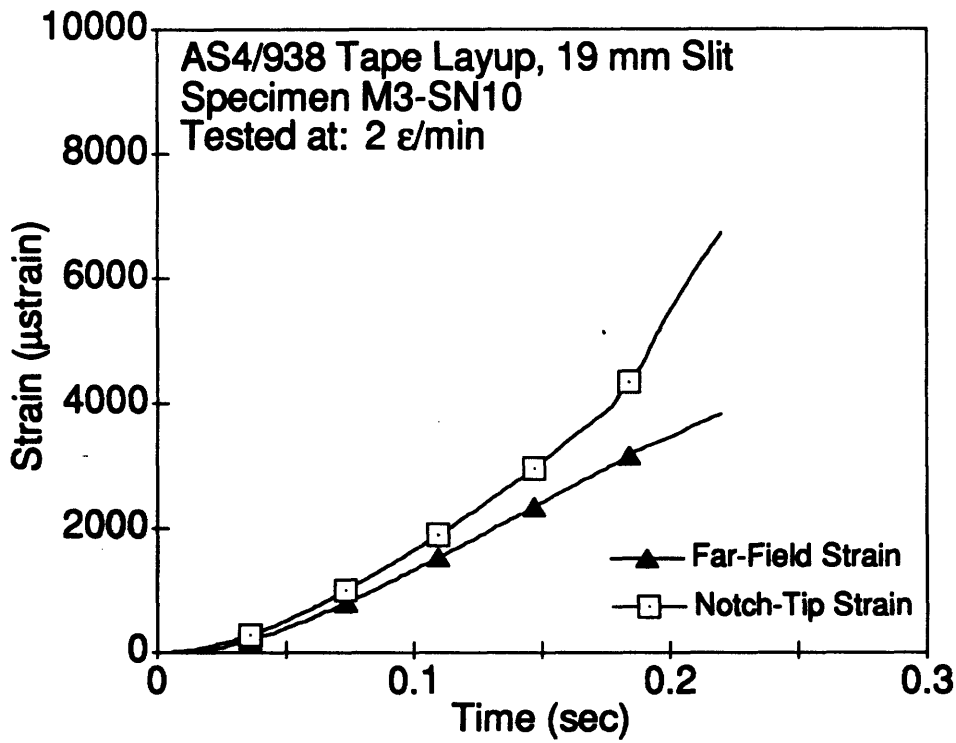
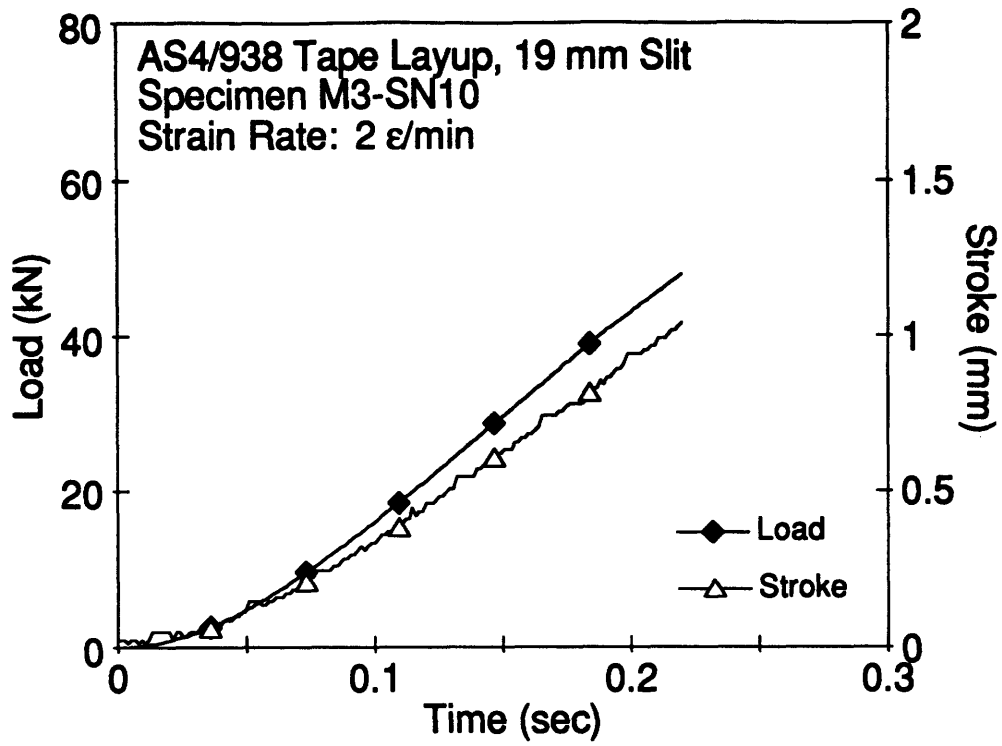


Figure E.40 Plots of Load, Stroke, Far-Field Strain and Notch-Tip Strain versus Time for Specimen M3-SN10.

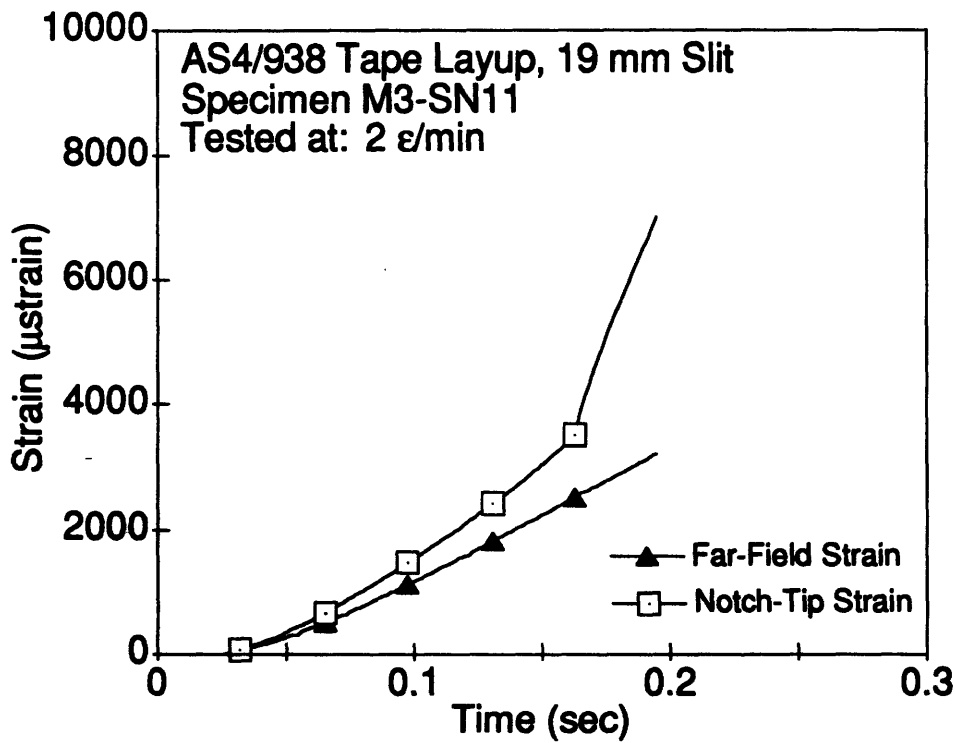
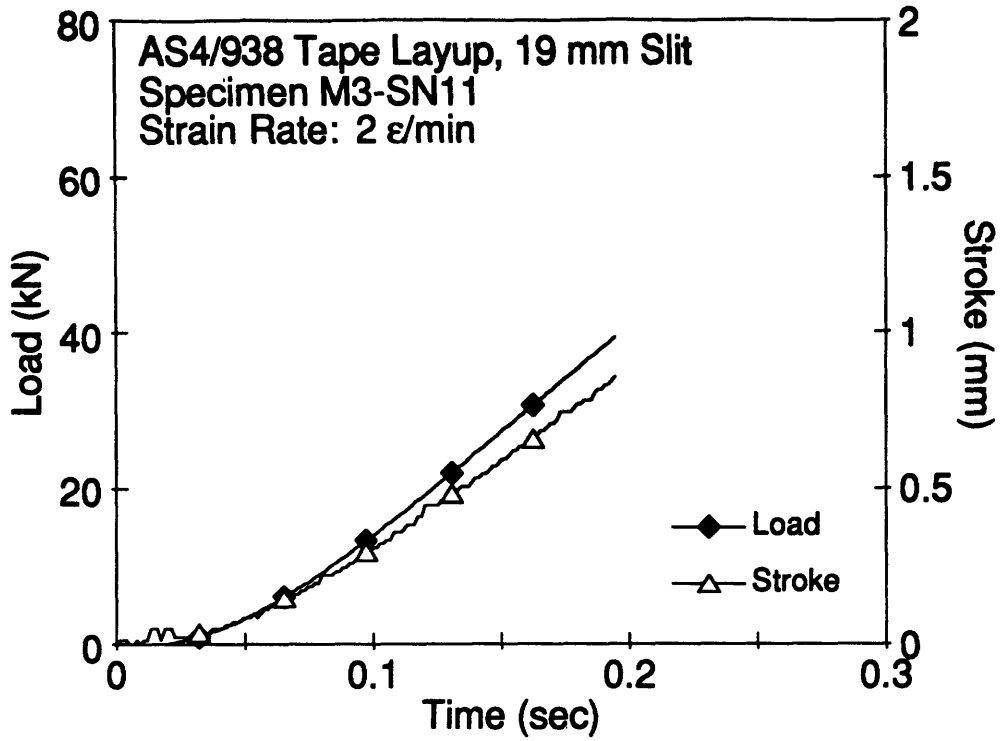


Figure E.41 Plots of Load, Stroke, Far-Field Strain and Notch-Tip Strain versus Time for Specimen M3-SN11.

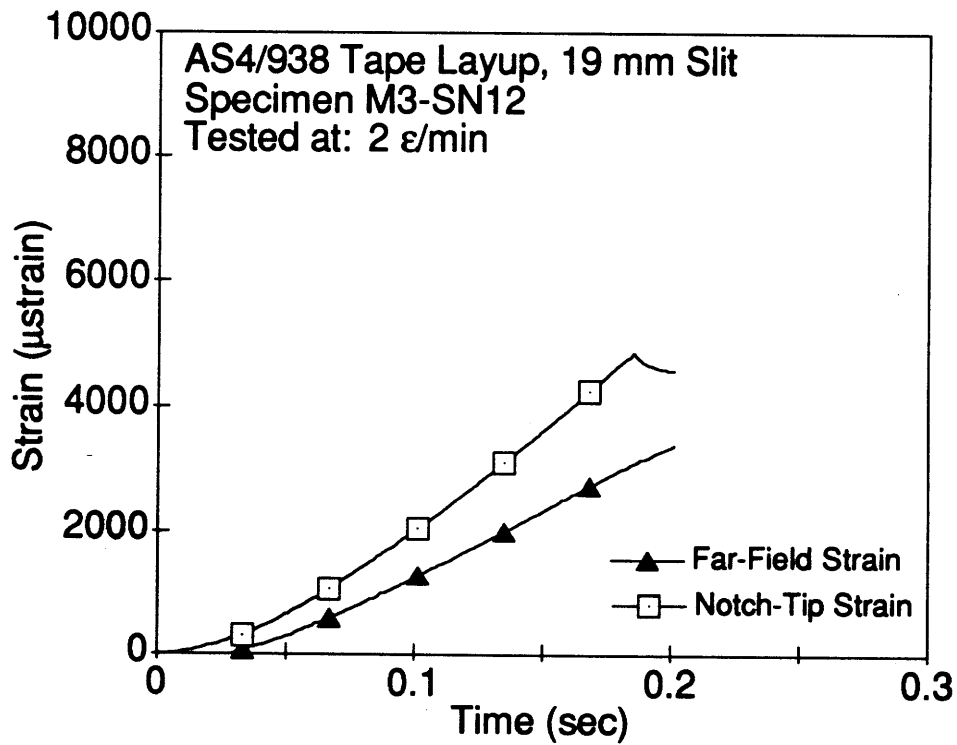
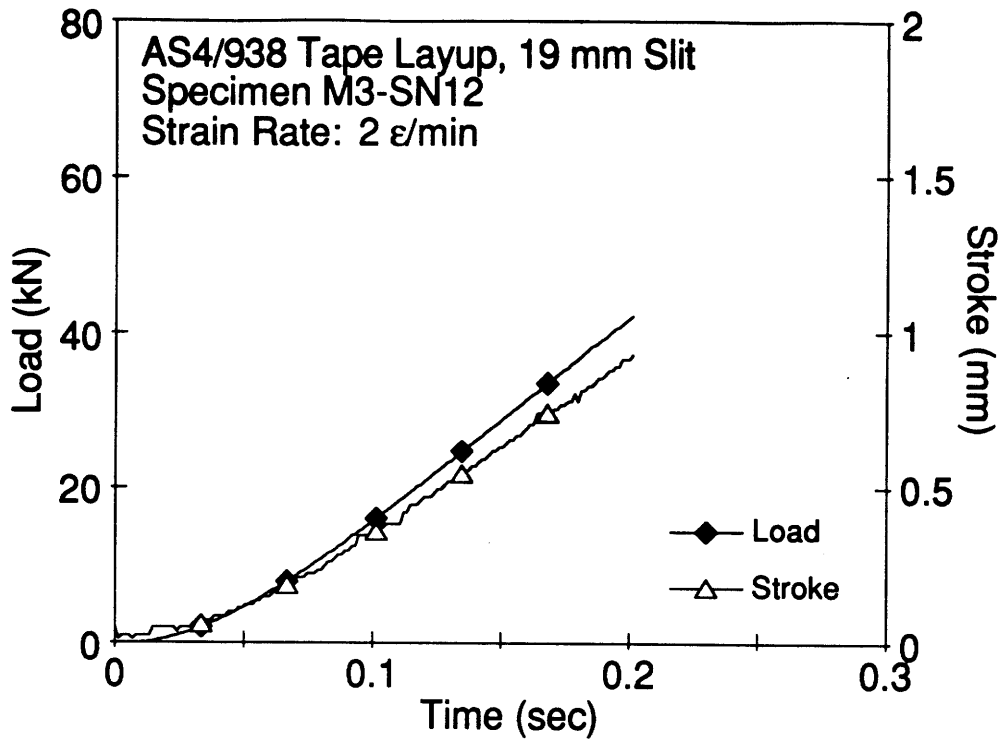


Figure E.42 Plots of Load, Stroke, Far-Field Strain and Notch-Tip Strain versus Time for Specimen M3-SN12.

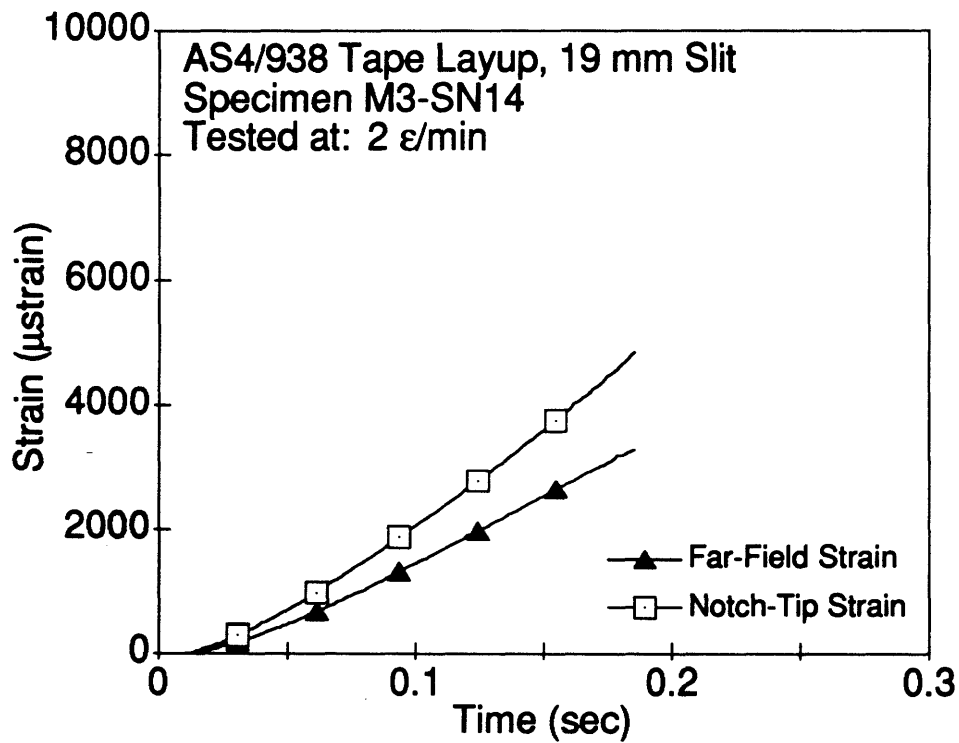
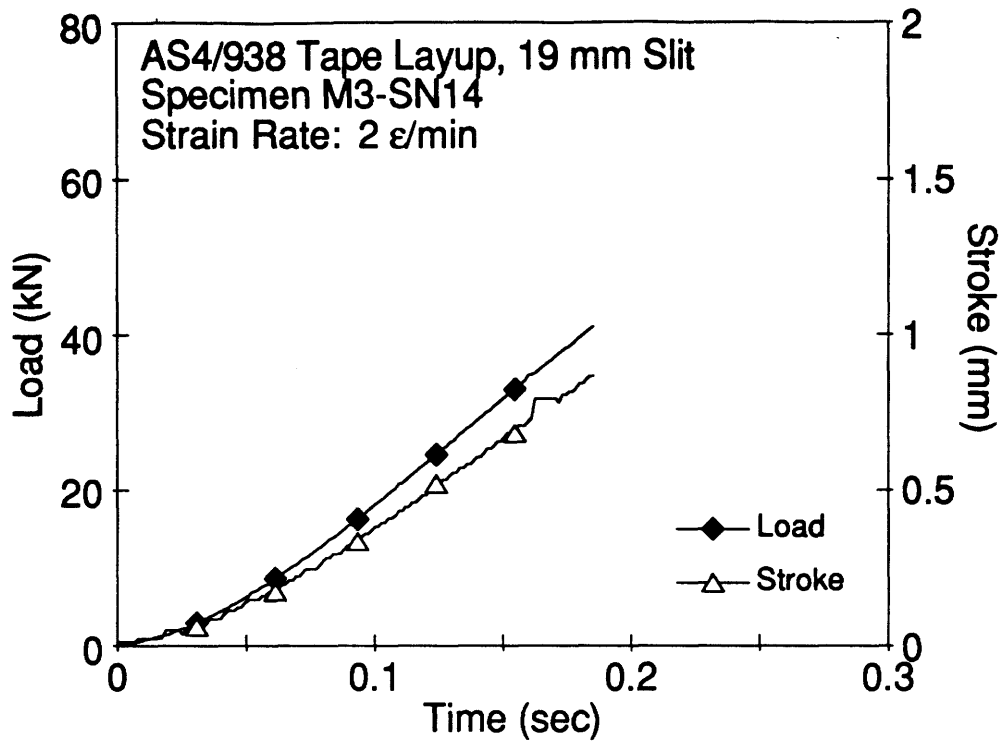


Figure E.43 Plots of Load, Stroke, Far-Field Strain and Notch-Tip Strain versus Time for Specimen M3-SN14.

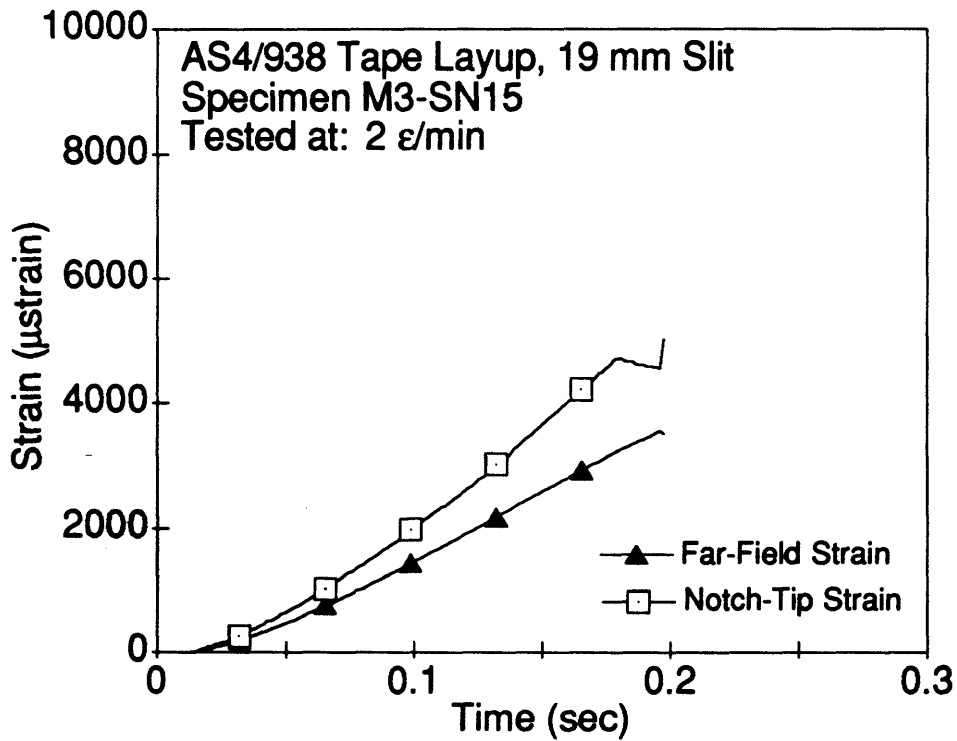
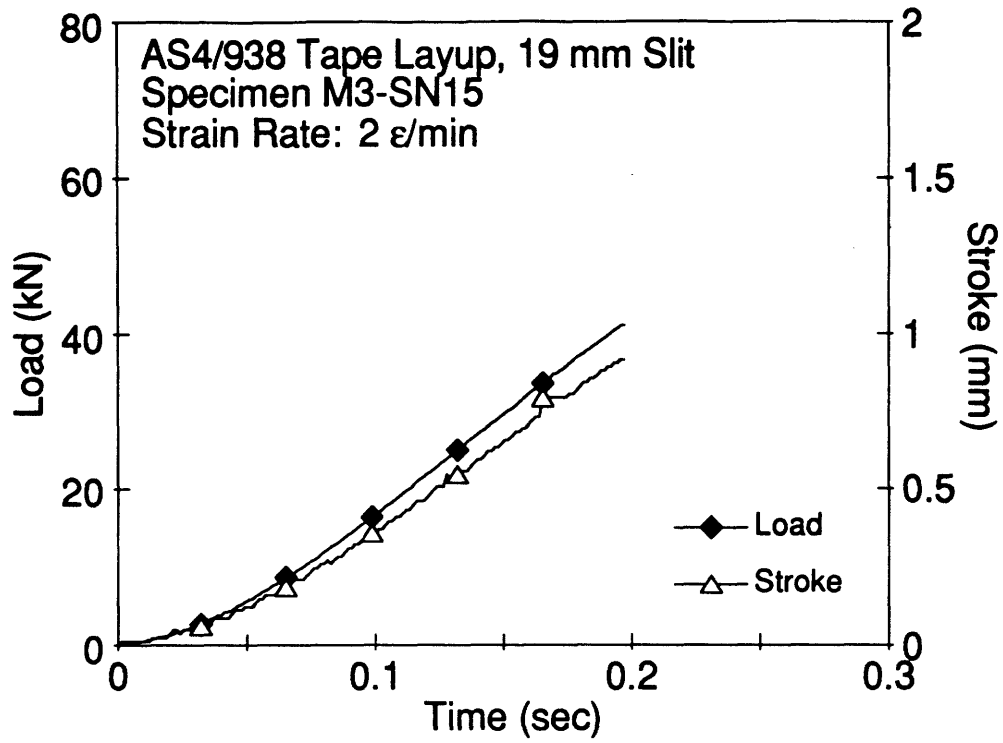


Figure E.44 Plots of Load, Stroke, Far-Field Strain and Notch-Tip Strain versus Time for Specimen M3-SN15.

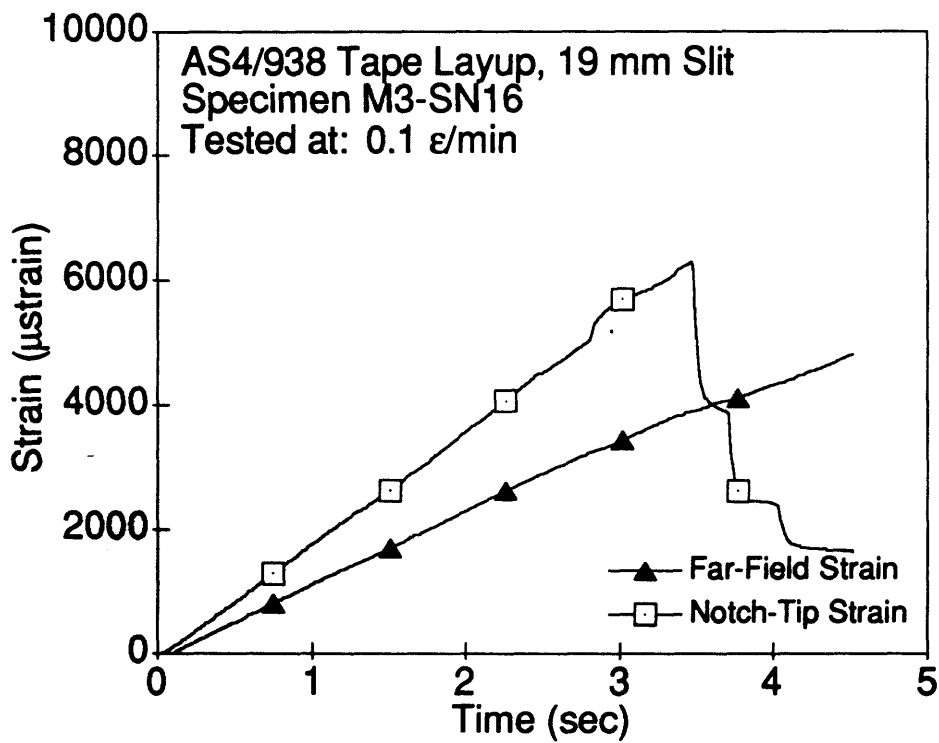
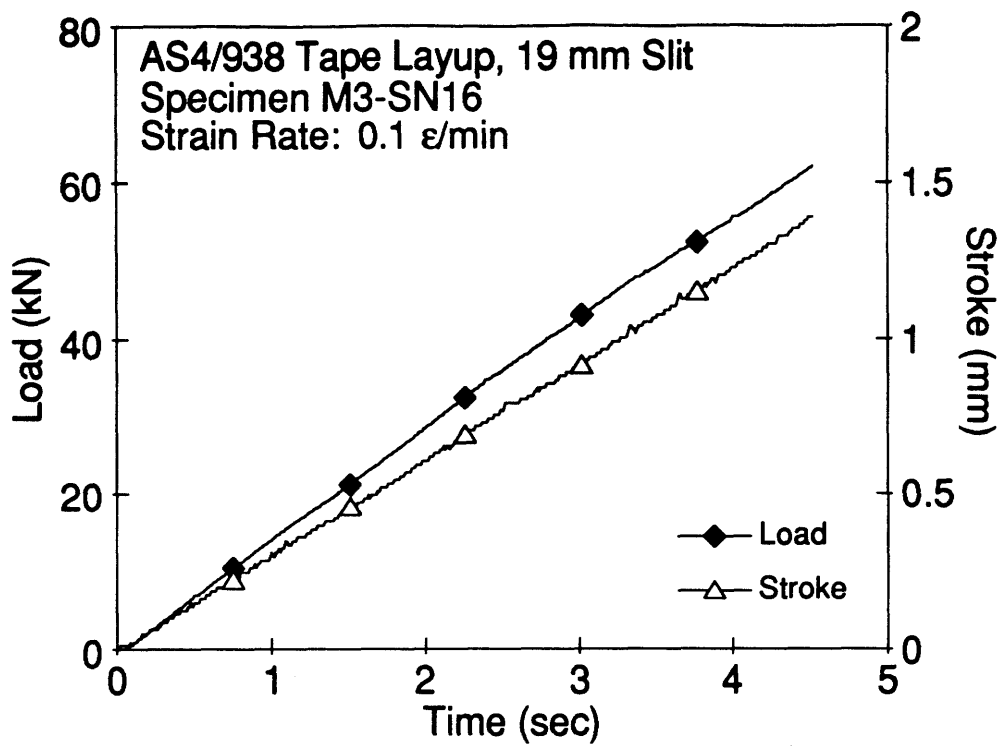


Figure E.45 Plots of Load, Stroke, Far-Field Strain and Notch-Tip Strain versus Time for Specimen M3-SN16.

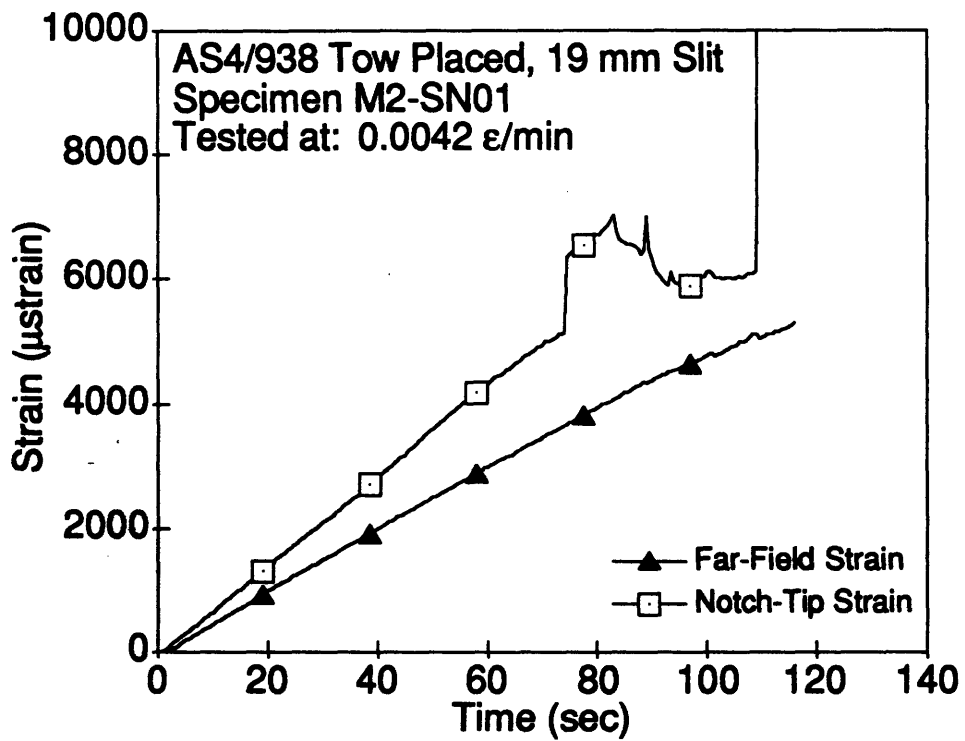
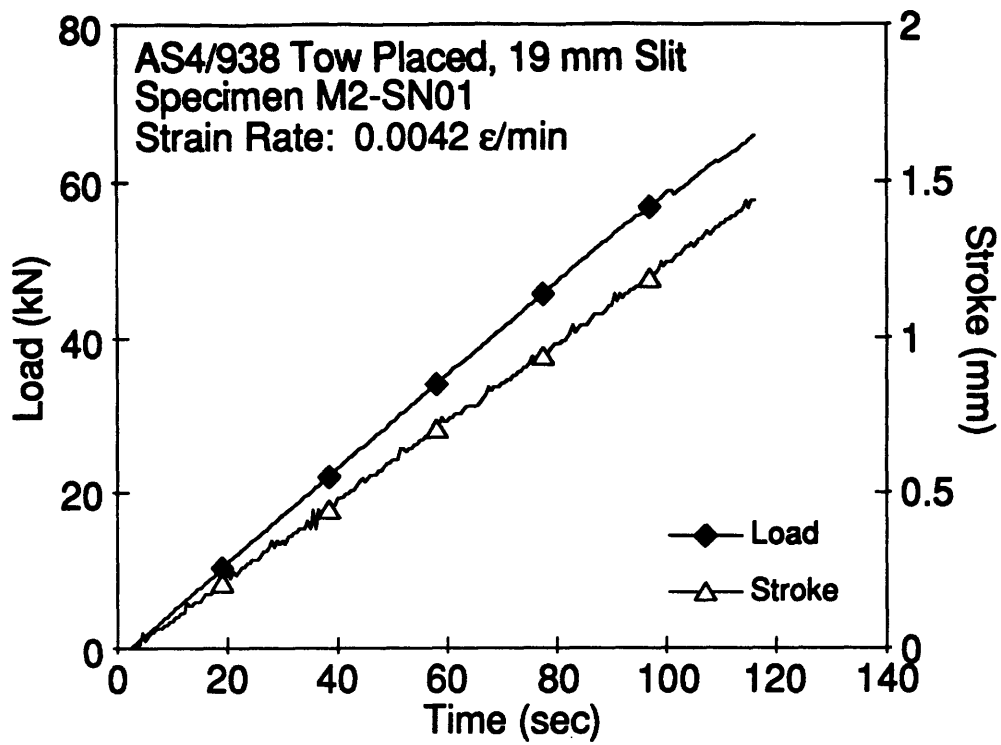


Figure E.46 Plots of Load, Stroke, Far-Field Strain and Notch-Tip Strain versus Time for Specimen M2-SN01.

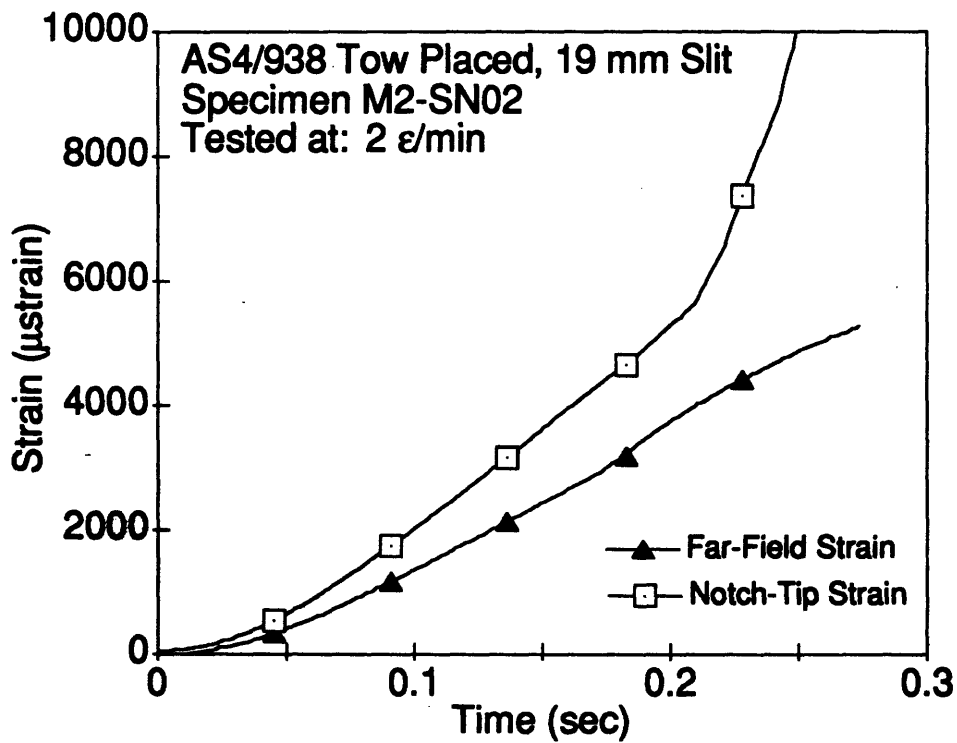
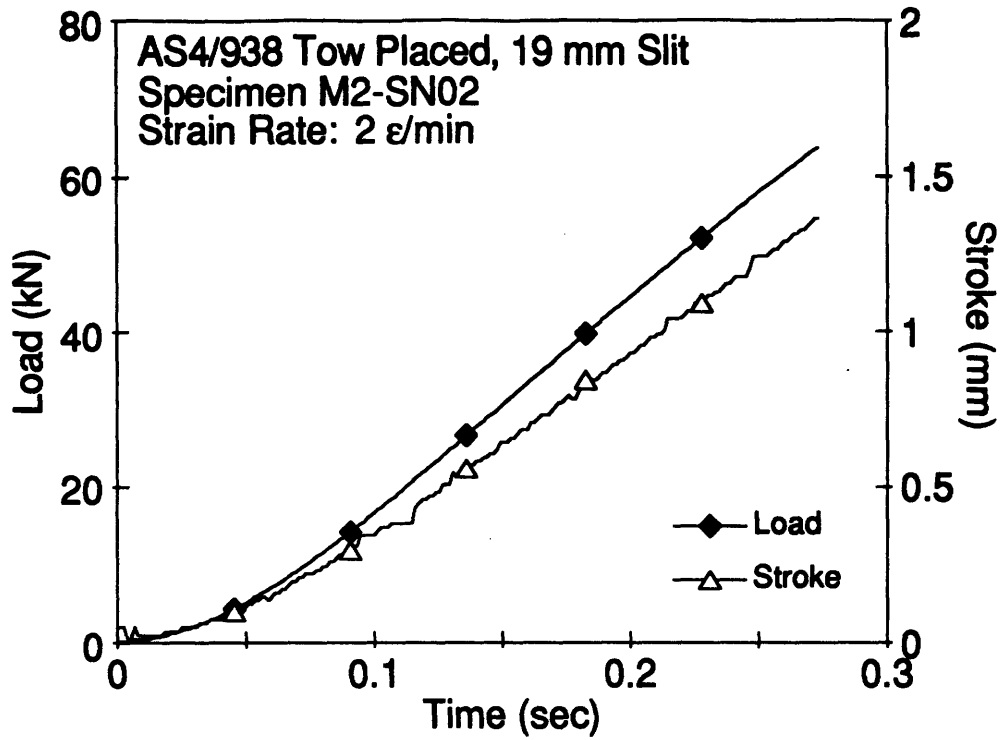


Figure E.47 Plots of Load, Stroke, Far-Field Strain and Notch-Tip Strain versus Time for Specimen M2-SN02.

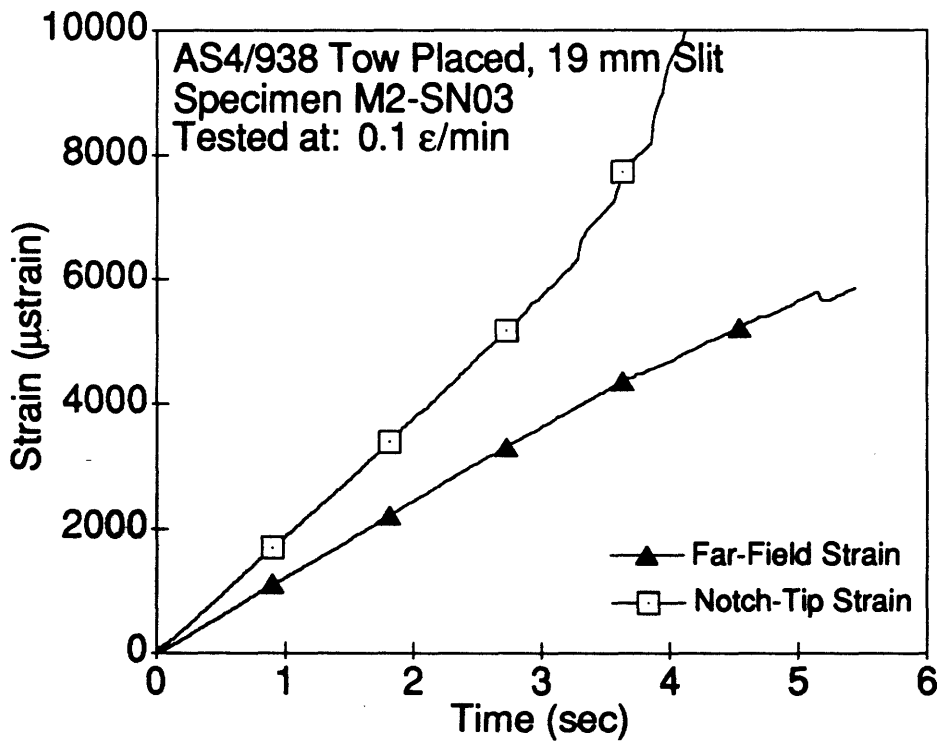
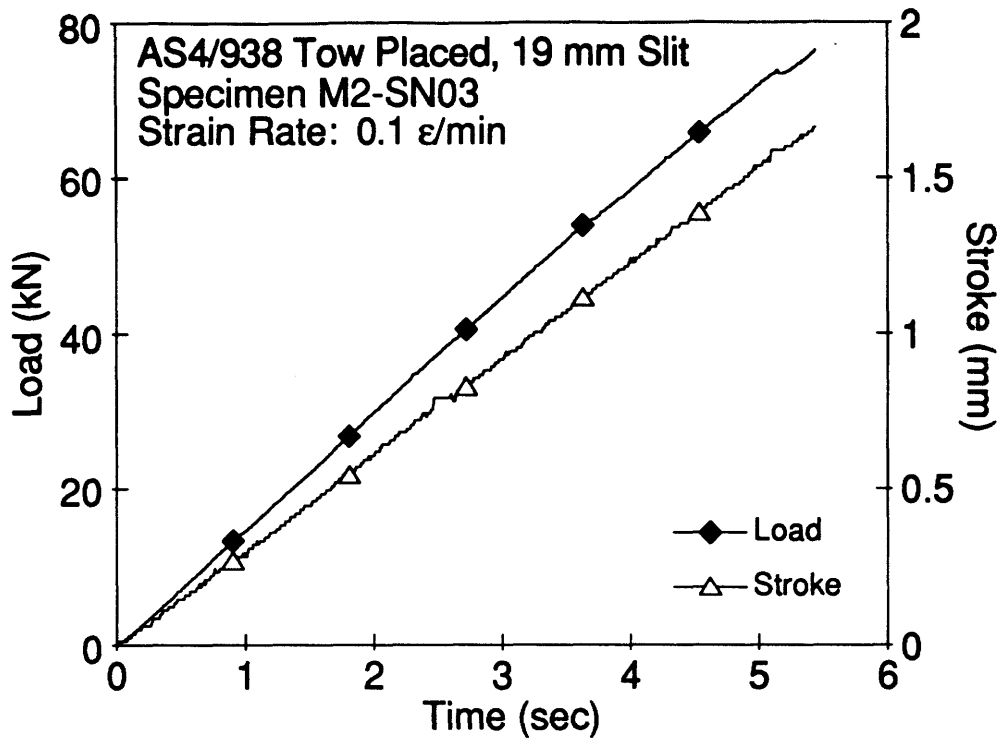


Figure E.48 Plots of Load, Stroke, Far-Field Strain and Notch-Tip Strain versus Time for Specimen M2-SN03.

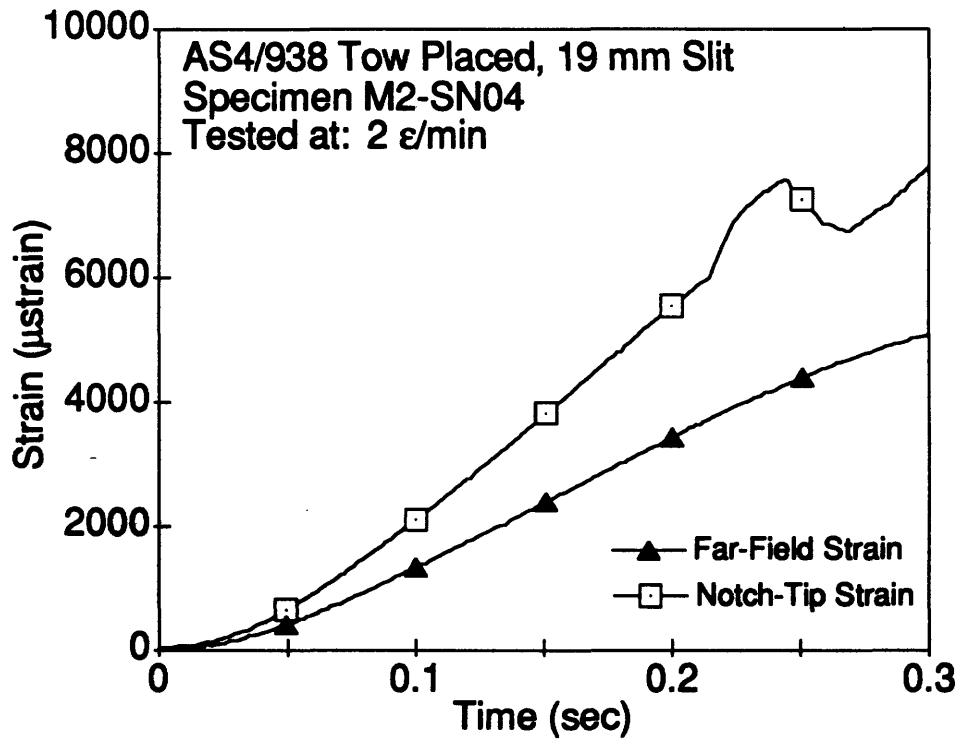
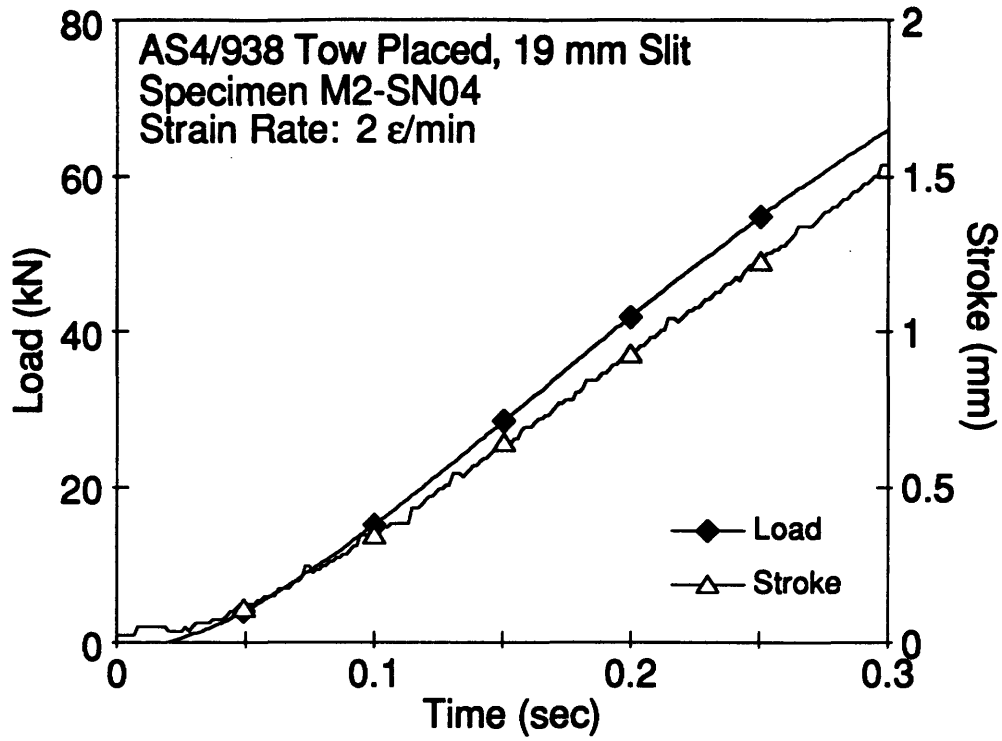


Figure E.49 Plots of Load, Stroke, Far-Field Strain and Notch-Tip Strain versus Time for Specimen M2-SN04.

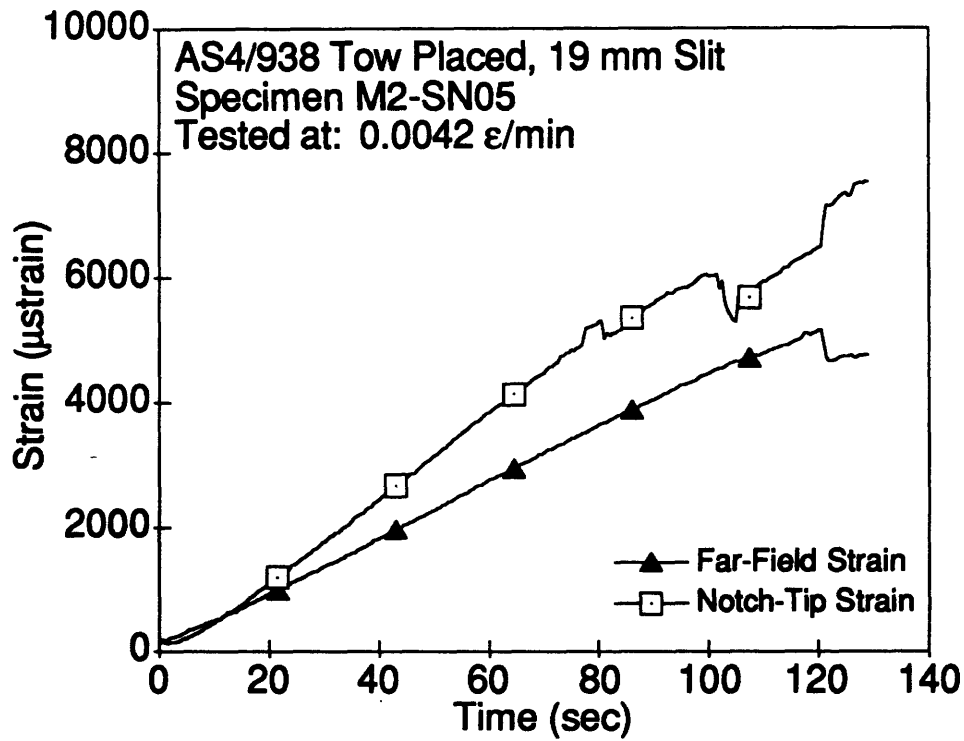
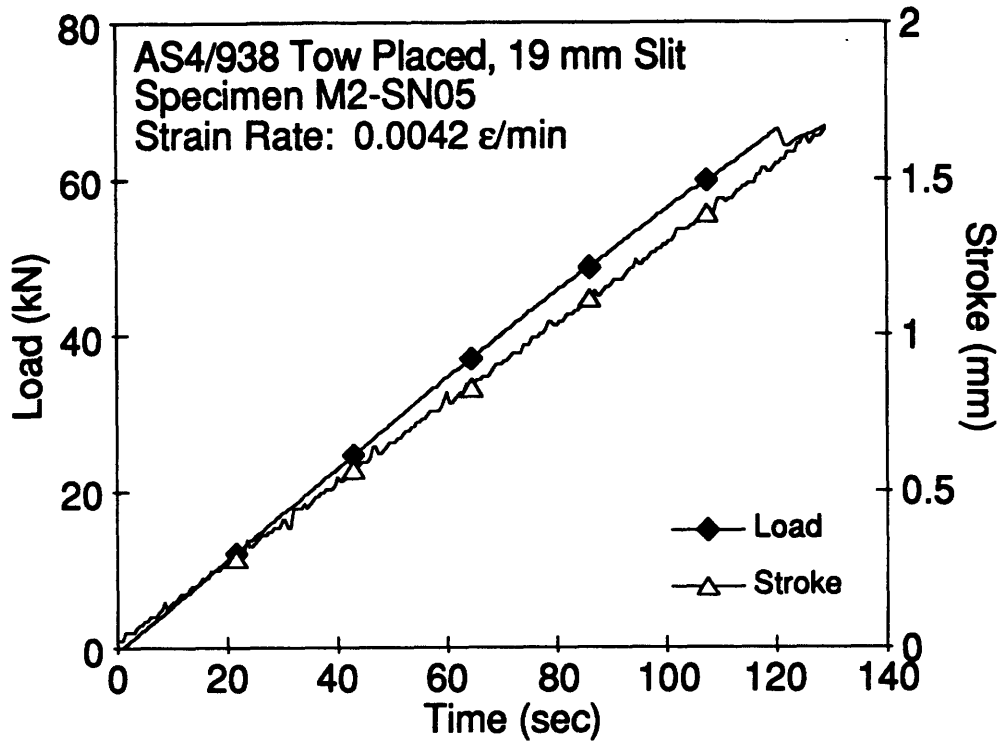


Figure E.50 Plots of Load, Stroke, Far-Field Strain and Notch-Tip Strain versus Time for Specimen M2-SN05.

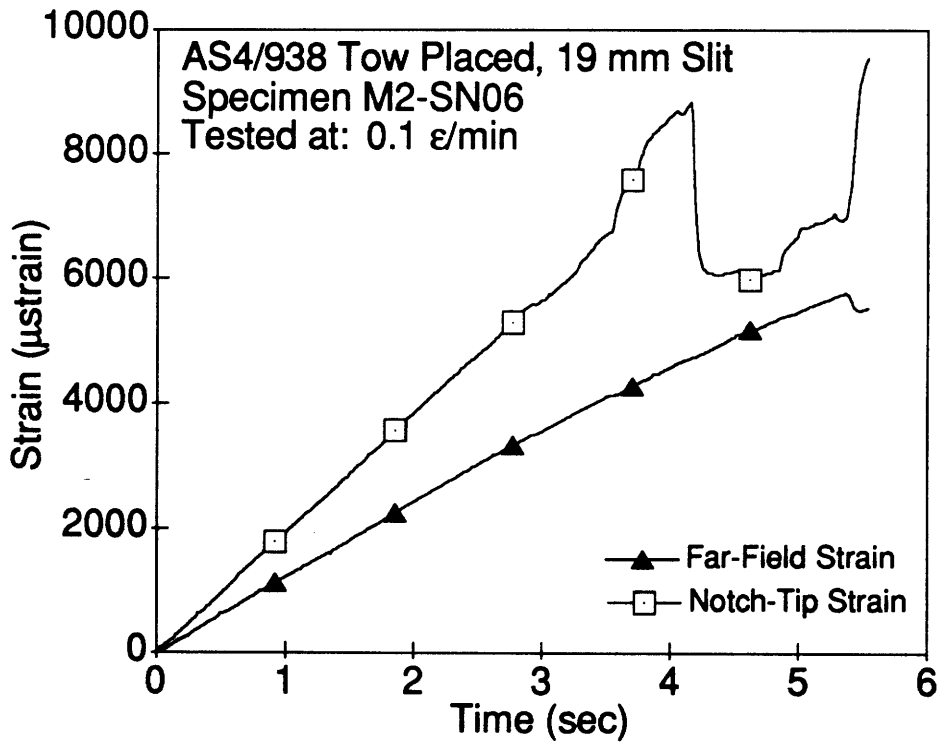
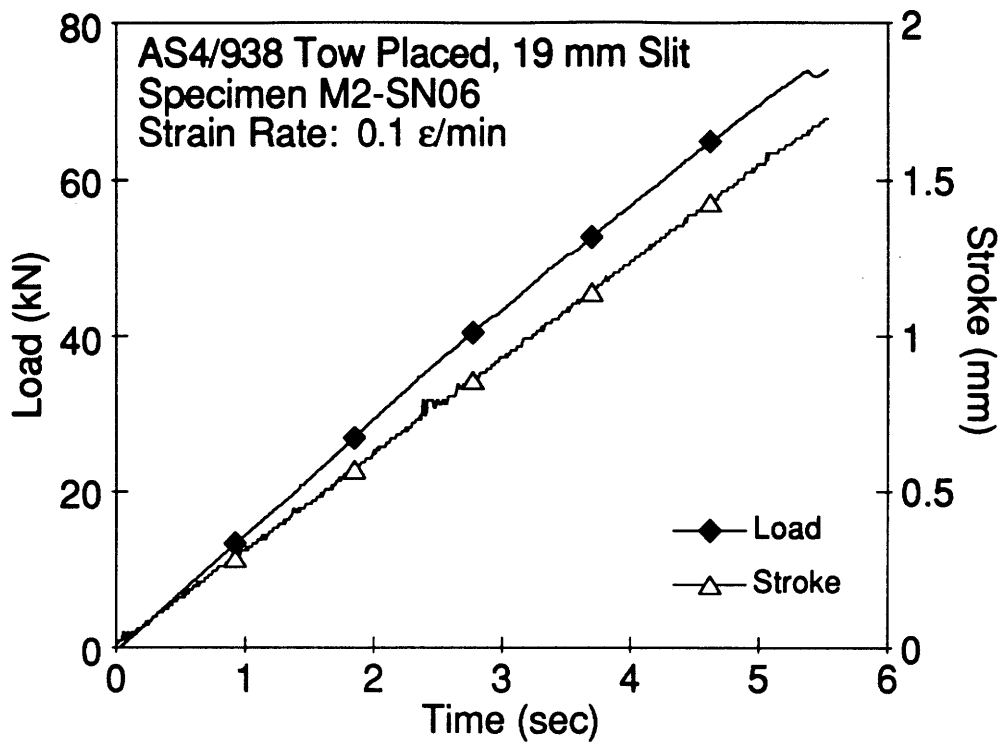


Figure E.51 Plots of Load, Stroke, Far-Field Strain and Notch-Tip Strain versus Time for Specimen M2-SN06.

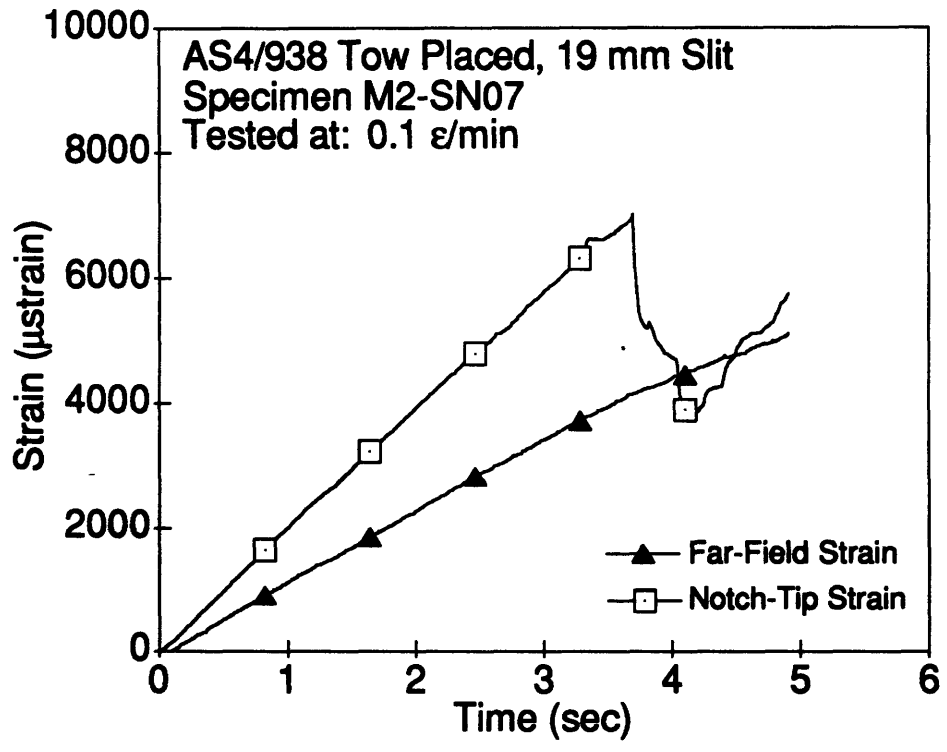
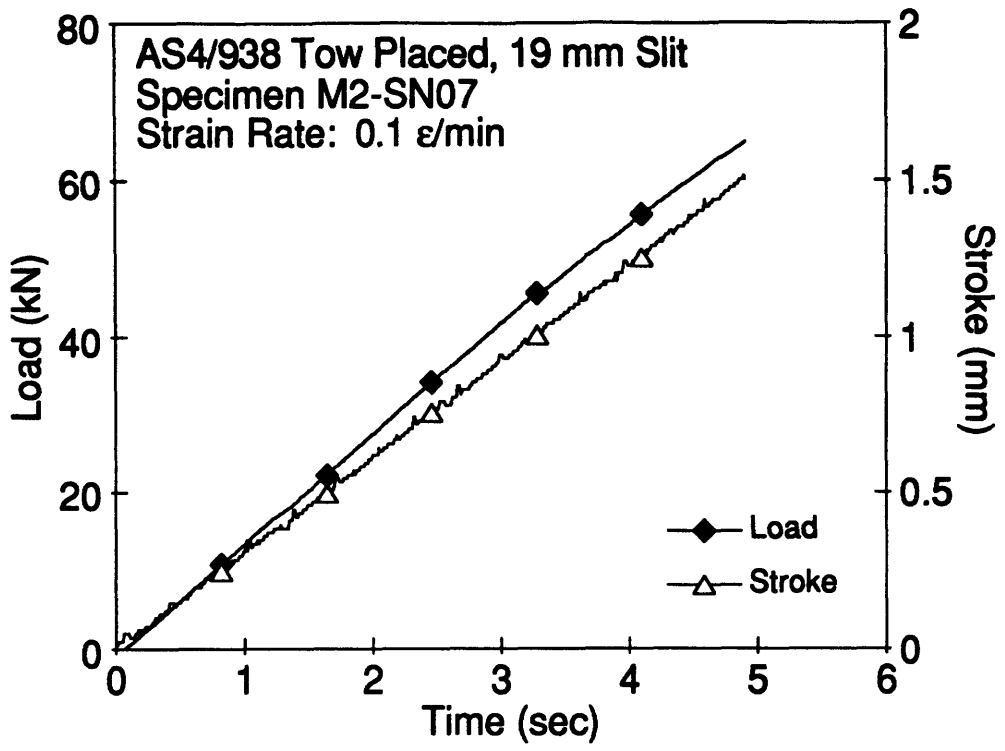


Figure E.52 Plots of Load, Stroke, Far-Field Strain and Notch-Tip Strain versus Time for Specimen M2-SN07.

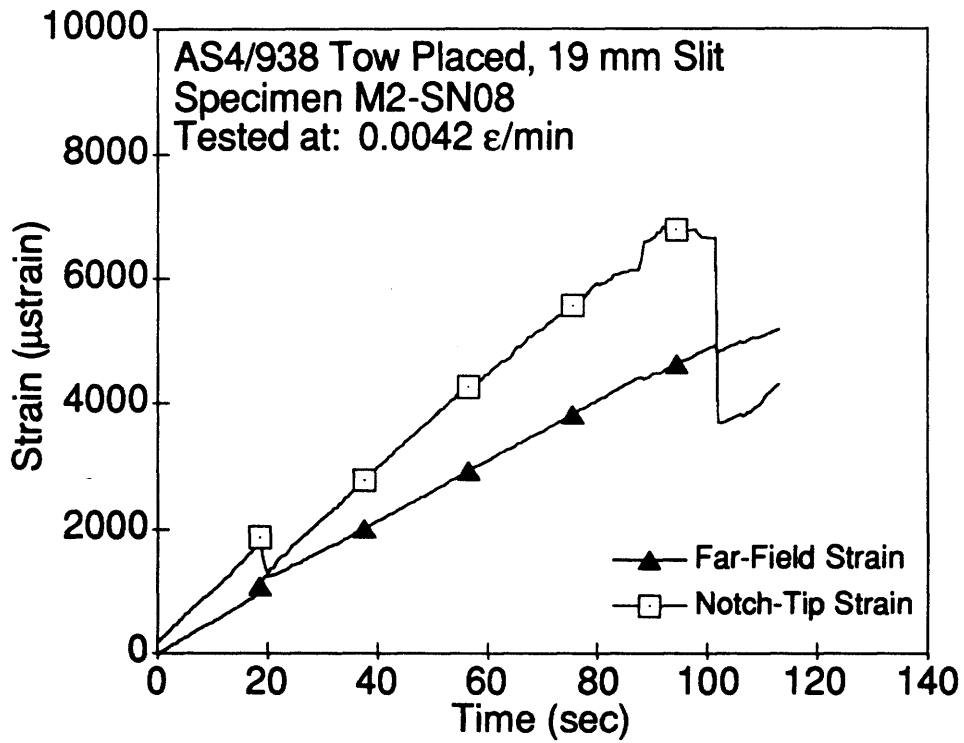
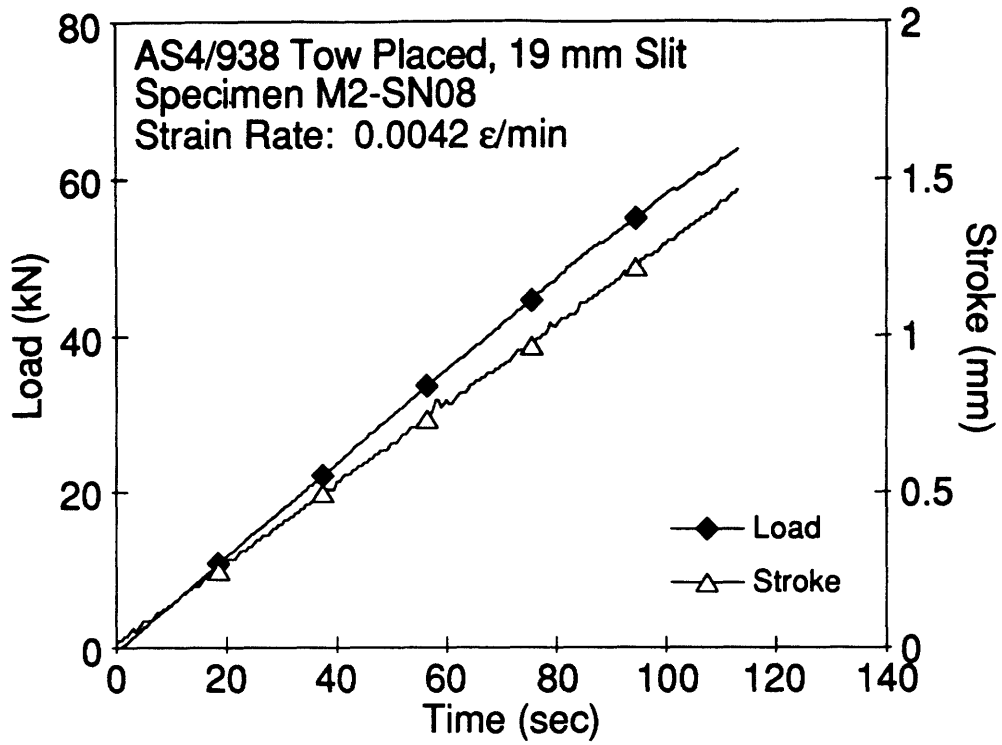


Figure E.53 Plots of Load, Stroke, Far-Field Strain and Notch-Tip Strain versus Time for Specimen M2-SN08.

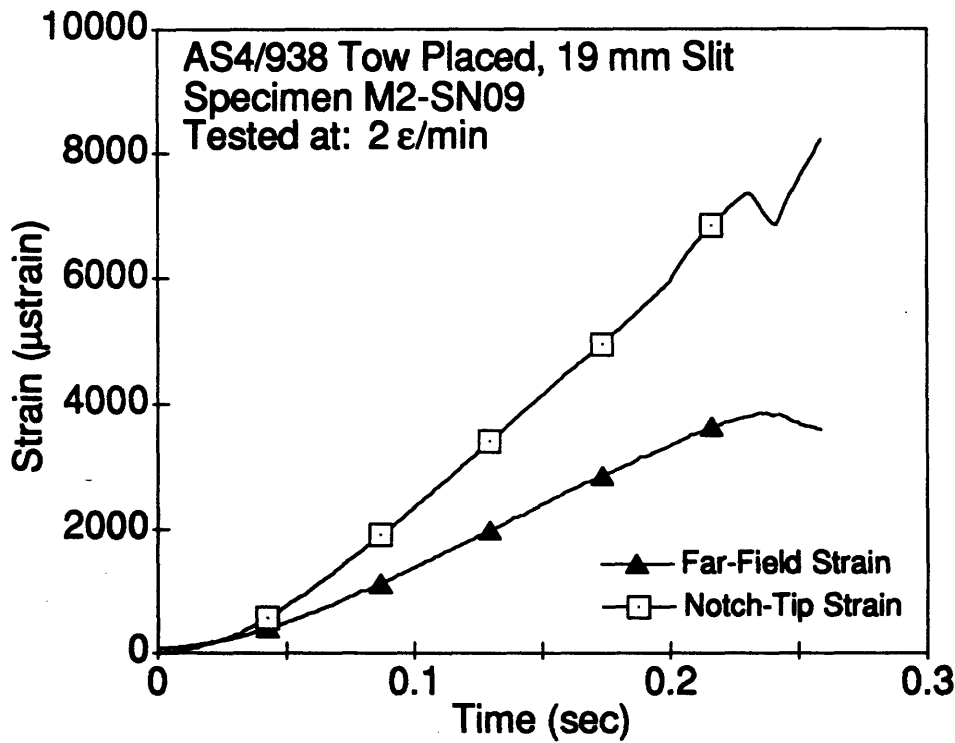
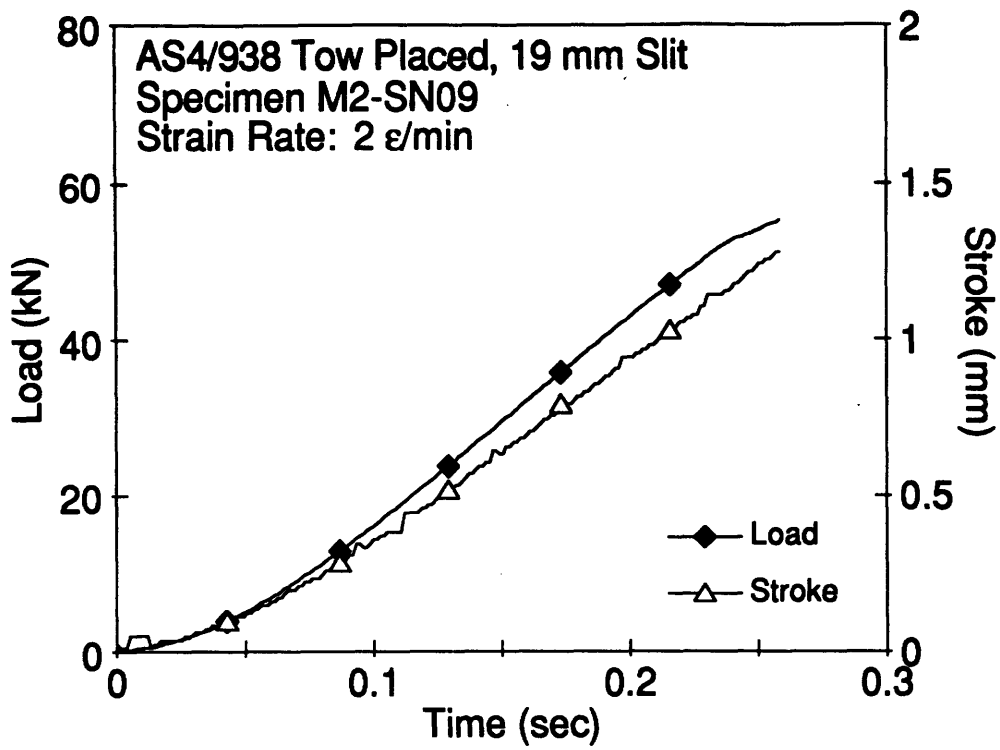


Figure E.54 Plots of Load, Stroke, Far-Field Strain and Notch-Tip Strain versus Time for Specimen M2-SN09.

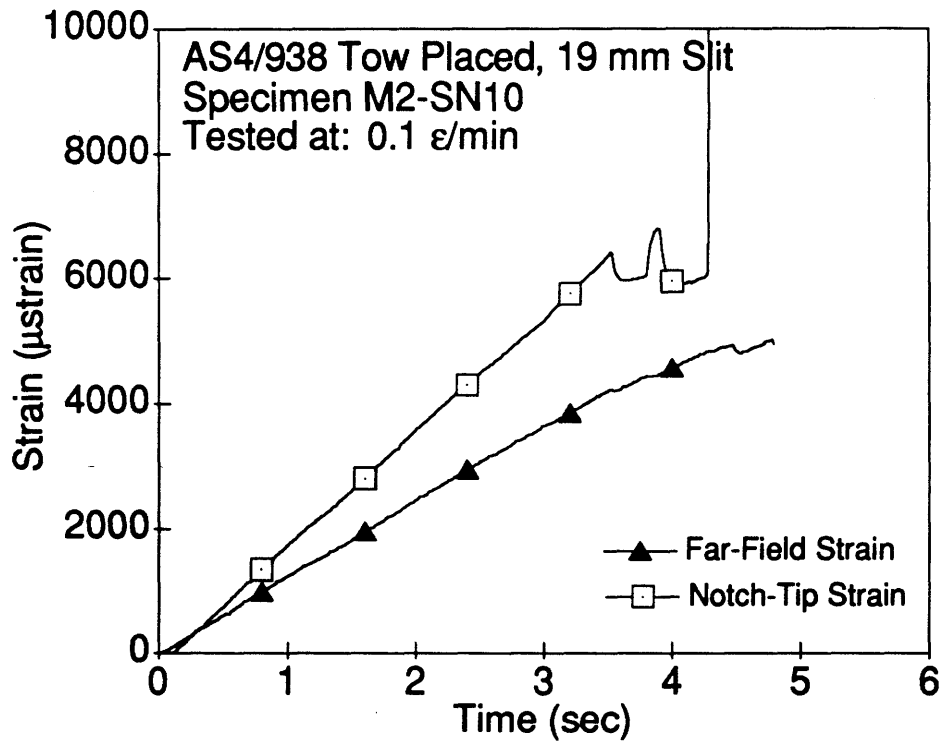
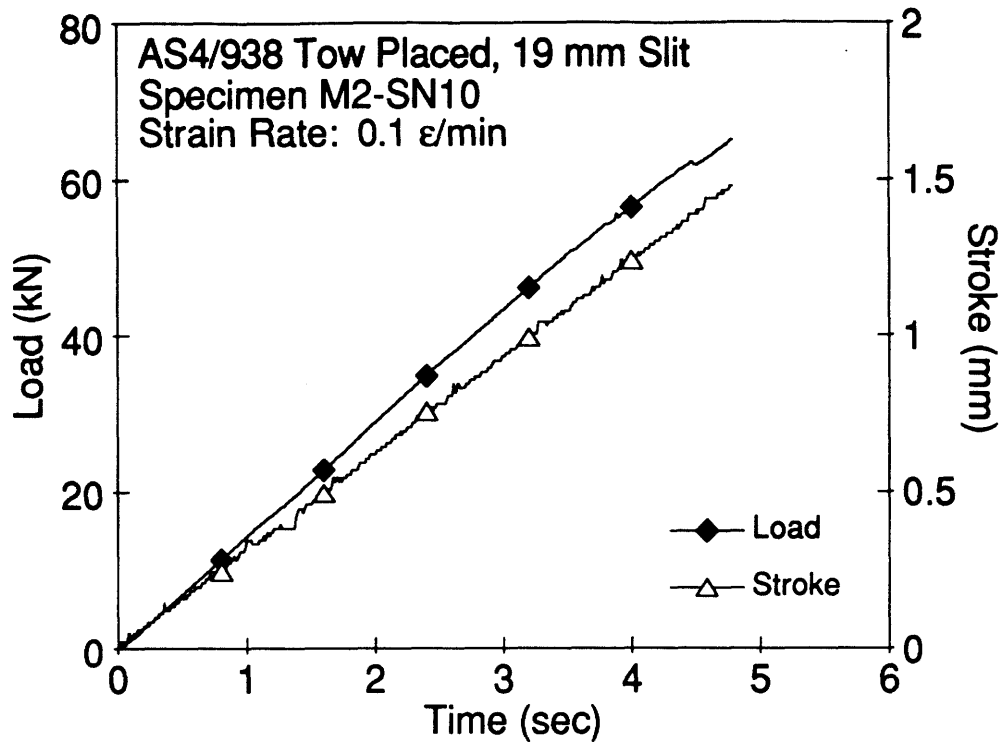


Figure E.55 Plots of Load, Stroke, Far-Field Strain and Notch-Tip Strain versus Time for Specimen M2-SN10.

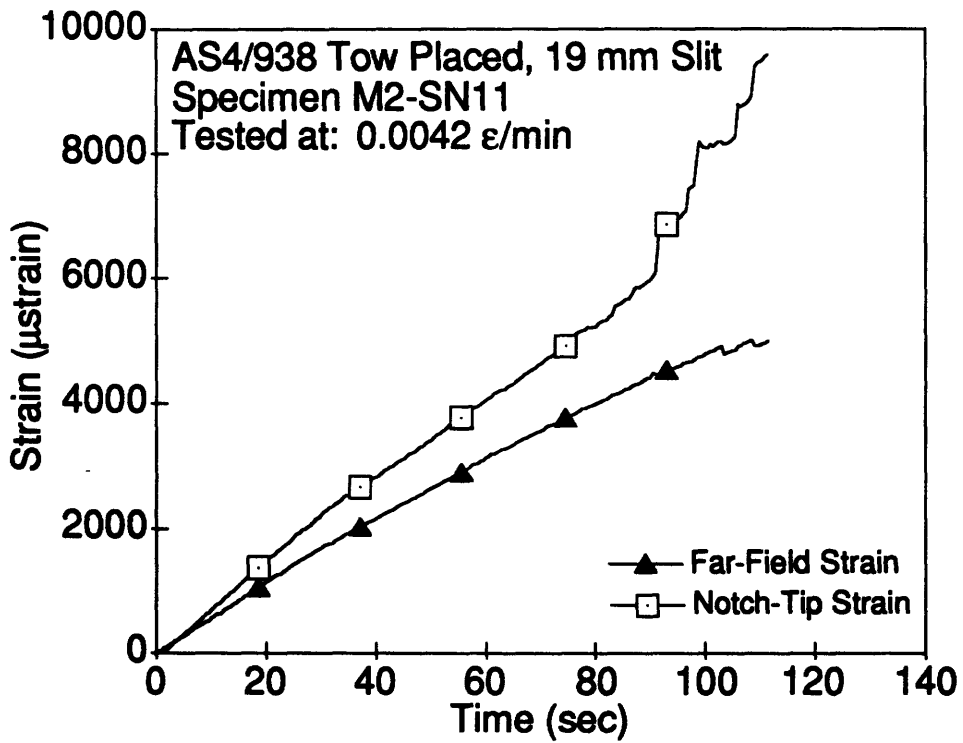
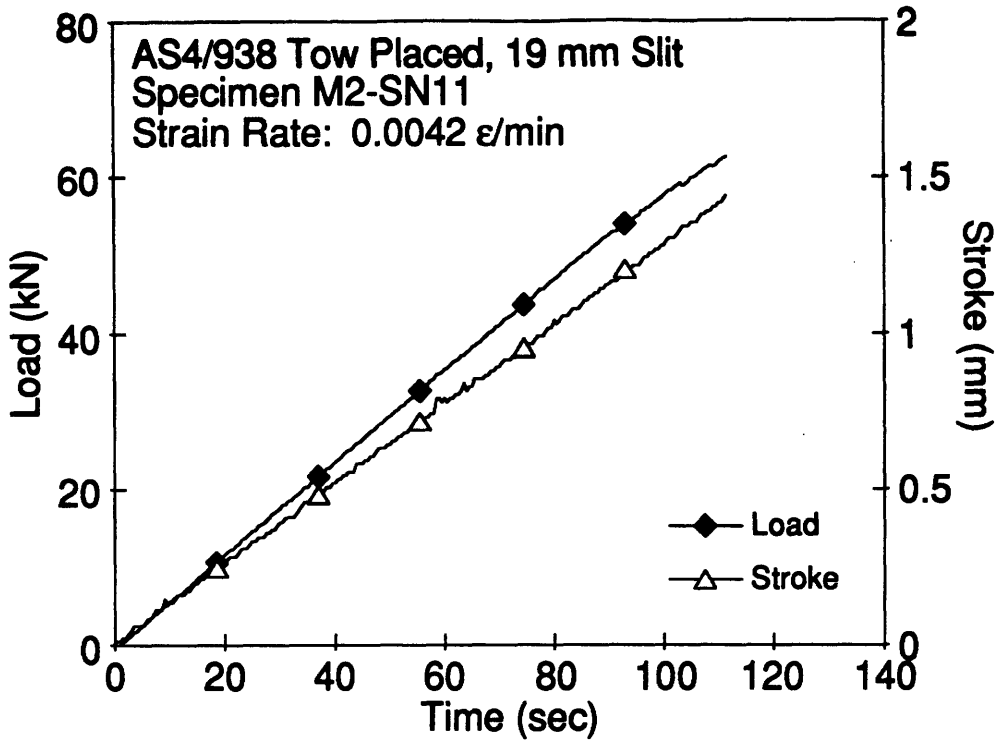


Figure E.56 Plots of Load, Stroke, Far-Field Strain and Notch-Tip Strain versus Time for Specimen M2-SN11.

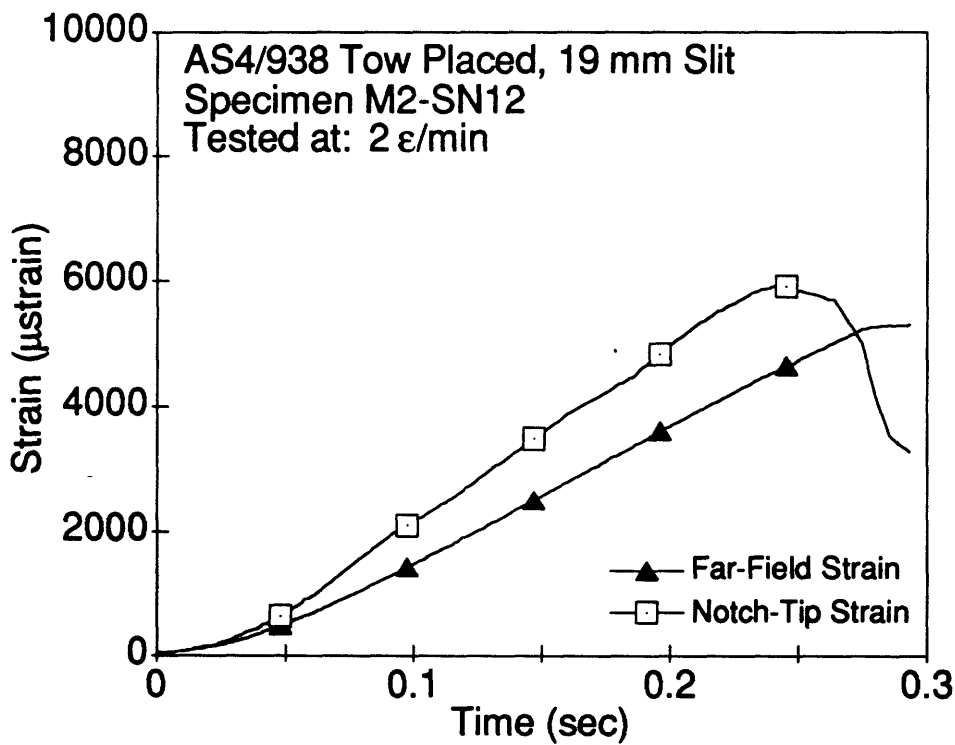
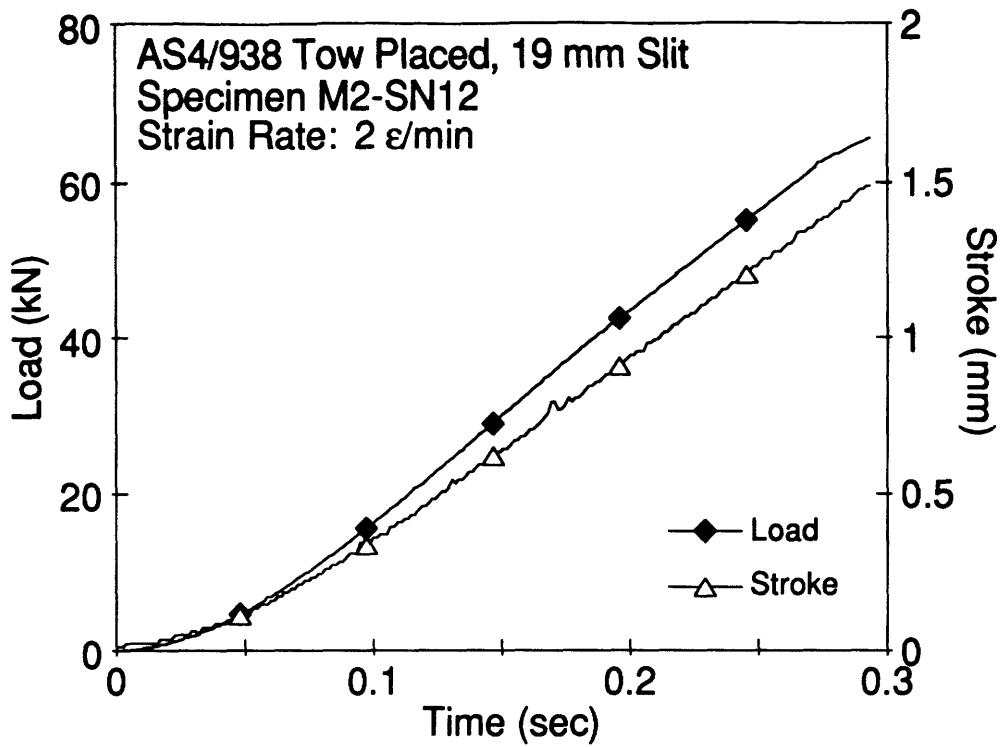


Figure E.57 Plots of Load, Stroke, Far-Field Strain and Notch-Tip Strain versus Time for Specimen M2-SN12.

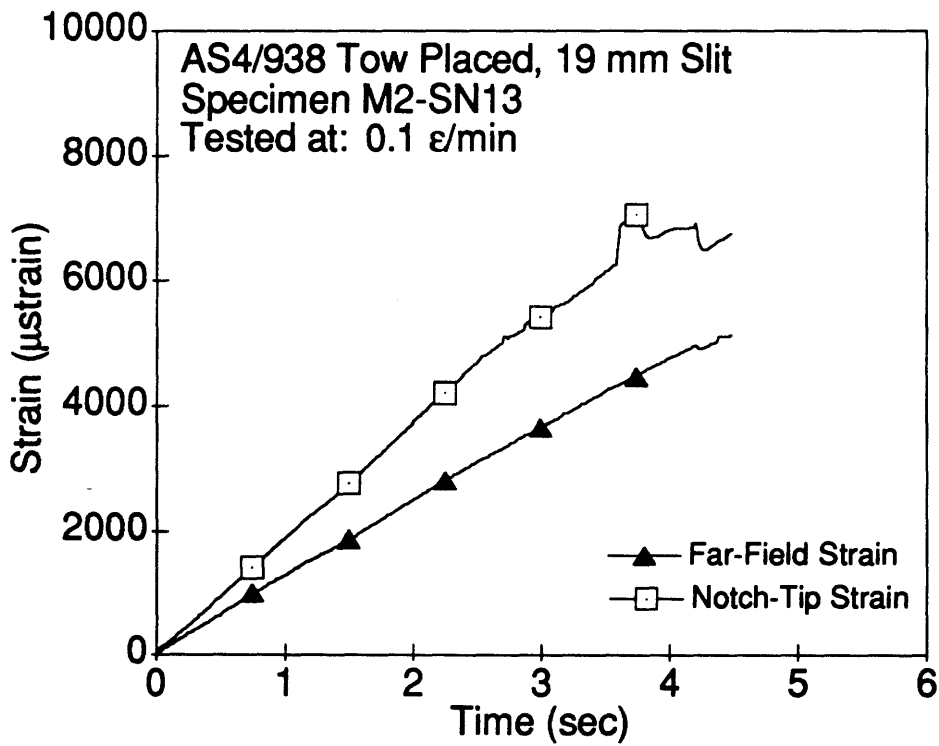
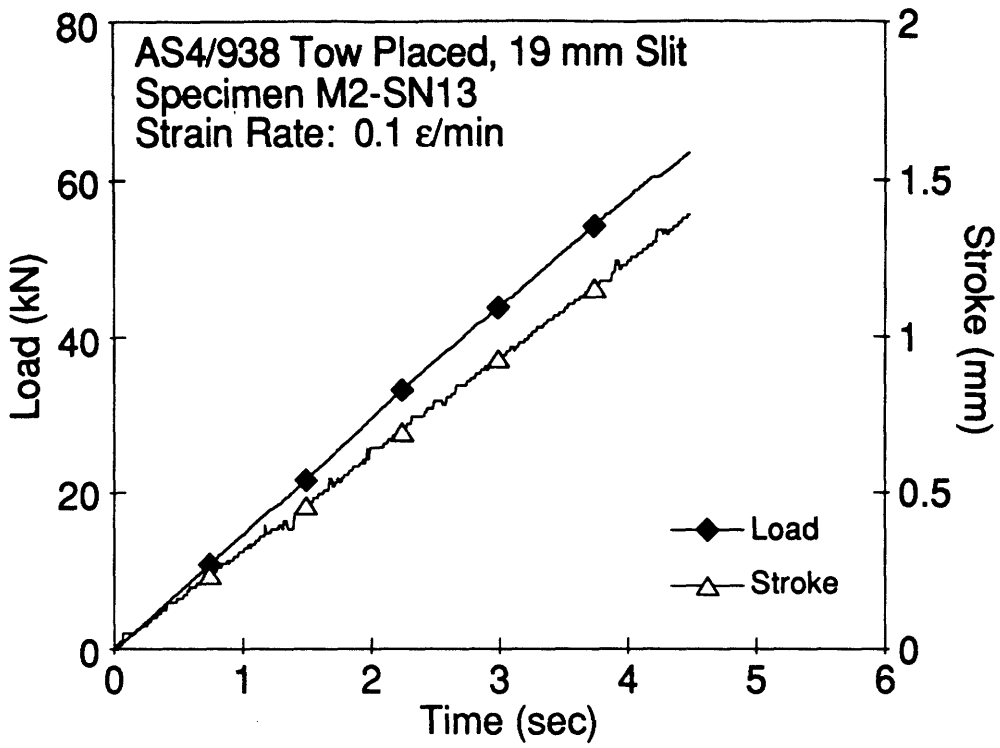


Figure E.58 Plots of Load, Stroke, Far-Field Strain and Notch-Tip Strain versus Time for Specimen M2-SN13.

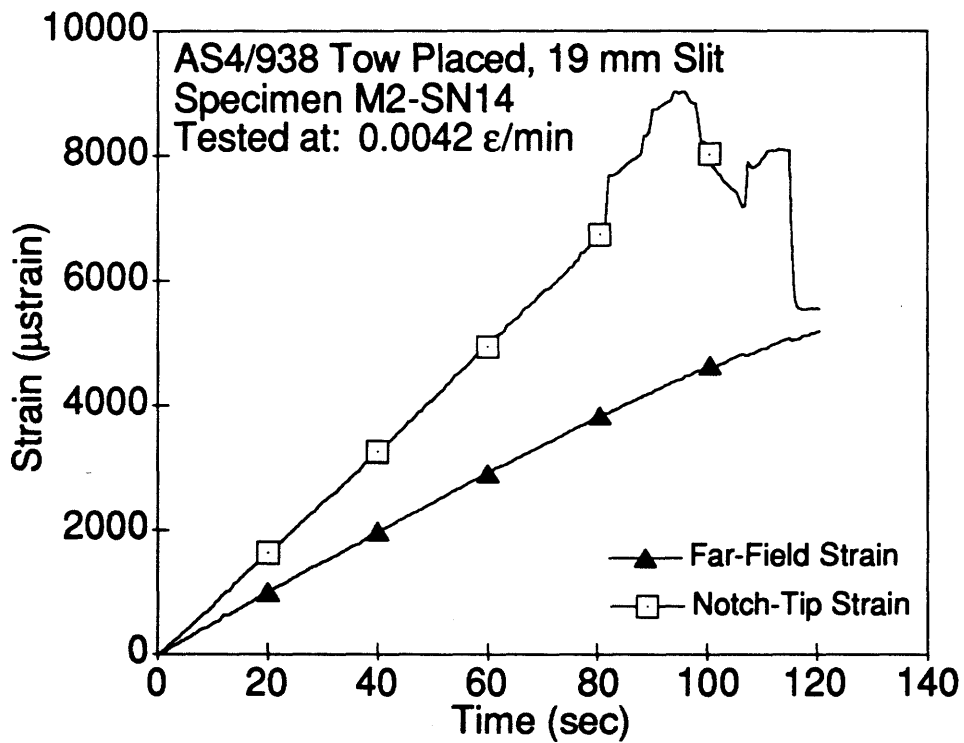
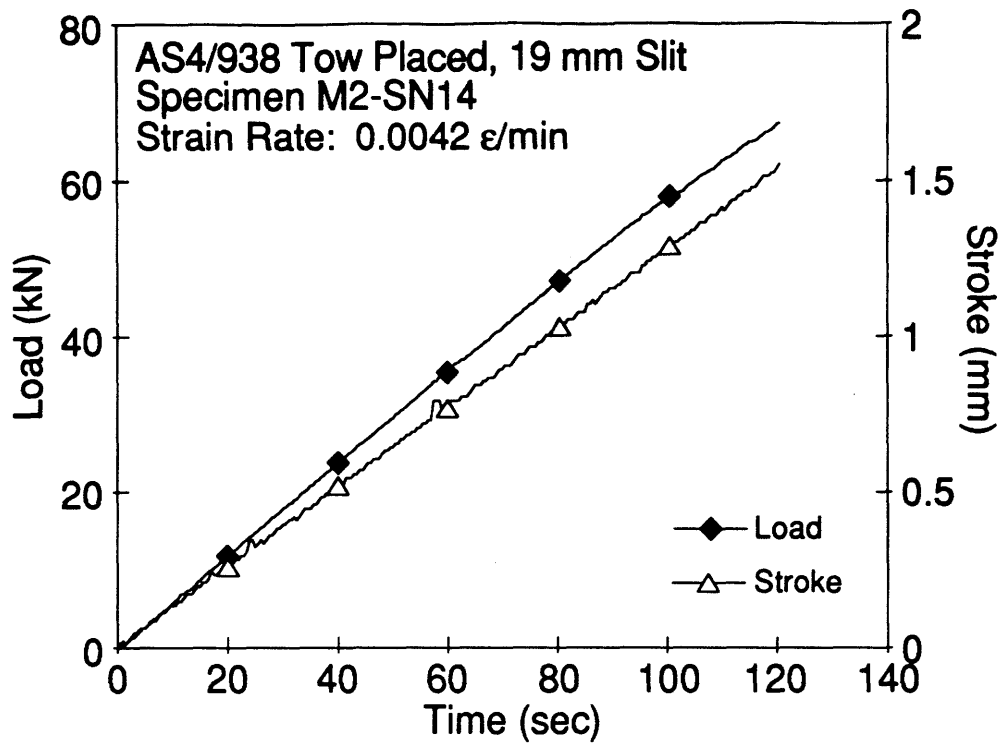


Figure E.59 Plots of Load, Stroke, Far-Field Strain and Notch-Tip Strain versus Time for Specimen M2-SN14.

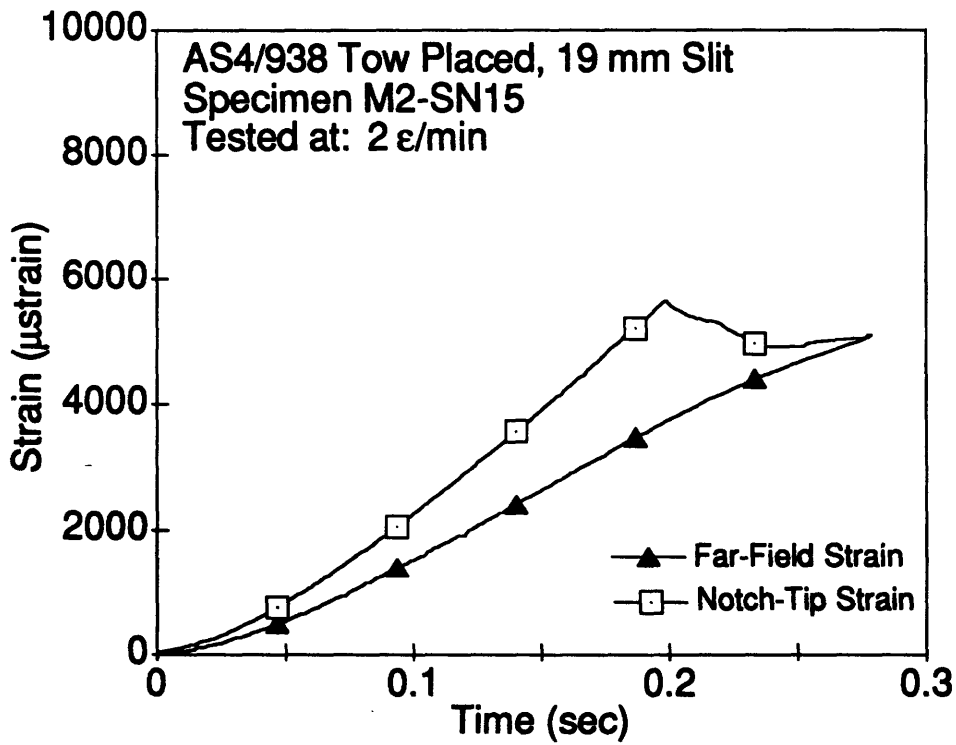
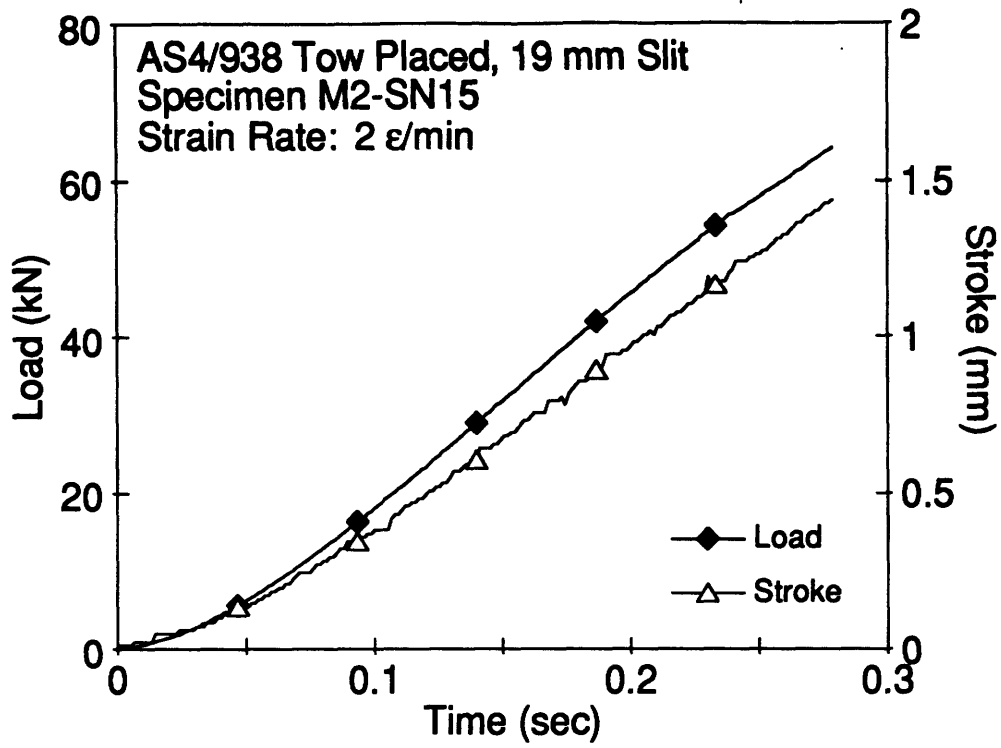


Figure E.60 Plots of Load, Stroke, Far-Field Strain and Notch-Tip Strain versus Time for Specimen M2-SN15.

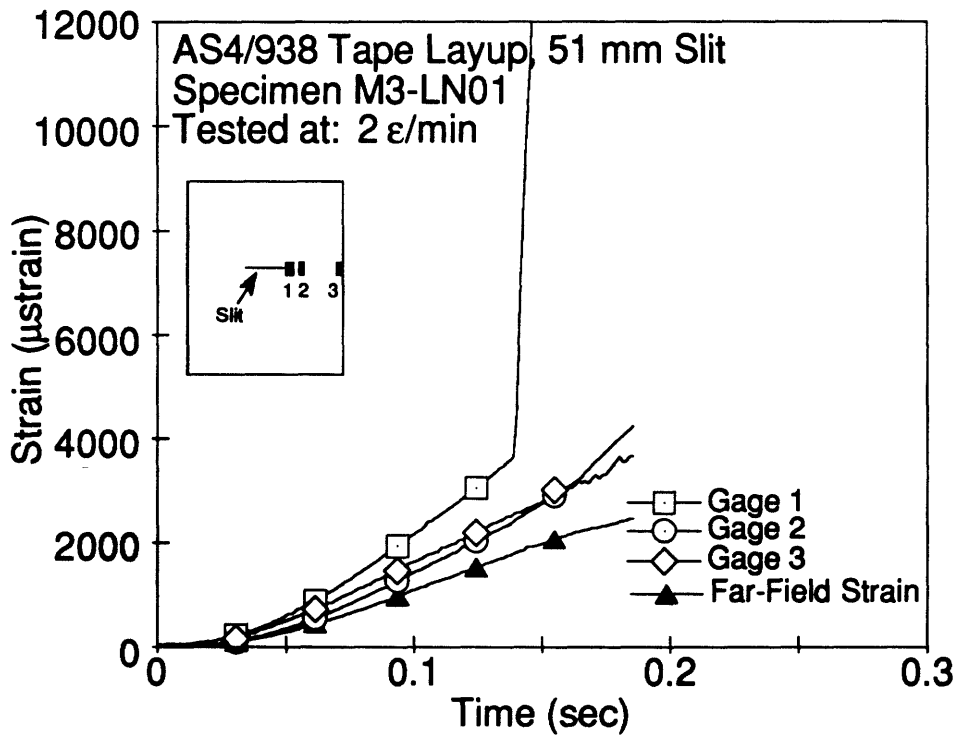
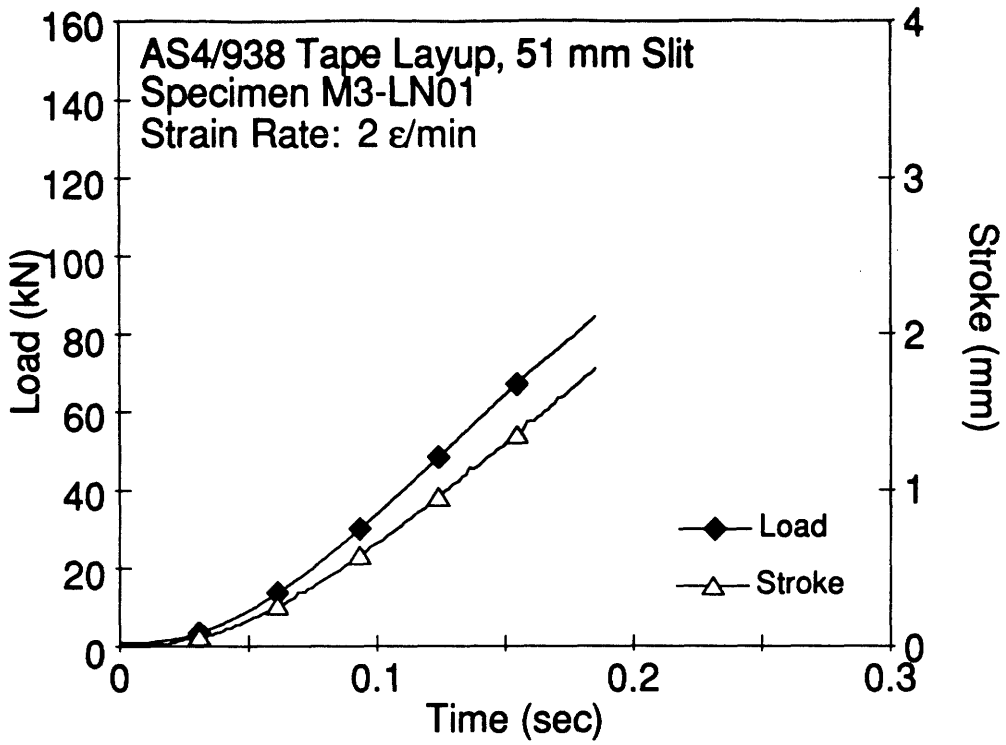


Figure E.61 Plots of Load, Stroke, Far-Field Strain and Strains from Notch-Tip versus Time for Specimen M3-LN01.

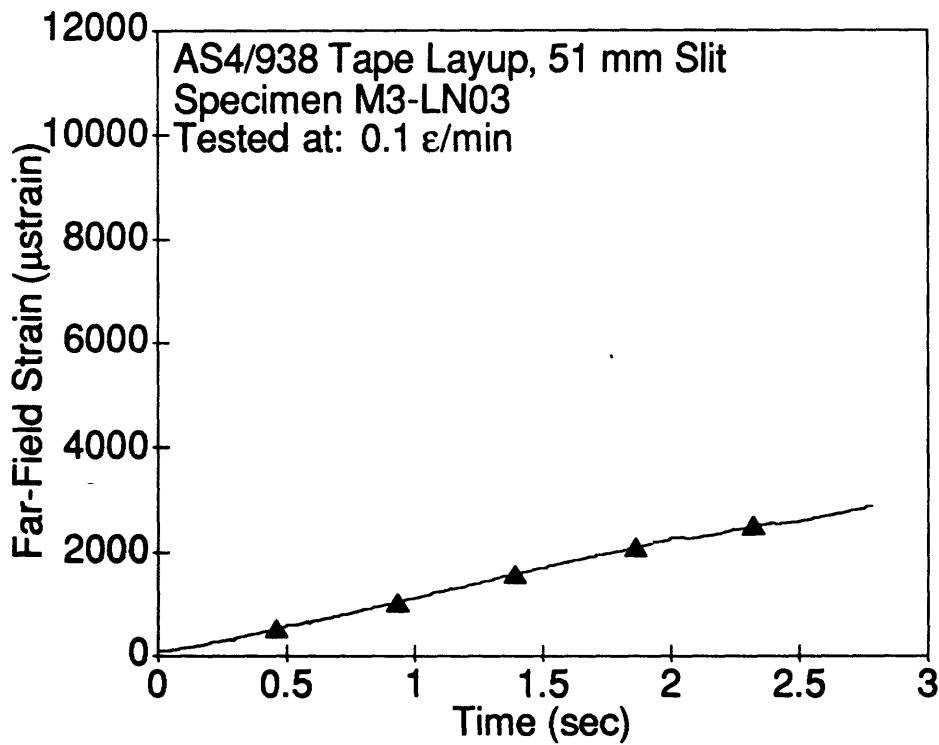
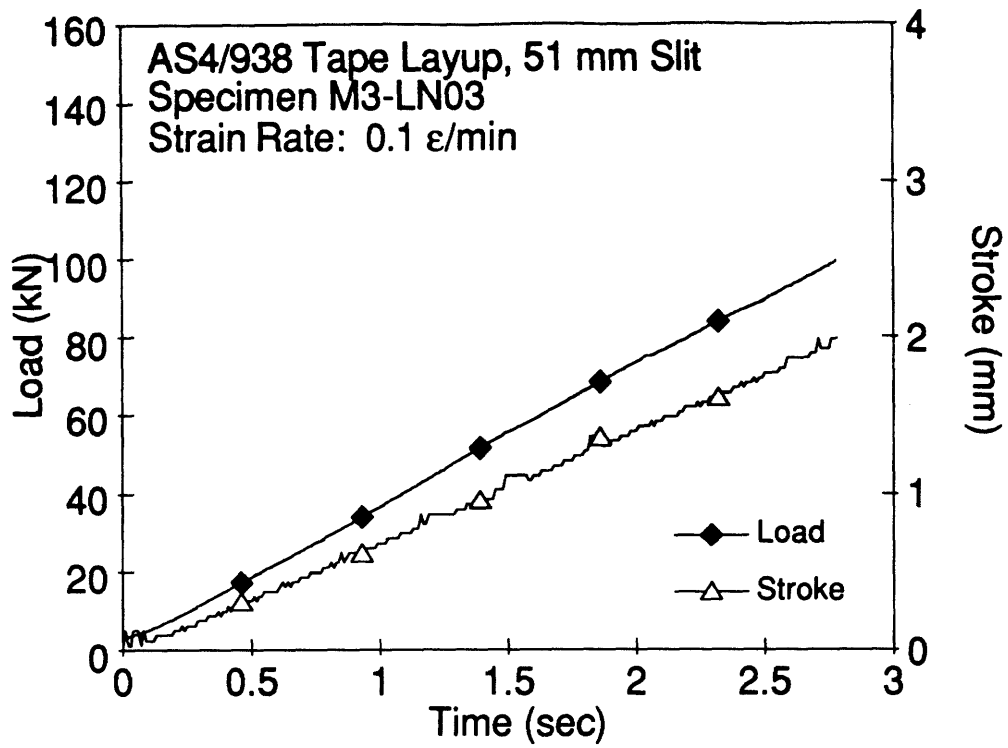


Figure E.62 Plots of Load, Stroke and Far-Field Strain versus Time for Specimen M3-LN03.

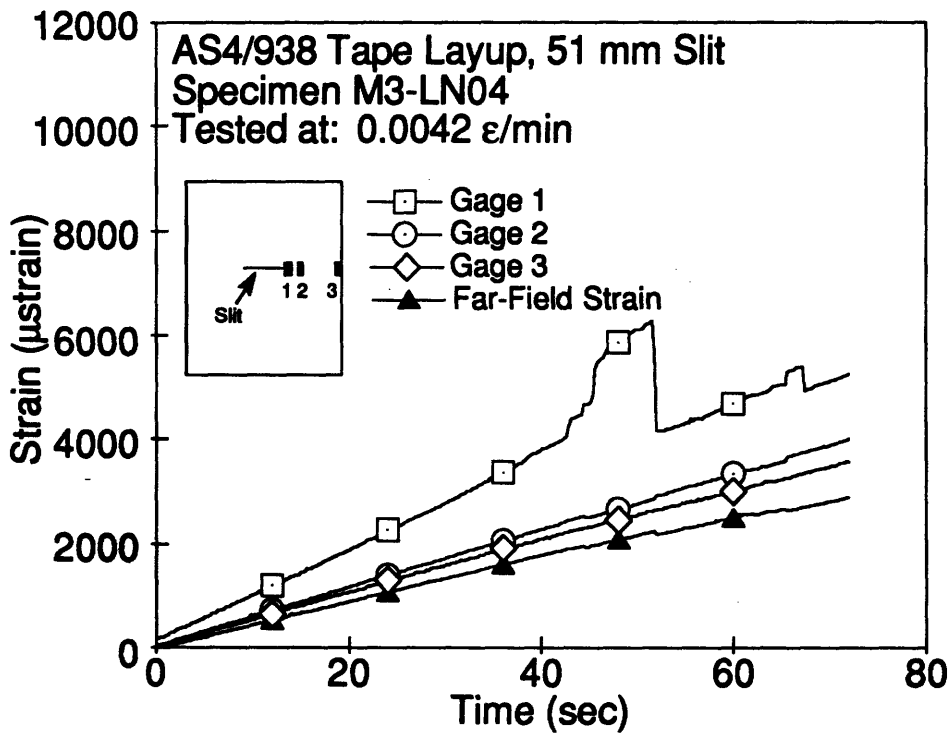
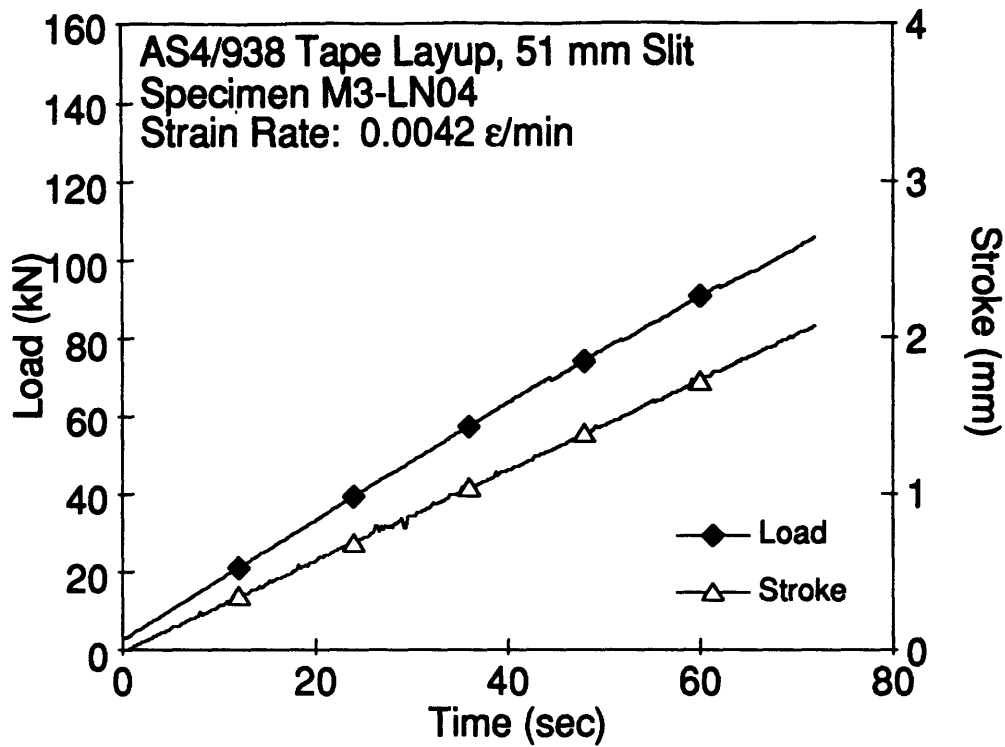


Figure E.63 Plots of Load, Stroke, Far-Field Strain and Strains from Notch-Tip versus Time for Specimen M3-LN04.

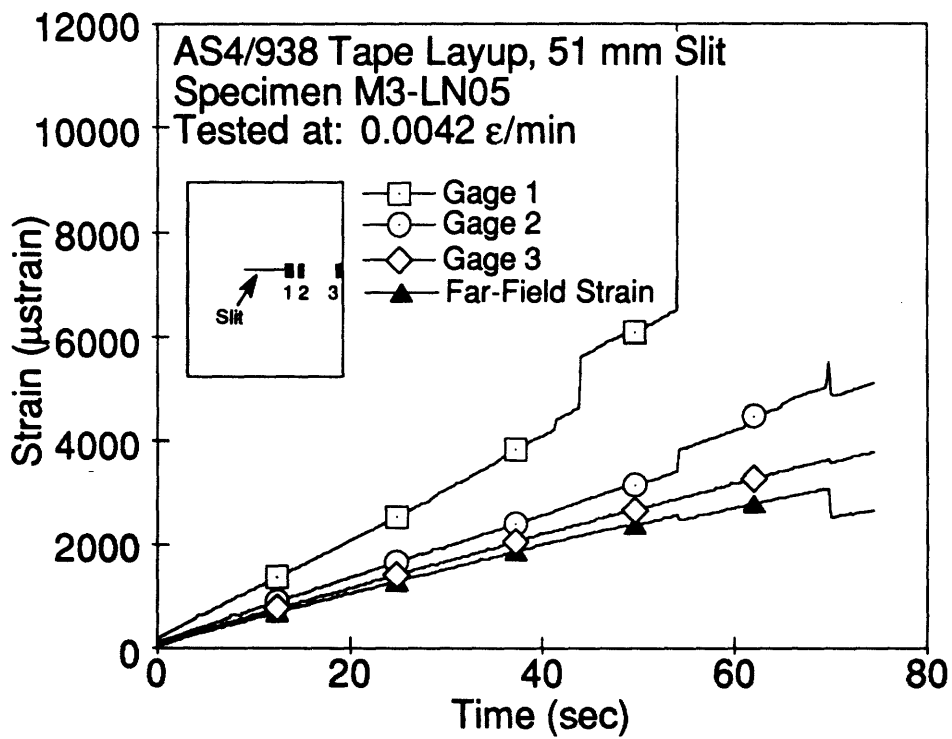
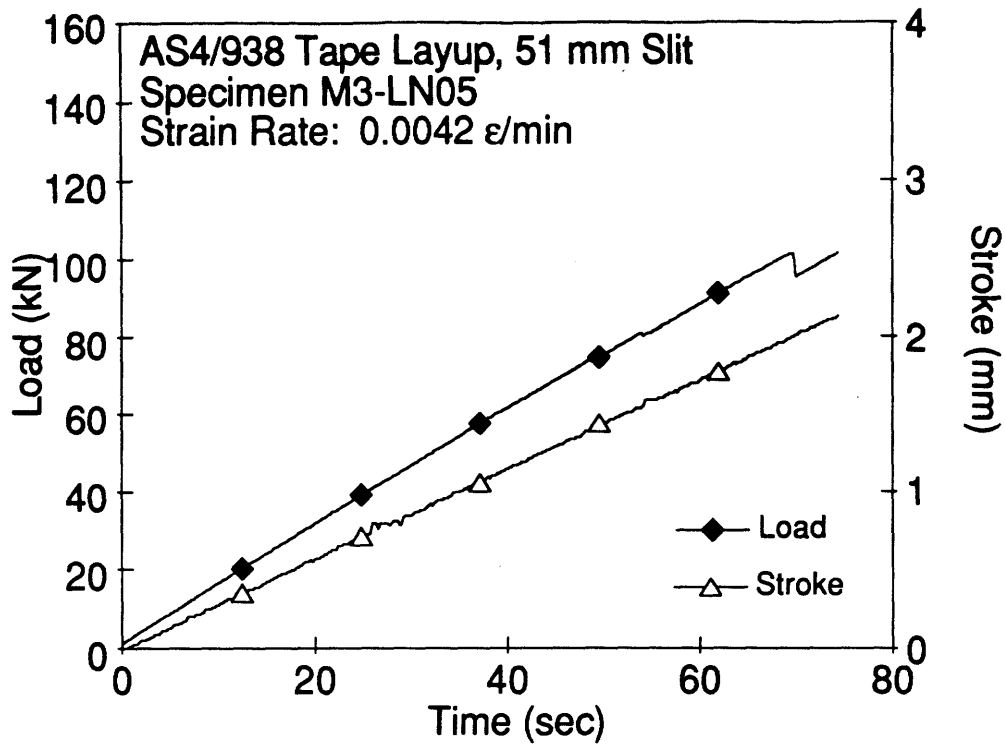


Figure E.64 Plots of Load, Stroke, Far-Field Strain and Strains from Notch-Tip versus Time for Specimen M3-LN05.

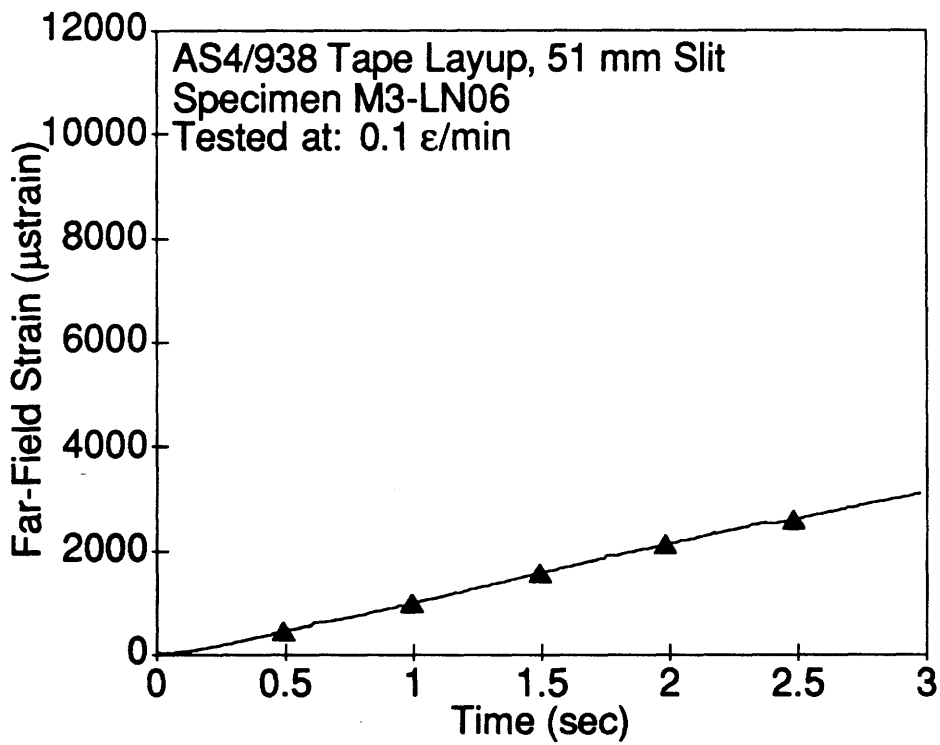
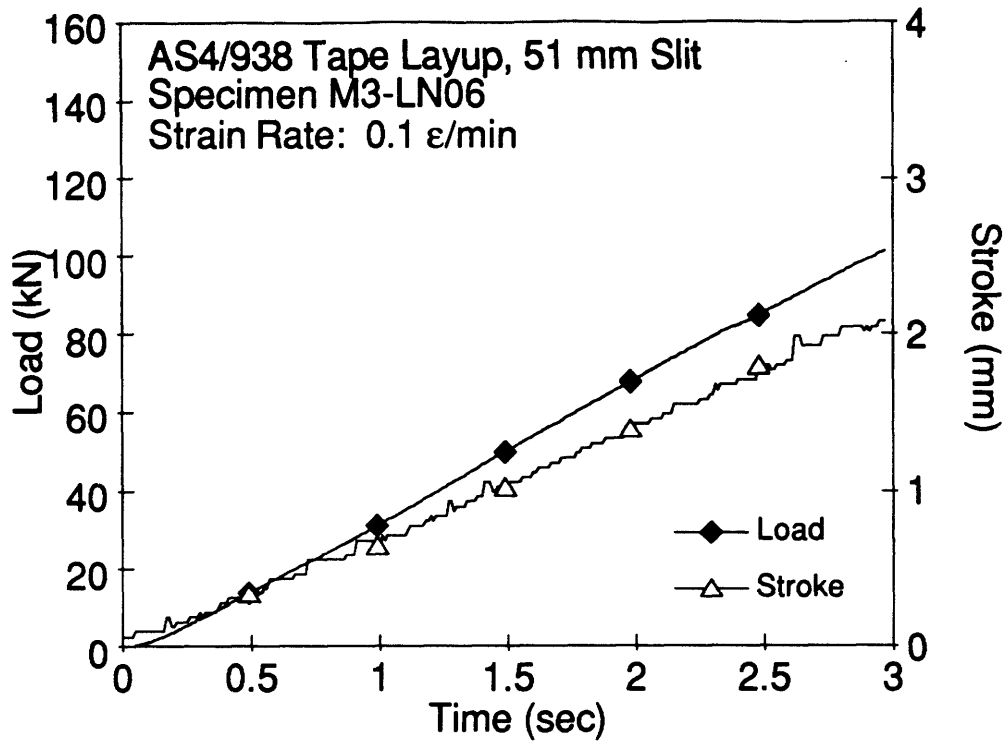


Figure E.65 Plots of Load, Stroke and Far-Field Strain versus Time for Specimen M3-LN06.

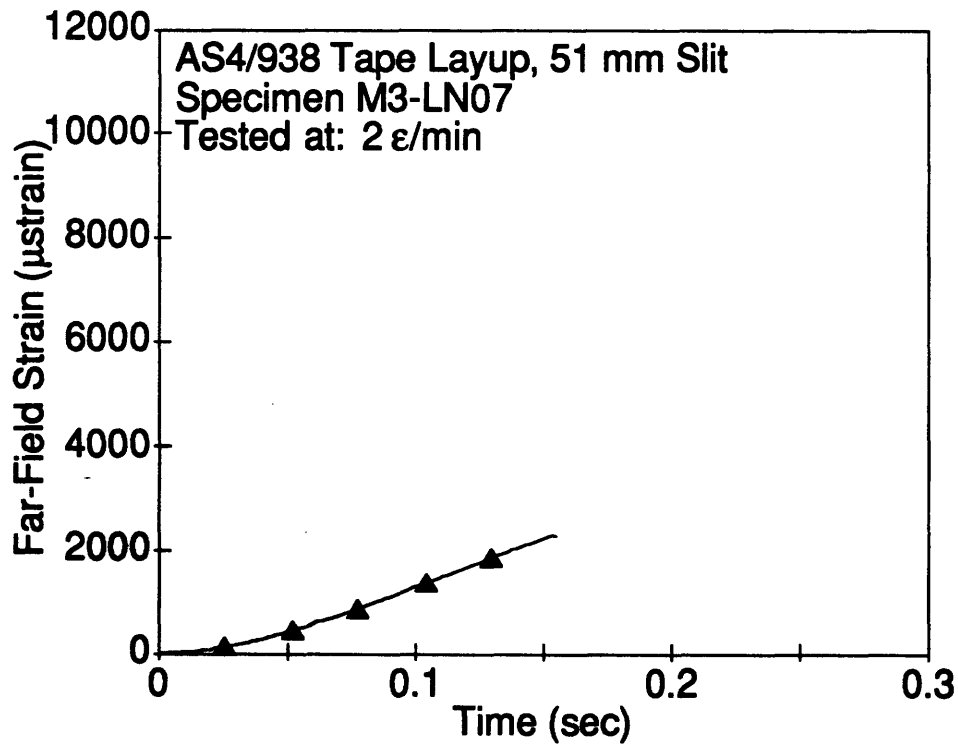
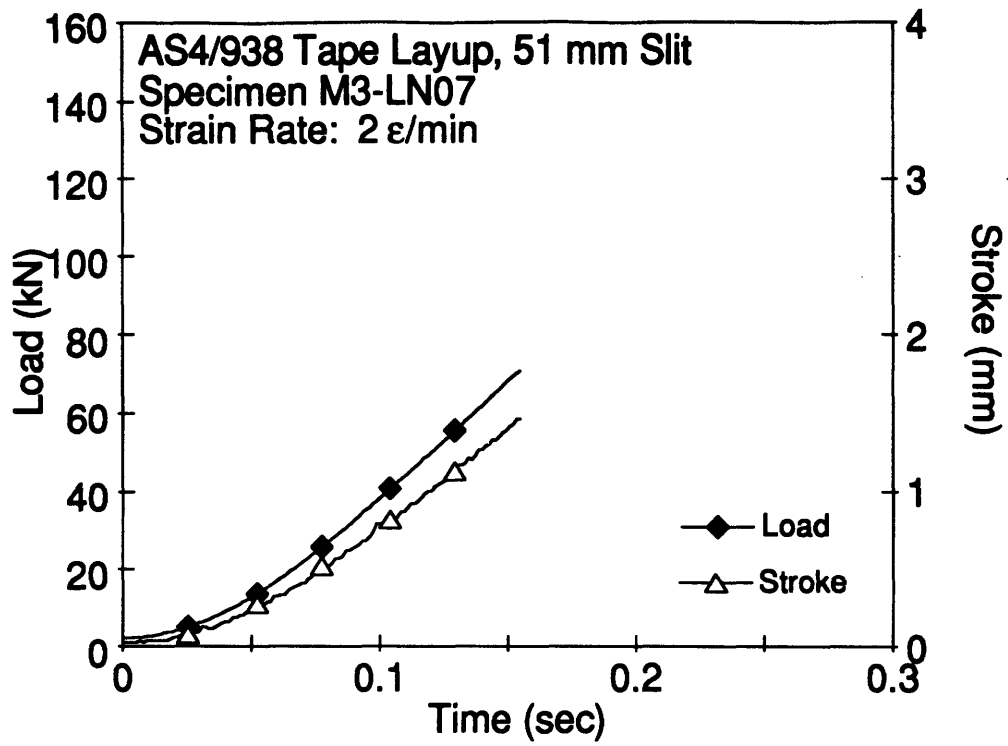


Figure E.66 Plots of Load, Stroke and Far-Field Strain versus Time for Specimen M3-LN07.

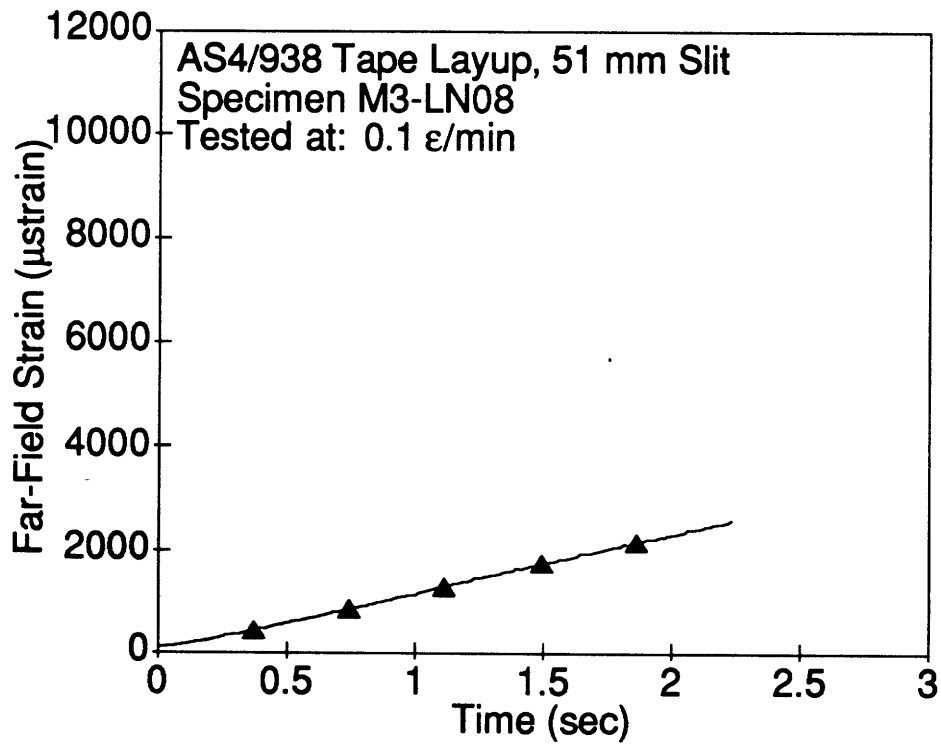
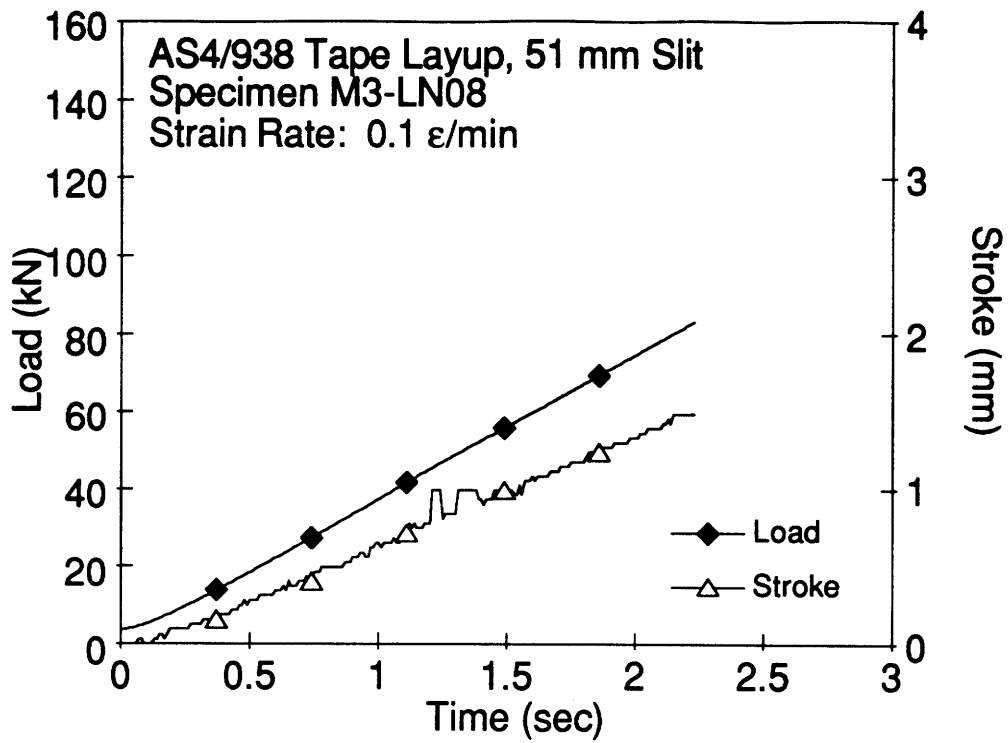


Figure E.67 Plots of Load, Stroke and Far-Field Strain versus Time for Specimen M3-LN08.

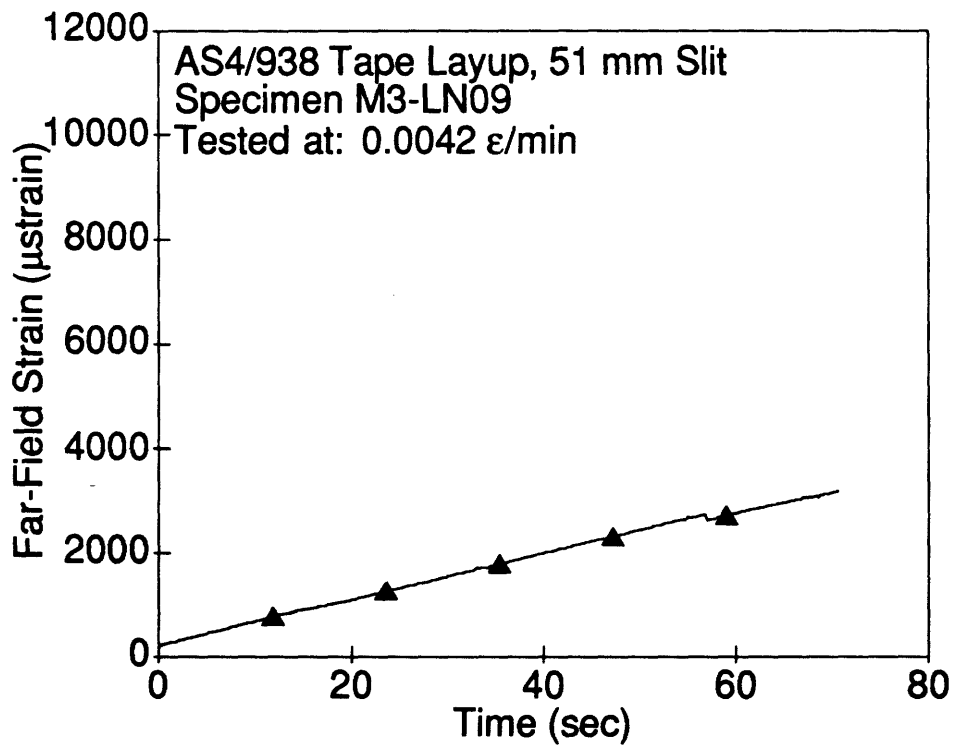
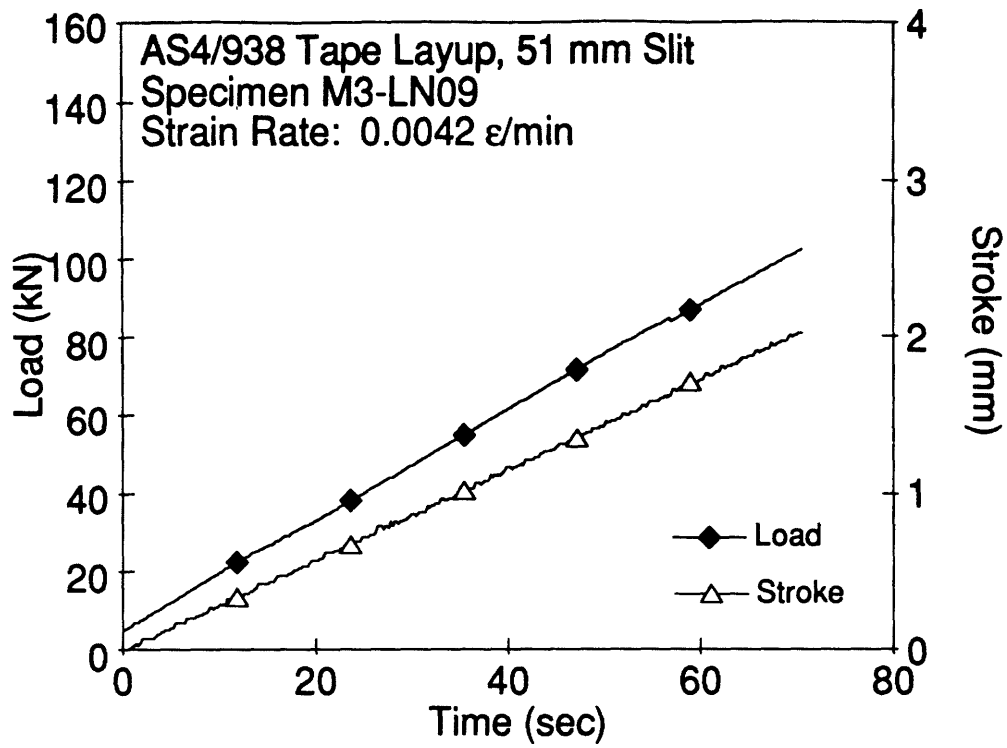


Figure E.68 Plots of Load, Stroke and Far-Field Strain versus Time for Specimen M3-LN09.

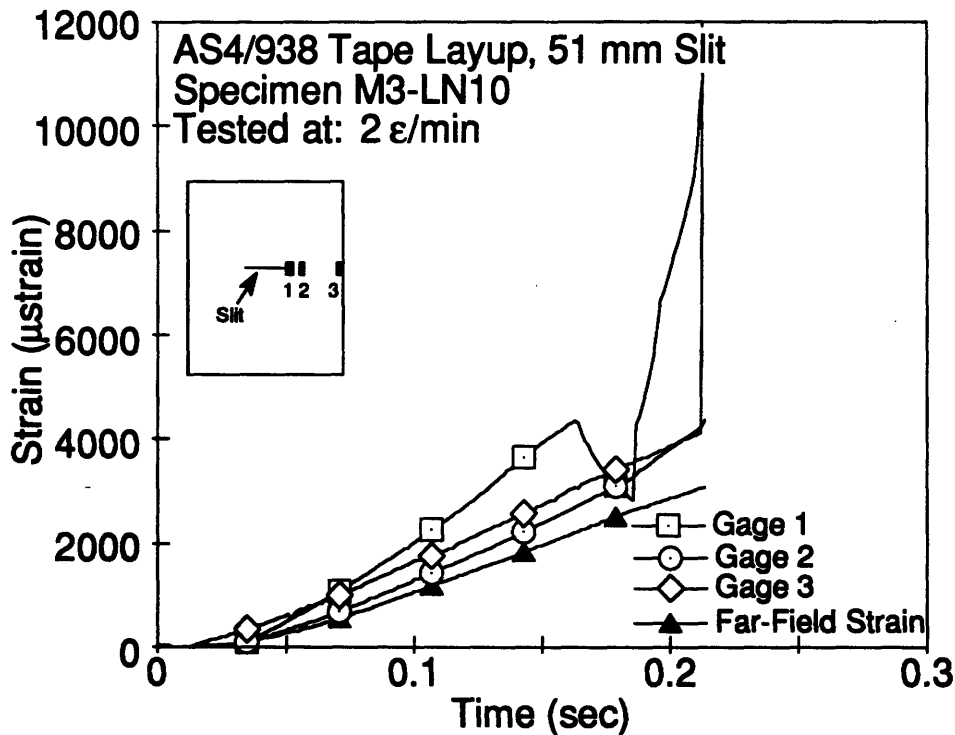
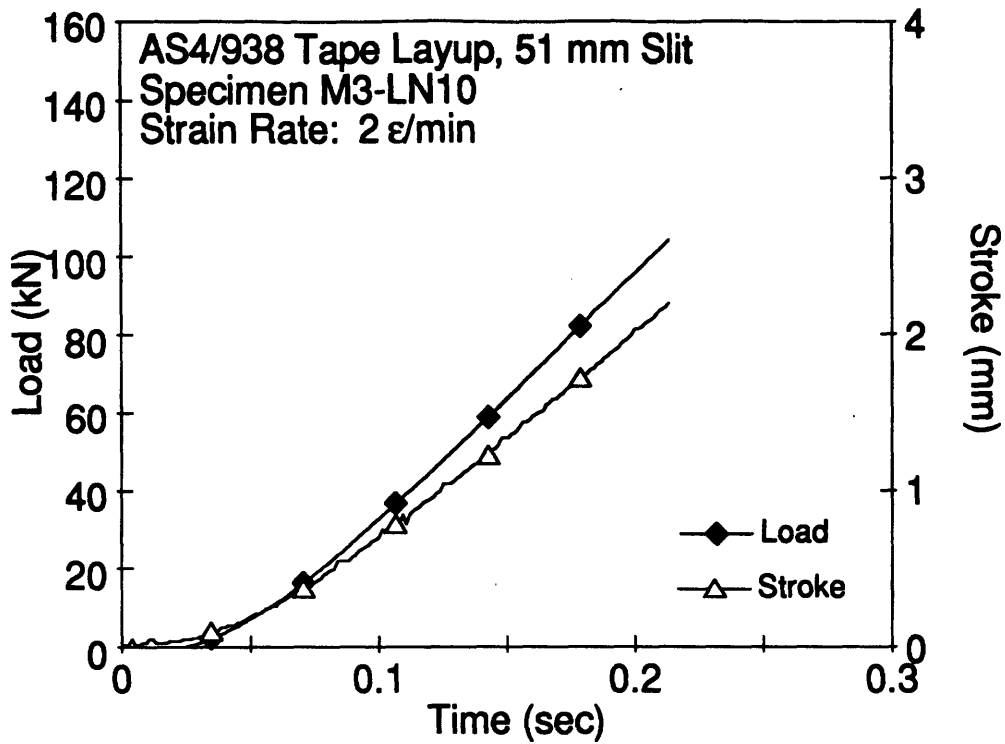


Figure E.69 Plots of Load, Stroke, Far-Field Strain and Strains from Notch-Tip versus Time for Specimen M3-LN10.

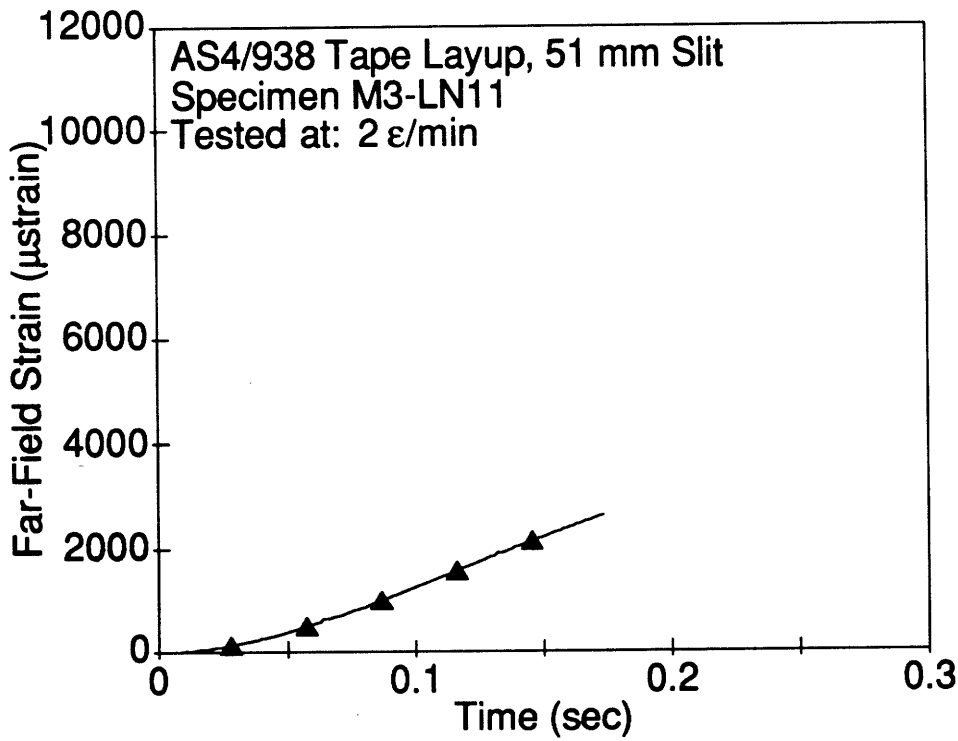
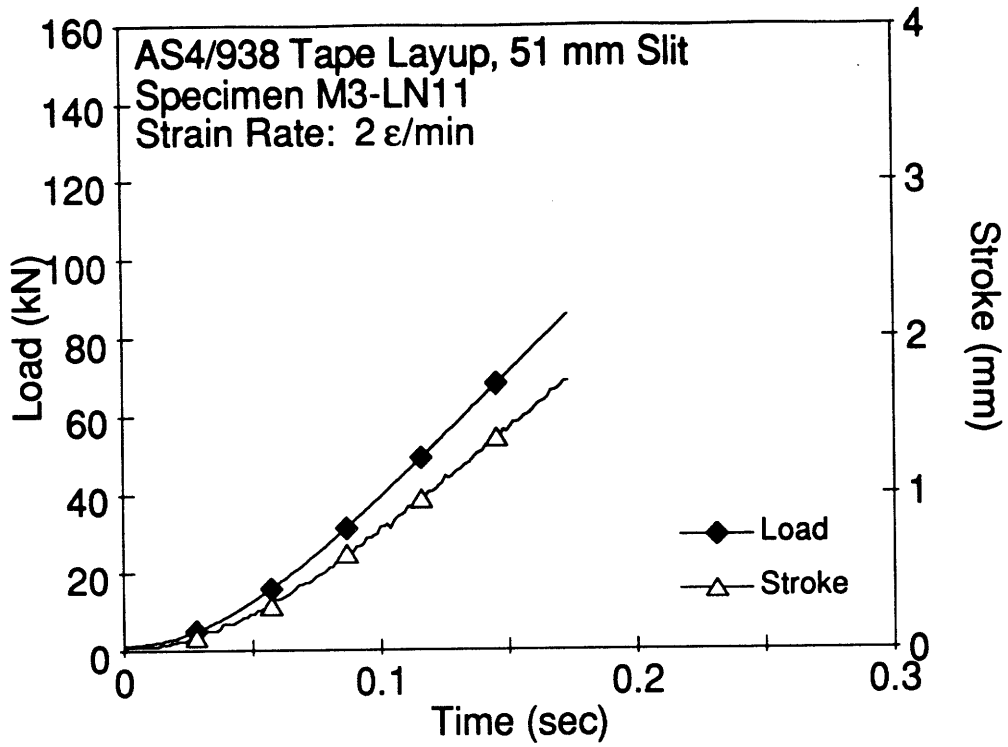


Figure E.70 Plots of Load, Stroke and Far-Field Strain versus Time for Specimen M3-LN11.

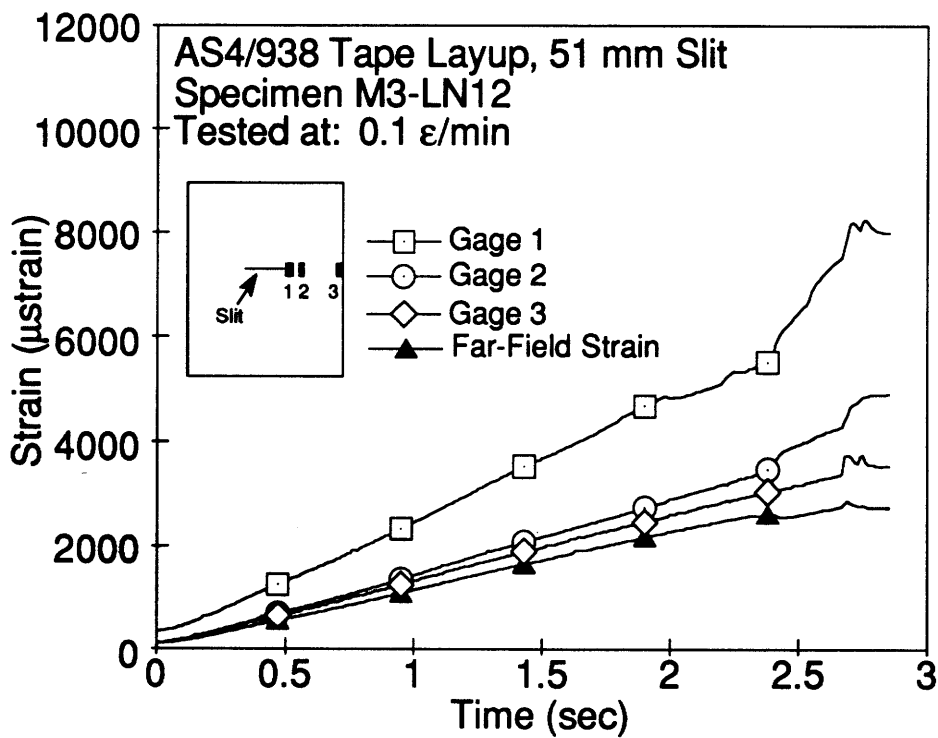
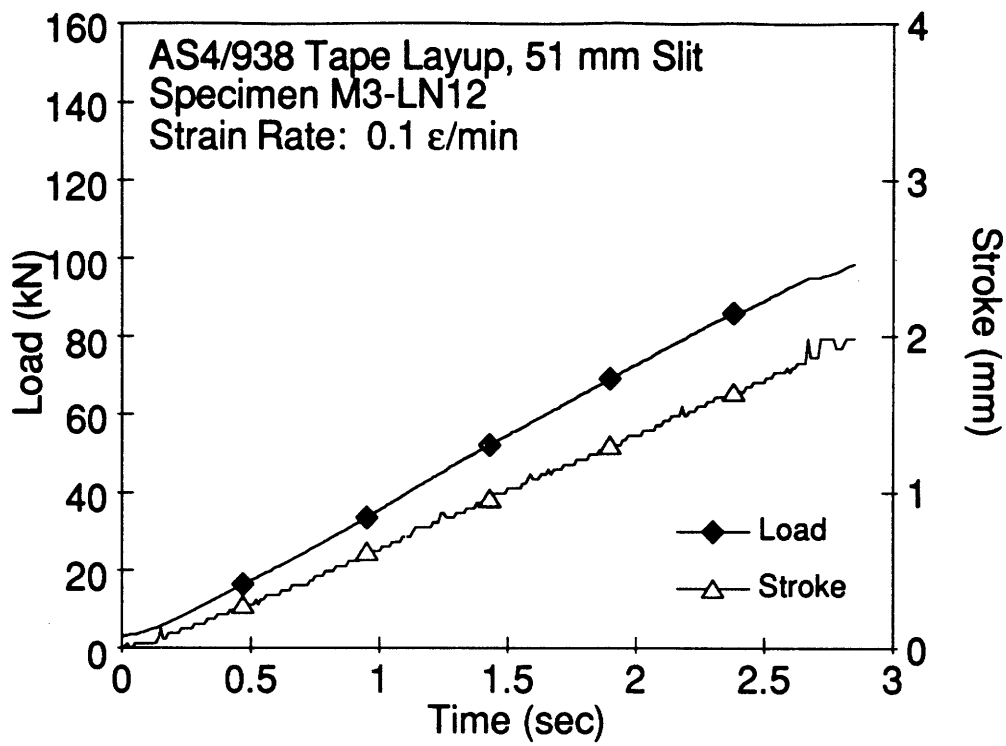


Figure E.71 Plots of Load, Stroke, Far-Field Strain and Strains from Notch-Tip versus Time for Specimen M3-LN12.

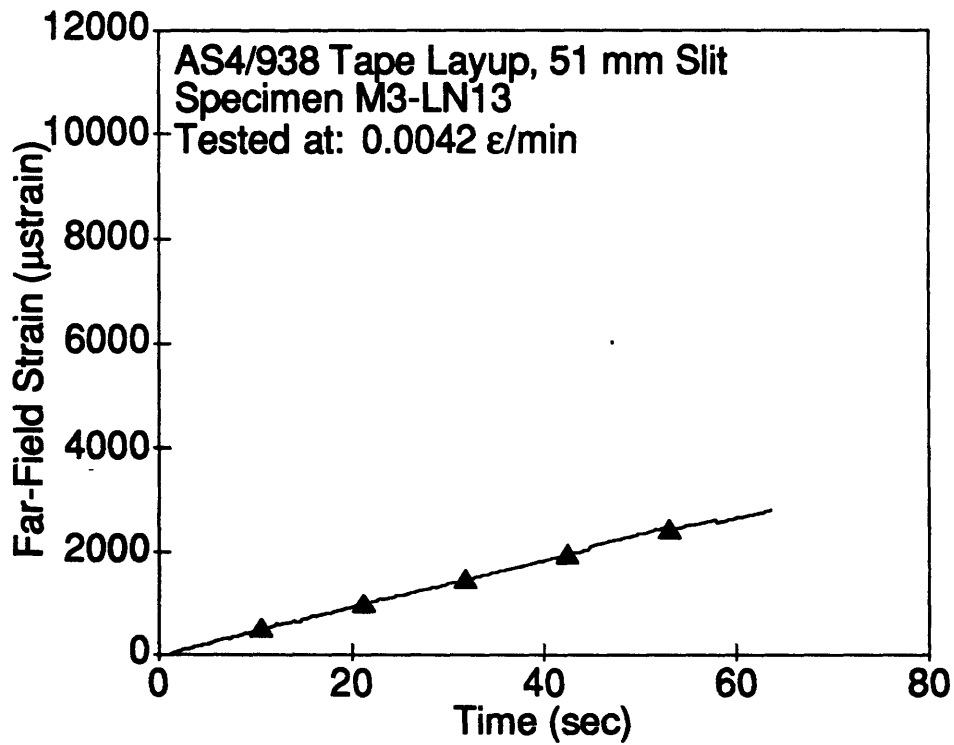
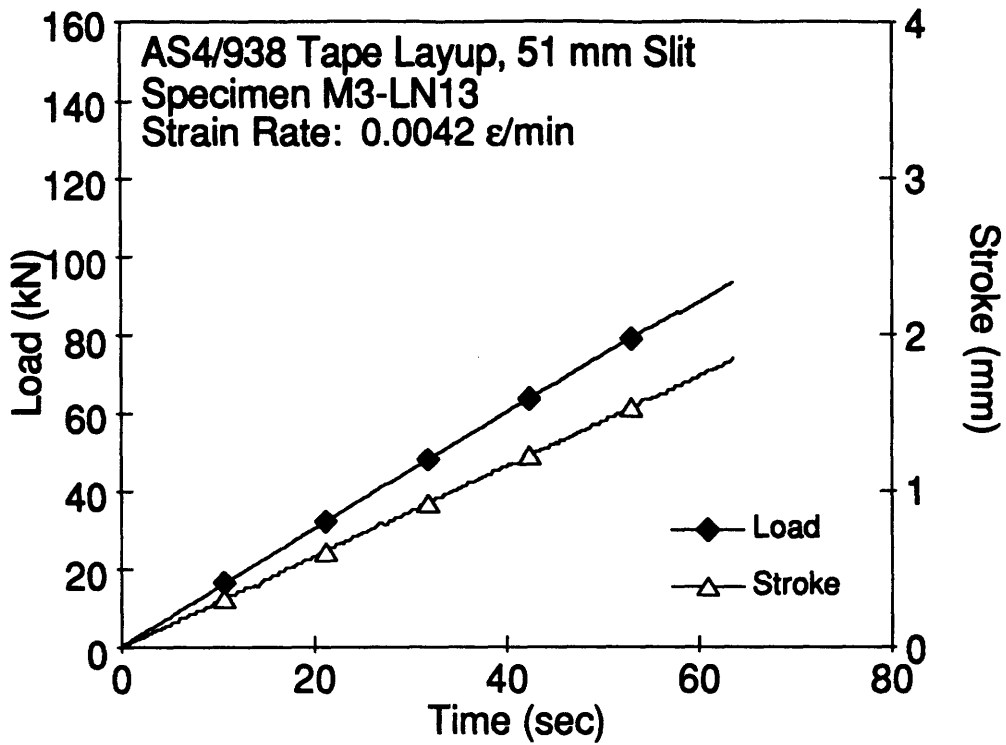


Figure E.72 Plots of Load, Stroke and Far-Field Strain versus Time for Specimen M3-LN13.

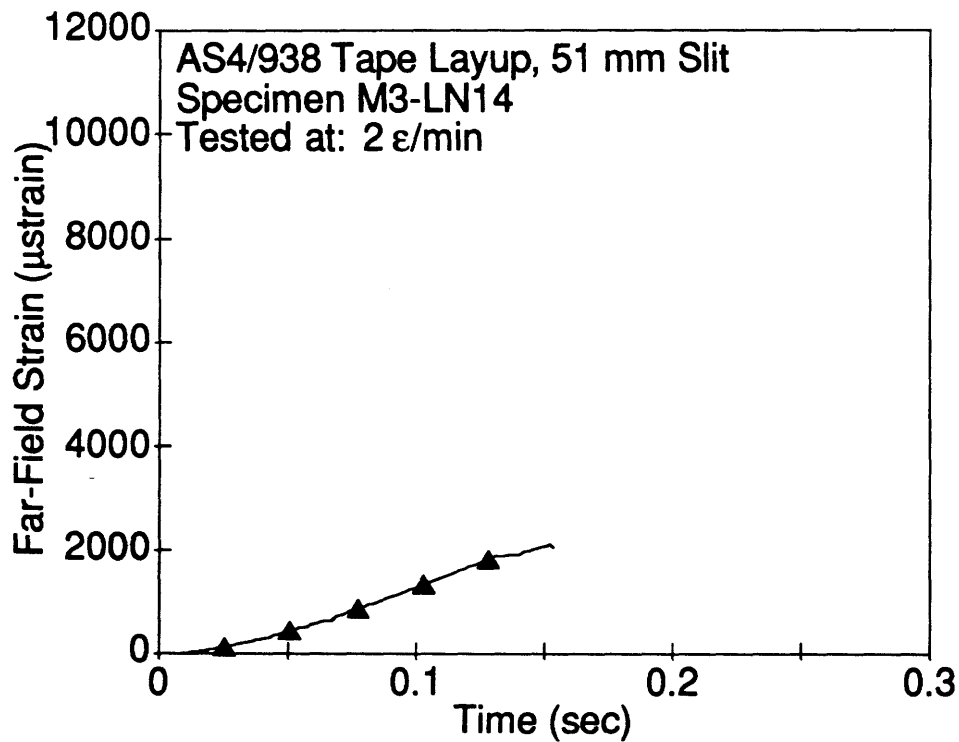
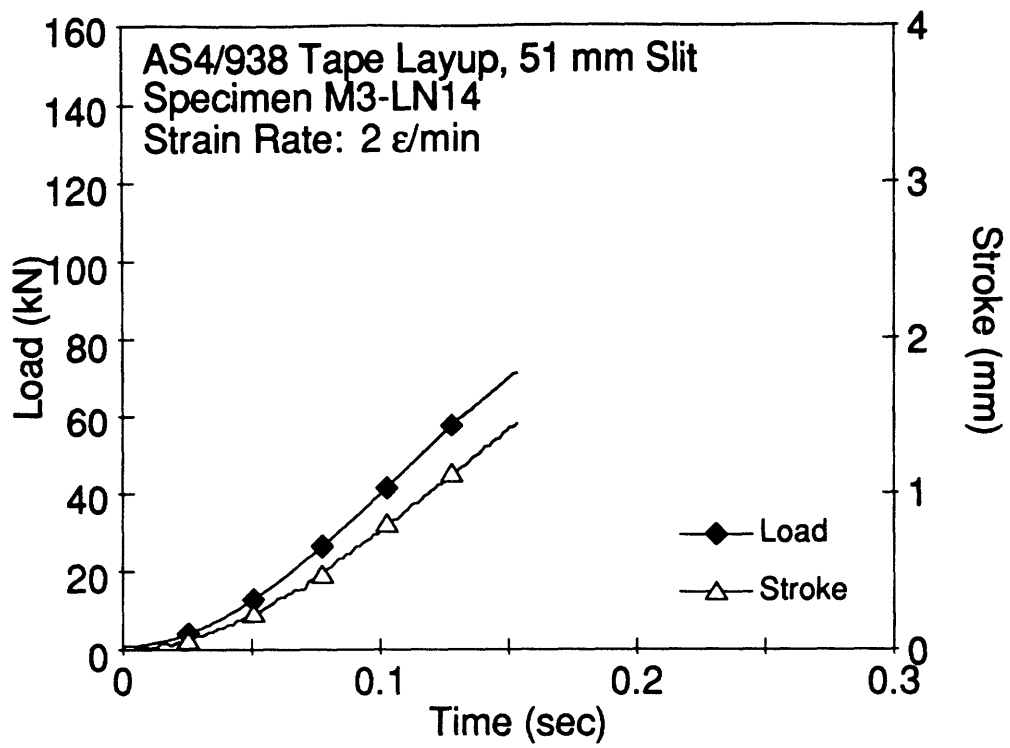


Figure E.73 Plots of Load, Stroke and Far-Field Strain versus Time for Specimen M3-LN14.

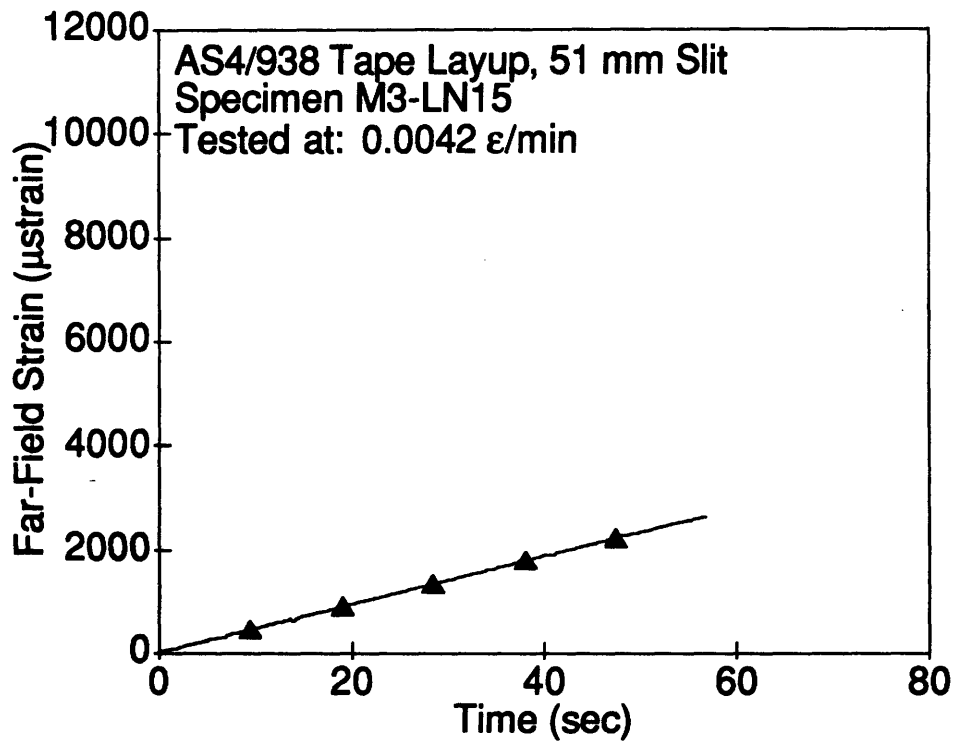
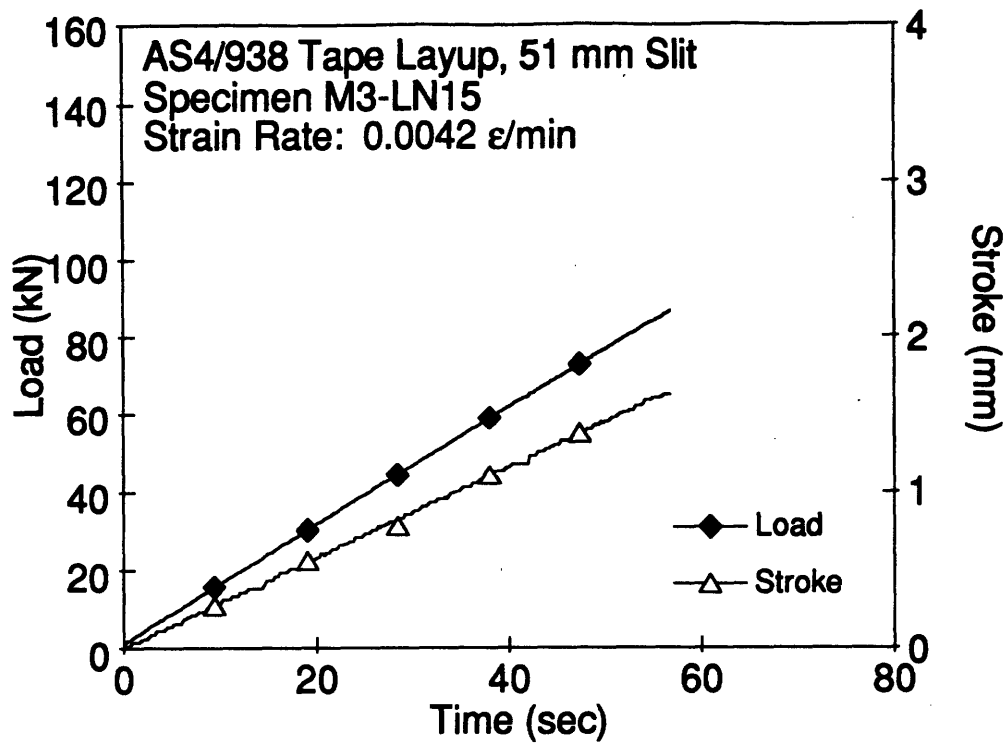


Figure E.74 Plots of Load, Stroke and Far-Field Strain versus Time for Specimen M3-LN15.

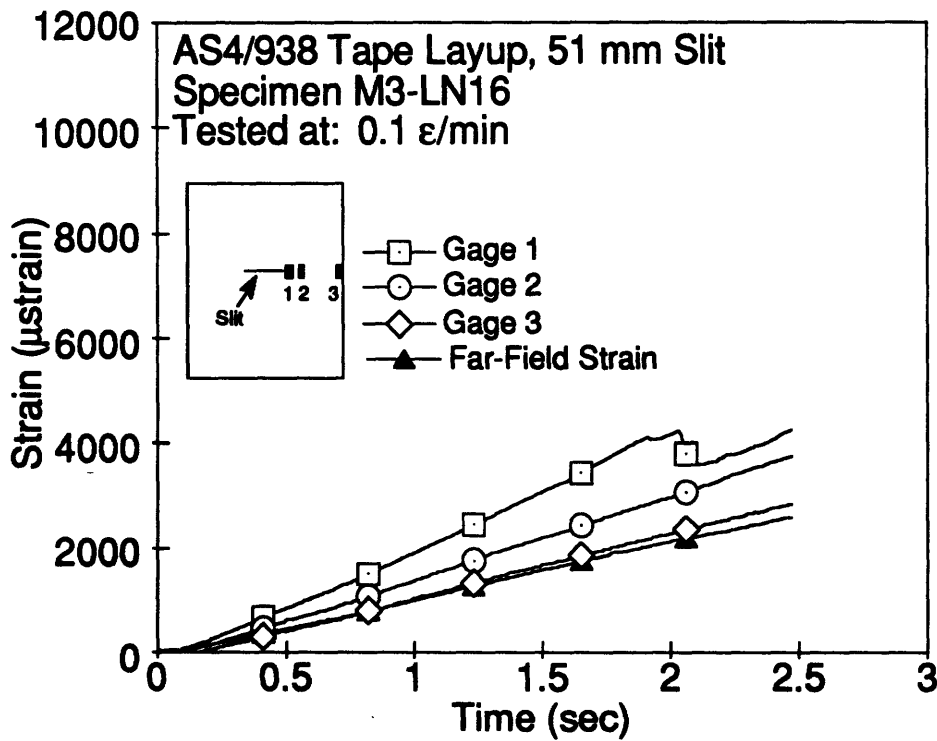
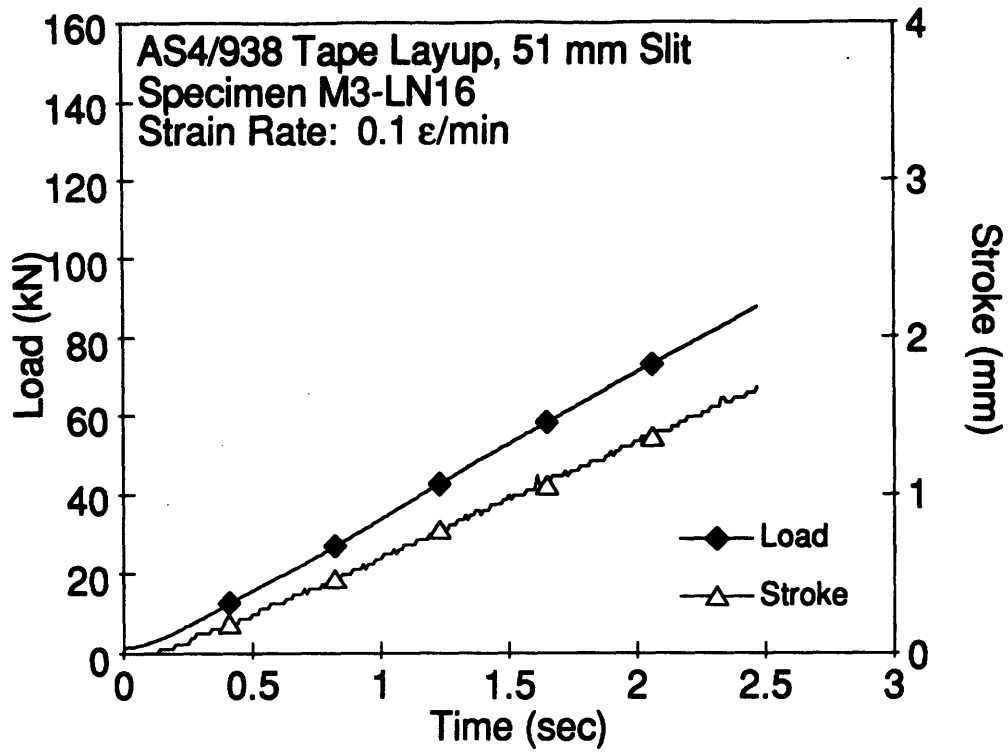


Figure E.75 Plots of Load, Stroke, Far-Field Strain and Strains from Notch-Tip versus Time for Specimen M3-LN16.

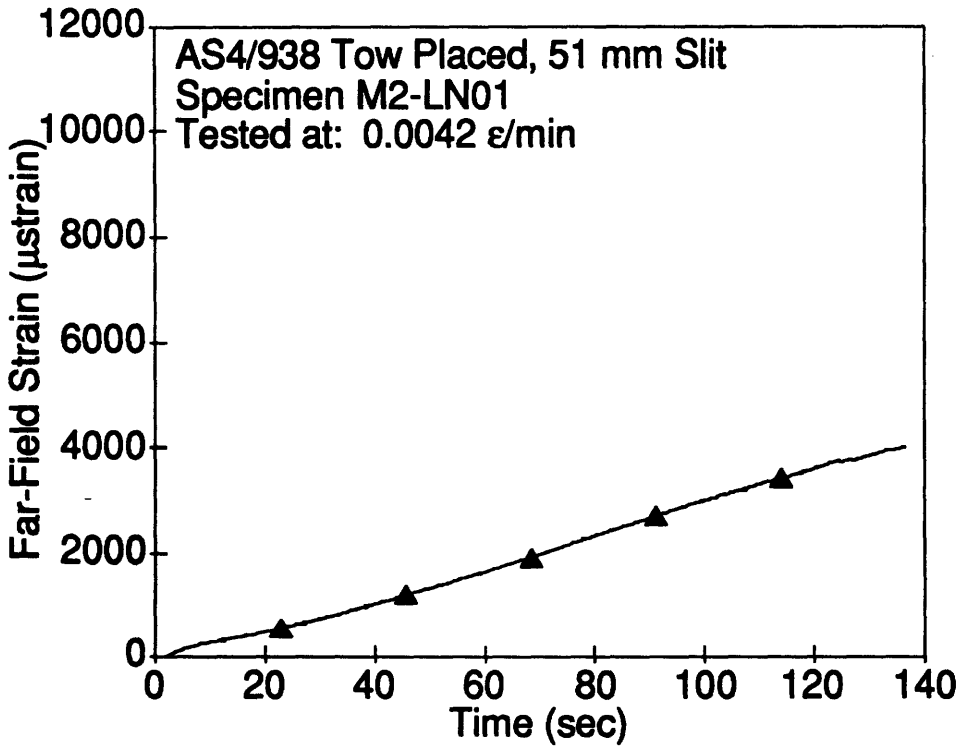
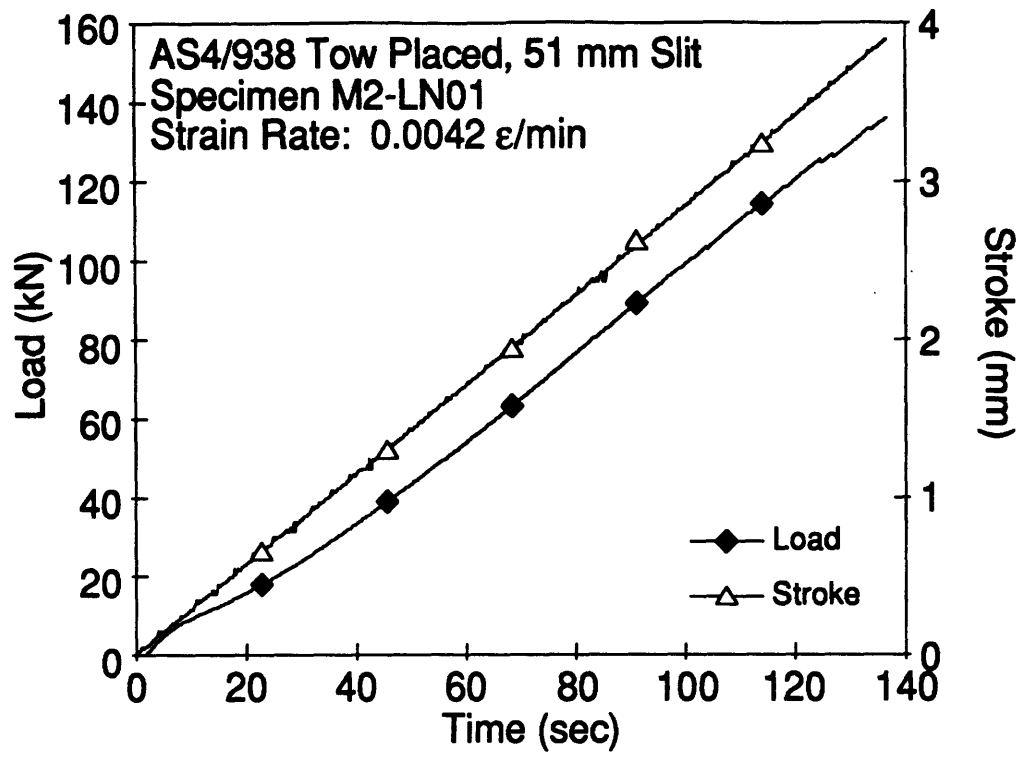


Figure E.76 Plots of Load, Stroke and Far-Field Strain versus Time for Specimen M2-LN01.

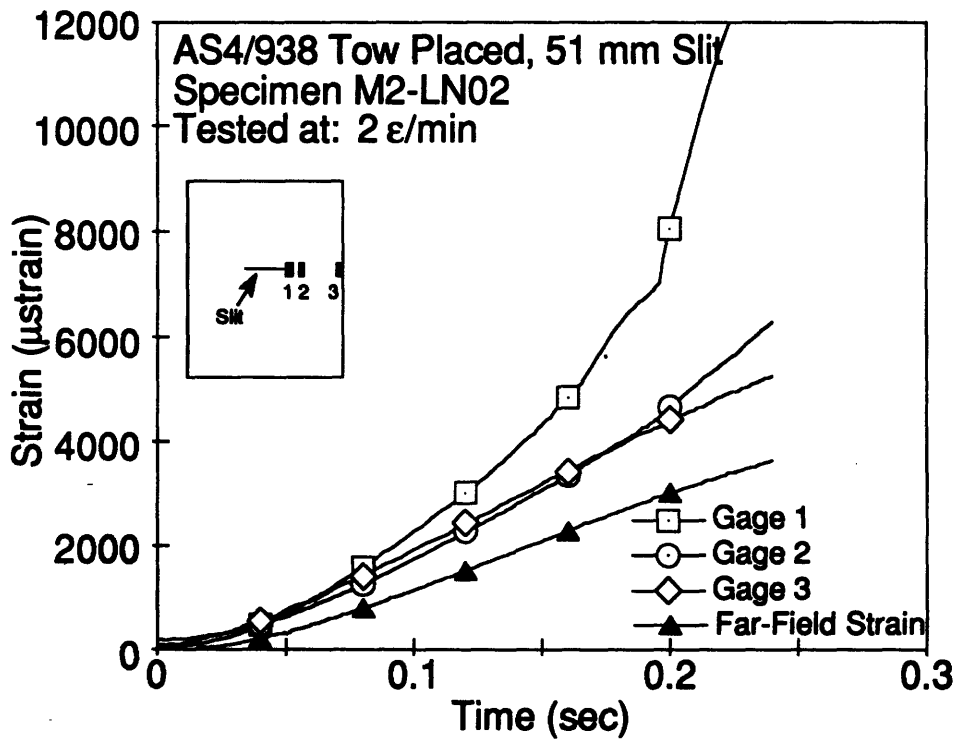
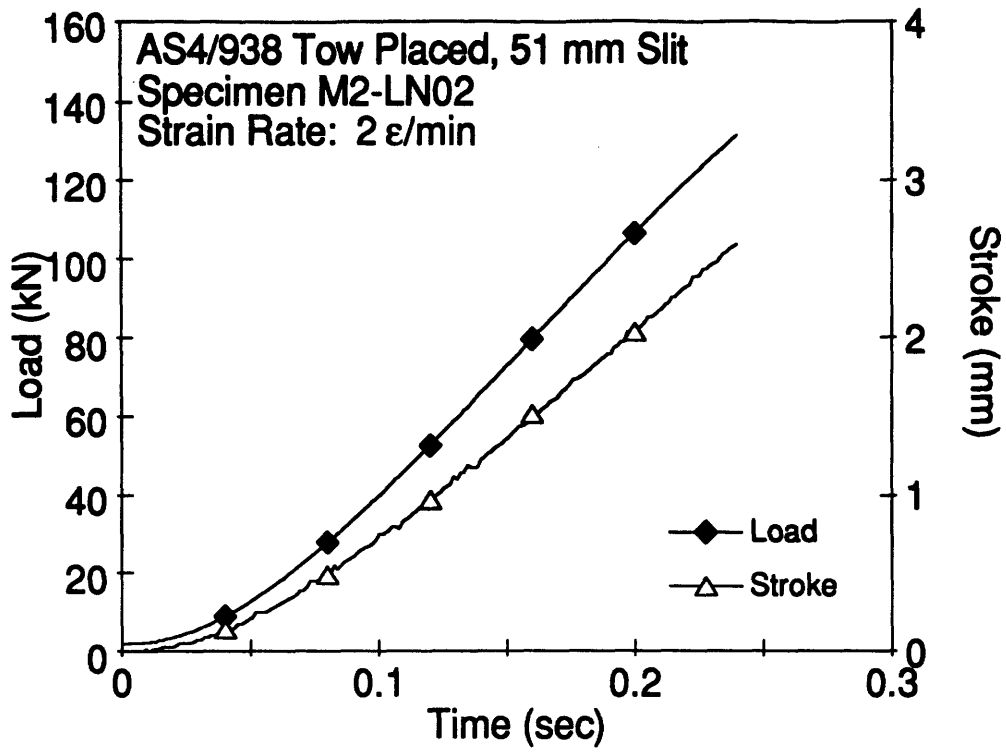


Figure E.77 Plots of Load, Stroke, Far-Field Strain and Strains from Notch-Tip versus Time for Specimen M2-LN02.

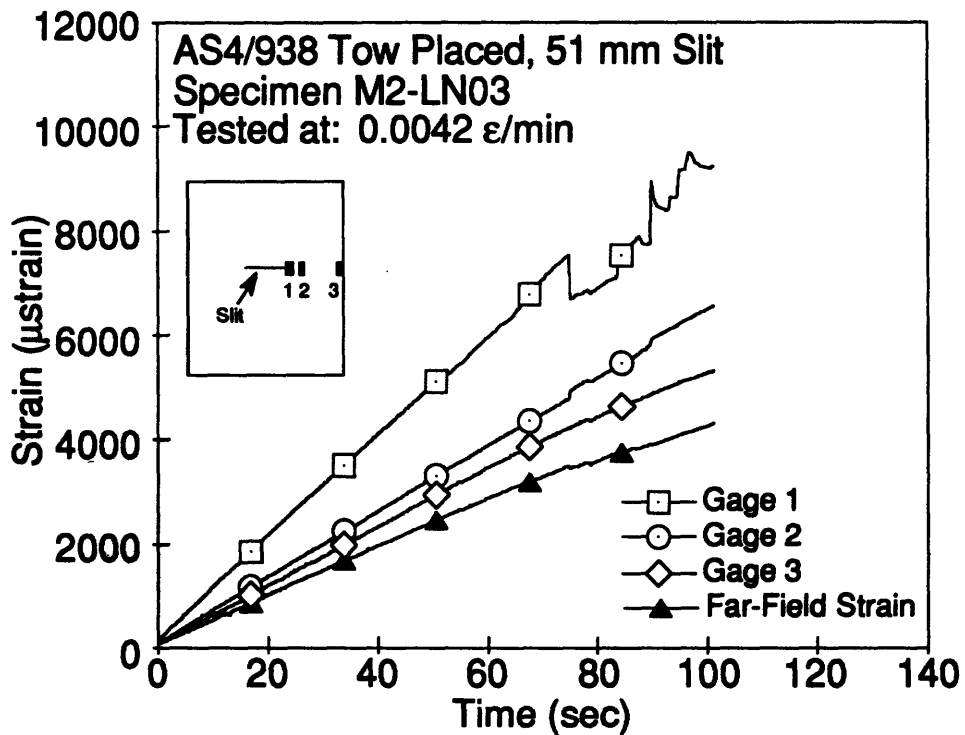
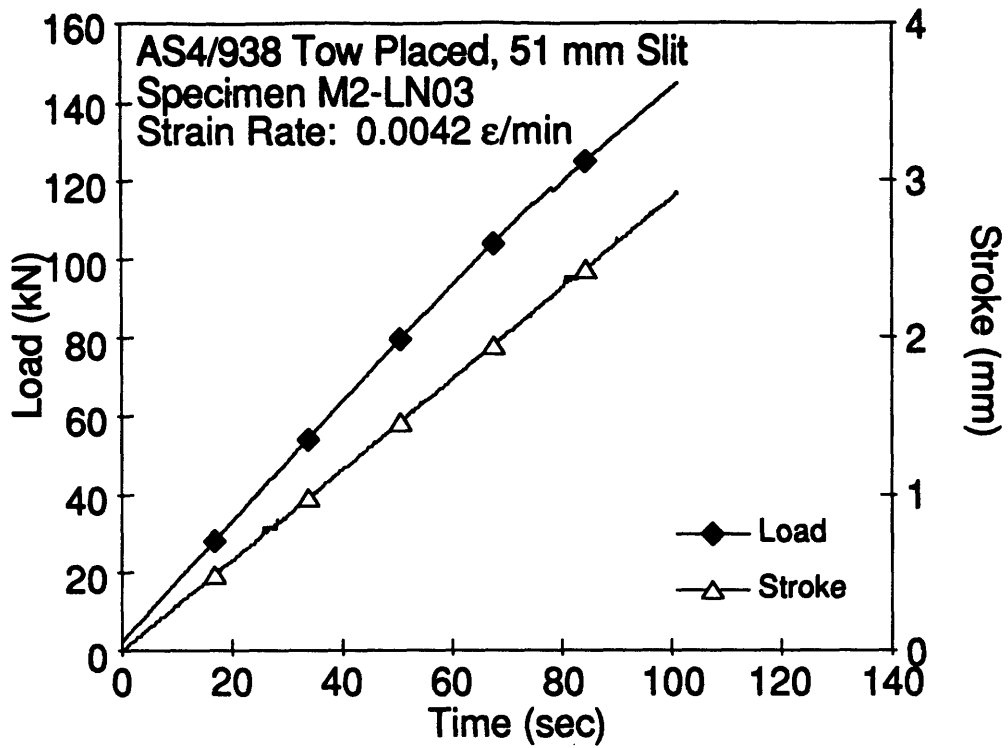


Figure E.78 Plots of Load, Stroke, Far-Field Strain and Strains from Notch-Tip versus Time for Specimen M2-LN03.

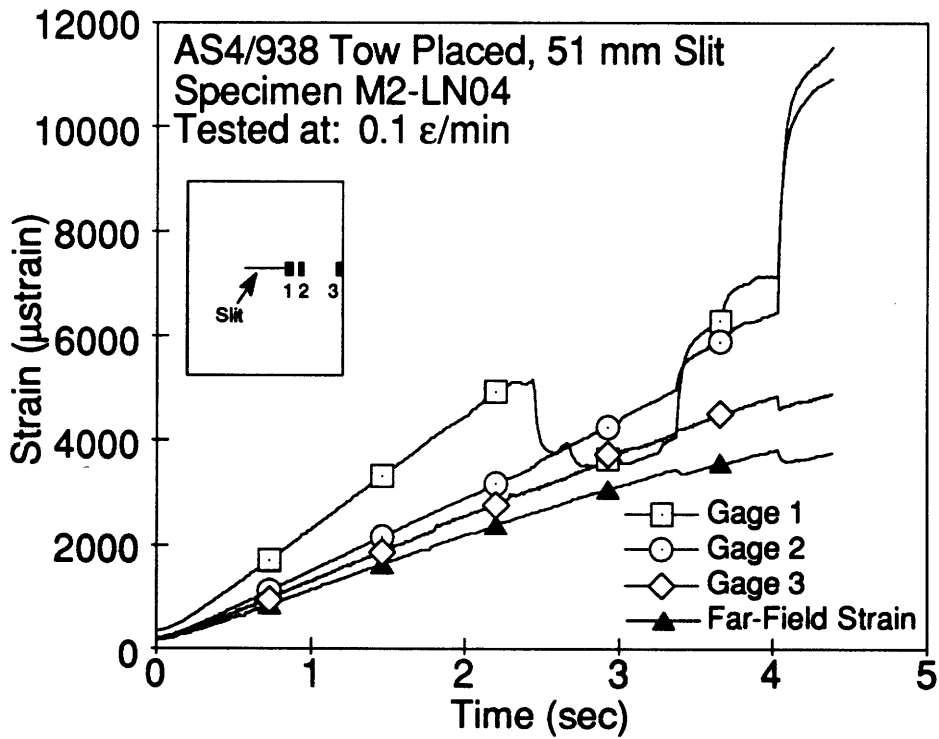
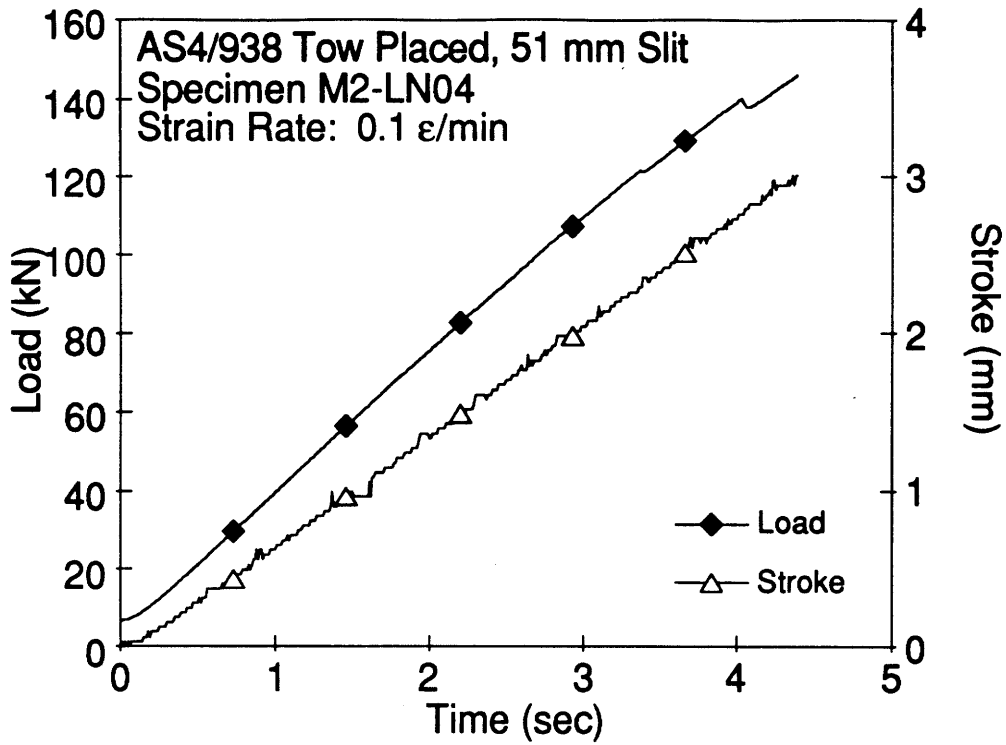


Figure E.79 Plots of Load, Stroke, Far-Field Strain and Strains from Notch-Tip versus Time for Specimen M2-LN04.

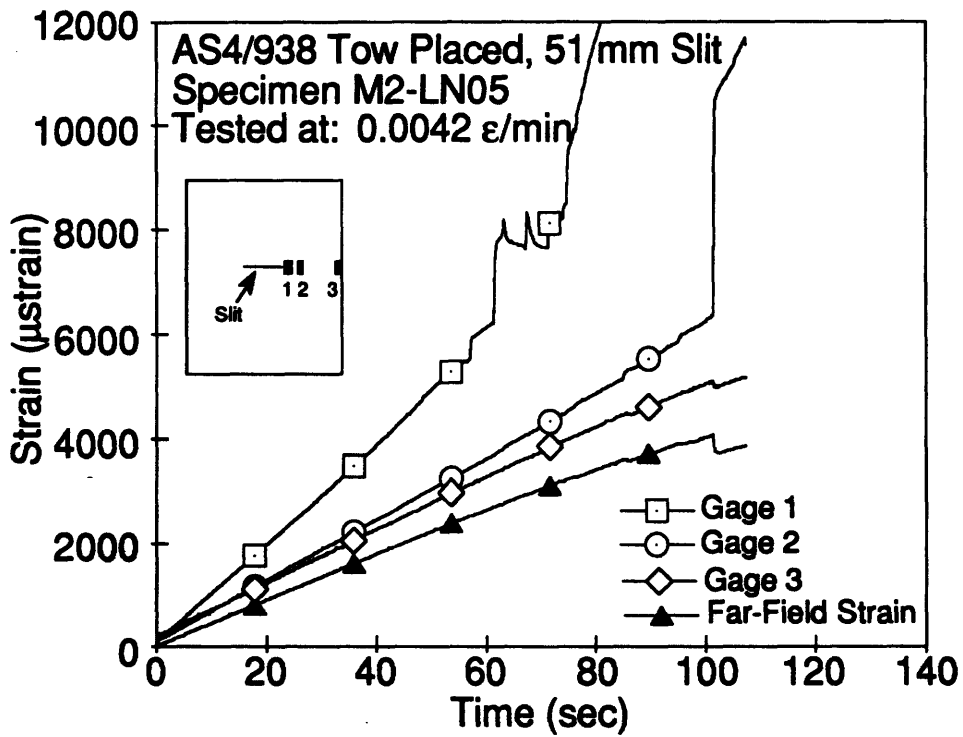
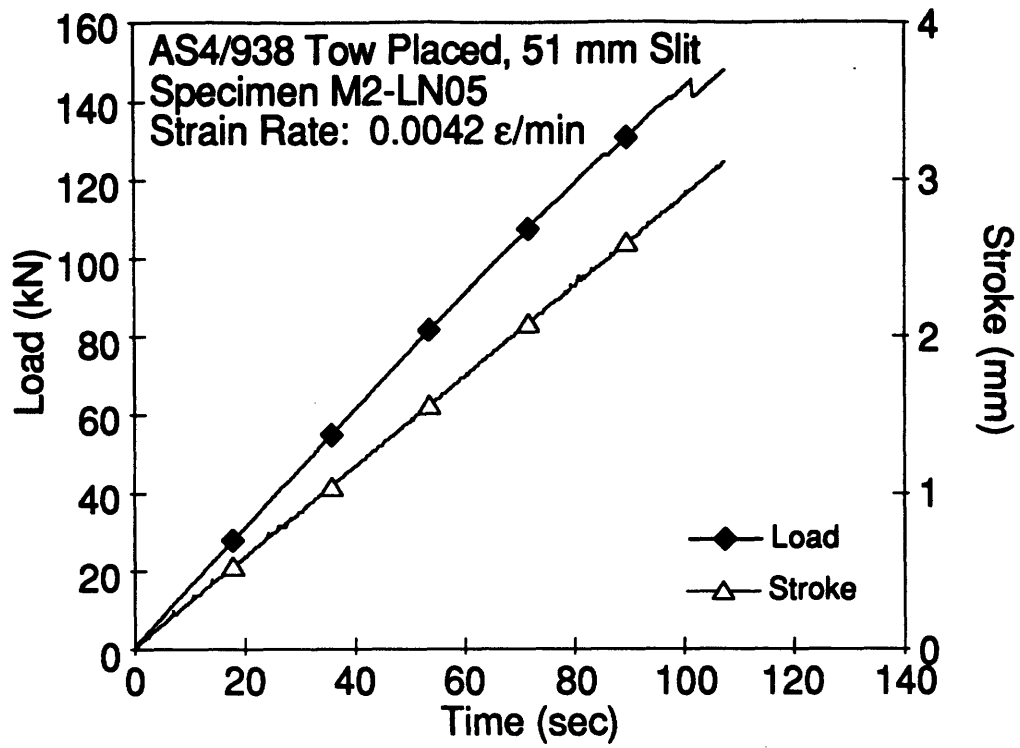


Figure E.80 Plots of Load, Stroke, Far-Field Strain and Strains from Notch-Tip versus Time for Specimen M2-LN05.

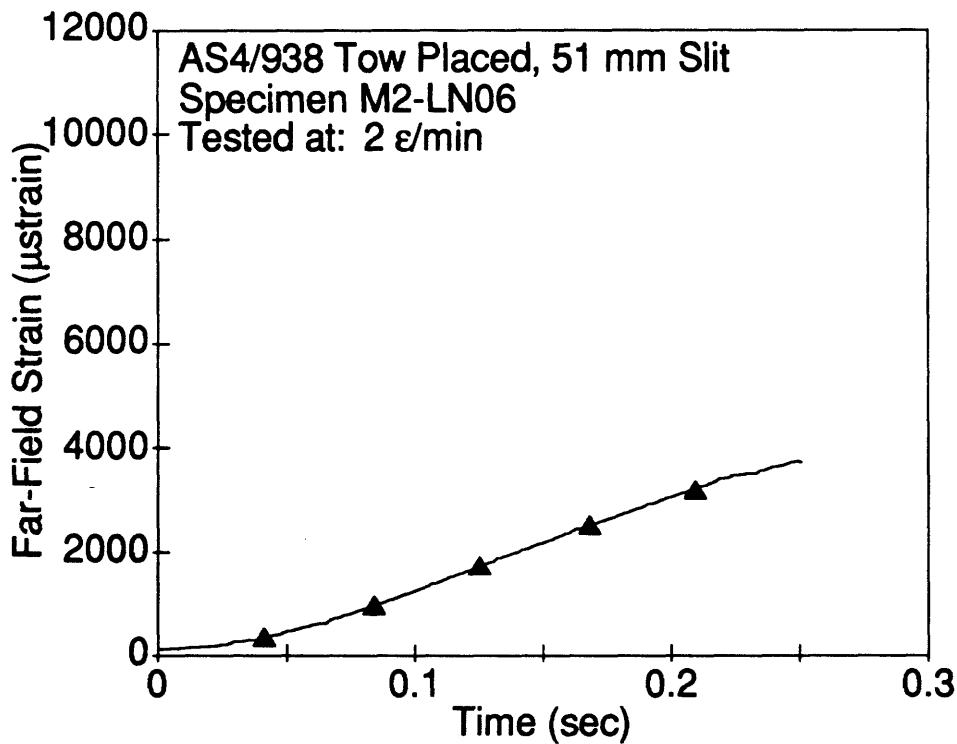
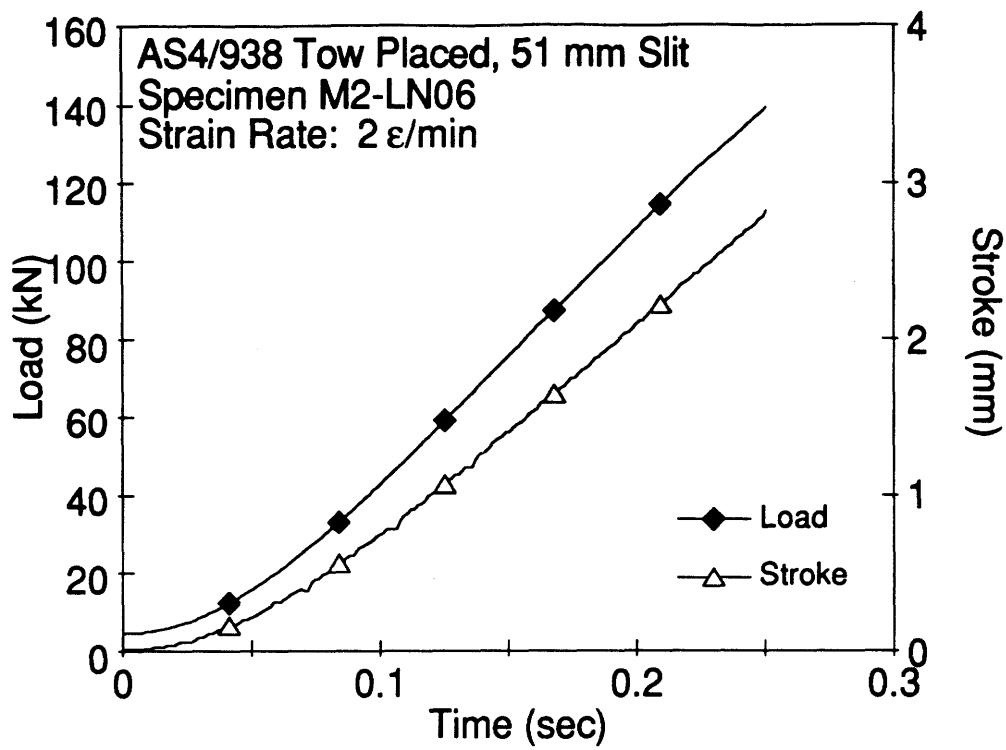


Figure E.81 Plots of Load, Stroke and Far-Field Strain versus Time for Specimen M2-LN06.

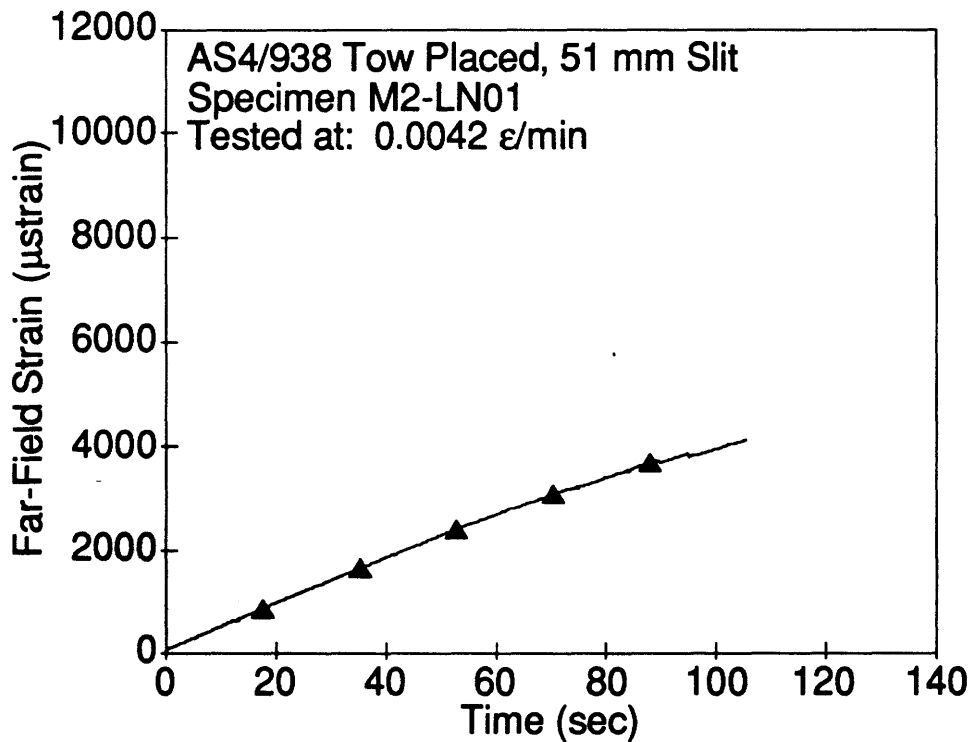
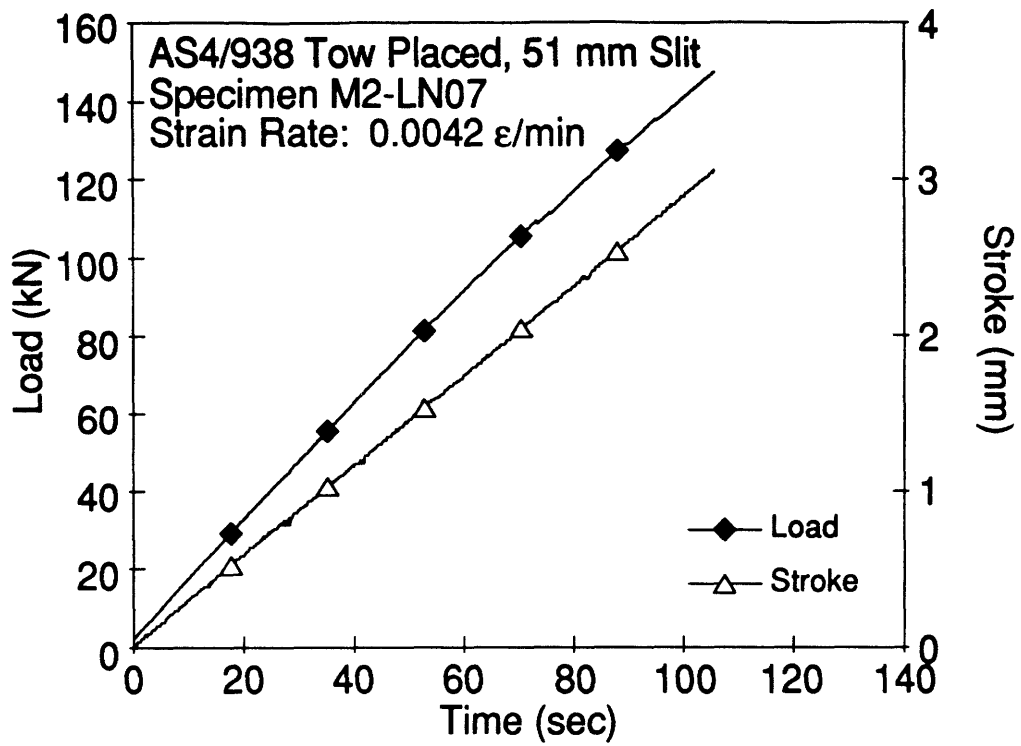


Figure E.82 Plots of Load, Stroke and Far-Field Strain versus Time for Specimen M2-LN07.

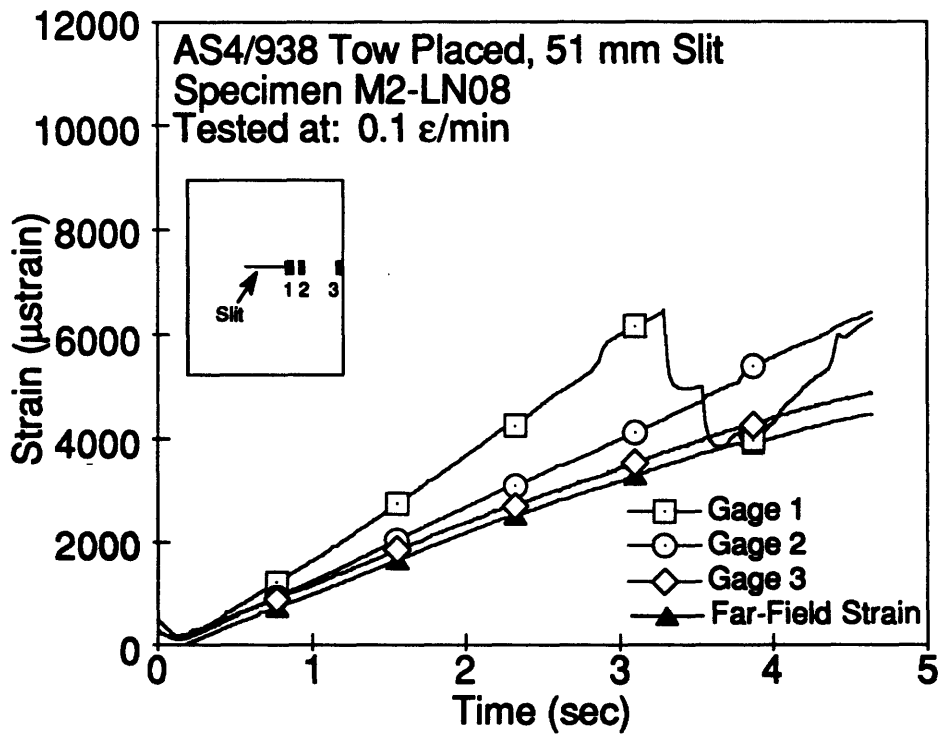
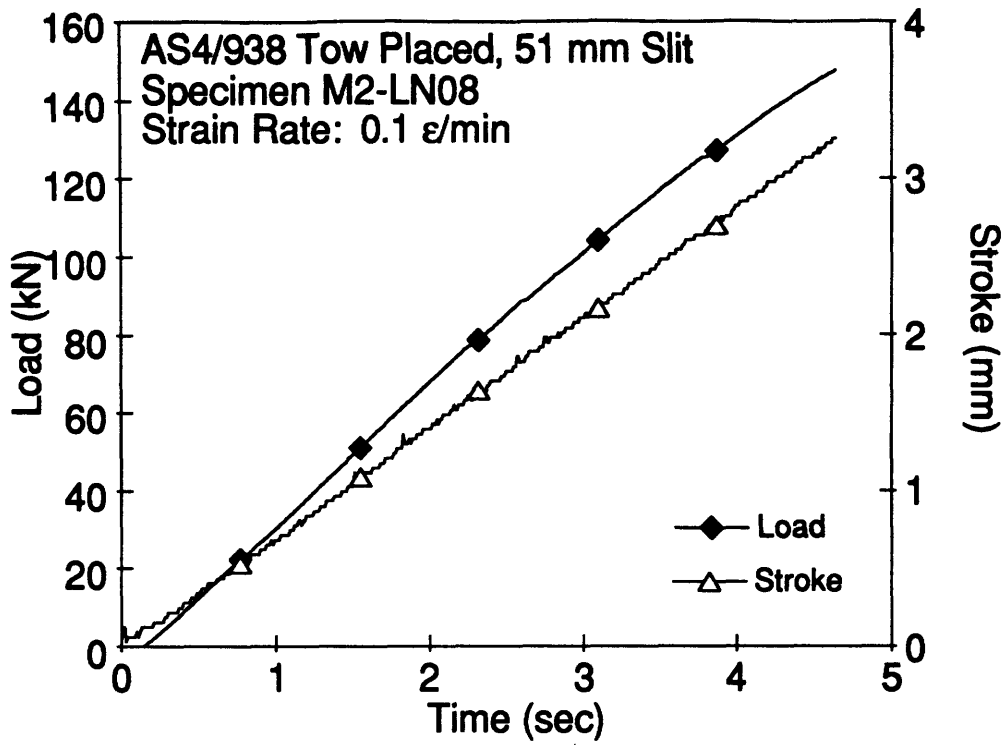


Figure E.83 Plots of Load, Stroke, Far-Field Strain and Strains from Notch-Tip versus Time for Specimen M2-LN08.

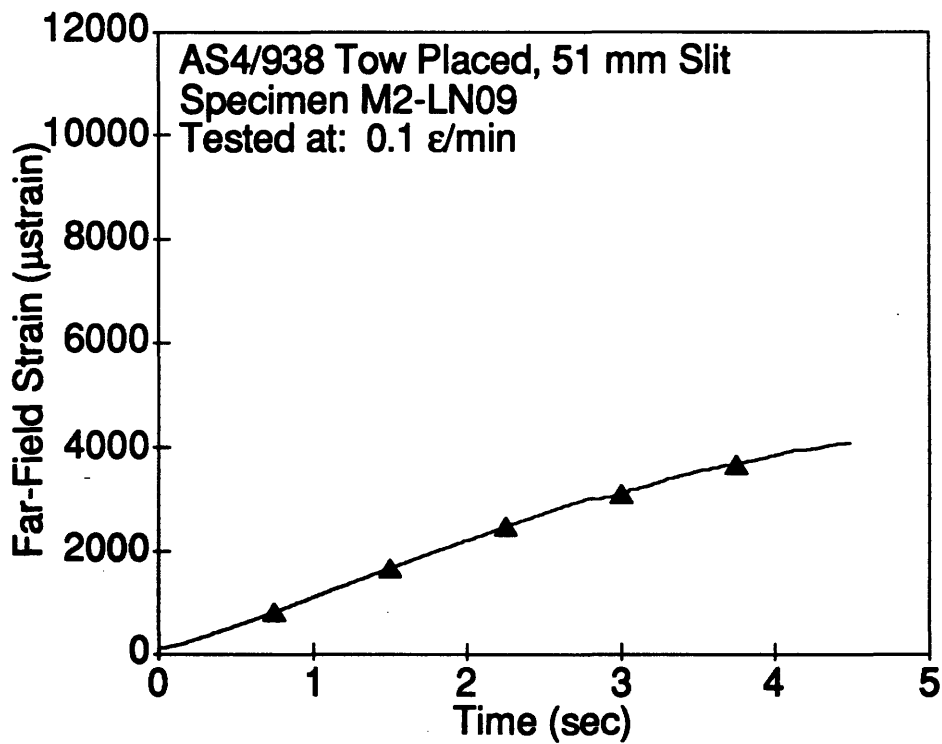
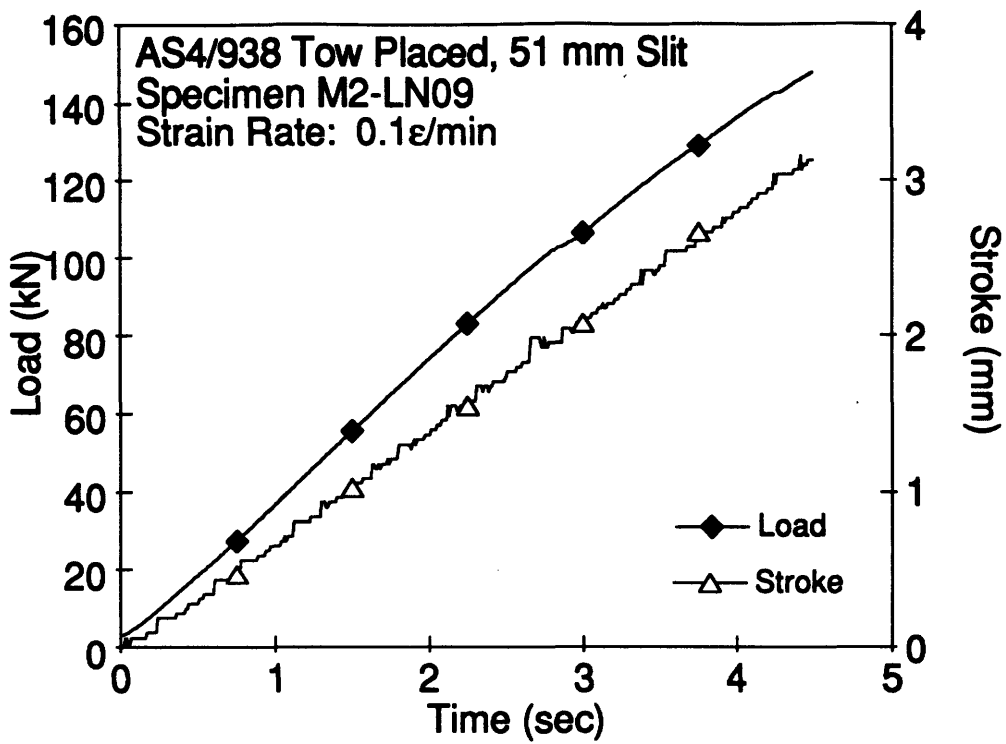


Figure E.84 Plots of Load, Stroke and Far-Field Strain versus Time for Specimen M2-LN09.

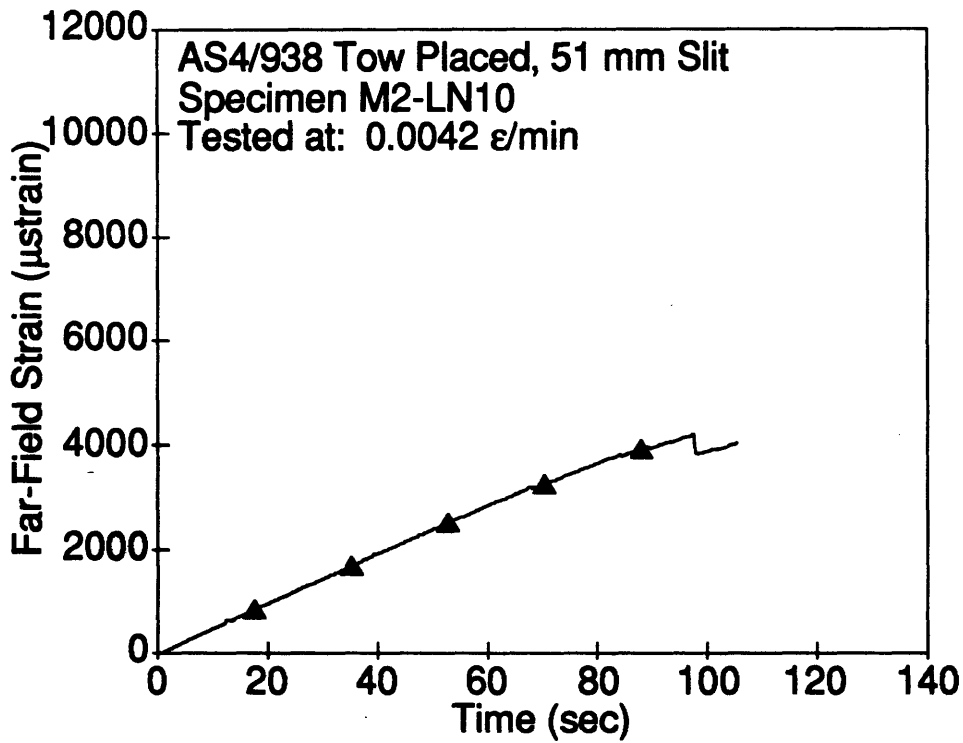
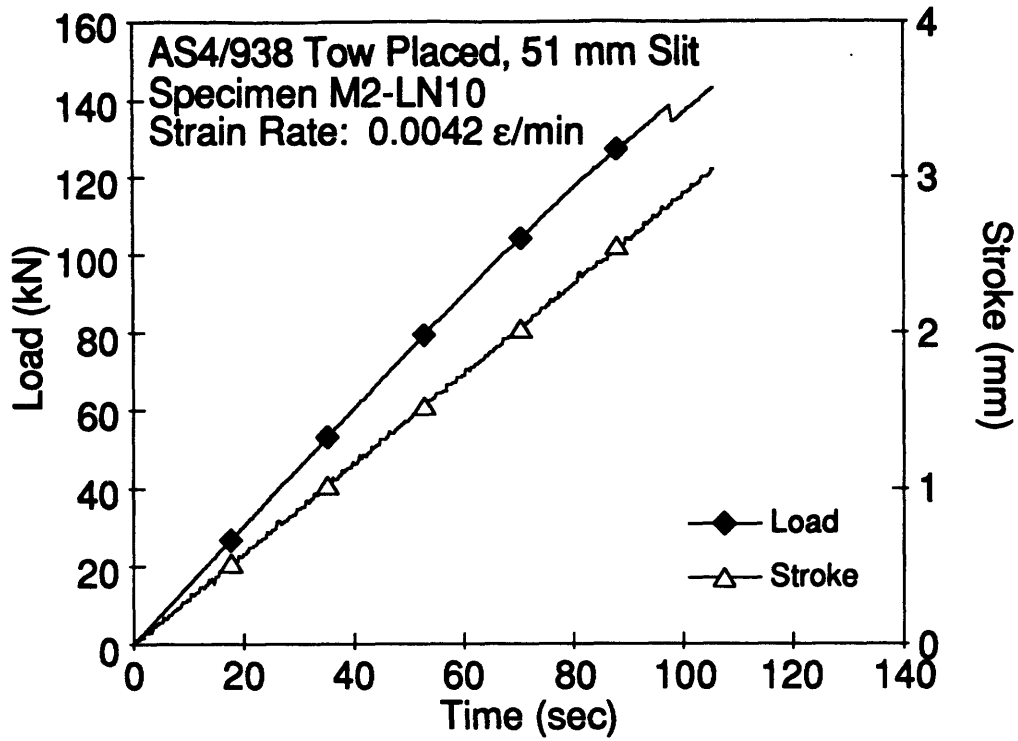


Figure E.85 Plots of Load, Stroke and Far-Field Strain versus Time for Specimen M2-LN10.

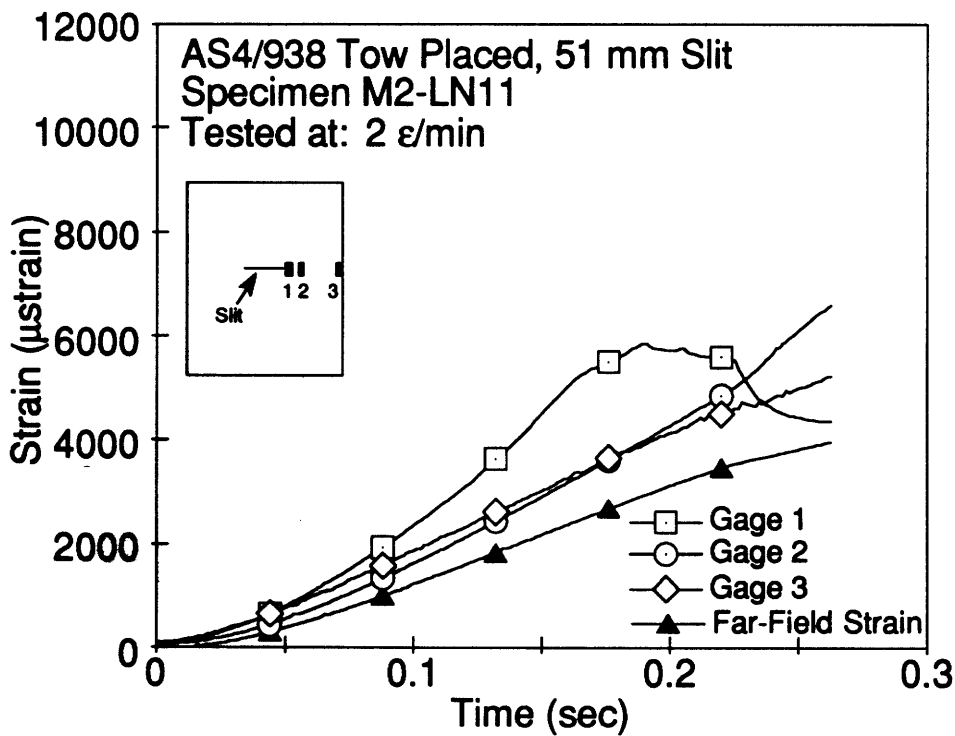
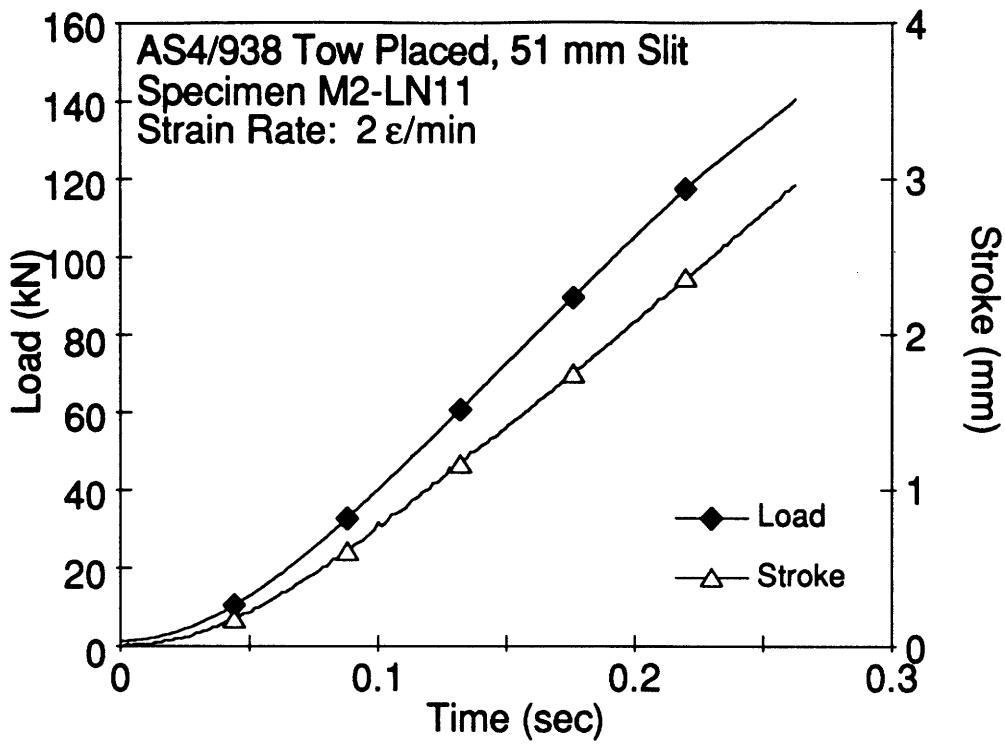


Figure E.86 Plots of Load, Stroke, Far-Field Strain and Strains from Notch-Tip versus Time for Specimen M2-LN11.

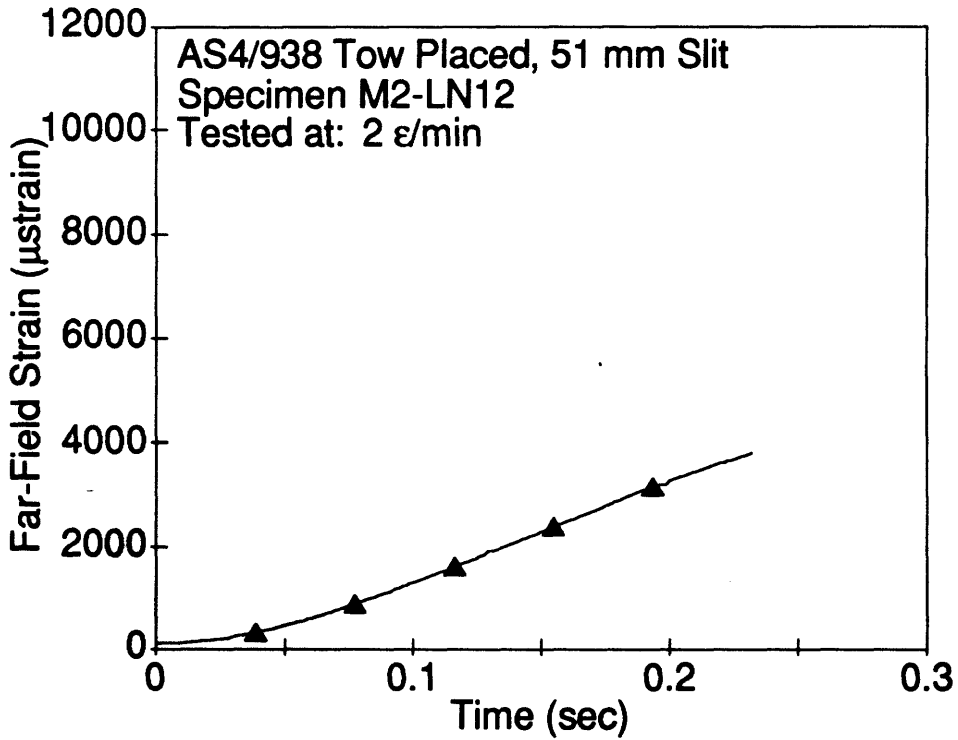
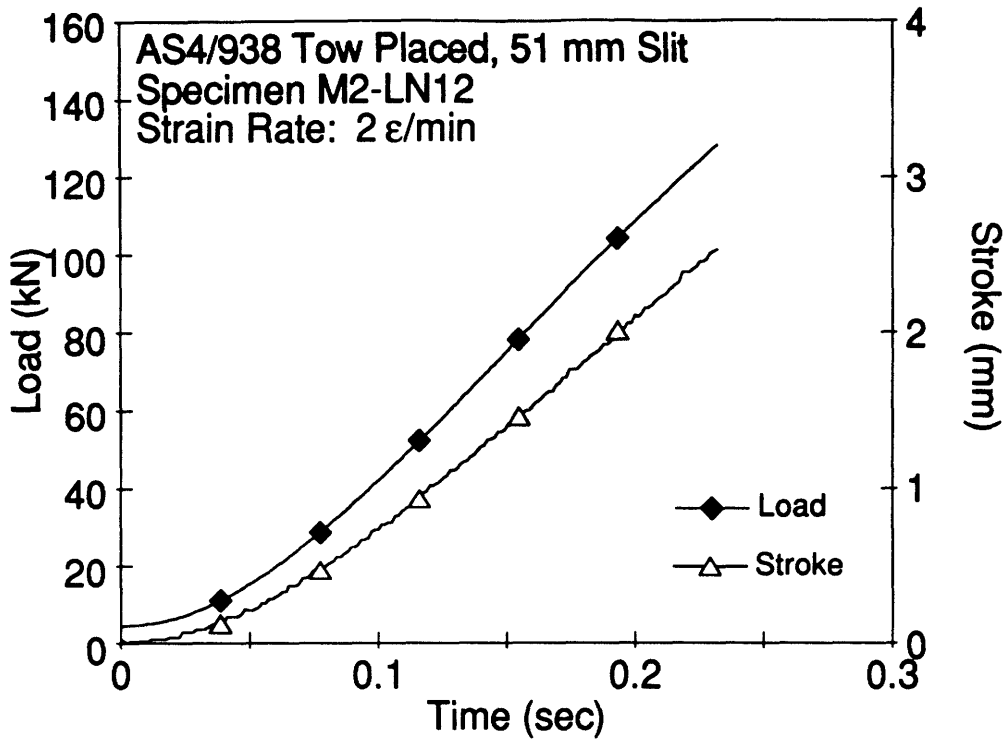


Figure E.87 Plots of Load, Stroke and Far-Field Strain versus Time for Specimen M2-LN12.

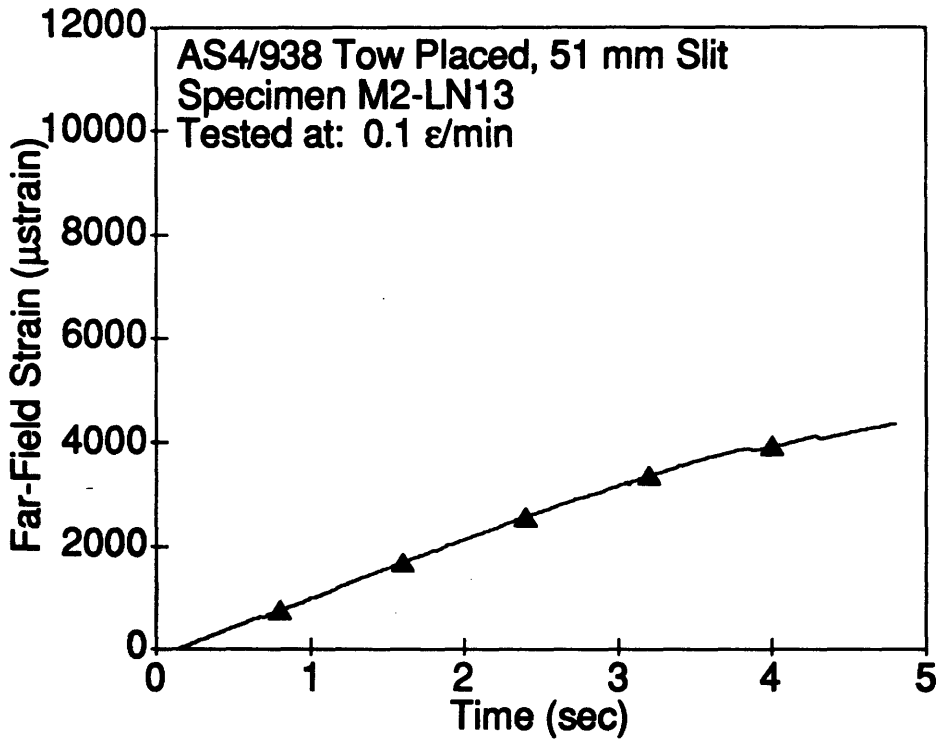
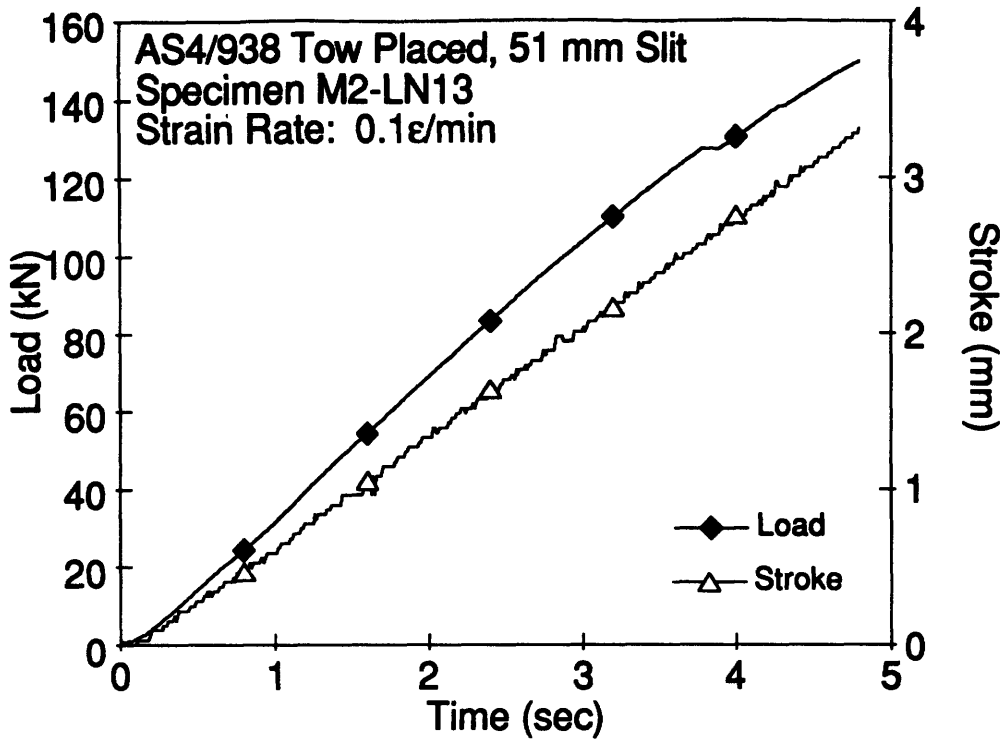


Figure E.88 Plots of Load, Stroke and Far-Field Strain versus Time for Specimen M2-LN13.

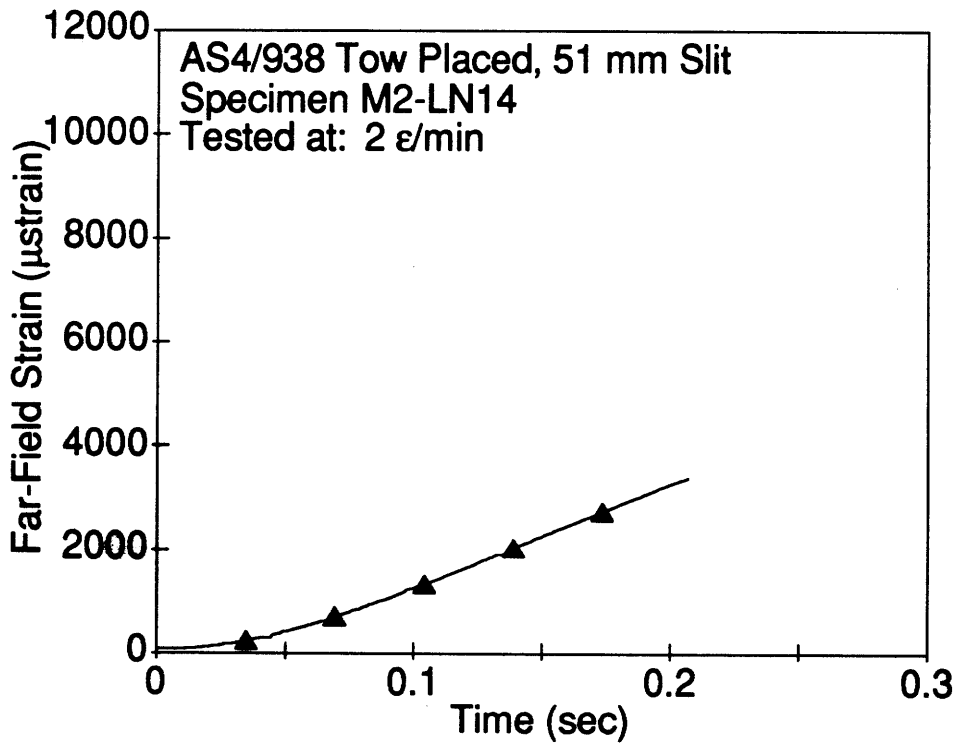
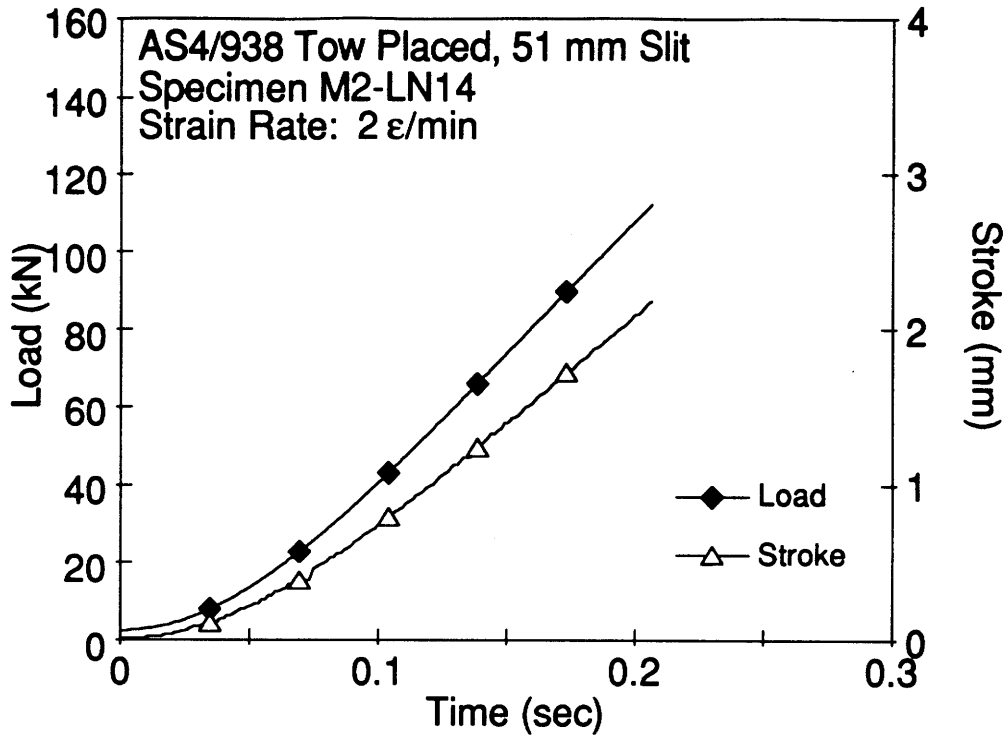


Figure E.89 Plots of Load, Stroke and Far-Field Strain versus Time for Specimen M2-LN14.

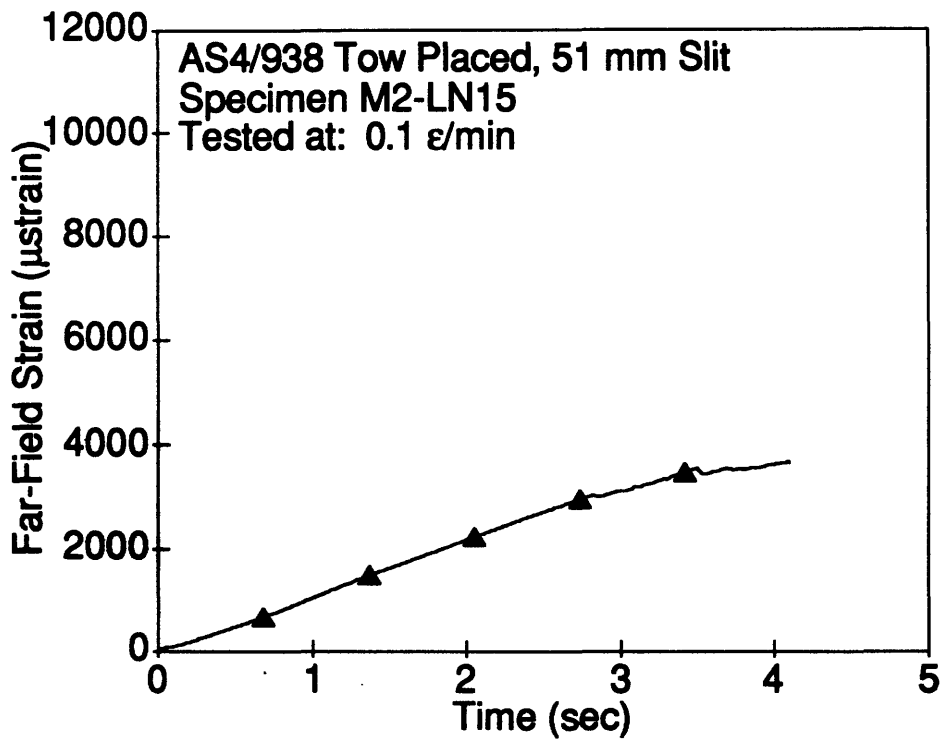
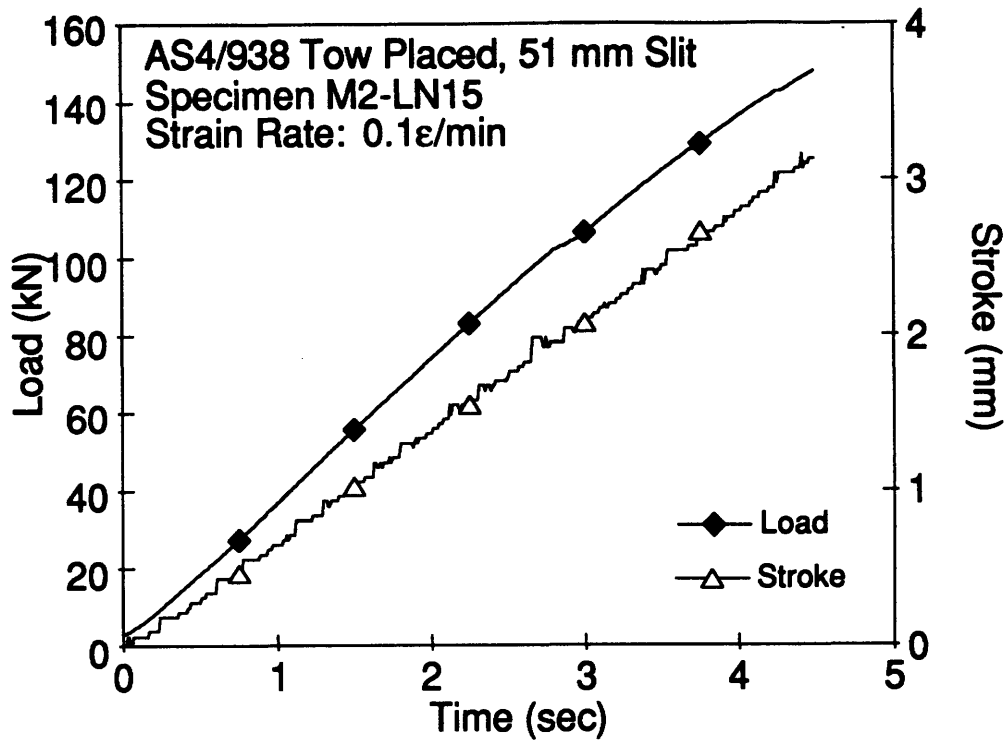


Figure E.90 Plots of Load, Stroke and Far-Field Strain versus Time for Specimen M2-LN15.